THÈSE

PRÉSENTÉE À

L'UNIVERSITÉ PIERRE ET MARIE CURIE

ÉCOLE DOCTORALE: Sciences Mathématiques de Paris Centre (ED 386)

Par **Thi Thao Phuong HOANG**

POUR OBTENIR LE GRADE DE

DOCTEUR

SPÉCIALITÉ: Mathématiques Appliquées

Méthodes de décomposition de domaine espace-temps pour la formulation mixte de problèmes d'écoulement et de transport en milieu poreux

---

Directeur de thèse: Jean E. Roberts

Co-directeurs de thèse: Caroline Japhet et Michel Kern

Soutenue le: 11 Décembre 2013

Devant la commission d'examen formée de:

M. Martin J. GANDER	Université de Genève	Rapporteur
M. Alexandre ERN	Université Paris-Est	Rapporteur
M. Marc LECONTE	ANDRA	Examinateur
M. Yvon MADAY	Université Paris VI	Président du jury
M. Pascal OMNES	CEA	Examinateur
Mme. Caroline JAPHET	Université Paris XIII	Co-directeur de thèse
M. Michel KERN	Inria Paris-Rocquencourt	Co-directeur de thèse
Mme. Jean E. ROBERTS	Inria Paris-Rocquencourt	Directeur de thèse

A THESIS

PRESENTED AT

UNIVERSITY OF PIERRE ET MARIE CURIE

DOCTORAL SCHOOL: Mathematical Sciences of Central Paris
(ED 386)

By **Thi Thao Phuong HOANG**

TO OBTAIN THE DEGREE OF

DOCTOR OF PHILOSOPHY

SPECIALITY: Applied Mathematics

Space-time domain decomposition methods for mixed formulations of flow and transport problems in porous media

---

Thesis advisor: Jean E. Roberts

Thesis co-advisors: Caroline Japhet and Michel Kern

Defended on: December 11th, 2013

In front of the examination committee consisting of:

M. Martin J. GANDER	The University of Geneva	Reviewer
M. Alexandre ERN	The University of Paris-Est	Reviewer
M. Marc LECONTE	ANDRA	Examiner
M. Yvon MADAY	The University of Paris VI	Chairman
M. Pascal OMNES	CEA	Examiner
Mme. Caroline JAPHET	The University of Paris XIII	Thesis co-advisor
M. Michel KERN	Inria Paris-Rocquencourt	Thesis co-advisor
Mme. Jean E. ROBERTS	Inria Paris-Rocquencourt	Thesis advisor

Résumé

Cette thèse présente une contribution aux développements de méthodes numériques pour la simulation d'écoulements en milieu poreux, en particulier par des méthodes de décomposition de domaine espace–temps qui permettent l'utilisation de pas de temps différents dans les différents sous–domaines. Nous étudions deux types de méthodes: la première est basée sur une généralisation de l'opérateur de Steklov–Poincaré au cas de problèmes dépendants du temps, et la seconde est basée sur la méthode de Relaxation d'Onde Optimisée de Schwarz (OSWR) dans laquelle des conditions de transmission plus générales (Robin ou Ventcell) sont utilisées pour accélérer la convergence de l'algorithme. Ces deux méthodes sont étudiées sur une formulation mixte qui est bien adaptée à la modélisation de l'écoulement et du transport en milieu poreux.

Nous considérons tout d'abord un problème de diffusion et formulons, pour chaque méthode, un problème sur l'interface espace–temps entre les sous–domaines. Le caractère bien posé de ces problèmes, avec des conditions aux limites de Dirichlet ou de Robin, est démontré. Les preuves de convergence de l'algorithme OSWR et de sa version semi–discrète sous forme mixte sont également données. Des expériences numériques sont menées en 2D pour comparer les performances des deux méthodes sur des problèmes fortement hétérogènes, et un préconditionneur de Neumann–Neumann dépendant du temps permet d'accélérer la première méthode.

Les deux méthodes sont ensuite étendues au cas d'une équation d'advection–diffusion, l'advection et la diffusion étant traitées séparément grâce une technique de séparation d'opérateurs, ce qui permet d'utiliser des pas de temps différents pour les deux phénomènes dans chaque sous-domaine. Des conditions de transmission sont proposées séparément pour l'advection et pour la diffusion. La convergence des méthodes est étudiée sur des exemples numériques, pour des problèmes en régime d'advection dominante ou de diffusion dominante, et leur précision en temps est étudiée dans le cas de grilles non–conformes en temps. Deux exemples inspirés de la simulation du stockage de déchets nucléaires sont étudiés, et la simulation sur des temps longs est réalisée par l'intermédiaire de fenêtres en temps.

Nous considérons également la méthode OSWR avec des conditions de transmission de Ventcell, étendues à la formulation mixte. Nous démontrons que les problèmes de sous–domaine avec des conditions aux limites de Ventcell sont bien posés. Nous comparons les performances des paramètres optimisés pour Ventcell et Robin dans le cas de problèmes hétérogènes pour une décomposition en deux sous–domaines.

Enfin, nous étudions l'extension des deux méthodes au cas où l'interface représente une fracture pour un modèle réduit d'écoulement dans un milieu poreux fracturé.

Mots-clés: décomposition de domaines espace–temps, formulation mixte, écoulement et transport en milieu poreux, problèmes hétérogènes, opérateur de Steklov–Poincaré dépendant du temps, Relaxation d'Onde de Schwarz Optimisée, grilles en temps non–conformes, fractures.

Abstract

This thesis contributes to the development of numerical methods for flow and transport in porous media, in particular, by using space-time domain decomposition methods that enable the use of different time steps in the subdomains. In this work, we study two types of methods: one is based on a generalization of the Steklov-Poincaré operator to time-dependent problems and one is based on the Optimized Schwarz Waveform Relaxation (OSWR) method in which more general (Robin or Ventcell) transmission conditions are used to accelerate the convergence of the method. These two methods are derived in a mixed formulation, which is well-suited to problems arising in the modeling of flow and transport in porous media.

We first consider the diffusion problem and formulate an interface problem on the space-time interfaces between the subdomains for each method. The well-posedness of the subdomain problem with either Dirichlet or Robin boundary conditions is shown. The convergence proofs of the OSWR algorithm and of the semi-discrete OSWR algorithm in mixed form with nonconforming time discretization are given. Numerical experiments in 2D comparing the performance of the two methods for strongly heterogeneous problems are carried out with a time-dependent Neumann-Neumann preconditioner with weight matrices being used to accelerate the first method.

We then extend both methods to the advection diffusion equation where operator splitting is used to treat the advection and the diffusion differently. Separate transmission conditions for the advection equation and for the diffusion equation are derived. Using numerical results for various test cases, both advection-dominated and diffusion-dominated problems, we compare the convergence of the two methods and analyze the accuracy in time given by each when nonconforming time grids are used. Two prototypes for nuclear waste disposal simulation are considered and time windows are used for long-term simulation.

We also consider the OSWR method with Ventcell transmission conditions extended to the mixed formulation. The subdomain problem with Ventcell boundary conditions is shown to be well-posed. We compare numerically, for a decomposition into two subdomains, the performance of the optimized Ventcell and Robin parameters for heterogeneous problems.

We finally study extensions of the two methods to the case in which the interface represents a discrete-fracture in a reduced fracture model for flow in a fractured porous medium.

Keywords: space-time domain decomposition, mixed formulations, flow and transport in porous media, heterogeneous problems, time-dependent Steklov-Poincaré operator, optimized Schwarz waveform relaxation, nonconforming time grids, fractures.

Acknowledgements

First of all, I would like to express my deep thanks to my advisors Jean E. Roberts, Caroline Japhet and Michel Kern for their guidance and support over the last three years. Working with you all was a great chance and a valuable experience for me. Thank you Michel, for making the first days of my PhD life become less difficult with your help and patience, your useful advices and your optimism. During my PhD, it was always comfortable and fruitful to discuss with you, especially when the answers to the problems somehow came out unexpectedly. Thank you Caroline, for being not only my advisor but also my friend. Your earnestness, inspiration and limitless energy for research have encouraged me a lot when I felt disappointed about my work. I will not forget interesting discussions we had which were not just about work but also about life and many other things. Thank you Jean, for generously sharing your knowledge and for helping me grow up as an independent researcher. I have learned so many things from you, most importantly, your wisdom, thoroughness, cautiousness and your thoughtfulness for others. You kindness always makes me feel so warm and I will remember you together with the "upwind operator" that saved my life at the last minutes.

I am also very thankful to my unofficial advisor Jérôme Jaffré for his advices and support. You have given me many opportunities to explore new things and have explained patiently to me - a young, lacking of experience, foreign student - the scientific conceptions that I haven't known before, the culture and history of France and Europe, and countless other things.

I am specially indebted to Prof. Pascal Omnes, who was my former professor of PUF, a joint program between France and Vietnam for the master degree in applied mathematics, for his recommendation which led to this thesis. You are always kind to all of your students and I am very glad that you have accepted to be a committee member.

I would like to express my grateful acknowledgement to Guillaume Pépin and Marc Leconte, who have provided me with realistic test cases for the numerical experiments in Chapter 2 and Chapter 3. Thank you Marc for useful discussions with you, for your great help and for your acceptance to be a committee member.

I am very grateful to Prof. Alexandre Ern and Prof. Martin J. Gander for kindly accepting to be the reviewers of this thesis. I highly appreciate your evaluation and comments on my work. I am also thankful to Prof. Yvon Maday for his acceptance to be the committee chief.

My next thank will go to the project team Pomdapi of Inria Paris-Rocquencourt, who was my "professional family" during my PhD. It was my pleasure to be a member

of this great team and I am obliged to you all, Françoise Clément, Jean-Charles Gilbert, Martin Vohralik, Pierre Weis and Hend Ben-Ameur, ... for being very nice to me. I am specially beholden to Ibtihel Ben-Gharbia for her great help and her friendship from my very first days at Inria. I also thank my friends, Fatma Cheikh, Emilie Joannopoulos, Alice Chiche, Elyes Ahmed, Nabil Birgle, Markus Köppel, Mohamed Riahi, Emna Hamraoui and Clément Franchini for helping me one way or another and for sharing enjoyable moments with me. I am additionally thankful to Daniel De Rauglaudre for his interesting problems which helped me be awake at the end of some tiring days.

For formalities and paperwork, I am much obliged to Nathalie Bonte and Catherine Chaix for their great help and for their excellent work.

I would like to express my gratitude to ANDRA and Inria who were the sponsors of this work. Thank you for giving me a chance to fulfill my doctoral studies and for offering favorable conditions to facilitate my work.

Many thanks to my best friends, Le Thuy Ngan and Tran Thi Ngoc Anh, and my Vietnamese friends in France, Tran Huong Lan, Vu Do Huy Cuong, Nguyen Thi Le Thu, Nguyen Thanh Nhan, Nguyen Dinh Liem, Ong Thanh Hai, Nguyen Thanh Binh, Nguyen Van Dang, Nguyen Tuan Hang, Luong Thi Hong Cam, Nguyen Thi Phuong Kieu, Nguyen Thanh Nam, Laurent Dang Quoc Tuan, ... for their encouragement and great help.

Finally, I am deeply grateful to my parents and my husband, my little sister, my brothers and my sisters-in-law for their ongoing support and their constant love. I am blessed because of you.

Contents

Résumé **i**

Abstract **iii**

Acknowledgements **v**

Introduction **1**

1 Modeling flow and transport in porous media **11**
1.1 Flow equations 12
1.1.1 Darcy's law 12
1.1.2 The equation of conservation of mass 13
1.2 Transport equations 14

2 Space-time domain decomposition for diffusion problems **17**
2.1 A model problem 17
2.2 A local problem with Robin boundary conditions 25
2.3 Space-time domain decomposition methods 30
2.3.1 Method 1: Using the time-dependent Steklov-Poincaré operator . 31
2.3.2 Method 2: Using Optimized Schwarz Waveform Relaxation 33
2.4 Nonconforming time discretizations and projections in time 39
2.4.1 For Method 1 39
2.4.2 For Method 2 40
2.5 Numerical results 43
2.5.1 A test case with a homogeneous medium 44
2.5.2 A test case with a heterogeneous medium 45
2.5.3 A porous medium test case 48

3 Space-time domain decomposition for advection-diffusion problems **53**
3.1 A model problem and operator splitting 54
3.2 Domain decomposition with operator splitting 56
3.2.1 Method 1: An extension of the time-dependent Steklov-Poincaré operator approach 60
3.2.2 Method 2: An extension of the Optimized Schwarz Waveform Relaxation approach 64
3.3 Nonconforming time discretizations 67
3.4 Numerical results 69
3.4.1 Test case 1: Piecewise constant coefficients 69

3.4.2 Test case 2: Rotating velocity 77
3.4.3 Test case 3: A near-field simulation 79
3.4.4 Test case 4: A simulation for a surface, nuclear waste storage . . 85

4 Extension to Ventcell transmission conditions 91
4.1 Stationary problems 92
4.1.1 Multidomain formulation with Ventcell transmission conditions . 93
4.1.2 Equivalence between the multidomain and the monodomain problems 94
4.1.3 Well-posedness of the Ventcell boundary value problem 96
4.1.4 An interface problem 99
4.1.5 Numerical results 100
4.2 Time-dependent diffusion problems 103
4.2.1 Multidomain formulation with Ventcell transmission conditions . 104
4.2.2 Well-posedness of the Ventcell boundary value problem 105
4.2.3 A space-time interface problem 108
4.2.4 Nonconforming discretization in time 109
4.2.5 Numerical results 110
4.3 Time-dependent advection-diffusion problems 116
4.3.1 An extension of the OSWR with Ventcell transmission conditions and operator splitting 116
4.3.2 Nonconforming time discretizations 120
4.3.3 Some comments on the approach with Ventcell transmission conditions and operator splitting 120

5 Application to reduced fracture models 123
5.1 The compressible flow model of a single-phase fluid 124
5.2 A reduced fracture model 125
5.2.1 Existence and uniqueness of the solution 127
5.3 Two space-time domain decomposition methods 130
5.3.1 Method 1: Using the time-dependent Steklov-Poincaré operator . 130
5.3.2 Method 2: Using Optimized Schwarz waveform relaxation 132
5.3.3 Nonconforming discretizations in time 136
5.4 Numerical results 138
5.5 Extension to transport problems 143
5.5.1 A model problem and operator splitting 143
5.5.2 Domain decomposition formulations 147
5.5.3 Nonconforming discretizations in time 151
5.5.4 Some remarks on numerical implementation 153

Conclusion and future work 155

Appendix A Convergence factor and optimized parameters 157
A.1 Stationary problems 157
A.1.1 Zero order (Robin) transmission conditions 160
A.1.2 Second order (Ventcell) transmission conditions 160
A.2 Time-dependent diffusion problems 161
A.2.1 Two half-space analysis 161

A.2.2 Three domain analysis 165
A.3 Reduced fracture model of the incompressible flow 168

Appendix B Discretizations in space using mixed finite element methods 171
B.1 A model problem and its mixed variational formulation 171
B.2 Semi-discrete approximations in space 173
B.3 Fully discrete problem with an implicit scheme in time 176
B.4 Detailed calculation of the matrices in the linear system 176
B.5 Mixed finite elements for Ventcell type boundary conditions 180

Appendix C Space-time domain decomposition with time windows 183

Bibliography 187

List of Figures

1 A possible layout for a deep geological repository provided by ANDRA. . 2

2.1 The decomposition of the domain into two subdomains where the interface is a plane in space and in time (in 2D). 30
2.2 Nonconforming time grids in the subdomains. 39
2.3 Left: Convergence curves with GMRES. Right: Level curves for the error in the vector field (in logarithmic scale) for various values of the parameters $\alpha_{1,2}$ and $\alpha_{2,1}$, where the red star shows the optimized parameters. 44
2.4 Convergence curves for different diffusion ratios: errors in c for Method 1 (red) and Method 2 (blue); errors in $\boldsymbol{r}$ for Method 1 (magenta) and Method 2 (green). 46
2.5 Level curves for the residual (in logarithmic scale) after 20 Jacobi iterations for various values of the parameters $\alpha_{1,2}$ and $\alpha_{2,1}$. The red star shows the optimized parameters computed by numerically minimizing the continuous convergence factor. 46
2.6 Errors in c (left) and $\boldsymbol{r}$ (right) in logarithmic scales between the reference and the multidomain solutions versus the time step for $\mathfrak{D} = 10$. . . 47
2.7 Errors in c (left) and $\boldsymbol{r}$ (right) in logarithmic scales between the reference and the multidomain solutions versus the time step for $\mathfrak{D} = 100$. . 47
2.8 Geometry of the domain. 48
2.9 The decomposition into 9 subdomains (blow up in the y-direction). . . . 48
2.10 Convergence curves for different time intervals with GMRES: error in c (on the left) and error in $\boldsymbol{r}$ (on the right), for short time $T = 200,000$ years (on top) and for long time $T = 1,000,000$ years (on bottom). . . . 50
2.11 Convergence curves for Method 2 using GMRES and Jacobi iteration: for short time $T = 200,000$ years (on the left) and for long time $T = 1,000,000$ years (on the right). 50
2.12 Snapshots of the multidomain solution after 20,000 years (top left), 100 000 years (top right), 200 000 years (bottom left), and 1,000,000 years (bottom right), with a blow up in the y-direction. 51
2.13 The relative residuals in logarithmic scales using GMRES for Method 1 (on the left) and Method 2 (with Opt. 2) (on the right). 51

3.1 A uniform partition in time with different time steps for advection and diffusion. 55

3.2 An illustration of the upwind concentration defined in the context of cell-centered finite volumes, the arrows represent the direction of the normal flux across the edges, $\int_E \boldsymbol{u}\cdot\boldsymbol{n}$, with $\boldsymbol{n}=(1,0)$. 57
3.3 An illustration of the upwind concentration in the context of domain decomposition, the arrows represent the direction of the normal flux across the edges (for a fixed normal vector $\boldsymbol{n}=(1,0)$). 58
3.4 Nonconforming time grids in the subdomains. 67
3.5 L^2-L^2 error in c (left) and in $\boldsymbol{r}$ (right) in logarithmic scale of the difference between the multidomain and the monodomain solutions versus the number of subdomain solves for $\mathrm{Pe_G}=100\sqrt{2}$. 70
3.6 Convergence curves with GMRES for $\mathrm{Pe_G}=\sqrt{2}$: L^2-L^2 error in the concentration c (left) and in the vector field $\boldsymbol{r}$ (right). 71
3.7 Convergence curves with GMRES for $\mathrm{Pe_G}=10\sqrt{2}$: L^2-L^2 error in the concentration c (left) and in the vector field $\boldsymbol{r}$ (right). 71
3.8 Convergence curves with GMRES for $\mathrm{Pe_G}=1000\sqrt{2}$: L^2-L^2 error in the concentration c (left) and in the vector field $\boldsymbol{r}$ (right). 72
3.9 For $\mathrm{Pe_G}=100\sqrt{2}$: Level curves for the error in the concentration (in logarithmic scale) after 20 Jacobi iterations for various values of the parameters $\alpha_{1,2}$ and $\alpha_{2,1}$, where the red star shows the optimized two-sided Robin parameters. 72
3.10 For $\mathrm{Pe_G}=100\sqrt{2}$: L^2-L^2 error in c (left) and in $\boldsymbol{r}$ (right) in logarithmic scale of the difference between the reference and the multidomain solutions versus the size of the time step. 74
3.11 For discontinuous coefficients: Convergence curves for the different algorithms using GMRES: L^2-L^2 error in c (left) and in $\boldsymbol{r}$ (right). 75
3.12 For discontinuous coefficients: Level curves for the error in $\boldsymbol{r}$ after 15 Jacobi iterations for various values of $\alpha_{1,2}$ and $\alpha_{2,1}$. 75
3.13 For discontinuous coefficients: L^2-L^2 error in c (left) and in $\boldsymbol{r}$ (right) in logarithmic scale of the difference between the reference and the multidomain solutions versus the size of the time step. 76
3.14 Left: Diffusion coefficient and corresponding maximum local Péclet number in each subdomain; Right: The rotating velocity field. 77
3.15 For rotating velocity: L^2-L^2 error in the concentration c for the different algorithms using GMRES: the advection-dominated case (left) and the diffusion-dominated case (right). 77
3.16 For rotating velocity: Level curves for the error in the concentration (in logarithmic scale) after 15 Jacobi iterations for various values of the parameters $\alpha_{1,2}$ and $\alpha_{2,1}$, where the red star the optimized Robin parameters. 78
3.17 For rotating velocity: L^2-L^2 error in c (left) and in $\boldsymbol{r}$ (right) in logarithmic scale of the difference between the reference and the multidomain solutions versus the size of the time step for the advection-dominated case. 79
3.18 The domain of calculation and its decomposition. 80
3.19 Darcy flow. 81

3.20 Convergence curves using GMRES: errors in c (on the left) and error in $\boldsymbol{r}$ (on the right). 81
3.21 Errors in c (left) and $\boldsymbol{r}$ (right) in logarithmic scales between the reference and the multidomain solutions versus the time step. 82
3.22 Relative residuals of GMRES for Method 1 (with the Neumann-Neumann preconditioner) and Method 2. 83
3.23 L^2-L^2 error in c(left) and in $\boldsymbol{r}$ (right) in logarithmic scales between the reference and the multidomain solutions. 83
3.24 Snapshots of the concentration in the repository (left) and in the host rock (right) after approximately 100 years, 5000 years, 10000 years and 20000 years respectively 84
3.25 The geometry of the test case. 85
3.26 The hydraulic head field and the decomposition of the domain. 86
3.27 Relative residuals of GMRES for Method 1 (with the Neumann-Neumann preconditioner) and Method 2. 87
3.28 L^2-L^2 error in c (left) and in $\boldsymbol{r}$ (right) in logarithmic scales between the reference and the multidomain solutions. 87
3.29 Snapshots of the concentration after 20 years, 50 years, 350 years and 500 years respectively. 88

4.1 L^2 error of the difference between the multidomain solution and the monodomain solution: with Jacobi iterations (left) and GMRES (right). 101
4.2 Level curves for the error in the velocity (in logarithmic scale) after some fixed number of Jacobi iterations for various values of the parameters α and β and for different permeability ratios $\mathscr{K}$. The red start shows the optimized parameters. 102
4.3 L^2 error in the pressure p for $\mathscr{K}=1$: Jacobi (left) and GMRES (right). . 102
4.4 L^2 error in the pressure p for $\mathscr{K}=10$: Jacobi (left) and GMRES (right). 103
4.5 L^2 error in the pressure p for $\mathscr{K}=100$: Jacobi (left) and GMRES (right). 103
4.6 Nonconforming time grids in the subdomains. 109
4.7 L^2-L^2 error in the concentration c and in the vector field $\boldsymbol{r}$ of the difference between the multidomain solution and the monodomain solution, using optimized Ventcell parameters. 111
4.8 L^2-L^2 error in the concentration c and in the vector field $\boldsymbol{r}$ with GMRES for the different algorithms. 112
4.9 Level curves for the error in the vector field for various values of α and β, where the red star shows the optimized Ventcell parameters. 112
4.10 L^2-L^2 error in the concentration c and in the vector field $\boldsymbol{r}$ with GMRES for the different algorithms and different diffusion ratios (the same legend applies to all three subfigures). 114
4.11 Level curves for the error in $\boldsymbol{r}$ after 12 Jacobi iterations for various values of the parameters α and β. The red star shows the optimized parameters. 115
4.12 L^2-L^2 error in c of the difference between the reference and the multidomain solutions versus the time step size for $\mathfrak{D}=10$ (left) and $\mathfrak{D}=100$ (right), using Ventcell transmission conditions. 116
4.13 Nonconforming time grids in the subdomains. 120

5.1 Left: The domain Ω with the fracture Ω_f. Right: The domain Ω with the interface-fracture γ. 125
5.2 Nonconforming time grids in the rock matrix and in the fracture. 137
5.3 Geometry of the test case where the fracture is considered as an interface. 139
5.4 Snapshots of the pressure field (left) and flow field (right) at $t = T/300$, $t = T/4$, $t = T/2$ and $t = T$ respectively (from top to bottom). 139
5.5 Convergence curves for the compressible flow: errors in p (on the left) and in $\boldsymbol{u}$ (on the right) - Method 1 with no preconditioner (blue), Method 1 with local preconditioner (green), Method 1 with Neumann-Neumann preconditioner (cyan) and Method 2 (red). 141
5.6 L^2 velocity error (in logarithmic scale) after 10 Jacobi iterations for various values of the Robin parameter. The red star shows the optimized parameters computed by numerically minimizing the continuous convergence factor. 141
5.7 Relative residual with GMRES for different time grids: Method 1 with the local preconditioner (green), Method 1 with the Neumann-Neumann preconditioner (cyan) and Method 2 (red). 142
5.8 L^2 pressure error in the rock matrix: Time grid 1 (blue), Time grid 2 (magenta), Time grid 3 (black). 142
5.9 L^2 pressure error in the fracture: Time grid 1 (blue), Time grid 2 (magenta), Time grid 3 (black). 143
5.10 Nonconforming advection and diffusion time grids in the rock matrix and in the fracture. 152

B.1 A conforming triangulation into rectangles. 177
B.2 The hat function $v_{i+1/2,j}\left(x_1\right)$. 178

List of Tables

2.1 Number of subdomain solves needed to reach a reduction of 10^{-6} of the errors for different algorithms, and for different values of the discretization parameters Δx and Δt. 45
2.2 Diffusion coefficients and corresponding nonconforming time steps. . . . 45
2.3 Number of subdomain solves needed to reach a reduction of 10^{-6} of the errors for different algorithms , and for different values of the discretization parameters Δx and Δt. 47

3.1 For $\mathrm{Pe}_G = 100\sqrt{2}$: Number of subdomain solves needed to reach a reduction of 10^{-6} in the error for the different algorithms , and for different values of the discretization parameters. 73
3.2 Data for the discontinuous test case. 74
3.3 For discontinuous coefficients: Number of subdomain solves required to reach a reduction of 10^{-6} in the error for the different algorithms , and for different values of the discretization parameters. 76
3.4 Data for flow and transport problems. 80
3.5 Data for flow and transport problems. 86

4.1 Number of iterations required to reach an error reduction of 10^{-6} in p and in $\boldsymbol{u}$ (in square brackets) for different permeability ratios, and for different values of the discretization parameter h. 101
4.2 Number of subdomain solves needed to reach an error reduction of 10^{-6} for continuous coefficients, using optimized Ventcell parameters. 113
4.3 Diffusion coefficients and corresponding nonconforming time steps. . . . 113
4.4 Number of subdomain solves needed to reach an error reduction of 10^{-6} for different diffusion ratios, using optimized weighted Ventcell parameters. 115

Introduction

Motivation: simulation of a deep geological repository

What can be done with the radioactive waste? In 1957, the National Research Council of the American National Academy of Sciences introduced the concept of a repository in a deep geological formation that would effectively isolate wastes from the biosphere for a time long enough for them to decay. In brief, the waste is first encapsulated in multiple-metal-barrier, waste packages and then is buried deep underground (about 300m-500m in depth) in a sufficiently stable environment. There are many technical challenges to deriving a full understanding of the long-term behavior and performance of such a repository. These are due to the physical characteristics of the flow system, the interaction of water with waste packages in the repository, the transport of radionuclides released from the packages due to corrosion, the chemical reactions that may occur, the possible presence of undetected or newly developed fractures, etc. This is a problem that involves scientists from many fields, hydrogeologists, physicists, chemists, mathematicians, biologists, engineers, etc. and that attracts more and more attention in many countries that have a sufficiently large amount of nuclear waste.

In France, ANDRA (l'Agence Nationale pour la gestion de Déchets RAdioactifs, *www.andra.fr*), who sponsored this thesis and provided data for more realistic numerical experiments, is the national radioactive waste management agency established in 1991 as a public body in charge of the long-term management of all radioactive waste. One of the purposes of ANDRA is to study the future performance of potential repositories to demonstrate that it is safe and that it will pose no significant environmental hazard due to possible leakages of the radioactive waste. Several different physical phenomena are involved: at the geologic scale, the main phenomena are the flow of water throughout the region of interest, and the subsequent possible migration of the radionuclides caused by the leak from the containers over time. At the repository scale, corrosion will cause formation of gas, so that two phase flow has to be taken into account. Furthermore, chemical interactions between the engineered barrier and the waste also play a role, as does the mechanical deformation due to the construction of the storage. The task can be carried out by modeling and simulating the multiphase, multicomponent flow and the transport of contaminants in a porous medium. In this work, we will only be concerned with large scale issues, and only deal with single phase flow and transport. Mathematically, one works with complex, coupled systems of (nonlinear) partial differential equations (PDEs) and tries to approximate their solutions as accurately and efficiently as possible. Additionally, the time interval for the experiment can be very long (about $10^3 - 10^6$ years due to the slow decay process of radioactive elements) and simulations may need to be repeated many times to carry

(a) Waste package 1.3m × Ø0.43m

(b) A repository 2km × 2km

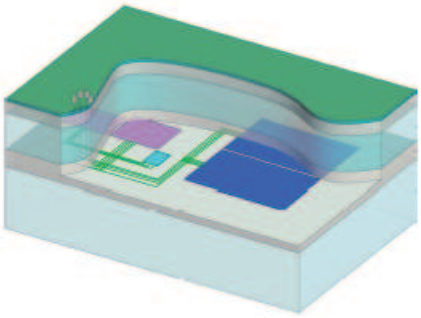

(c) Geological formation 20km × 20km × 500m

Figure 1: A possible layout for a deep geological repository provided by ANDRA.

out a sensitivity analysis. Thus there is a need for efficient simulators to deal with this problem. One is confronted with the following challenges:

- The simulations involve objects with very different length scales, from 1 meter (or even less if the possibility of fractures is considered) to hundreds or thousands of meters, and with complex geometries (see Figure 1). Consequently, local refinements in different zones may be required.
- The domain of calculation is actually a union of several subdomains representing various geological layers involved in the simulation and regions in and around the repository. These subdomains may have very different hydrogeological properties, which causes strong heterogeneity in space. In addition, the various physical or chemical processes involved might occur on very different time scales that may vary over several orders of magnitude.

One possible way to efficiently carry out such a simulation is to use domain decomposition methods: the domain of calculation Ω is decomposed into several subdomains Ω_i, then instead of solving a problem defined on the whole domain, we solve the subproblems defined on the subdomains and couple them through the use of well-chosen transmission conditions on the interfaces between subdomains. This approach is well-adapted to our original problem for three reasons: firstly, it reduces the problem on a very complex and large domain (which may be very expensive or even impossible to implement) to problems of smaller size; secondly, it makes possible the use of different numerical schemes for spatial discretization for different subdomains adapted to their physical properties (thus the refinements can be handled locally in each subdomain); thirdly, the subdomain problems can be solved in parallel on supercomputers

with many processors so that the computational time may be reduced significantly. For a dynamic system (i.e. changing with time), a straightforward extension of such an approach is to first discretize the system in time, then apply domain decomposition to solve the resulting stationary problem at each time step. Consequently, a single time step is applied for all subdomains, which is not computationally efficient due to very different time scales involved in the simulation. Hence we search for a method that enables different time discretizations in the subdomains as well as different spatial discretizations. The idea is using an iterative procedure to decouple the dynamic system into dynamic subsystems defined on the subdomains, to solve the time-dependent problem independently in each subdomain, and then to exchange information between the subdomains on the space-time interfaces. This method, namely the space-time domain decomposition method or global-in-time domain decomposition, may be enhanced by using time windows, i.e. the long time interval is divided into several smaller subintervals, called time windows, and the problem is then solved in the time windows sequentially.

In this thesis, we consider the linear transport problem with both advection and diffusion. Dispersion can be handled in a way similar to what has been done for diffusion, however, we haven't taken into account the impact of dispersion in our numerical implementations. The aim of this thesis is to derive and analyze domain decomposition methods with local time stepping for this type of parabolic equation before moving on to more complicated models.

The object of the work: Space-time domain decomposition in mixed formulations

Domain decomposition methods originated from the work of H. A. Schwarz [105] in 1870, in which he proposed an iterative method, now called the Schwarz alternating method, to prove the existence of harmonic functions on irregular regions (such as a region consisting of a rectangle and a circle which intersect). Since the mid-1980s, due to the development of parallel computer architectures and multiprocessor supercomputer designs, one has witnessed a strong development of numerical methods for partial differential equations (PDEs) based on the concept of domain decomposition, see, e.g., [55, 15, 4, 20] and the references therein. We cite in particular the work of P. L. Lions [85] (see also [83, 84]) introducing a parallelizable nonoverlapping domain decomposition method based on Robin transmission conditions, which lays the corner stone for a school of domain decomposition methods to which one of the two methods developed in this thesis belongs. We refer to the books [101, 109, 94] and the references therein for an overview of this subject and the website of the annual international domain decomposition method conference, *ddm.org*, for an increasingly large amount of research and numerical algorithms using domain decomposition for different types of linear and nonlinear PDEs. It should be noted that domain decomposition methods have a close relation with the numerical methods for the solution of linear algebraic systems.

For parabolic equations, there are three possible classes of domain decomposition methods (as acknowledged in [45]) :

- Domain decomposition in space: the equation is first discretized in time using

an implicit scheme and the classical domain decomposition methods is then used for solving the stationary problems at each time step (see, e.g. [78, 23] and the references therein). Consequently, the same time discretization must be used in each subdomain, which restricts the possibility of using numerical approximations adapted to the physics of the subdomain problem. In the context of using parallel computing, this approach is costly as information needs to be exchanged at every time step of the discretization.

- Domain decomposition in time: the equation is first discretized in space to obtain a large system of ordinary differential equations, then a waveform relaxation algorithm is used for solving such a system. Multi-splitting algorithm [76], multigrid dynamic iteration method [69] and convolution SOR waveform relaxation algorithm [70] are examples of this class, where the analysis is carried out in an algebraic view and thus it is difficult to interpret the physical properties such as information exchange on the interfaces in this case. See the cited papers and the references therein for more detail about this approach.

- Space-time domain decomposition: a space-time domain decomposition method is derived at continuous level so that the time-dependent problems are solved in each subdomain (resulting from a spatial decomposition) and the information is then exchanged over space-time interfaces between subdomains. As a result, different numerical schemes both in space and in time can be used in the subdomains and less communication cost is needed (in terms of parallel computations) as the data is transferred over the whole time interval. Such an approach using the waveform relaxation algorithm and the overlapping Schwarz domain decomposition has been simultaneously and independently introduced in [51, 54]. However, the resulting iterative algorithm was shown to converge slowly (with a constant overlap). Then by using the idea of the Optimized Schwarz method [72, 44], optimal transmission conditions were derived for parabolic problems [47, 90, 12] and the new method was introduced, namely, the Optimized Schwarz Waveform Relaxation method (more details about this method will be given in the following).

Our work concentrates on the last of these classes as it provides a natural and simple way to efficiently deal with problems with strong heterogeneities. We apply such a space-time domain decomposition method to model flow and transport in porous media. In particular, we focus on the use of local time stepping and only treat conforming spatial discretizations. There are many works on nonconforming grids in space, for example: mortar finite elements (see, e.g.[13, 113, 114]), mortar mixed finite elements (see, e.g. [38, 115]), methods based on Schwarz algorithms with optimized Robin transmission conditions (see [2, 50, 1]).

In order to handle efficiently the advection-diffusion problem, especially when advection is dominant, we use operator splitting [68] to treat the advection and the diffusion separately and differently. It was shown that (see, e.g. [29, 30, 95]) approximating the advection explicitly and the diffusion implicitly can reduce the numerical diffusion. In [6, Chapter 2, p.14–32], numerical results in 1D comparing the three schemes - fully implicit, explicit-implicit and operator splitting with sub-time steps for the advection - show that the operator splitting gives good approximations both for

homogeneous and for heterogeneous problems and at the same time makes possible the optimal use of time steps for the advection and the diffusion. In particular, for an advection-dominated problem, one may take a smaller time step, satisfying the CFL condition, for the advection while much larger time step can be used for the diffusion. Throughout the thesis, due to operator splitting, we study first the domain decomposition methods for the pure diffusion equation, then extend the results to the coupled advection-diffusion problem.

In addition, as the conservation of mass is essential for the application that we envisage, we use conservative cell-centered techniques for discretization in space such as mixed finite element methods, mixed hybrid finite element methods or finite volume methods. In particular we have chosen to use mixed methods. Mixed finite element methods are numerical discretization methods first used by engineers in the mid 1960's for problems in solid mechanics; see [111, 63, 64]. A mathematical analysis of the basic method was given by F. Brezzi in 1974 [21], and the most widely used approximation spaces associated with the method were introduced by P.-A.Raviart and J.-M. Thomas in 1977 [102]. From the mid 1980's these methods began to be used for calculation of the flow field in reservoir simulation problems in particular because they give an approximation simultaneously, and to the same order, of both the velocity field and the pressure field [32, 34, 39, 24]. They were also considered to be particularly appropriate methods for this problem because they are conservative and even locally conservative. These same properties have made these methods interesting for many other problems in which flow in a porous medium must be calculated: modeling flow in and around underground nuclear waste repositories, studying seawater infiltration into aquifers, evaluating the feasibility of CO2 sequestration, to name a few. If these discretization methods have still today not become the method of choice for large industrial codes in the oil industry they are nonetheless much studied with respect to porous medium applications in both the academic and engineering literature. For a development from a mathematical point of view see [22] or [104] or from a more engineering point of view see [25] or [26, Chapter 4.5]. The mixed formulation with two types of variables is very well-suited for using domain decomposition [56], especially since one has available both Dirichlet and Neumann data on the boundary.

In this work, we develop two space-time domain decomposition methods as follows:

1. The first method (called Method 1 in this thesis) is a global-in-time substructuring method which uses a Steklov-Poincaré type operator. Steklov-Poincaré operators are interface operators that enforce the classical transmission conditions on the interfaces between subdomains. They were introduced for stationary problems [3, 112, 14, 100] as natural mathematical tools for analyzing domain decomposition algorithms for both homogeneous and heterogeneous problems. The convergence of an iterative procedure associated with the discrete counterpart of any Steklov-Poincaré operator (namely, the Schur complement matrix) is accelerated by a use of the Neumann-Neumann preconditioner [99, 19, 31] which is a local preconditioner defined by solving Neumann boundary problems in the subdomains. For a decomposition into many subdomains a technique called Balancing Domain Decomposition (BDD) preconditioner was introduced and analyzed in [88, 89], and in [28] for mixed finite elements. In brief, the method "involves at each iteration the solution of a local problem with Dirich-

let data, a local problem with Neumann data and a "coarse grid" problem to propagate information globally and to insure the consistency of the Neumann problems" [28]. It was shown that the condition number is independent of the coefficient jumps between the subdomains and of the number of subdomains, and it grows only as the square of the logarithm of the ratio of the subdomain size to the element size in both two and three dimensions. Extension of Steklov-Poincaré operators to parabolic problems was given in [35, 52] in which uniform time steps are considered and the iterations are then performed at each time step.

In this work, we extend the method to the case of unsteady problems and in the context of operator splitting, and construct the time-dependent Steklov-Poincaré operator. For parabolic problems, we need only the Neumann-Neumann preconditioner [80] as there are no difficulties concerning consistency for time-dependent Neumann problems. Of course one could make use of the idea of the "coarse grid" to ensure a convergence rate independent of the number of subdomains. However, this idea has not been pursued for lack of time.

2. The second method (Method 2) uses the Optimized Schwarz Waveform Relaxation (OSWR) approach. The OSWR algorithm is an iterative method that computes in the subdomains over the whole time interval, exchanging space-time boundary data through more general (Robin or Ventcell) transmission operators in which coefficients can be optimized to improve convergence rates. For stationary problems, Robin and Ventcell transmission conditions for the alternating Schwarz method were proposed in [96] and the optimized conditions were introduced in [71, 74]. See [44] for an overview of the Optimized Schwarz methods. In the context of mixed formulations, the classical Schwarz algorithm with Robin transmission conditions for stationary problems with mixed finite elements was analyzed in [33]. In this thesis, we extend the Optimized Schwarz methods with Ventcell transmission condition to the mixed settings.

   The OSWR method was introduced for parabolic and hyperbolic problems in [47] and was extended to advection-reaction-diffusion problems with constant coefficients in [90]. The optimization of the Robin or Ventcell parameters was analyzed in [45, 90, 12] and extended to discontinuous coefficients in [46, 16, 60]. Extensions to heterogeneous problems and non-matching time grids were introduced in [46, 17]. More precisely, in [17, 59], discontinuous Galerkin (DG) for the time discretization of the OSWR was introduced to handle non-conforming time grids, in one dimension with discontinuous coefficients. This approach was extended to the two dimensional case in [61, 62]. One of the advantages of the DG method in time is that a rigorous analysis can be carried out for any degree of accuracy and local time-stepping, with different time steps in different subdomains (see [61, 62]). A suitable time projection between subdomains was obtained by an optimal projection algorithm without any additional grid, as in [50] (see also [49] for efficient projection algorithms for higher dimensions). These papers use Lagrange finite elements. An extension to vertex-centered finite volume schemes and nonlinear problems is given in [57].

   In this thesis, we study an extension of the OSWR method with Robin transmission conditions to the mixed formulation and in the context of operator splitting.

In order to improve the convergence of the method, we also consider the Ventcell transmission conditions in the mixed setting. Moreover, this type of transmission conditions is concerned when we extend the OSWR method to a reduced fracture model since the equation in the fracture is also second order.

The well-posedness of the subdomain problems involved in each method is presented using Galerkin's method and suitable a priori estimates [81, 18, 65]. In [106, 107] demonstrations using semigroups are given for nonlinear evolution problems.

For each method, we transform the multidomain problem into an interface problem on the space-time interfaces between subdomains. Different time discretizations are enabled by applying the projection algorithm in [50] to exchange information on the space-time interfaces, for the lowest order DG method in time. The discrete counterpart of the interface problem is solved iteratively using a Richardson iteration or can be accelerated by a Krylov method such as GMRES. Numerical experiments are carried out for different test cases, including realistic prototypes arising from the simulation of an underground nuclear waste storage, to investigate and compare the performance of the two methods and to analyze the accuracy in time of the nonconforming time grids.

We finally extend the two methods to model flow and transport in a porous medium with fractures. A discrete-fracture model where the fracture is treated as an interface of co-dimension 1 (see [5, 92] and the references therein) is considered. An extension of Method 1 is straightforward while for Method 2, a new formulation is derived to adapt to the coupled system of the reduced fracture model. Existence of a weak solution to the subdomain problem involved in each method is shown. For the compressible flow problem, numerical studies are carried out.

Contents of the thesis

This thesis consists of four main parts:

1. For pure diffusion problems: we have formulated the time dependent Steklov-Poincaré operator and the time dependent Neumann-Neumann preconditioner with weight matrices to handle heterogeneous problems (the convergence of a Richardson iteration for the primal formulation of the heat equation was independently introduced and analyzed in [79]). The corresponding semi-discrete-in-time interface problem with the lowest order DG method and nonconforming time steps is presented; we have extended the OSWR method with optimized Robin transmission conditions to the mixed formulation and prove the convergence of the OSWR algorithm in mixed form for the continuous problem and for the semi-discrete problem in time with nonconforming time discretizations. The well-posedness of the subdomain problems involved in each method (with either Dirichlet or Robin boundary conditions) is shown. Numerical experiments in 2D for both homogeneous and heterogeneous problems with a decomposition into two/multiple subdomains are presented, in which the performance of the two methods is investigated and the two are compared. The accuracy in time of the solution is analyzed when nonconforming time grids are used.

   The work in this section is the object of the publication [66].

2. For advection-diffusion problems: using operator splitting, we have introduced new schemes by extending the two methods derived for pure diffusion problems to the advection-diffusion couplings, where the transmission conditions consist of one equation for the advection and two equations for the diffusion (which are similar to that of the pure diffusion case). For each method, a fully discrete interface problem is formulated in a way such that it is equivalent to the original problem defined on the whole domain. We study and compare the numerical performance of the two methods, and use time windows to perform test cases arising from the near-field simulation of a nuclear waste repository site and of a surface waste storage site.

3. For the OSWR method with Ventcell transmission conditions: we have formulated, in mixed form, the multi-domain problem with Ventcell transmission conditions by introducing Lagrange multipliers on the interface; we then obtain a subdomain problem coupling between a PDE defined in the subdomain and another PDE with one less dimension on the interface. For elliptic problems, such a subdomain problem is well-posed using an extension of the inf-sup condition [22, 104]; for parabolic problem, the existence of weak solutions is shown using Galerkin's method and a priori estimates. For each case, an interface problem is derived using the (time-dependent) Ventcell-to-Ventcell operator. We compare numerically the performance of Ventcell and Robin transmission conditions for strongly heterogeneous problems and for a decomposition into two symmetric subdomains in 2D.

4. For reduced fracture models: we have extended the method based on the Steklov-Poincaré type operator for incompressible flow [92, 7] to the case of compressible flow, in which different time steps in the fracture and in the surrounding medium can be used. In addition, we have introduced a new method using the idea of the OSWR approach in which the transmission conditions on the fracture-interface are rewritten equivalently in the form of Ventcell-to-Robin type conditions. Extensions of both methods to the advection-diffusion equation are given.

The rest of the thesis is organised as follows: in Chapter 1, we briefly present the models for flow and transport in porous media considered in this work. The subject of Chapter 2 is domain decomposition methods for the pure diffusion problem written in mixed form. Method 1 and Method 2 with Robin transmission conditions are introduced and analyzed. We extend the results in Chapter 2 to the advection-diffusion equation with operator splitting, which is presented in Chapter 3. In Chapter 4, Method 2 with Ventcell transmission conditions is studied both for elliptic and parabolic equations in a mixed formulation. An extension of the two methods to the reduced fracture models is derived and investigated in Chapter 5 for incompressible flow and transport of a contaminant in a fractured porous medium. This thesis also includes three appendices where we present successively the 2D convergence factor used to calculate the optimized parameters of the OSWR algorithms (Appendix A), the detailed discretization in space using the mixed finite element method with the lowest order Raviart-Thomas spaces on rectangle (Appendix B), and the use of time windows for space-time domain decomposition methods (Appendix C).

Major contributions of the thesis

The main contribution of this thesis is the extension of two space-time domain decomposition methods to mixed finite elements. The first method uses physical transmission conditions and the second method uses more general (Robin or Ventcell) transmission conditions which optimize the convergence rate of the algorithm. One of the difficulties was to treat the Ventcell conditions, or more precisely to treat the tangential derivatives occuring in the Ventcell operators, with mixed finite elements. The methods are then extended to treat advection and diffusion differently through operator splitting. The main difficulty was to take into account the different ways of coupling the unknowns on the interfaces (for the advection and for the diffusion). Two domain decomposition methods are obtained both of which make possible the use of different time steps in the different subdomains, both for the diffusion and for the advection. An extension to the case in which the interface represents a discrete fracture in a reduced model for flow in a fractured porous medium is also given. Ideas related to those used to treat the Ventcell conditions for a simple interface make possible the introduction of an optimization parameter into the transmission conditions on the fracture.

Chapter 1

Modeling flow and transport in porous media

This chapter presents mathematical models for the single phase fluid flow and the transport of a component in a fluid phase in porous media. We briefly present the partial differential equations (PDEs) that govern the physical processes and introduce the terminology and notation used throughout this thesis. For details of how these PDEs are derived, we refer to many books on this topic, e.g. [11, 26] and the references therein.

A porous medium such as the subsurface consists of a solid matrix and a void space, occupied by one or more fluid phases. In this work, we will only be concerned by the one phase flow case, that is we assume that the void space is filled by water. When we study transport, we will additionally assume that the concentration of the dissolved species is small enough that the "filled with water" assumption is still valid.

In this work, we employ the common approach of modeling the porous medium as a continuum. This means that all considered quantities, such as pressure, velocity or species concentration are actually averages of microscopic quantities over a *representative elementary volume*, or REV, cf. references above. An REV is usually defined as a portion of space that is

1. large enough that averages over the REV are meaningful, and do not depend on the precise size of the region,

2. small enough that making the approximation that the volume is "infinitesimal" (so that the usual balance equations still make sense).

The averages should then not depend on the precise size of the REV. The description of the porous medium in terms of quantities averaged over an REV is referred to as the macroscopic description.

It is only over an REV that the concept of porosity makes sense: it measures how much of the REV is occupied by the void. Similarly, Darcy's law (described in the next section) is the macroscopic law governing flow. It was originally proposed by H. Darcy in 1856 as an experimental observation. Note that Darcy's law can also be obtained by homogenization from the Stokes equations at the microscopic level (see for instance [67]), but this method is based on a different approach than the REV approach.

1.1 Flow equations

Water flow through an aquifer is modeled mathematically by Darcy's law together with the equation of conservation of mass.

1.1.1 Darcy's law

Darcy's law expresses the linear relationship between a volumetric fluid velocity and the pressure gradient:

$$\boldsymbol{u} = -\frac{\boldsymbol{\kappa}}{\mu}\left(\nabla P - \rho g \nabla z\right), \tag{1.1}$$

where

- $\boldsymbol{u}$ (m/s) is the Darcy velocity,
- P (Pa) is the fluid pressure, recall that

$$1\,\text{Pa} = 1\,\text{N/m}^2, \quad \text{and} \;\; 1\,\text{N} = 1\,\text{kg}\cdot\text{m/s}^2.$$

- $\boldsymbol{\kappa}$ is the absolute permeability tensor of the porous medium: $\boldsymbol{\kappa} = (\kappa)_{ij}$ where κ_{ij} (m^2) for $i, j = 1, 2, 3$, is the intrinsic permeability.
- μ (Pa·s) is the dynamic viscosity of the fluid.
- ρ (kg/m^3) is the fluid density.
- g (m/s^2) is the magnitude of the gravitational acceleration.
- z (m) is the depth.

Note that the density ρ is a function of fluid pressure, concentration of dissolved contaminants and temperature of the fluid: $\rho = \rho(P, c, T)$ and the porosity ϕ is a function of fluid pressure: $\phi = \phi(P)$. Here and throughout this thesis, we assume that ρ is constant as a function of P, c and T. Consequently, equation (1.1) can be rewritten equivalently in two different ways as follows:

1st interpretation

$$\boldsymbol{u} = -\boldsymbol{K}\nabla p, \tag{1.2}$$

where

- $\boldsymbol{K} = \dfrac{\boldsymbol{\kappa}}{\mu}$ is called the permeability tensor and its components are measured in $\text{m}^2/(\text{Pa}\cdot\text{s})$.
- p (Pa) is defined by $p := P + \rho g z$ and we shall refer to p as the pressure in the following chapters.

2nd interpretation

$$\boldsymbol{u} = -\mathbb{K}\nabla h, \tag{1.3}$$

where

- $\mathbb{K} = \dfrac{\boldsymbol{\kappa}\rho g}{\mu}$ is called the hydraulic conductivity tensor and its components are measured in m/s.
- h (m) is the hydraulic head defined by

$$h := \frac{P}{\rho g} + z. \tag{1.4}$$

Note that the two equations (1.2) and (1.3) are mathematically equivalent and either of them can be used depending on the physical description of the problem.

1.1.2 The equation of conservation of mass

The mass conservation equation describing the mass flow in a small element of a saturated porous medium is given by

$$\frac{\partial(\phi\rho)}{\partial t} = -\operatorname{div}(\rho\boldsymbol{u}) + q, \tag{1.5}$$

where q is the external sources or sinks. As ρ is constant, equation (1.5) becomes

$$\frac{\partial\phi}{\partial P}\frac{\partial P}{\partial t} = -\operatorname{div}(\boldsymbol{u}) + \frac{q}{\rho}, \tag{1.6}$$

Due to the slightly compressible fluid is present, it is necessary to introduce the specific storage S_s (m^{-1}):

$$S_s = g\frac{\partial\phi\rho}{\partial P} = g\,\rho\frac{\partial\phi}{\partial P}.$$

Then using the definition of h in (1.4) and from (1.6) we obtain

$$S_s\frac{\partial h}{\partial t} = -\operatorname{div}(\boldsymbol{u}) + \frac{q}{\rho}. \tag{1.7}$$

This together with equation (1.7) gives a closed system for a compressible flow with two unknowns - the scalar h and the vector field $\boldsymbol{u}$:

$$\begin{aligned} \boldsymbol{u} &= -\mathbb{K}\nabla h, && \text{in } \Omega\times(0,T),\\ S_s\frac{\partial h}{\partial t} + \operatorname{div}(\boldsymbol{u}) &= \frac{q}{\rho}, && \text{in } \Omega\times(0,T), \end{aligned} \tag{1.8}$$

for a porous medium domain Ω and some fixed time $T > 0$. This system is completed by defining the boundary and initial conditions. There are three most popular types of boundary conditions as follows:

- Dirichlet boundary condition:

$$h = h_d \quad \text{on } \partial\Omega\times(0,T).$$

- Neumann boundary condition:

$$\boldsymbol{u}\cdot\boldsymbol{n} = \Psi \quad \text{on } \partial\Omega\times(0,T),$$

  where $\boldsymbol{n}$ is the outward unit vector normal to $\partial\Omega$.

- Mixed (or Robin) boundary condition:

$$-\boldsymbol{u}\cdot\boldsymbol{n} + \alpha h = \psi \quad \text{on } \partial\Omega\times(0,T),$$

  for $\alpha > 0$ given.

The initial condition is defined by

$$h(\cdot,0) = h_0 \quad \text{in } \Omega.$$

Incompressible flow or steady state flow equation

In our application, the flow is assumed to be incompressible: $S_s = 0$ and no source nor sink is present. In this case, system (1.8) becomes

$$\begin{aligned} \boldsymbol{u} &= -\mathbb{K}\nabla h, && \text{in } \Omega,\\ \operatorname{div}(\boldsymbol{u}) &= 0, && \text{in } \Omega, \end{aligned} \tag{1.9}$$

or equivalently

$$\begin{aligned} \boldsymbol{u} &= -\boldsymbol{K}\nabla p, && \text{in } \Omega,\\ \operatorname{div}(\boldsymbol{u}) &= 0, && \text{in } \Omega. \end{aligned} \tag{1.10}$$

In the next section, we will make use of either of these systems for the water flow involved in the transport process of contaminants dissolved in the water.

1.2 Transport equations

The quantity of a dissolved species in a fluid phase is measured by its (molar) concentration, expressed in moles per litre of solution. The transport of such a component is governed first by the general balance equation:

$$\phi\frac{\partial c}{\partial t} + \operatorname{div}\boldsymbol{j} = f, \tag{1.11}$$

where

- c is the concentration of the dissolved contaminant,
- $\boldsymbol{j}$ is the flux of the species, that is the amount of the species going through a unit surface per unit time.
- f is a source term.

The complete description needs a specification of the flux $\boldsymbol{j}$. This involved three main phenomena: advection, (molecular) diffusion and dispersion. The first two are common to most flow models, while the third one is specific to porous media. The flux will then be a sum of three fluxes. We deal briefly with each phenomenon:

Advection is the species being carried along the flow, without its shape undergoing any deformation. The corresponding flux is

$$\boldsymbol{j}_{\text{adv}} = \boldsymbol{u}c.$$

Molecular diffusion is caused by the Brownian motion of the molecules in the fluid. It is expressed by Fick's law:

$$\boldsymbol{j}_{\text{diff}} = -D_e \nabla c,$$

where D_e is the effective diffusion coefficient of the medium (m^2/s). It is related to the molecular diffusion coefficient D_m by

$$D_e = \phi\, D_m.$$

Since D_e includes the porosity in its definition, it is a macroscopic quantity.

Dispersion is a phenomenon specific to porous media: it is a macroscopic way of taking into the small scale variations of the velocity, due to the microscopic heterogeneities in the medium. There exists several theories to write the dispersive flux, and all of them are phenomenological. The most commonly employed is Scheidegger model, for which the dispersive flow is written as

$$\boldsymbol{j}_{\text{disp}} = |\boldsymbol{u}| \left(\alpha_L \mathbf{E}(\boldsymbol{u}) + \alpha_T \mathbf{E}^{\perp}(\boldsymbol{u}) \right) \nabla c, \tag{1.12}$$

where α_L and α_T (both in m) are, respectively, the longitudinal and transverse dispersion coefficients, $|\boldsymbol{u}|$ is the Euclidean norm of $\boldsymbol{u} = (\boldsymbol{u}_1, \boldsymbol{u}_2, \boldsymbol{u}_3)$, $|\boldsymbol{u}| = \sqrt{\boldsymbol{u}_1^2 + \boldsymbol{u}_2^2 + \boldsymbol{u}_3^2}$, $\mathbf{E}$ is the orthogonal projection along the velocity,

$$\mathbf{E} = \frac{1}{|\boldsymbol{u}|^2} \begin{pmatrix} \boldsymbol{u}_1^2 & \boldsymbol{u}_1\boldsymbol{u}_2 & \boldsymbol{u}_1\boldsymbol{u}_3 \\ \boldsymbol{u}_2\boldsymbol{u}_1 & \boldsymbol{u}_2^2 & \boldsymbol{u}_2\boldsymbol{u}_3 \\ \boldsymbol{u}_3\boldsymbol{u}_1 & \boldsymbol{u}_3\boldsymbol{u}_2 & \boldsymbol{u}_3^2 \end{pmatrix}$$

and $\mathbf{E}^{\perp} = \boldsymbol{I} - \mathbf{E}$.

Equation (1.12) simply expresses the fact that, in a first approximation, dispersion has a tendency to spread the concentration plume, but does more (α_L is usually larger than α_T) in the direction of the flow than in the direction transverse to it.

By replacing the flux $\boldsymbol{j}$ in equation (1.11) by the sum of the 3 fluxes $\boldsymbol{j}_{\text{adv}} + \boldsymbol{j}_{\text{diff}} + \boldsymbol{j}_{\text{disp}}$, one obtains the general transport equation:

$$\phi \frac{\partial c}{\partial t} - \text{div}\ (c\boldsymbol{u} - \boldsymbol{D}(\boldsymbol{u})\nabla c) = f, \tag{1.13}$$

where we have denoted by by $D(u)$ the diffusion-dispersion tensor

$$D(u) = D_e I + |\boldsymbol{u}| \left(\alpha_L \mathbf{E}(\boldsymbol{u}) + \alpha_T \mathbf{E}^{\perp}(\boldsymbol{u}) \right).$$

Even though they are different physical phenomena, it will be convenient to treat diffusion and dispersion together, as acting in the same way as diffusion with an anisotropic tensor.

Chapter 2

Space-time domain decomposition for diffusion problems

Contents

2.1 A model problem 17
2.2 A local problem with Robin boundary conditions 25
2.3 Space-time domain decomposition methods 30
2.3.1 Method 1: Using the time-dependent Steklov-Poincaré operator . . 31
2.3.2 Method 2: Using Optimized Schwarz Waveform Relaxation 33
2.4 Nonconforming time discretizations and projections in time 39
2.4.1 For Method 1 39
2.4.2 For Method 2 40
2.5 Numerical results 43
2.5.1 A test case with a homogeneous medium 44
2.5.2 A test case with a heterogeneous medium 45
2.5.3 A porous medium test case 48

This chapter consists of three main parts. In the first part, we consider the time-dependent diffusion problem written in a mixed formulation and prove its well-posedness for Dirichlet and Robin boundary conditions by using Galerkin's method and a priori estimates. In the second part, two nonoverlapping domain decomposition methods - the Steklov-Poincaré operator and the Optimized Schwarz waveform relaxation (OSWR) - are formulated through an introduction of the space-time interface problems. We consider the semi-discrete problems in time using different time grids in the subdomains. Convergence proofs for the continuous and semi-discrete OSWR algorithms in mixed form are given. In the third part, we present numerical results for different test cases to study and compare the performance of the two methods.

2.1 A model problem

In this section we define our model problem and show the existence and uniqueness of its solution. For an open, bounded domain Ω of $\mathbb{R}^d$ $(d = 2, 3)$ with Lipschitz boundary

$\partial\Omega$ and some fixed time $T > 0$, we consider the following time-dependent diffusion problem

$$\phi\,\partial_t c + \text{div}\,(-\boldsymbol{D}\nabla c) = f, \quad \text{in } \Omega\times(0,T), \tag{2.1}$$

with boundary and initial conditions

$$\begin{aligned} c &= 0, \quad \text{on } \partial\Omega\times(0,T),\\ c(\cdot,0) &= c_0, \quad \text{in } \Omega. \end{aligned} \tag{2.2}$$

Here c is the concentration of a contaminant dissolved in a fluid, f the source term, ϕ the porosity and $\boldsymbol{D}$ a symmetric time independent diffusion tensor (see Chapter 1 for a detailed description). Here and throughout this chapter, unless explicitly stated otherwise, we assume that ϕ is bounded above and below by positive constants, $0 < \phi_- \le \phi(x) \le \phi_+$, and that there exist positive constants δ_- and δ_+ such that $\varsigma^T\boldsymbol{D}^{-1}(x)\varsigma \ge \delta_-|\varsigma|^2$, and $|\boldsymbol{D}(x)\varsigma| \le \delta_+|\varsigma|$, for a.e. $x\in\Omega$ and $\forall\varsigma\in\mathbb{R}^d$. For simplicity, we have imposed a homogeneous Dirichlet boundary condition on $\partial\Omega$. In practice, we may use non-homogeneous Dirichlet and Neumann boundary conditions for which the analysis remains valid (see Section 2.2 for the extension to Robin boundary conditions).

We now rewrite (2.1) in an equivalent mixed form by introducing the vector field $\boldsymbol{r} := -\boldsymbol{D}\nabla c$. This yields

$$\begin{aligned} \phi\,\partial_t c + \text{div}\,\boldsymbol{r} &= f, \quad \text{in } \Omega\times(0,T),\\ \nabla c + \boldsymbol{D}^{-1}\boldsymbol{r} &= 0, \quad \text{in } \Omega\times(0,T). \end{aligned} \tag{2.3}$$

To write the variational formulation for (2.3) (see [22, 104]), we introduce the spaces

$$M = L^2(\Omega) \text{ and } \Sigma = H(\text{div},\Omega).$$

We multiply the first and second equations in (2.3) by $\mu\in M$ and $\boldsymbol{\nu}\in\Sigma$ respectively, then integrate over Ω and apply Green's formula to obtain:

For a.e. $t\in(0,T)$, find $c(t)\in M$ and $\boldsymbol{r}(t)\in\Sigma$ such that

$$\begin{aligned} (\phi\,\partial_t c,\mu) + (\text{div}\,\boldsymbol{r},\mu) &= (f,\mu), \quad \forall\mu\in M,\\ -(\text{div}\,\boldsymbol{\nu},c) + (\boldsymbol{D}^{-1}\boldsymbol{r},\boldsymbol{\nu}) &= 0, \quad \forall\boldsymbol{\nu}\in\Sigma, \end{aligned} \tag{2.4}$$

together with initial condition (2.2).

Here and in the following, we will use the convention that if V is a space of functions, then we write $\boldsymbol{V}$ for a space of vector functions having each component in V. We also denote by $(\cdot,\cdot)$ the inner product in $L^2(\Omega)$ or $\boldsymbol{L^2(\Omega)}$ and $\|\cdot\|$ the $L^2(\Omega)$-norm or $\boldsymbol{L^2(\Omega)}$-norm.

Remark 2.1. *Throughout this manuscript, we will treat various physical problems. Each will be written in a mixed formulation and for each we will need a space of scalar functions and a space of vector functions. We use the notation M for the former and Σ for the latter, even though the definitions will change somewhat from problem to problem as we will point out when these changes are made.*

The well-posedness of problem (2.4) is shown in [81, 18], with an argument based on Galerkin's method and a priori estimates:

Theorem 2.2. *If f is in $L^2(0,T;L^2(\Omega))$ and c_0 in $H^1_0(\Omega)$ then problem* (2.4), (2.2) *has a unique solution*

$$(c,\boldsymbol{r}) \in H^1(0,T;L^2(\Omega)) \times \left(L^2(0,T;H(\mathrm{div}\,,\Omega)) \cap L^\infty(0,T;\boldsymbol{L^2(\Omega)})\right).$$

Moreover, if $\boldsymbol{D}$ is in $\boldsymbol{W^{1,\infty}(\Omega)}$, f in $H^1(0,T;L^2(\Omega))$ and c_0 in $H^2(\Omega)\cap H^1_0(\Omega)$, then

$$(c,\boldsymbol{r}) \in W^{1,\infty}(0,T;L^2(\Omega)) \times \left(L^\infty(0,T;H(\mathrm{div}\,,\Omega)) \cap H^1(0,T;\boldsymbol{L^2(\Omega)})\right).$$

Remark 2.3. *We give the proof of Theorem 2.2 in the finite dimensional setting since some technical points (those involving $\partial_t \boldsymbol{r}$, or $\boldsymbol{r}$ at time $t=0$) can only be defined by their finite dimensional Galerkin approximation. This is not surprising given the differential-algebraic structure of system* (2.35)*: the second equation has no time derivative. In DAE theory it is well known that the algebraic equations have to be differentiated a number of times (this is what defines the index), and that this imposes compatibility conditions between the initial data (note that $\boldsymbol{r}(0)$ is not given). The index has been extended to PDEs, see for instance [93].*

The proof of Theorem 2.2 is carried out in several steps: in Lemma 2.4 we first construct solutions of certain finite-dimensional approximations of (2.4), then we derive suitable energy estimates in Lemma 2.5 and prove the first part of the theorem. The higher regularity of the solution is obtained from the estimates given in Lemma 2.6.

We need first to introduce some notations: Let $\{\mu_n \mid n \in \mathbb{N}\}$ be a Hilbert basis of M and $\{\boldsymbol{v}_n \mid n \in \mathbb{N}\}$ be a Hilbert basis of Σ. For each pair of positive integers n and m, we denote by M_n the finite dimensional subspace spanned by $\{\mu_i\}_{i=1}^n$, and Σ_m the finite dimensional subspace spanned by $\{\boldsymbol{v}_i\}_{i=1}^m$. Now let $c_n : [0,T] \to M_n$ and $\boldsymbol{r}_m : [0,T] \to \Sigma_m$ be the solution of the following problem

$$\begin{array}{rll} (\phi\,\partial_t c_n, \mu_i) + (\mathrm{div}\,\boldsymbol{r}_m, \mu_i) & = (f(t),\mu_i), & \forall i = 1,\dots,n, \\ -(\mathrm{div}\,\boldsymbol{v}_j, c_n) + (\boldsymbol{D}^{-1}\boldsymbol{r}_m, \boldsymbol{v}_j) & = 0, & \forall j = 1,\dots,m, \end{array} \tag{2.5}$$

with

$$(c_n(0),\mu_i) = (c_0,\mu_i), \quad \forall i = 1,\dots,n. \tag{2.6}$$

Lemma 2.4. (Construction of approximate solutions) *For each pair $(n,m) \in \mathbb{N}^2$, $n,m \geq 1$, there exists a unique solution $(c_n,\boldsymbol{r}_m)$ to problem* (2.5).

Proof. We introduce the following notations

$(\boldsymbol{F}_n(t))_i = (f(t),\mu_i)$, $(\boldsymbol{C}_0)_i = (c_0,\mu_i)$, $(\boldsymbol{W}_n)_{ij} = (\phi\mu_j,\mu_i)$, $\forall\, 1 \leq i,j \leq n$,

$(\boldsymbol{A}_m)_{ij} = (\boldsymbol{D}^{-1}\boldsymbol{v}_j,\boldsymbol{v}_i)$, $\forall\, 1 \leq i,j \leq m$, $(\boldsymbol{B}_{nm})_{ij} = (\mathrm{div}\,\boldsymbol{v}_j,\mu_i)$, $\forall\, 1 \leq i \leq n, 1 \leq j \leq m$.

We also denote by $\boldsymbol{C}_n(t)$ the vector of degrees of freedom of $c_n(t)$ with respect to the basis $\{\mu_i\}_{i=1}^n$ and $\boldsymbol{R}_m(t)$ that of $\boldsymbol{r}_m(t)$ with respect to the basis $\{\boldsymbol{v}_i\}_{i=1}^m$. With this notation, (2.5) may be rewritten as

$$\boldsymbol{W}_n \frac{d\boldsymbol{C}_n}{dt}(t) + \boldsymbol{B}_{nm}\boldsymbol{R}_m(t) = \boldsymbol{F}_n(t), \tag{2.7a}$$

$$-\boldsymbol{B}_{nm}^T\boldsymbol{C}_n(t) + \boldsymbol{A}_m\boldsymbol{R}_m(t) = 0, \tag{2.7b}$$

$$\boldsymbol{C}_n(0) = \boldsymbol{C}_0. \tag{2.7c}$$

As $\boldsymbol{A}_m$ is a symmetric and positive definite square matrix of size m (because of the assumptions concerning $\boldsymbol{D}$), $\boldsymbol{A}_m$ is invertible. Thus (2.7b) implies

$$\boldsymbol{R}_m(t) = \boldsymbol{A}_m^{-1}\boldsymbol{B}_{nm}^T\boldsymbol{C}_n(t). \tag{2.8}$$

Substituting (2.8) into (2.7a) and as $\boldsymbol{W}_n$ is invertible, we obtain

$$\frac{d\boldsymbol{C}_n}{dt}(t) + \boldsymbol{W}_n^{-1}\boldsymbol{B}_{nm}\boldsymbol{A}_m^{-1}\boldsymbol{B}_{nm}^T\boldsymbol{C}_n(t) = \boldsymbol{W}_n^{-1}\boldsymbol{F}_n(t), \quad \text{for a.e. } t \in [0,T]. \tag{2.9}$$

This is a system of n linear ODEs of order 1 with initial condition (2.7c). Hence, there exists a unique function $\boldsymbol{C}_n \in (C([0,T]))^n$ with $\frac{d\boldsymbol{C}_n}{dt} \in \left(L^2(0,T)\right)^n$ satisfying (2.9) and (2.7c) (see [37]). From (2.8) we obtain $\boldsymbol{R}_m \in (C([0,T]))^m$ such that $\frac{d\boldsymbol{R}_m}{dt} \in \left(L^2(0,T)\right)^m$ and then $(c_n, \boldsymbol{r}_m)$, which is the unique solution to (2.5). □

In the next step, we derive some suitable a priori estimates similar to those given in [81] but in a more detailed manner.

Lemma 2.5. *There exists a constant C independent of n and m such that*

$$\|c_n\|_{L^\infty(0,T;L^2(\Omega))} + \|\partial_t c_n\|_{L^2(0,T;L^2(\Omega))} + \|\boldsymbol{r}_m\|_{L^\infty(0,T;\boldsymbol{L^2(\Omega)})} + \|\boldsymbol{r}_m\|_{L^2(0,T;H(\mathrm{div},\Omega))} \\ \leq C(\|c_0\|_{H_0^1(\Omega)} + \|f\|_{L^2(0,T;L^2(\Omega))}), \quad \forall n,m \geq 1.$$

Proof. We prove this lemma by deriving successively the estimates on c_n, $\partial_t c_n$ and $\boldsymbol{r}_m$, and finally on $\mathrm{div}\,\boldsymbol{r}_m$ for the $H(\mathrm{div},\Omega)$-norm.

• Let $n,m \geq 1$ and take $c_n(t) \in M_n$ and $\boldsymbol{r}_m(t) \in \Sigma_m$ as the test functions in (2.5)

$$\begin{aligned} (\phi\,\partial_t c_n, c_n) + (\mathrm{div}\,\boldsymbol{r}_m, c_n) &= (f, c_n), \\ -(\mathrm{div}\,\boldsymbol{r}_m, c_n) + (\boldsymbol{D}^{-1}\boldsymbol{r}_m, \boldsymbol{r}_m) &= 0. \end{aligned}$$

Adding these two equations, we obtain

$$(\phi\,\partial_t c_n, c_n) + (\boldsymbol{D}^{-1}\boldsymbol{r}_m, \boldsymbol{r}_m) = (f, c_n).$$

Using the properties of ϕ and $\boldsymbol{D}$, and applying the Cauchy-Schwarz inequality, we get

$$\begin{aligned} (\phi\,\partial_t c_n, c_n) = \frac{1}{2}\frac{d}{dt}(\phi c_n(t), c_n(t)) &\geq \frac{\phi_-}{2}\frac{d}{dt}\|c_n(t)\|^2, \\ (\boldsymbol{D}^{-1}\boldsymbol{r}_m(t), \boldsymbol{r}_m(t)) &\geq \delta_-\|\boldsymbol{r}_m(t)\|, \\ (f(t), c_n(t)) \leq \|f(t)\|\,\|c_n(t)\| &\leq \frac{1}{2\phi_-}\|f(t)\|^2 + \frac{\phi_-}{2}\|c_n(t)\|^2. \end{aligned}$$

As $\phi_- > 0$, we deduce that

$$\frac{d}{dt}\|c_n(t)\|^2 + \frac{2\delta_-}{\phi_-}\|\boldsymbol{r}_m(t)\|^2 \leq \frac{1}{\phi_-^2}\|f(t)\|^2 + \|c_n(t)\|^2.$$

Integrating this inequality over $(0,t)$ for $t \in [0,T]$, we find

$$\|c_n(t)\|^2 + \frac{2\delta_-}{\phi_-}\int_0^t \|\boldsymbol{r}_m(s)\|^2 ds \leq \|c(0)\|^2 + \frac{1}{\phi_-^2}\int_0^t \|f(s)\|^2 ds + \int_0^t \|c_n(s)\|^2 ds, \tag{2.10}$$

since $\|c_n(0)\|^2 = \sum_{i=1}^{n}(c_0,\mu_i)^2 \le \sum_{i=1}^{\infty}(c_0,\mu_i)^2 = \|c_0\|^2$.

Thus (2.10) implies

$$\|c_n(t)\|^2 \le (\|c_0\|^2 + \frac{1}{\phi_-^2}\|f\|^2_{L^2(0,T;L^2(\Omega))}) + \int_0^t \|c_n(s)\|^2 ds.$$

Applying Gronwall's lemma, there exists C independent of n or m such that

$$\|c_n\|^2_{L^\infty(0,T;L^2(\Omega))} \le C(\|c_0\|^2 + \|f\|^2_{L^2(0,T;L^2(\Omega))}), \tag{2.11}$$

• Now we derive the estimate for $\partial_t c_n$: Taking $\partial_t c_n \in M_n$ as the test function in the first equation of (2.5), we obtain

$$(\phi\,\partial_t c_n, \partial_t c_n) + (\operatorname{div} \boldsymbol{r}_m, \partial_t c_n) = (f, \partial_t c_n). \tag{2.12}$$

Differentiating the second equation of (2.5) with respect to t, we find

$$-(\operatorname{div} \boldsymbol{v}, \partial_t c_n) + (\boldsymbol{D}^{-1}\partial_t \boldsymbol{r}_m, \boldsymbol{v}) = 0, \quad \forall \boldsymbol{v} \in \Sigma_m. \tag{2.13}$$

Then we take $\boldsymbol{r}_m$ as the test function in (2.13)

$$(\boldsymbol{D}^{-1}\partial_t \boldsymbol{r}_m, \boldsymbol{r}_m) - (\operatorname{div} \boldsymbol{r}_m, \partial_t c_n) = 0. \tag{2.14}$$

Adding (2.12) and (2.14), we see that

$$(\phi\,\partial_t c_n, \partial_t c_n) + (\boldsymbol{D}^{-1}\partial_t \boldsymbol{r}_m, \boldsymbol{r}_m) = (f, \partial_t c_n).$$

As $\boldsymbol{D}$ is symmetric and positive definite, by applying the Cauchy-Schwarz inequality to the right hand side as well as using the property of ϕ, we obtain

$$\phi_-\|\partial_t c_n(t)\|^2 + \frac{d}{dt}\|\sqrt{\boldsymbol{D}^{-1}}\boldsymbol{r}_m(t)\|^2 \le \frac{1}{\phi_-}\|f(t)\|^2. \tag{2.15}$$

Integrating (2.15) over $(0,t)$ for $t \in [0,T]$, we find

$$\phi_- \int_0^t \|\partial_t c_n(s)\|^2 ds + \|\sqrt{\boldsymbol{D}^{-1}}\boldsymbol{r}_m(t)\|^2 \le \|\sqrt{\boldsymbol{D}^{-1}}\boldsymbol{r}_m(0)\|^2 + \frac{1}{\phi_-}\int_0^t \|f(s)\|^2 ds. \tag{2.16}$$

To bound $\|\boldsymbol{r}_m(0)\|$, we take $\boldsymbol{r}_m \in \Sigma_m$ as the test function in the second equation of (2.5) and let $t = 0$

$$(\boldsymbol{D}^{-1}\boldsymbol{r}_m(0), \boldsymbol{r}_m(0)) = (\operatorname{div} \boldsymbol{r}_m(0), c_n(0)). \tag{2.17}$$

Noting that (2.17) holds for all $n, m \ge 1$, we bound the left-hand side as before and let $n \to \infty$. Since $c_n(0) \to c_0$ in $L^2(\Omega)$ and $c_0 \in H_0^1(\Omega)$, we have by Green's formula

$$\delta_-\|\boldsymbol{r}_m(0)\|^2 \le (\operatorname{div} \boldsymbol{r}_m(0), c_0) = (\boldsymbol{r}_m(0), -\nabla c_0) \le \|\boldsymbol{r}_m(0)\|\,\|\nabla c_0\|.$$

Thus

$$\|\boldsymbol{r}_m(0)\| \le C\|c_0\|_{H_0^1(\Omega)}. \tag{2.18}$$

This along with (2.16) yields

$$\|\partial_t c_n\|^2_{L^2(0,T;L^2(\Omega))} + \|\boldsymbol{r}_m\|^2_{L^\infty(0,T;\boldsymbol{L^2(\Omega)})} \le C(\|c_0\|^2_{H_0^1(\Omega)} + \|f\|^2_{L^2(0,T;L^2(\Omega))}),\ \forall n, m \ge 1. \tag{2.19}$$

There only remains to show that $\|\text{div}\,\boldsymbol{r}_m\|_{L^2(0,T;\boldsymbol{L^2(\Omega)})}$ is bounded.
• Fixing $m \ge 1$, as $\text{div}\,\boldsymbol{r}_m(t) \in M$ we can write

$$\text{div}\,\boldsymbol{r}_m(t) = \sum_{i=1}^{\infty} \xi_m^i(t)\mu_i,\ \text{for a.e. } t \in (0,T), \tag{2.20}$$

where $\xi_m^i(t) = (\text{div}\,\boldsymbol{r}_m(t), \mu_i)$. Now we fix $n \ge 1$ and multiply the first equation of (2.5) by $\xi_m^i(t)$, sum over $i = 1, \dots, n$, we see that

$$(\text{div}\,\boldsymbol{r}_m, \sum_{i=1}^{n} \xi_m^i \mu_i) \le \frac{1}{2}(\|f\| + C\|\partial_t c_n\|)^2 + \frac{1}{2}\|\sum_{i=1}^{n} \xi_m^i \mu_i\|^2. \tag{2.21}$$

Integrating with respect to time and recalling (2.19), we find

$$\int_0^T (\text{div}\,\boldsymbol{r}_m, \sum_{i=1}^{n} \xi_m^i \mu_i) dt \le C(\|f\|^2_{L^2(0,T;L^2(\Omega))} + \|c_0\|^2_{H_0^1(\Omega)}) + \frac{1}{2}\int_0^T \|\sum_{i=1}^{n} \xi_m^i \mu_i\|^2 dt.$$

Let $n \to \infty$ and recall (2.20), we obtain

$$\int_0^T \|\text{div}\,\boldsymbol{r}_m\|^2 dt \le C(\|f\|^2_{L^2(0,T;L^2(\Omega))} + \|c_0\|^2_{H_0^1(\Omega)}) + \frac{1}{2}\int_0^T \|\text{div}\,\boldsymbol{r}_m\|^2 dt.$$

Thus

$$\|\text{div}\,\boldsymbol{r}_m\|^2_{L^2(0,T;L^2(\Omega))} \le C(\|f\|^2_{L^2(0,T;L^2(\Omega))} + \|c_0\|^2_{H_0^1(\Omega)}).$$

On the other hand, by recalling inequality (2.10) with $t = T$ and by (2.11), we find

$$\|\boldsymbol{r}_m\|^2_{L^2(0,T;\boldsymbol{L^2(\Omega)})} \le C(\|c_0\|^2 + \|f\|^2_{L^2(0,T;L^2(\Omega))}).$$

Hence,

$$\begin{aligned}\|\boldsymbol{r}_m\|^2_{L^2(0,T;H(\text{div},\Omega))} &= \|\boldsymbol{r}_m\|^2_{L^2(0,T;(L^2(\Omega))^2)} + \|\text{div}\,\boldsymbol{r}_m\|^2_{L^2(0,T;L^2(\Omega))} \\ &\le C(\|f\|^2_{L^2(0,T;L^2(\Omega))} + \|c_0\|^2_{H_0^1(\Omega)}), \quad \forall m \ge 1,\end{aligned}$$

which ends the proof of Lemma 2.5. □

We now prove the first part of Theorem 2.2: there exists a unique solution $(c, \boldsymbol{r})$ in $H^1(0,T;L^2(\Omega)) \times L^2(0,T;H(div\,,\Omega)) \cap L^\infty(0,T;\boldsymbol{L^2(\Omega)})$ of problem (2.3).

Proof. The proof of the first part of Theorem 2.2 follows the following steps:.
• Lemma 2.5 implies that for the sequences $\{c_n\}_{n=1}^\infty$ and $\{\boldsymbol{r}_m\}_{m=1}^\infty$ defined by (2.5) and (2.6), $\{c_n\}_{n=1}^\infty$ is bounded in $L^2(0,T;L^2(\Omega))$, $\{\partial_t c_n\}_{n=1}^\infty$ is bounded in $L^2(0,T;L^2(\Omega))$ and $\{\boldsymbol{r}_m\}_{m=1}^\infty$ is bounded in $L^2(0,T;H(\text{div}\,,\Omega)) \cap L^\infty(0,T;\boldsymbol{L^2(\Omega)})$. Thus, there exist subsequences, still denoted by $\{c_n\}_{n=1}^\infty$ and $\{\boldsymbol{r}_m\}_{m=1}^\infty$ and functions $c \in L^2(0,T;L^2(\Omega))$ with $\partial_t c \in L^2(0,T;L^2(\Omega))$ and $\boldsymbol{r} \in L^2(0,T;H(\text{div}\,,\Omega)) \cap L^\infty(0,T;\boldsymbol{L^2(\Omega)})$ such that

$$\begin{aligned}&c_n \rightharpoonup c \text{ in } L^2(0,T;L^2(\Omega)),\\ &\partial_t c_n \rightharpoonup \partial_t c \text{ in } L^2(0,T;L^2(\Omega)),\\ &\boldsymbol{r}_m \rightharpoonup \boldsymbol{r} \text{ in } L^2(0,T;H(\text{div}\,,\Omega)).\end{aligned} \tag{2.22}$$

• Next let $\eta \in C^1([0,T];M_{n_0})$, $\boldsymbol{w} \in C^1([0,T];\Sigma_{m_0})$ for $n_0, m_0 \geq 1$. We choose $n \geq n_0$ and $m \geq m_0$, take η and $\boldsymbol{w}$ as the test functions in (2.5) and then integrate with respect to time

$$\begin{aligned} \int_0^T (\phi \partial_t c_n, \eta) + (\operatorname{div} \boldsymbol{r}_m, \eta) dt &= \int_0^T (f, \eta) dt, \\ \int_0^T -(\operatorname{div} \boldsymbol{w}, c_n) + (\boldsymbol{D}^{-1} \boldsymbol{r}_m, \boldsymbol{w}) dt &= 0. \end{aligned} \tag{2.23}$$

Because of the weak convergence in (2.22), we also have

$$\begin{aligned} \int_0^T (\phi \partial_t c, \eta) + (\operatorname{div} \boldsymbol{r}, \eta) dt &= \int_0^T (f, \eta) dt, \\ \int_0^T -(\operatorname{div} \boldsymbol{w}, c) + (\boldsymbol{D}^{-1} \boldsymbol{r}, \boldsymbol{w}) dt &= 0. \end{aligned} \tag{2.24}$$

Since the spaces of test functions $\eta, \boldsymbol{w}$ are dense in $L^2(0,T;M)$ and $L^2(0,T;\Sigma)$ respectively, it follows from (2.24) that (2.4) holds for a.e. $t \in (0,T)$ (see [37]).

• There remains to show that $c(0) = c_0$. Toward this end, we take $\eta \in C^1([0,T];M_{n_0})$ with $\eta(T) = 0$. It follows from the first equation of (2.24) that

$$-\int_0^T (\phi \partial_t \eta, c) + (\operatorname{div} \boldsymbol{r}, \eta) dt = \int_0^T (f, \eta) dt + (\phi c(0), \eta(0)). \tag{2.25}$$

Similarly, from the first equation of (2.23) we deduce

$$-\int_0^T (\phi \partial_t \eta, c_n) + (\operatorname{div} \boldsymbol{r}_m, \eta) dt = \int_0^T (f, \eta) dt + (\phi c_n(0), \eta(0)).$$

Using (2.22), we obtain

$$-\int_0^T (\phi \partial_t \eta, c) + (\operatorname{div} \boldsymbol{r}, \eta) dt = \int_0^T (f, \eta) dt + (\phi c_0, \eta(0)), \tag{2.26}$$

since $c_n(0) \to c_0$ in $L^2(\Omega)$. As $\eta(0)$ is arbitrary, by comparing (2.25) and (2.26) we conclude that $c(0) = c_0$.

• For the uniqueness, as the equations are linear, it suffices to check that $c = 0$ and $\boldsymbol{r} = 0$ for $f = 0$ and $c_0 = 0$. To prove this, we set $\mu = c$ and $\boldsymbol{v} = \boldsymbol{r}$ in (2.4) (for $f = 0$) and add the two resulting equations:

$$\frac{1}{2} \frac{d}{dt} (\phi c, c) + (\boldsymbol{D}^{-1} \boldsymbol{r}, \boldsymbol{r}) = 0.$$

Using the property of ϕ and the fact that $(\boldsymbol{D}^{-1} \boldsymbol{r}, \boldsymbol{r}) \geq \delta_- \|\boldsymbol{r}\|^2 \geq 0$, then integrating with respect to t we see that

$$\phi_- \|c(t)\|^2 + 2\delta_- \int_0^t \|\boldsymbol{r}(s)\|^2_{\boldsymbol{L^2(\Omega)}} ds \leq 0, \quad \text{for a.e. } t \in (0,T),$$

where $c(0) = c_0 = 0$. Thus $c = 0$ and $\boldsymbol{r} = 0$ for a.e. $t \in (0,T)$. □

We now prove the second part of Theorem 2.2. The higher regularity of the solution to (2.3) is obtained by using the following lemma.

Lemma 2.6. (Estimates for improved regularity) *Assume that* $\boldsymbol{D}$ *is in* $\boldsymbol{W^{1,\infty}(\Omega)}$, c_0 *in* $H^2(\Omega) \cap H_0^1(\Omega)$ *and* f *in* $H^1(0,T;L^2(\Omega))$ *then*

$$\|\partial_t c\|_{L^\infty(0,T;L^2(\Omega))} + \|\boldsymbol{r}\|_{L^\infty(0,T;H(\mathrm{div},\Omega))} + \|\partial_t \boldsymbol{r}\|_{L^2(0,T;\boldsymbol{L^2(\Omega)})} \leq C(\|f\|_{H^1(0,T;L^2(\Omega))} + \|c_0\|_{H^2(\Omega)}).$$

Proof. As $f \in H^1(0,T;L^2(\Omega))$, the solutions of the ODE system (2.7) are more regular in time than before (i.e. up to second-order time derivatives).

Let $n, m \geq 1$. First, we differentiate the first equation of (2.5) with respect to t

$$(\phi \partial_{tt} c_n, \mu_i) + (\mathrm{div}\, \partial_t \boldsymbol{r}_m, \mu_i) = (\partial_t f, \mu_i), \quad \forall i = 1, \ldots, n,$$

then we take $\partial_t c_n$ as the test function

$$(\phi \partial_{tt} c_n, \partial_t c_n) + (\mathrm{div}\, \partial_t \boldsymbol{r}_m, \partial_t c_n) = (\partial_t f, \partial_t c_n). \tag{2.27}$$

Similarly, we differentiate the second equation of (2.5) with respect to t

$$(\boldsymbol{D}^{-1} \partial_t \boldsymbol{r}_m, \boldsymbol{v}_i) - (\mathrm{div}\, v_i, \partial_t c_n) = 0, \quad \forall i = 1, \ldots, m,$$

and take $\partial_t \boldsymbol{r}_m$ as the test function

$$(\boldsymbol{D}^{-1} \partial_t \boldsymbol{r}_m, \partial_t \boldsymbol{r}_m) - (\mathrm{div}\, \partial_t \boldsymbol{r}_m, \partial_t c_n) = 0. \tag{2.28}$$

Adding (2.27) and (2.28), we find

$$(\phi \partial_{tt} c_n, \partial_t c_n) + (\boldsymbol{D}^{-1} \partial_t \boldsymbol{r}_m, \partial_t \boldsymbol{r}_m) = (\partial_t f, \partial_t c_n).$$

Bounding $(\boldsymbol{D}^{-1} \partial_t \boldsymbol{r}_m, \partial_t \boldsymbol{r}_m) \geq \delta_- \|\partial_t \boldsymbol{r}_m\|^2$, using the assumption about ϕ and applying the Cauchy-Schwarz inequality, we obtain

$$\frac{d}{dt}\|\partial_t c_n\|^2 + \frac{2\delta_-}{\phi_-}\|\partial_t \boldsymbol{r}_m\|^2 \leq \frac{1}{\phi_-^2}\|\partial_t f\|^2 + \|\partial_t c_n\|^2.$$

For each $t \in [0,T]$, we may integrate over $(0,t)$ to obtain

$$\|\partial_t c_n(t)\|^2 + \frac{2\delta_-}{\phi_-}\int_0^t \|\partial_t \boldsymbol{r}_m\|^2 ds \leq \|\partial_t c_n(0)\|^2 + \frac{1}{\phi_-^2}\int_0^t \|\partial_t f\|^2 ds + \int_0^t \|\partial_t c_n\|^2 ds. \tag{2.29}$$

In order to bound $\|\partial_t c_n(0)\|$, we use the first equation of (2.5) (with $\partial_t c_n$ as the test function, at $t = 0$) to obtain

$$\|\partial_t c_n(0)\| \leq C(\|\mathrm{div}\, \boldsymbol{r}_m(0)\| + \|f(0)\|).$$

Using the second equation of (2.5) at $t = 0$, and then let $n \to \infty$ to get

$$(\boldsymbol{D}^{-1} \boldsymbol{r}_m(0) + \nabla c_0, \boldsymbol{v}) = 0, \quad \forall \boldsymbol{v} \in \Sigma_m.$$

Thus, using density argument and $c_0 \in H_0^1(\Omega) \cap H^2(\Omega)$, we obtain $\boldsymbol{D}^{-1} \boldsymbol{r}_m(0) = -\nabla c_0$ in $H^1(\Omega)$. Then, we bound

$$\|\partial_t c_n(0)\|^2 \leq C(\|c_0\|^2_{H^2(\Omega)} + \|f(0)\|^2). \tag{2.30}$$

Replacing (2.30) in (2.29), we obtain

$$\|\partial_t c_n(t)\|^2 + \frac{2\delta_-}{\phi_-}\int_0^t \|\partial_t \boldsymbol{r}_m\|^2 ds \leq C(\|c_0\|^2_{H^2(\Omega)} + \|f\|^2_{H^1(0,T;L^2(\Omega))}) + \int_0^t \|\partial_t c_n\|^2 ds. \quad (2.31)$$

It now follows from (2.31) and Gronwall's lemma that

$$\|\partial_t c_n\|^2_{L^\infty(0,T;L^2(\Omega))} + \frac{2\delta_-}{\phi_-}\|\partial_t \boldsymbol{r}_m\|^2_{L^2(0,T;\boldsymbol{L^2(\Omega)})} \leq C(\|c_0\|^2_{H^2(\Omega)} + \|f\|^2_{H^1(0,T;L^2(\Omega))}). \quad (2.32)$$

Recalling (2.21) and using (2.32), we obtain

$$(\operatorname{div} \boldsymbol{r}_m, \sum_{i=1}^n \xi^i_m \mu_i) \leq C(\|c_0\|^2_{H^2(\Omega)} + \|f\|^2_{H^1(0,T;L^2(\Omega))}) + \frac{1}{2}\|\sum_{i=1}^n \xi^i_m \mu_i\|^2.$$

Then, let $n \to \infty$, we see that

$$\|\operatorname{div} \boldsymbol{r}_m\|^2_{L^\infty(0,T;L^2(\Omega))} \leq C(\|c_0\|^2_{H^2(\Omega)} + \|f\|^2_{H^1(0,T;L^2(\Omega))}).$$

This along with (2.19) gives

$$\|\boldsymbol{r}_m\|^2_{L^\infty(0,T;H(\operatorname{div},\Omega))} \leq C(\|c_0\|^2_{H^2(\Omega)} + \|f\|^2_{H^1(0,T;L^2(\Omega))}). \quad (2.33)$$

The lemma now follows from (2.32), (2.33) and (2.22). □

In the sequel, we will consider two domain decomposition methods for solving (2.4), (2.2). The first one involves local Dirichlet subproblems whose well-posedness is an extension of Theorem 2.2. In the second approach, the optimized Schwarz waveform relaxation method, we shall impose Robin transmission conditions on the interfaces. Thus, we extend the well-posedness results above to the case of Robin boundary conditions.

2.2 A local problem with Robin boundary conditions

In this section, we consider problem (2.1)-(2.2) with Robin boundary conditions on $\partial\Omega \times (0,T)$:

$$-\boldsymbol{r}\cdot\boldsymbol{n} + \alpha c = g, \quad \text{on } \partial\Omega \times (0,T), \quad (2.34)$$

where α defined on $\partial\Omega$ is a time independent positive, bounded coefficient and g is a space-time function. We define $\breve{\alpha} := \dfrac{1}{\alpha}$ and suppose that $0 < \kappa_1 \leq \breve{\alpha} \leq \kappa_2$ a.e. in $\partial\Omega$. We denote by $(\cdot,\cdot)_{\partial\Omega}$ and $\|\cdot\|_{\partial\Omega}$ the inner product and norm in $L^2(\partial\Omega)$ respectively. To derive a variational formulation corresponding to boundary condition (2.34), we introduce the following Hilbert space

$$\widetilde{\Sigma} = \mathscr{H}(\operatorname{div},\Omega) := \{\boldsymbol{v} \in H(\operatorname{div},\Omega) |\ \boldsymbol{v}\cdot\boldsymbol{n} \in L^2(\partial\Omega)\},$$

equipped with the norm

$$\|\boldsymbol{v}\|^2_{\mathscr{H}(\mathrm{div},\Omega)} := \|\boldsymbol{v}\|_{H(\mathrm{div},\Omega)} + \|\boldsymbol{v}\cdot\boldsymbol{n}\|^2_{\partial\Omega}.$$

The weak problem with Robin boundary conditions may now be written as follows:

For a.e. $t \in (0,T)$, find $c(t) \in M$ and $\boldsymbol{r}(t) \in \widetilde{\Sigma}$ such that

$$\begin{array}{rll} (\phi\,\partial_t c, \mu) + (\mathrm{div}\,\boldsymbol{r}, \mu) & = (f,\mu), & \forall \mu \in M, \\ -(\mathrm{div}\,\boldsymbol{v}, c) + (\boldsymbol{D}^{-1}\boldsymbol{r}, \boldsymbol{v}) + (\breve{\alpha}\boldsymbol{r}\cdot\boldsymbol{n}, \boldsymbol{v}\cdot\boldsymbol{n})_{\partial\Omega} & = -(\breve{\alpha} g, \boldsymbol{v}\cdot\boldsymbol{n})_{\partial\Omega}, & \forall \boldsymbol{v} \in \widetilde{\Sigma}. \end{array} \tag{2.35}$$

Theorem 2.7. *If f is in $L^2(0,T;L^2(\Omega))$, g in $H^1(0,T;L^2(\partial\Omega))$ and c_0 in $H^1(\Omega)$, then problem* (2.35)*,* (2.2) *has a unique solution*

$$(c,\boldsymbol{r}) \in H^1(0,T;L^2(\Omega)) \times \left(L^2(0,T;\mathscr{H}(\mathrm{div},\Omega)) \cap L^\infty(0,T;\boldsymbol{L^2(\Omega)})\right).$$

Moreover, if $\boldsymbol{D}$ is in $\boldsymbol{W^{1,\infty}(\Omega)}$, f in $H^1(0,T;L^2(\Omega))$ and c_0 in $H^2(\Omega)$ then

$$(c,\boldsymbol{r}) \in W^{1,\infty}(0,T;L^2(\Omega)) \times \left(L^\infty(0,T;\mathscr{H}(\mathrm{div},\Omega)) \cap H^1(0,T;\boldsymbol{L^2(\Omega)})\right).$$

Proof. The proof of Theorem 2.7 relies on energy estimates and Gronwall's lemma, together with a Galerkin method, as for the proof of Theorem 2.2. We only present here the parts of the proof that are different from those of the proof of Theorem 2.2. We construct the finite-dimensional approximation problems to (2.35) as follows

$$\begin{array}{rll} (\phi\,\partial_t c_n, \mu_i) + (\mathrm{div}\,\boldsymbol{r}_m, \mu_i) & = (f,\mu_i), & 1 \le i \le n, \\ -(\mathrm{div}\,\tilde{\boldsymbol{v}}_j, c_n) + (\boldsymbol{D}^{-1}\boldsymbol{r}_m, \tilde{\boldsymbol{v}}_j) + (\breve{\alpha}\boldsymbol{r}_m\cdot\boldsymbol{n}, \tilde{\boldsymbol{v}}_j\cdot\boldsymbol{n})_{\partial\Omega} & = (-\breve{\alpha} g, \tilde{\boldsymbol{v}}_j\cdot\boldsymbol{n})_{\partial\Omega}, & 1 \le j \le m, \end{array} \tag{2.36}$$

where $c_n \in M_n$, $\boldsymbol{r}_m \in \widetilde{\Sigma}_m$ and $\tilde{\boldsymbol{v}}_i, i = 1,\dots,m$ is the basis of $\widetilde{\Sigma}_m$. We then rewrite (2.36) in matrix form as in (2.7):

$$\begin{aligned} \boldsymbol{W}_n \frac{d\boldsymbol{C}_n}{dt}(t) + \tilde{\boldsymbol{B}}_{nm}\tilde{\boldsymbol{R}}_m(t) &= \boldsymbol{F}_n(t), \\ -\tilde{\boldsymbol{B}}^T_{nm}\boldsymbol{C}_n(t) + \tilde{\boldsymbol{A}}_m\tilde{\boldsymbol{R}}_m(t) &= \boldsymbol{G}_m(t), \end{aligned}$$

where $\tilde{\boldsymbol{R}}_m$ is the vector of degrees of freedom of $\boldsymbol{r}_m$ with respect to the basis $\{\tilde{\boldsymbol{v}}_i\}_{i=1}^m$;

$$(\tilde{\boldsymbol{A}}_m)_{ij} = (\boldsymbol{D}^{-1}\tilde{\boldsymbol{v}}_j, \tilde{\boldsymbol{v}}_i) + (\breve{\alpha}\tilde{\boldsymbol{v}}_j\cdot\boldsymbol{n}, \tilde{\boldsymbol{v}}_i\cdot\boldsymbol{n})_{\partial\Omega}, \qquad \forall 1 \le i,j \le m,$$

is symmetric and positive-definite,

$$(\tilde{\boldsymbol{B}}_{nm})_{ij} = (\mathrm{div}\,\tilde{\boldsymbol{v}}_j, \mu_i) \text{ and } (\boldsymbol{G}_m(t))_i = (-\breve{\alpha} g(t), \tilde{\boldsymbol{v}}_i\cdot\boldsymbol{n})_{\partial\Omega}, \quad \forall\, 1 \le i \le n, 1 \le j \le m.$$

Thus, there exists a unique solution $(c_n, \boldsymbol{r}_m)$ to (2.36).

Now to prove the existence of a solution to (2.35), we derive suitable energy estimates in the same manner as in Section 2.1 but with an extra term $\boldsymbol{r}\cdot\boldsymbol{n}$ on the boundary.

Lemma 2.8. *Let $f \in L^2(0,T;L^2(\Omega))$, $g \in H^1(0,T;L^2(\partial\Omega)$ and $c_0 \in H^1(\Omega)$.*

The following estimates hold

$$\begin{aligned} (i)\ & \|c\|_{L^\infty(0,T;L^2(\Omega))} + \|\boldsymbol{r}\|_{L^2(0,T;\boldsymbol{L^2(\Omega)})} + \|\boldsymbol{r}\cdot\boldsymbol{n}\|_{L^2(0,T;L^2(\partial\Omega))} \\ &\qquad \le C(\|c_0\|_{L^2(\Omega)} + \|f\|_{L^2(0,T;L^2(\Omega))} + \|g\|_{L^2(0,T;L^2(\partial\Omega))}), \\ (ii)\ & \|\partial_t c\|_{L^2(0,T;L^2(\Omega))} + \|\boldsymbol{r}\|_{L^\infty(0,T;\boldsymbol{L^2(\Omega)})} + \|\boldsymbol{r}\cdot\boldsymbol{n}\|_{L^\infty(0,T;L^2(\partial\Omega))} \\ &\qquad \le C(\|c_0\|_{H^1(\Omega)} + \|f\|_{L^2(0,T;L^2(\Omega))} + \|g\|_{H^1(0,T;L^2(\partial\Omega))}), \\ (iii)\ & \|\boldsymbol{r}\|_{L^2(0,T;\mathscr{H}(div,\Omega))} \le C(\|c_0\|_{H^1(\Omega)} + \|f\|_{L^2(0,T;L^2(\Omega))} + \|g\|_{H^1(0,T;L^2(\partial\Omega))}). \end{aligned}$$

Lemma 2.9. (Estimates with greater regularity) *Assume that* $\boldsymbol{D}$ *is in* $\boldsymbol{W^{1,\infty}(\Omega)}$, c_0 *in* $H^2(\Omega)$, f *in* $H^1(0,T;L^2(\Omega))$ *and* g *in* $H^1(0,T;L^2(\partial\Omega))$, *then*

$$\begin{aligned}\|\partial_t c\|_{L^\infty(0,T;L^2(\Omega))} + \|\boldsymbol{r}\|_{L^\infty(0,T;\mathscr{H}(\mathrm{div},\Omega))} + \|\partial_t \boldsymbol{r}\|_{L^2(0,T;\boldsymbol{L^2(\Omega)})} \\ \leq C(\|f\|_{H^1(0,T;L^2(\Omega))} + \|c_0\|_{H^2(\Omega)} + \|g\|_{H^1(0,T;L^2(\partial\Omega))}).\end{aligned}$$

Proof. (of Lemma 2.8). In order to prove *(i)*, as before, we take c_n and $\boldsymbol{r}_m$ as test functions in (2.36) and add the two equations:

$$(\phi\,\partial_t c_n, c_n) + \left(\boldsymbol{D}^{-1}\boldsymbol{r}_m, \boldsymbol{r}_m\right) + \left(\check{\alpha}\boldsymbol{r}_m\cdot\boldsymbol{n}, \boldsymbol{r}_m\cdot\boldsymbol{n}\right)_{\partial\Omega} = (f, c_n) + \left(-\check{\alpha}g, \boldsymbol{r}_m\cdot\boldsymbol{n}\right)_{\partial\Omega}.$$

The assumptions concerning ϕ, $\boldsymbol{D}$ and $\check{\alpha}$ give

$$(\phi\,\partial_t c_n, c_n) \geq \frac{\phi_-}{2}\frac{d}{dt}\|c_n\|^2,\ \ (\boldsymbol{D}^{-1}\boldsymbol{r}_m, \boldsymbol{r}_m) \geq \delta_-\|\boldsymbol{r}_m\|^2,\ \ \left(\check{\alpha}\boldsymbol{r}_m\cdot\boldsymbol{n}, \boldsymbol{r}_m\cdot\boldsymbol{n}\right)_{\partial\Omega} \geq \kappa_1\|\boldsymbol{r}_m\cdot\boldsymbol{n}\|^2_{\partial\Omega},$$

and the Cauchy-Schwarz inequality:

$$|\ (f, c_n)\ | \leq \|f\|\|c_n\| \leq \frac{1}{2\phi_-}\|f\|^2 + \frac{\phi_-}{2}\|c_n\|^2. \tag{2.37}$$

Similarly, for each $\epsilon > 0$,

$$|-\left(\check{\alpha}g, \boldsymbol{r}_m\cdot\boldsymbol{n}\right)_{\partial\Omega}| \leq \kappa_2\|g\|_{\partial\Omega}\,\|\boldsymbol{r}_m\cdot\boldsymbol{n}\|_{\partial\Omega} \leq \kappa_2\left(\frac{1}{2\epsilon}\|g\|^2_{\partial\Omega} + \frac{\epsilon}{2}\|\boldsymbol{r}_m\cdot\boldsymbol{n}\|^2_{\partial\Omega}\right). \tag{2.38}$$

Choosing $\epsilon = \dfrac{\kappa_1}{\kappa_2}$, we then obtain

$$\frac{\phi_-}{2}\frac{d}{dt}\|c_n\|^2 + \delta_-\|\boldsymbol{r}_m\|^2 + \frac{\kappa_1}{2}\|\boldsymbol{r}_m\cdot\boldsymbol{n}\|^2_{\partial\Omega} \leq \frac{1}{2\phi_-}\|f\|^2 + \frac{\kappa_2^2}{2\kappa_1}\|g\|^2_{\partial\Omega} + \frac{\phi_-}{2}\|c_n\|^2.$$

Integrating this inequality over $(0,t)$ for $t\in(0,T]$, and using $\|c_n(0)\|^2 \leq \|c_0\|^2$, we get

$$\begin{aligned}\|c_n(t)\|^2 + \frac{2\delta_-}{\phi_-}\int_0^t \|\boldsymbol{r}_m(s)\|^2\,ds + \frac{\kappa_1}{\phi_-}\int_0^t \|\boldsymbol{r}_m(s)\cdot\boldsymbol{n}\|^2_{\partial\Omega}\,ds \\ \leq C\left(\|c_0\|^2 + \|f\|^2_{L^2(0,T;L^2(\Omega))} + \|g\|^2_{L^2(0,T;L^2(\partial\Omega))}\right) + \int_0^t \|c_n(s)\|^2\,ds,\end{aligned}$$

with $C = \max(1, \dfrac{1}{\phi_-^2}, \dfrac{\kappa_2^2}{\phi_-\kappa_1})$. Then an application of Gronwall's lemma completes the proof of (i).

For *(ii)*, we follow the same steps as in (2.12)-(2.15): taking $\partial_t c_n \in L^2(0,T;M)$ as the test function in the first equation of (2.36), we obtain

$$(\phi\,\partial_t c, \partial_t c) + (\mathrm{div}\,\boldsymbol{r}_m, \partial_t c) = (f, \partial_t c). \tag{2.39}$$

Differentiating the second equation of (2.36) with respect to t, we obtain

$$-(\mathrm{div}\,\boldsymbol{v}, \partial_t c_n) + (\boldsymbol{D}^{-1}\partial_t\boldsymbol{r}_m, \boldsymbol{v}) + (\check{\alpha}\partial_t\boldsymbol{r}_m\cdot\boldsymbol{n}, \boldsymbol{v}\cdot\boldsymbol{n})_{\partial\Omega} = -(\check{\alpha}\partial_t g, \boldsymbol{v}\cdot\boldsymbol{n})_{\partial\Omega},\ \forall\boldsymbol{v}\in\widetilde{\Sigma}.$$

Then we take $\boldsymbol{v} = \boldsymbol{r}_m$ in the previous equation and add the resulting equation to (2.39) to obtain

$$(\phi\,\partial_t c_n, \partial_t c_n) + (\boldsymbol{D}^{-1}\partial_t \boldsymbol{r}_m, \boldsymbol{r}_m) + \left(\breve{\alpha}\partial_t \boldsymbol{r}_m\cdot\boldsymbol{n}, \boldsymbol{r}_m\cdot\boldsymbol{n}\right)_{\partial\Omega} = (f, \partial_t c_n) - \left(\breve{\alpha}\partial_t g, \boldsymbol{r}_m\cdot\boldsymbol{n}\right)_{\partial\Omega}.$$

As $\boldsymbol{D}$ is symmetric and positive definite, by applying the Cauchy-Schwarz inequality to the right hand side as well as using the property of ϕ, we obtain

$$\phi_-\|\partial_t c\|^2 + \frac{1}{2}\frac{d}{dt}\|\sqrt{\boldsymbol{D}^{-1}}\boldsymbol{r}_m\|^2 + \frac{\kappa_1}{2}\frac{d}{dt}\|\boldsymbol{r}_m\cdot\boldsymbol{n}\|^2_{\partial\Omega} \leq |\ (f, \partial_t c)\ | + |\ \left(\breve{\alpha}\partial_t g, \boldsymbol{r}_m\cdot\boldsymbol{n}\right)_{\partial\Omega}\ |\,.$$

We then apply the Cauchy-Schwarz inequality for the right-hand side (as in (2.37), (2.38), replacing c and g by $\partial_t c$ and $\partial_t g$), and take $\epsilon = \dfrac{\kappa_1}{\kappa_2}$, $C = \max(\dfrac{1}{\phi_-}, \dfrac{\kappa_2^2}{\kappa_1})$ to obtain

$$\phi_-\|\partial_t c_n\|^2 + \frac{d}{dt}\|\sqrt{\boldsymbol{D}^{-1}}\boldsymbol{r}_m\|^2 + \kappa_1\frac{d}{dt}\|\boldsymbol{r}_m\cdot\boldsymbol{n}\|^2_{\partial\Omega} \leq C\left(\|f\|^2 + \|\partial_t g\|^2_{\partial\Omega}\right) + \kappa_1\|\boldsymbol{r}_m\cdot\boldsymbol{n}\|^2_{\partial\Omega}.$$

Integrating over $(0,t)$ for $t\in[0,T]$, we find

$$\begin{aligned}\phi_-\int_0^t \|\partial_t c_n(s)\|^2 ds + \|\sqrt{\boldsymbol{D}^{-1}}\boldsymbol{r}_m(t)\|^2 + \kappa_1\|\boldsymbol{r}_m(t)\cdot\boldsymbol{n}\|^2_{\partial\Omega}&\\ \leq C(\|f\|^2_{L^2(0,T;L^2(\Omega))} + \|g\|^2_{H^1(0,T;L^2(\partial\Omega))}) + \|\sqrt{\boldsymbol{D}^{-1}}\boldsymbol{r}_m(0)\|^2 + \kappa_1\|\boldsymbol{r}_m(0)\cdot\boldsymbol{n}\|^2_{\partial\Omega}&\\ + \kappa_1\int_0^t \|\boldsymbol{r}_m(s)\cdot\boldsymbol{n}\|^2_{\partial\Omega} ds.&\quad (2.40)\end{aligned}$$

So there only remains to bound the term $(\|\sqrt{\boldsymbol{D}^{-1}}\boldsymbol{r}_m(0)\|^2 + \kappa_1\|\boldsymbol{r}_m(0)\cdot\boldsymbol{n}\|^2_{\partial\Omega})$. Toward this end, we use the second equation of (2.36) with $\boldsymbol{v} = \boldsymbol{r}_m$ and for $t = 0$ to obtain:

$$\delta_-\|\boldsymbol{r}_m(0)\|^2 + \kappa_1\|\boldsymbol{r}_m(0)\cdot\boldsymbol{n}\|^2 \leq (\operatorname{div}\boldsymbol{r}_m(0), c_n(0)) + \left(-\breve{\alpha}g(0), \boldsymbol{r}_m(0)\cdot\boldsymbol{n}\right)_{\partial\Omega}.$$

Let $n\to\infty$, as $c_n(0)\to c_0$ we have

$$\begin{aligned}\delta_-\|\boldsymbol{r}_m(0)\|^2 + \kappa_1\|\boldsymbol{r}_m(0)\cdot\boldsymbol{n}\|^2 &\leq (\operatorname{div}\boldsymbol{r}_m(0), c_0) + \left(-\breve{\alpha}g(0), \boldsymbol{r}_m(0)\cdot\boldsymbol{n}\right)_{\partial\Omega}\\ &\leq (-\boldsymbol{r}_m(0), \nabla c_0) + \left(c_0 - \breve{\alpha}g(0), \boldsymbol{r}_m(0)\cdot\boldsymbol{n}\right)_{\partial\Omega}\\ &\leq \frac{\delta_-}{2}\|\boldsymbol{r}_m(0)\|^2 + \frac{1}{2\delta_-}\|\nabla c_0\|^2 + \frac{\kappa_1}{2}\|\boldsymbol{r}_m(0)\cdot\boldsymbol{n}\|^2 + \frac{\kappa_2}{2\kappa_1}\|c_0 - g(0)\|^2_{\partial\Omega},\end{aligned}$$

or

$$\delta_-\|\boldsymbol{r}_m(0)\|^2 + \kappa_1\|\boldsymbol{r}_m(0)\cdot\boldsymbol{n}\|^2 \leq C\left(\|c_0\|^2_{H^1(\Omega)} + \|g\|^2_{H^1(0,T;L^2(\partial\Omega))}\right).$$

This along with (2.40) and Gronwall's lemma yields (ii). We now estimate $\|\operatorname{div}\boldsymbol{r}_m\|^2$ as in Section 2.1: we derive (2.21) from (2.20) and the first equation of (2.36) (after multiplying by $\xi^i_m(t)$ and summing over $i = 1,\dots,n$). Then, using the bound for $\|\partial_t c\|_{L^2(0,T;L^2(\Omega))}$ in (ii), we obtain

$$\|\operatorname{div}\boldsymbol{r}_m\|^2_{L^2(0,T;L^2(\Omega))} \leq C(\|c_0\|^2_{H^1(\Omega)} + \|f\|^2_{L^2(0,T;L^2(\Omega))} + \|g\|^2_{H^1(0,T;L^2(\partial\Omega))}). \quad (2.41)$$

This along with (i) gives

$$\|\boldsymbol{r}_m\|^2_{L^2(0,T;\mathscr{H}(\operatorname{div},\Omega))} \leq C(\|c_0\|^2_{H^1(\Omega)} + \|f\|^2_{L^2(0,T;L^2(\Omega))} + \|g\|^2_{H^1(0,T;L^2(\partial\Omega))}),$$

and the proof of Lemma 2.8 is completed. □

We now prove Lemma 2.9 for the higher regularity of the solution to (2.3).

Proof. (of Lemma 2.9). Let $n, m \geq 1$. Differentiate both equations of (2.36) with respect to t, take $\mu = \partial_t c_n$ and $\boldsymbol{v} = \partial_t \boldsymbol{r}_m$ as the test functions, and add the two resulting equations to obtain

$$(\phi \partial_{tt} c_n, \partial_t c_n) + (\boldsymbol{D}^{-1} \partial_t \boldsymbol{r}_m, \partial_t \boldsymbol{r}_m) + (\check{\alpha} \partial_t \boldsymbol{r}_m \cdot \boldsymbol{n}, \partial_t \boldsymbol{r}_m \cdot \boldsymbol{n})_{\partial\Omega} = (\partial_t f, \partial_t c_n) - (\check{\alpha} \partial_t g, \partial_t \boldsymbol{r}_m \cdot \boldsymbol{n})_{\partial\Omega}.$$

Then, the assumptions concerning ϕ, $\boldsymbol{D}$, $\check{\alpha}$, and the Cauchy-Schwarz inequality give

$$\frac{\phi_-}{2} \frac{d}{dt} \|\partial_t c_n\|^2 + \delta_- \|\partial_t \boldsymbol{r}_m\|^2 + \frac{\kappa_1}{2} \|\partial_t \boldsymbol{r}_m \cdot \boldsymbol{n}\|^2_{\partial\Omega} \leq \frac{1}{2\phi_-} \|\partial_t f\|^2 + \frac{\kappa_2^2}{2\kappa_1} \|\partial_t g\|^2_{\partial\Omega} + \frac{\phi_-}{2} \|\partial_t c_n\|^2.$$

Integrating this inequality over $(0, t)$, for $t \in (0, T]$, we obtain

$$\begin{aligned} &\|\partial_t c_n(t)\|^2 + \frac{2\delta_-}{\phi_-} \int_0^t \|\partial_t \boldsymbol{r}_m(s)\|^2 \, ds + \frac{\kappa_1}{\phi_-} \int_0^t \|\partial_t \boldsymbol{r}_m(s) \cdot \boldsymbol{n}\|^2_{\partial\Omega} \, ds \\ &\leq C(\|\partial_t c_n(0)\|^2 + \|\partial_t f\|^2_{L^2(0,T;L^2(\Omega))} + \|\partial_t g\|^2_{L^2(0,T;L^2(\partial\Omega))}) + \int_0^t \|\partial_t c_n(s)\|^2 \, ds, \end{aligned} \tag{2.42}$$

with $C = \max(1, \frac{1}{\phi_-^2}, \frac{\kappa_2^2}{\phi_- \kappa_1})$. To bound $\|\partial_t c_n(0)\|$, we use the first equation of (2.36) at $t = 0$ with $\mu = \partial_t c_n$, and the Cauchy-Schwarz inequality to obtain

$$\|\partial_t c_n(0)\|^2 \leq C(\|f(0)\|^2 + \|\operatorname{div} \boldsymbol{r}_m(0)\|^2) \leq C(\|f(0)\|^2 + \|c_0\|^2_{H^2(\Omega)}).$$

Here we have used the fact that $\boldsymbol{D}^{-1} \boldsymbol{r}_m(0) = -\nabla c_n(0)$ in $\mathscr{D}'(\Omega)$ given by the second equation of (2.36), and hence in $L^2(\Omega)$ since $c_0 \in H^2(\Omega)$. From this inequality and (2.42), we have

$$\begin{aligned} &\|\partial_t c_n(t)\|^2 + \frac{2\delta_-}{\phi_-} \int_0^t \|\partial_t \boldsymbol{r}_m(s)\|^2 \, ds + \frac{\kappa_1}{\phi_-} \int_0^t \|\partial_t \boldsymbol{r}_m(s) \cdot \boldsymbol{n}\|^2_{\partial\Omega} \, ds \\ &\leq C(\|c_0\|^2_{H^2(\Omega)} + \|f\|^2_{H^1(0,T;L^2(\Omega))} + \|g\|^2_{H^1(0,T;L^2(\partial\Omega))}) + \int_0^t \|\partial_t c_n\|^2 ds. \end{aligned} \tag{2.43}$$

It now follows from (2.43) and Gronwall's lemma that

$$\begin{aligned} &\|\partial_t c_n\|_{L^\infty(0,T;L^2(\Omega))} + \|\partial_t \boldsymbol{r}_m\|_{L^2(0,T;\boldsymbol{L^2(\Omega)})} + \|\partial_t \boldsymbol{r}_m \cdot \boldsymbol{n}\|_{L^2(0,T;L^2(\partial\Omega))} \\ &\leq C(\|c_0\|^2_{H^2(\Omega)} + \|f\|^2_{H^1(0,T;L^2(\Omega))} + \|g\|^2_{H^1(0,T;L^2(\partial\Omega))}). \end{aligned} \tag{2.44}$$

To obtain the estimate in the $\mathscr{H}(\operatorname{div}, \Omega)$-norm, we follow the same steps as for (2.41) to obtain

$$\|\operatorname{div} \boldsymbol{r}_m\|^2_{L^\infty(0,T;L^2(\Omega))} \leq C(\|c_0\|^2_{H^2(\Omega)} + \|f\|^2_{H^1(0,T;L^2(\Omega))} + \|g\|^2_{H^1(0,T;L^2(\partial\Omega))}).$$

This along with the inequality (i) of Lemma 2.8 gives

$$\|\boldsymbol{r}\|^2_{L^\infty(0,T;\mathscr{H}(\operatorname{div},\Omega))} \leq C(\|c_0\|^2_{H^2(\Omega)} + \|f\|^2_{H^1(0,T;L^2(\Omega))} + \|g\|^2_{H^1(0,T;L^2(\partial\Omega))}). \tag{2.45}$$

The lemma now follows from (2.44) and (2.45). □

Thanks to Lemma 2.8, we can finish the proof of Theorem 2.7 using similar arguments as for the proof of Theorem 2.2. □

2.3 Space-time domain decomposition methods

In this section, we present two nonoverlapping domain decomposition methods for solving problem (2.3). For simplicity, we consider a decomposition of Ω into two non overlapping subdomains Ω_1 and Ω_2 separated by an interface Γ (see Figure 2.1):

$$\Omega_1 \cap \Omega_2 = \emptyset; \quad \Gamma = \partial\Omega_1 \cap \partial\Omega_2 \cap \Omega, \quad \Omega = \Omega_1 \cup \Omega_2 \cup \Gamma.$$

Also for the sake of simplicity we have assumed throughout this section and the next that the boundary condition given on $\partial\Omega$ is a homogeneous Dirichlet condition. However, the analysis given below can be generalized to the case of multiple subdomains and more general boundary conditions (see Section 2.5).

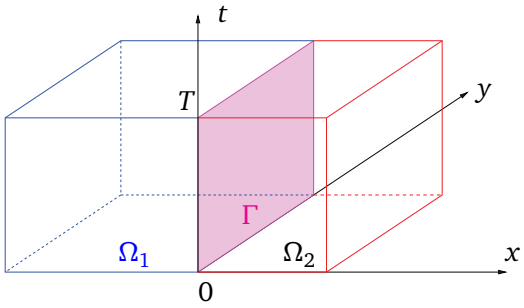

Figure 2.1: The decomposition of the domain into two subdomains where the interface is a plane in space and in time (in 2D).

For $i = 1, 2$, let $\boldsymbol{n}_i$ denote the unit outward pointing vector field on $\partial\Omega_i$, and for any scalar, vector or tensor valued function φ defined on Ω, let φ_i denote the restriction of φ to Ω_i. Using this notation, problem (2.3) can be reformulated as an equivalent multidomain problem consisting of the following space-time subdomain problems

$$\begin{aligned} \phi_i \partial_t c_i + \operatorname{div} \boldsymbol{r}_i &= f && \text{in } \Omega_i \times (0,T), \\ \nabla c_i + \boldsymbol{D}_i^{-1} \boldsymbol{r}_i &= 0 && \text{in } \Omega_i \times (0,T), \\ c_i &= 0 && \text{on } \big(\partial\Omega_i \cap \partial\Omega\big) \times (0,T), \\ c_i(0) &= c_0 && \text{in } \Omega_i, \end{aligned} \qquad \text{for } i = 1,2, \tag{2.46}$$

together with the transmission conditions on the space-time interface

$$\begin{aligned} & c_1 = c_2 \\ & \boldsymbol{r}_1 \cdot \boldsymbol{n}_1 + \boldsymbol{r}_2 \cdot \boldsymbol{n}_2 = 0 \end{aligned} \qquad \text{on } \Gamma \times (0,T), \tag{2.47}$$

Alternatively, and equivalently, one may impose the transmission conditions

$$\begin{aligned} -\boldsymbol{r}_1 \cdot \boldsymbol{n}_1 + \alpha_{1,2} c_1 &= -\boldsymbol{r}_2 \cdot \boldsymbol{n}_1 + \alpha_{1,2} c_2 \\ -\boldsymbol{r}_2 \cdot \boldsymbol{n}_2 + \alpha_{2,1} c_2 &= -\boldsymbol{r}_1 \cdot \boldsymbol{n}_2 + \alpha_{2,1} c_1 \end{aligned} \qquad \text{on } \Gamma \times (0,T), \tag{2.48}$$

where $\alpha_{1,2}$ and $\alpha_{2,1}$ are a pair of positive parameters. The first method that we consider is based on (2.46) together with the "natural" transmission conditions (2.47) while the second method is based on (2.46) together with the Robin transmission conditions (2.48). For the latter method the parameters $\alpha_{i,j}$ may be optimized to improve the convergence rate of the iterative scheme (see [12, 45, 46, 48]). For details of how this optimization is carried out, see Appendix A.2.

For both methods the multidomain problem is formulated through the use of interface operators as a problem posed on the space-time interface. For the first method

the interface operators are time-dependent Steklov-Poincaré (Dirichlet-to-Neumann) operators while for the second they are Robin-to-Robin operators. Associated with a Jacobi algorithm this latter method is known as the Optimized Schwarz Waveform Relaxation (OSWR) method. Rewriting the OSWR method as a space-time interface problem solved by a more general (Krylov) method was done in [57]; here we extend that work to a problem written in mixed form.

2.3.1 Method 1: Using the time-dependent Steklov-Poincaré operator

To introduce the interface problem for this method we introduce several operators, but first we define some notation:

$$\Lambda = H^1(0,T;H^{\frac{1}{2}}_{00}(\Gamma)), \quad \text{and, for } i=1,2, \quad M_i = L^2(\Omega_i) \quad \text{and} \quad \Sigma_i = H(\mathrm{div}\,,\Omega_i),$$

where the space $H^{\frac{1}{2}}_{00}(\Gamma)$ is the interpolated space of index $1/2$ between $H^1_0(\Gamma)$ and $L^2(\Gamma)$ (see, e.g., [82, p. 72]). We also define

$$H^1_*(\Omega_i) = \{v \in H^1(\Omega_i),\ v = 0 \text{ over } \partial\Omega_i \cap \partial\Omega\}, \text{ for } i = 1,2. \tag{2.49}$$

Next, let $\mathscr{D}_i, i = 1,2$, be the solution operator that associates to the boundary, right-hand-side, and initial data (λ, f, c_0) the solution $(c_i, \boldsymbol{r}_i)$ of the subdomain problem

$$\begin{aligned} \phi_i \partial_t c_i + \mathrm{div}\,\boldsymbol{r}_i &= f && \text{in } \Omega_i \times (0,T), \\ \nabla c_i + \boldsymbol{D}_i^{-1}\boldsymbol{r}_i &= 0 && \text{in } \Omega_i \times (0,T), \\ c_i &= 0 && \text{on } \big(\partial\Omega_i \cap \partial\Omega\big) \times (0,T), \\ c_i &= \lambda && \text{on } \Gamma \times (0,T), \\ c_i(0) &= c_0 && \text{in } \Omega_i. \end{aligned} \tag{2.50}$$

An extension of Theorem 2.2 (to the case of non-homogeneous Dirichlet boundary conditions) guarantees that

$$\begin{array}{rccc} \mathscr{D}_i: & \Lambda \times L^2(0,T;L^2(\Omega_i)) \times H^1_*(\Omega_i) & \longrightarrow & H^1(0,T;M_i) \times L^2(0,T;\Sigma_i) \\ & (\lambda, f, c_0) & \mapsto & (c_i, \boldsymbol{r}_i) = (c_i(\lambda,f,c_0), \boldsymbol{r}_i(\lambda,f,c_0)) \end{array}$$

is a well defined operator. We also make use of the normal trace operator

$$\begin{array}{rccc} \mathscr{F}_i: & H^1(0,T;M_i)) \times L^2(0,T;\Sigma_i) & \longrightarrow & L^2(0,T;(H^{\frac{1}{2}}_{00}(\Gamma))') \\ & (c_i, \boldsymbol{r}_i) & \mapsto & \boldsymbol{r}_i \cdot \boldsymbol{n}_i|_{\Gamma\times(0,T)} \end{array}$$

to define the following operators:

$$\begin{array}{rccc} \mathscr{S}_i: & \Lambda & \longrightarrow & L^2(0,T;(H^{\frac{1}{2}}_{00}(\Gamma))') \\ & \lambda & \mapsto & -\mathscr{F}_i\mathscr{D}_i(\lambda,0,0) \end{array}$$

and

$$\begin{array}{rccc} \chi_i: & L^2(0,T;L^2(\Omega_i)) \times H^1_*(\Omega_i) & \longrightarrow & L^2(0,T;(H^{\frac{1}{2}}_{00}(\Gamma))') \\ & (f, c_0) & \mapsto & \mathscr{F}_i\mathscr{D}_i(0,f,c_0). \end{array}$$

Now letting $\mathscr{S} = \mathscr{S}_1 + \mathscr{S}_2$ and $\chi = \chi_1 + \chi_2$ we may rewrite problem (2.46), (2.47) as the interface problem

$$\mathscr{S}\lambda = \chi(f, c_0), \qquad \text{on } \Gamma \times (0,T). \tag{2.51}$$

The weak formulation of this problem is then

Find $\lambda \in \Lambda$ such that:

$$\int_0^T \langle \mathscr{S}\lambda, \eta\rangle = \int_0^T \langle \chi(f, c_0), \eta\rangle, \quad \forall \eta \in \Lambda, \tag{2.52}$$

where $\langle\cdot,\cdot\rangle$ denotes the duality pairing between $H_{00}^{\frac{1}{2}}(\Gamma)$ and $(H_{00}^{\frac{1}{2}}(\Gamma))'$, and the operator $\mathscr{S}$ is the time-dependent Steklov-Poincaré operator.

Remark 2.10. *The interface problem* (2.51) *is derived in such a way that it is equivalent to the multidomain problem* (2.46) *with the physical transmission conditions* (2.47)*. Thus* (2.51) *is equivalent to the original problem* (2.3)*, which implies that problem* (2.51) *is well-posed.*

To investigate the properties of the operator $\mathscr{S}_i, i = 1, 2$, we write the weak formulation of problem (2.50) for $f = 0$ and $c_0 = 0$:

For a.e. $t \in (0, T)$, find $c_i(t) \in M_i$ and $\boldsymbol{r}_i(t) \in \Sigma_i$ such that

$$\begin{aligned} \frac{d}{dt}(\phi_i c_i, \mu)_{\Omega_i} + (\operatorname{div} \boldsymbol{r}_i, \mu)_{\Omega_i} &= 0, && \forall \mu \in M_i, \\ -(\operatorname{div} \boldsymbol{v}, c_i)_{\Omega_i} + (\boldsymbol{D}_i^{-1}\boldsymbol{r}_i, \boldsymbol{v})_{\Omega_i} &= -\int_\Gamma \lambda(\boldsymbol{v}\cdot\boldsymbol{n}_i), && \forall \boldsymbol{v} \in \Sigma_i. \end{aligned} \tag{2.53}$$

For $\lambda \in \Lambda$ and for $i = 1, 2$, we will denote by $(c_i(\lambda), \boldsymbol{r}_i(\lambda))$ the solution of (2.53) for the data function λ. Then for $\eta, \lambda \in \Lambda$ and for almost every $t \in (0, T)$, we have

$$\begin{aligned} (\phi_i \partial_t c_i(\lambda), c_i(\eta))_{\Omega_i} + (\operatorname{div} \boldsymbol{r}_i(\lambda), c_i(\eta))_{\Omega_i} &= 0, \\ -(\operatorname{div} \boldsymbol{r}_i(\eta), c_i(\lambda))_{\Omega_i} + (\boldsymbol{D}_i^{-1}\boldsymbol{r}_i(\lambda), \boldsymbol{r}_i(\eta))_{\Omega_i} &= -\int_\Gamma \lambda(\boldsymbol{r}_i(\eta)\cdot\boldsymbol{n}_i). \end{aligned}$$

Now adding the first equation to the second equation in which the roles of λ and η are reversed, integrating over time and summing on i, we obtain

$$\sum_{i=1}^2 \int_0^T \left((\phi_i \partial_t c_i(\lambda), c_i(\eta))_{\Omega_i} + (\boldsymbol{D}_i^{-1}\boldsymbol{r}_i(\eta), \boldsymbol{r}_i(\lambda))_{\Omega_i}\right) = -\sum_{i=1}^2 \int_0^T \int_\Gamma \eta(\boldsymbol{r}_i(\lambda)\cdot\boldsymbol{n}_i).$$

Thus we see that

$$\int_0^T \langle \mathscr{S}\lambda, \eta\rangle = -\sum_{i=1}^2 \int_0^T \int_\Gamma (\boldsymbol{r}_i(\lambda)\cdot\boldsymbol{n}_i)\eta = \sum_{i=1}^2 \int_0^T \left((\phi_i \partial_t c_i(\lambda), c_i(\eta))_{\Omega_i} + (\boldsymbol{D}_i^{-1}\boldsymbol{r}_i(\lambda), \boldsymbol{r}_i(\eta))_{\Omega_i}\right),$$

from which we conclude that $\mathscr{S}$ is a positive definite but non-symmetric, space-time interface operator. Thus a direct proof of the existence and uniqueness of the solution of the space-time interface problem (2.52) does not follow in a standard way as for the elliptic problems (see [101, p. 5]), and we have not pursued this question here.

Nonetheless, we solve a discretized version of problem (2.51) iteratively by using a Krylov method (here GMRES): the right hand side is computed (only once, it does not change with the iteration) by solving problem (2.50) in each subdomain with $\lambda = 0$ and then calculating the jump of the flux across the space-time interface; then for a given vector η defined on $\Gamma \times (0, T)$, the matrix vector product is obtained (at each iteration)

by solving subdomain problem (2.50) with $\lambda = \eta$ and with $f = 0$ and, $c_0 = 0$, then computing the jump of the flux on $\Gamma \times (0,T)$. Once the discrete approximation to λ is obtained, we can construct the multidomain solution of the discretized problem.

Following the work in [80, 89] for elliptic problems with strong heterogeneities, we apply a Neumann-Neumann type preconditioner enhanced with averaging weights:

$$\left(\sigma_1 \mathscr{S}_1^{-1} + \sigma_2 \mathscr{S}_2^{-1}\right) \mathscr{S} \lambda = \tilde{\chi}, \tag{2.54}$$

where $\sigma_i : \Gamma \times (0,T) \to [0,1]$ is such that $\sigma_1 + \sigma_2 = 1$, and $\mathscr{S}_i^{-1}$, the Neumann-to-Dirichlet operator, is the (pseudo)-inverse of $\mathscr{S}_i$, for $i = 1,2$, defined as follows

$$\begin{array}{rccc} \mathscr{S}_i^{-1} : & L^2(0,T;(H_{00}^{\frac{1}{2}}(\Gamma))') & \longrightarrow & \Lambda \\ & \varphi & \mapsto & c_i(\varphi)_{|\Gamma\times(0,T)}, \end{array}$$

where $(c_i(\varphi), \boldsymbol{r}_i(\varphi)), i = 1,2$, is the solution of

$$\begin{array}{rcl} \phi_i \partial_t c_i + \nabla \cdot \boldsymbol{r}_i &= 0 & \text{in } \Omega_i \times (0,T), \\ \nabla c_i + \boldsymbol{D}_i^{-1} \boldsymbol{r}_i &= 0 & \text{in } \Omega_i \times (0,T), \\ c_i &= 0 & \text{on } \left(\partial\Omega_i \cap \partial\Omega\right) \times (0,T), \\ -\boldsymbol{r}_i \cdot \boldsymbol{n}_i &= \varphi & \text{on } \Gamma \times (0,T), \\ c_i(0) &= 0 & \text{in } \Omega_i. \end{array}$$

Remark 2.11. *There is no analysis on the convergence of the GMRES algorithm for solving the interface problem* (2.51)*. One can perform Richardson iterations for this problem and study the convergence of the corresponding algorithm (and hopefully, GMRES may converge faster). This has been done using detailed properties of the Green's function for the case of a homogeneous problem by F. Kwok (see [79]); it is difficult to generalize this analysis to the case of heterogeneous media.*

2.3.2 Method 2: Using Optimized Schwarz Waveform Relaxation

The function spaces needed to derive the interface formulation of Method 2 are

$$\Xi := H^1(0,T;L^2(\Gamma)), \quad \text{and, for } i = 1,2, \quad M_i = L^2(\Omega_i) \quad \text{and} \quad \widetilde{\Sigma}_i = \mathscr{H}(\text{div}\,, \Omega_i).$$

To define the Robin-to-Robin operator we first define for $i = 1,2$, the following solution operator $\mathscr{R}_i$ which depends on the parameter $\alpha_{i,j};\ j = 3 - i$:

$$\begin{array}{rccc} \mathscr{R}_i : & \Xi \times L^2(0,T;L^2(\Omega_i)) \times H^1_*(\Omega_i) & \longrightarrow & \Xi \times H^1(0,T;M_i) \times L^2(0,T;\widetilde{\Sigma}_i) \\ & (\xi, f, c_0) & \mapsto & (\xi, c_i, \boldsymbol{r}_i) = (\xi, c_i(\xi,f,c_0), \boldsymbol{r}_i(\xi,f,c_0)) \end{array}$$

where $(c_i, \boldsymbol{r}_i) = (c_i(\xi,f,c_0), \boldsymbol{r}_i(\xi,f,c_0))$ is the solution to the problem

$$\begin{array}{rcl} \phi_i \partial_t c_i + \text{div}\, \boldsymbol{r}_i &= f & \text{in } \Omega_i \times (0,T), \\ \nabla c_i + \boldsymbol{D}_i^{-1} \boldsymbol{r}_i &= 0 & \text{in } \Omega_i \times (0,T), \\ c_i &= 0 & \text{on } \left(\partial\Omega_i \cap \partial\Omega\right) \times (0,T), \\ -\boldsymbol{r}_i \cdot \boldsymbol{n}_i + \alpha_{i,j} c_i &= \xi & \text{on } \Gamma \times (0,T), \\ c_i(0) &= c_0 & \text{in } \Omega_i. \end{array} \tag{2.55}$$

(As stated earlier the parameters $\alpha_{i,j}$ will be chosen is such a way as to optimize the convergence of the algorithm). The existence and uniqueness of the solution of problem (2.55) is guaranteed by Theorem 2.7.

Next, to impose the interface conditions (2.48) we will need the following interface operators defined for $i = 1, 2$, and $j = 3 - i$:

$$\begin{aligned}\mathscr{B}_i : \left(\Xi \times H^1(0,T;M_j) \times L^2(0,T;\widetilde{\Sigma}_j)\right) \cap \mathrm{Im}(\mathscr{R}_j) &\longrightarrow \quad \Xi \\ (\xi, c_j, \boldsymbol{r}_j) &\mapsto (-\boldsymbol{r}_j \cdot \boldsymbol{n}_i + \frac{\alpha_{i,j}}{\alpha_{j,i}}(\xi + \boldsymbol{r}_j \cdot \boldsymbol{n}_j))|_{\Gamma\times(0,T)}\end{aligned}$$

Remark 2.12. *To see that $Im(\mathscr{B}_i) \subset \Xi$ (instead of simply $L^2(0,T;L^2(\Gamma))$, we note that* (2.35) *implies that $\boldsymbol{D}^{-1}\boldsymbol{r}(t) = -\nabla c(t)$ in $\mathscr{D}'(\Omega)$ for a.e. $t \in (0,T)$. Since $\boldsymbol{r}(t)$ is in $H(div\ ,\Omega)$, we have $c(t) \in H^1(\Omega)$, for a.e. $t \in (0,T)$. Consequently, $c_i(t)$ is in $H^1(0,T;H^1(\Omega_i))$. This along with the fact that $\xi \in \Xi$ implies that $\boldsymbol{r}_i \cdot \boldsymbol{n}_i|_{\Gamma\times(0,T)} \in \Xi$.*

Now, defining

$$\begin{aligned}\mathscr{S}_R : \quad \Xi \times \Xi \quad &\longrightarrow \quad \Xi \times \Xi \\ \begin{pmatrix}\xi_1 \\ \xi_2\end{pmatrix} \quad &\mapsto \quad \begin{pmatrix}\xi_1 - \mathscr{B}_1\mathscr{R}_2(\xi_2, 0, 0) \\ \xi_2 - \mathscr{B}_2\mathscr{R}_1(\xi_1, 0, 0)\end{pmatrix}\end{aligned} \tag{2.56}$$

and

$$\begin{aligned}\chi_R : \quad L^2(0,T;L^2(\Omega_i)) \times H^1_*(\Omega_i) \quad &\longrightarrow \quad \Xi \times \Xi \\ (f, c_0) \quad &\mapsto \quad \begin{pmatrix}\mathscr{B}_1\mathscr{R}_2(0, f, c_0) \\ \mathscr{B}_2\mathscr{R}_1(0, f, c_0)\end{pmatrix},\end{aligned}$$

we can write the interface problem as

$$\mathscr{S}_R \begin{pmatrix}\xi_1 \\ \xi_2\end{pmatrix} = \chi_R(f, c_0) \quad \text{on } \Gamma \times (0,T). \tag{2.57}$$

We then write (2.57) in weak form as

Find $(\xi_1, \xi_2) \in \Xi \times \Xi$ such that

$$\int_0^T \int_\Gamma \mathscr{S}_R \begin{pmatrix}\xi_1 \\ \xi_2\end{pmatrix} \cdot \begin{pmatrix}\zeta_1 \\ \zeta_2\end{pmatrix} = \int_0^T \int_\Gamma \chi_R(f, c_0) \cdot \begin{pmatrix}\zeta_1 \\ \zeta_2\end{pmatrix}, \ \ \forall (\zeta_1, \zeta_2) \in \Xi \times \Xi. \tag{2.58}$$

Remark 2.13. *The counterpart to Remark 2.10 is that the interface problem* (2.57) *is well-posed due to the fact that it is equivalent to the multidomain problem* (2.46) *with Robin transmission conditions* (2.48).

In order to study the interface operator $\mathscr{S}_R$, we proceed as in Section 2.3.1 by giving the weak formulation of the relevant subdomain problems (here (2.55) for $i = 1, 2$ and $j = 3 - 1$) for $f = 0$ and $c_0 = 0$:

For a.e. $t \in (0,T)$, find $c_i(t) \in M_i$ and $\boldsymbol{r}_i(t) \in \widetilde{\Sigma}_i$ such that, $\forall \mu \in M_i$ and $\forall \boldsymbol{v} \in \widetilde{\Sigma}_i$,

$$\begin{aligned}\frac{d}{dt}(\phi_i c_i, \mu)_{\Omega_i} + (\mathrm{div}\, \boldsymbol{r}_i, \mu)_{\Omega_i} &= 0, \\ -(\mathrm{div}\, \boldsymbol{v}, c_i)_{\Omega_i} + (\boldsymbol{D}_i^{-1}\boldsymbol{r}_i, \boldsymbol{v})_{\Omega_i} + \int_\Gamma \frac{1}{\alpha_{i,j}}(\boldsymbol{r}_i \cdot \boldsymbol{n}_i)(\boldsymbol{v} \cdot \boldsymbol{n}_i) &= -\int_\Gamma \frac{1}{\alpha_{i,j}}\xi(\boldsymbol{v} \cdot \boldsymbol{n}_i).\end{aligned} \tag{2.59}$$

Now for any $\zeta \in \Xi$ letting $c_i(\zeta) \in H^1(0,T;M_i)$ and $\boldsymbol{r}_i(\zeta) \in L^2(0,T;\widetilde{\Sigma}_i)$ be such that $\mathscr{R}_i(\zeta,0,0) = (\zeta, c_i(\zeta), \boldsymbol{r}_i(\zeta))$, we have for any pair of elements ξ and ζ in Ξ and for a.e. $t \in (0,T)$ that

$$\begin{aligned}(\phi_i \partial_t c_i(\xi), c_i(\zeta))_{\Omega_i} + (\operatorname{div} \boldsymbol{r}_i(\xi), c_i(\zeta))_{\Omega_i} &= 0,\\ -(\operatorname{div} \boldsymbol{r}_i(\zeta), c_i(\xi))_{\Omega_i} + (\boldsymbol{D}_i^{-1}\boldsymbol{r}_i(\xi), \boldsymbol{r}_i(\zeta))_{\Omega_i} + \int_\Gamma \frac{1}{\alpha_{i,j}} (\boldsymbol{r}_i(\xi)\cdot\boldsymbol{n}_i)(\boldsymbol{r}_i(\zeta)\cdot\boldsymbol{n}_i)&\\ = -\int_\Gamma \frac{1}{\alpha_{i,j}} \xi(\boldsymbol{r}_i(\zeta)\cdot\boldsymbol{n}_i).&\end{aligned}$$

Next we add the first of these two equations to the second in which the roles of ζ and ξ have been interchanged to obtain

$$\begin{aligned}(\phi_i \partial_t c_i(\xi), c_i(\zeta))_{\Omega_i} + (\boldsymbol{D}_i^{-1}\boldsymbol{r}_i(\xi), \boldsymbol{r}_i(\zeta))_{\Omega_i} + \int_\Gamma \frac{1}{\alpha_{i,j}} (\boldsymbol{r}_i(\xi)\cdot\boldsymbol{n}_i)(\boldsymbol{r}_i(\zeta)\cdot\boldsymbol{n}_i)&\\ = -\int_\Gamma \frac{1}{\alpha_{i,j}} \zeta(\boldsymbol{r}_i(\xi)\cdot\boldsymbol{n}_i),&\end{aligned} \tag{2.60}$$

and this holds for any pair of elements ξ and ζ in Ξ. Now we consider the case in which the parameters $\alpha_{i,j}$, $i = 1,2$, $j = 3-i$, are constant and apply (2.60) with $\xi = \xi_j$ and $\zeta = \zeta_i$, to obtain

$$\begin{aligned}\int_0^T \int_\Gamma \mathscr{S}_R \begin{pmatrix}\xi_1\\ \xi_2\end{pmatrix} \cdot \begin{pmatrix}\zeta_1\\ \zeta_2\end{pmatrix} = \sum_{i=1}^{2} \int_0^T \Big\{ \int_\Gamma (\xi_i - \frac{\alpha_{i,j}}{\alpha_{j,i}}\xi_j)\zeta_i + (\alpha_{1,2}+\alpha_{2,1}) \Big\{ (\phi_i \partial_t c_i(\xi_j), c_i(\zeta_i))_{\Omega_i}&\\ + (\boldsymbol{D}_i^{-1}\boldsymbol{r}_i(\xi_j), \boldsymbol{r}_i(\zeta_i))_{\Omega_i} + \int_\Gamma \frac{1}{\alpha_{i,j}} (\boldsymbol{r}_i(\xi_j)\cdot\boldsymbol{n}_i)(\boldsymbol{r}_i(\zeta_i)\cdot\boldsymbol{n}_i) \Big\} \Big\}&\end{aligned}$$

As for Method 1, we obtain a non-symmetric, space-time interface operator, but here it is also not positive definite. We solve the discretized problem iteratively using Jacobi iterations or GMRES: the right hand side is computed (only once) by solving subdomain problem (2.55) with $\xi = 0$ and then calculating the discrete Robin terms (corresponding to the discrete counterpart of operator $\mathscr{B}_i, i = 1,2$) on the space-time interface; for a given pair of vectors (ξ_1, ξ_2), the matrix vector product is obtained (at each iteration) by solving, for $i = 1,2$, problem (2.55) in $\Omega_i \times (0,T)$ with $\xi = \xi_i$ and with $f = 0$ and, $c_0 = 0$, then computing the jump of the Robin data on $\Gamma \times (0,T)$ (using (2.56)). Performing Jacobi iterations for problem (2.57) is equivalent to the OSWR algorithm, and in the next subsection we show that the algorithm (in mixed form) converges.

2.3.2.1 The OSWR algorithm

We consider the general case in which Ω is decomposed into I non-overlapping subdomains Ω_i. We denote by $\Gamma_{i,j}$ the interface between two neighboring subdomains Ω_i and Ω_j, $\Gamma_{i,j} = \partial\Omega_i \cap \partial\Omega_j \cap \Omega$. Let $\mathscr{N}_i$ be the set of indices of the neighbors of the subdomain Ω_i, $i = 1,\ldots,I$. The OSWR method may be written as follows: at the k^{th} iteration, we solve in each subdomain the problem

$$\begin{aligned}\phi_i \partial_t c_i^k + \operatorname{div} \boldsymbol{r}_i^k &= f, && \text{in } \Omega_i \times (0,T),\\ \nabla c_i^k + \boldsymbol{D}_i^{-1}\boldsymbol{r}_i^k &= 0, && \text{in } \Omega_i \times (0,T),\\ -\boldsymbol{r}_i^k \cdot \boldsymbol{n}_i + \alpha_{i,j} c_i^k &= -\boldsymbol{r}_j^{k-1}\cdot\boldsymbol{n}_i + \alpha_{i,j} c_j^{k-1}, && \text{on } \Gamma_{i,j} \times (0,T), \forall j \in \mathscr{N}_i,\end{aligned} \tag{2.61}$$

where, for $i = 1, \dots, I$, $j \in \mathcal{N}_i$, $\alpha_{i,j} > 0$ is a Robin parameter. The initial value is that of c_0 in each subdomain. Moreover, $\left(g_{i,j}\right) := -\boldsymbol{r}_j^0 \cdot \boldsymbol{n}_i + \alpha_{i,j} c_j^0$ is an initial guess on $\Gamma_{i,j}$, for $i = 1, \dots, I$, $j \in \mathcal{N}_i$, in order to start the first iterate.

Remark 2.14. *Problem* (2.61) *results from the application of Jacobi iterations for the interface problem* (2.57) *(for the case of two subdomains). This can be seen by writing the interface problem for* (2.61) *(following the same steps as in Subsection 2.3.2):*

$$\begin{pmatrix} \xi_1^k - \mathscr{B}_1 \mathscr{R}_2(\xi_2^{k-1}, 0, 0) \\ \xi_2^k - \mathscr{B}_2 \mathscr{R}_1(\xi_1^{k-1}, 0, 0) \end{pmatrix} = \chi_R(f, c_0), \quad \text{on } \Gamma \times (0,T),$$

or equivalently,

$$\begin{pmatrix} \xi_1^k \\ \xi_2^k \end{pmatrix} = \begin{pmatrix} \xi_1^{k-1} \\ \xi_2^{k-1} \end{pmatrix} + \chi_R(f, c_0) - \mathscr{S}_R \begin{pmatrix} \xi_1^{k-1} \\ \xi_2^{k-1} \end{pmatrix}, \quad \text{on } \Gamma \times (0,T).$$

The variational formulation of (2.61) is written as follows:

For a.e. $t \in (0,T)$, find $c_i^k(t) \in L^2(\Omega_i)$ and $\boldsymbol{r}_i^k(t) \in \mathscr{H}(\mathrm{div}, \Omega_i)$ such that

$$\begin{aligned} (\phi_i \partial_t c_i^k, \mu_i)_{\Omega_i} + (\nabla \cdot \boldsymbol{r}_i^k, \mu_i)_{\Omega_i} &= (f, \mu_i)_{\Omega_i}, && \forall \mu_i \in L^2(\Omega_i), \\ -(\nabla \cdot \boldsymbol{v}_i, c_i^k)_{\Omega_i} + (\boldsymbol{D}_i^{-1} \boldsymbol{r}_i^k, \boldsymbol{v}_i)_{\Omega_i} &= \sum_{j \in \mathcal{N}_i} \int_{\Gamma_{i,j}} c_i^k (-\boldsymbol{v}_i \cdot \boldsymbol{n}_i), && \forall \boldsymbol{v}_i \in \mathscr{H}(\mathrm{div}, \Omega_i), \end{aligned} \tag{2.62}$$

for $i = 1, \cdots, I$.

Theorem 2.15. *Let $\boldsymbol{D} \in \boldsymbol{W^{1,\infty}(\Omega)}$, $f \in H^1(0,T; L^2(\Omega))$ and $c_0 \in H^2(\Omega) \cap H_0^1(\Omega)$ and let $\alpha_{i,j} \in L^\infty(\partial\Omega_i)$ be such that $\alpha_{i,j} \geq \alpha_0 > 0$ for $i = 1, \dots, I$, $j \in \mathcal{N}_i$. Algorithm* (2.62)*, initialized by $(g_{i,j})$ in $H^1\left(0,T; L^2\left(\Gamma_{i,j}\right)\right)$, $i = 1, \dots, I$, $j \in \mathcal{N}_i$, defines a unique sequence of iterates*

$$(c_i^k, \boldsymbol{r}_i^k) \in W^{1,\infty}(0,T; L^2(\Omega_i)) \times \left(L^2(0,T; \mathscr{H}(\mathrm{div}, \Omega_i)) \cap H^1(0,T; \boldsymbol{L^2(\Omega_i)}) \right),$$

for $i = 1, \dots, I$, that converges to the weak solution $(c, \boldsymbol{r})$ of problem (2.3).

Proof. The sequence $(c_i^k, \boldsymbol{r}_i^k)_k$ is well-defined according to Theorem 2.7 and Remark 2.12. Now, to prove the convergence of algorithm (2.61), as the equations are linear, we can take $f = 0$ and $c_0 = 0$ and show that the sequence $\left(c_i^k, \boldsymbol{r}_i^k\right)_k$ of iterates converges to zero in suitable norms.

Choosing $\mu_i = c_i^k$ and $\boldsymbol{v}_i = \boldsymbol{r}_i^k$ in (2.62), then adding the two resulting equations and replacing the boundary term by using the equation

$$\begin{aligned} &\left(-\boldsymbol{r}_i^k \cdot \boldsymbol{n}_i + \alpha_{i,j} c_i^k\right)^2 - \left(-\boldsymbol{r}_i^k \cdot \boldsymbol{n}_i - \alpha_{j,i} c_i^k\right)^2 \\ &\qquad = 2\left(\alpha_{i,j} + \alpha_{j,i}\right) c_i^k \left(-\boldsymbol{r}_i^k \cdot \boldsymbol{n}_i\right) + \left(\alpha_{i,j}^2 - \alpha_{j,i}^2\right) \left(c_i^k\right)^2, \end{aligned} \tag{2.63}$$

we obtain

$$\begin{aligned} &(\phi_i \partial_t c_i^k, c_i^k)_{\Omega_i} + \left(\boldsymbol{D}_i^{-1} \boldsymbol{r}_i^k, \boldsymbol{r}_i^k\right)_{\Omega_i} + \sum_{j \in \mathcal{N}_i} \int_{\Gamma_{i,j}} \frac{1}{2\left(\alpha_{i,j} + \alpha_{j,i}\right)} \left(-\boldsymbol{r}_i^k \cdot \boldsymbol{n}_i - \alpha_{j,i} c_i^k\right)^2 \\ &\quad = \sum_{j \in \mathcal{N}_i} \int_{\Gamma_{i,j}} \frac{1}{2\left(\alpha_{i,j} + \alpha_{j,i}\right)} \left(-\boldsymbol{r}_i^k \cdot \boldsymbol{n}_i + \alpha_{i,j} c_i^k\right)^2 + \frac{1}{2} \sum_{j \in \mathcal{N}_i} \int_{\Gamma_{i,j}} \left(\alpha_{j,i} - \alpha_{i,j}\right) \left(c_i^k\right)^2. \end{aligned}$$

We then integrate over $(0,t)$ for a.e. $t \in (0,T]$ and apply the Robin boundary conditions. By using the properties of ϕ and $\boldsymbol{D}$ and using the fact that the Robin coefficients $\alpha_{i,j}$ belong to $L^\infty\left(\Gamma_{i,j}\right)$, $i \in 1,\cdots,I$, $j \in \mathcal{N}_i$ and that c_i^k belongs to $H^1(\Omega_i)$ (see Remark 2.12), we apply the trace theorem and obtain, for some constant C,

$$\phi_- \|c_i^k(t)\|_{\Omega_i}^2 + 2\delta_- \int_0^t \|\boldsymbol{r}_i^k(s)\|_{\Omega_i}^2 ds + \sum_{j\in\mathcal{N}_i} \int_0^t \int_{\Gamma_{i,j}} \frac{1}{\alpha_{i,j}+\alpha_{j,i}} \left(-\boldsymbol{r}_i^k \cdot \boldsymbol{n}_i - \alpha_{j,i} c_i^k\right)^2$$
$$\leq \sum_{j\in\mathcal{N}_i} \int_0^t \int_{\Gamma_{i,j}} \frac{1}{\alpha_{i,j}+\alpha_{j,i}} \left(-\boldsymbol{r}_j^{k-1} \cdot \boldsymbol{n}_i + \alpha_{i,j} c_j^{k-1}\right)^2 + C \int_0^t \|c_i^k(s)\|_{\Omega_i}^2 ds.$$

Now we sum over all subdomains and define for $k \geq 1$ and for a.e. $t \in (0,T]$

$$E^k(t) = \sum_{i=1}^I \left(\phi_- \|c_i^k(t)\|_{\Omega_i}^2 + 2\delta_- \int_0^t \|\boldsymbol{r}_i^k(s)\|_{\Omega_i}^2 ds \right),$$
$$B^k(t) = \sum_{i=1}^I \sum_{j\in\mathcal{N}_i} \int_0^t \int_{\Gamma_{i,j}} \frac{1}{\alpha_{i,j}+\alpha_{j,i}} \left(-\boldsymbol{r}_j^k \cdot \boldsymbol{n}_i + \alpha_{i,j} c_j^k\right)^2.$$

Then we have, for all $k > 0$

$$E^k(t) + B^k(t) \leq B^{k-1}(t) + C \sum_{i=1}^I \int_0^t \|c_i^k(s)\|_{\Omega_i}^2 ds.$$

Now sum over the iterates for any given $K > 0$:

$$\sum_{k=1}^K E^k(t) \leq B^0(t) + C \sum_{k=1}^K \sum_{i=1}^I \int_0^t \|c_i^k(s)\|_{\Omega_i}^2 ds, \tag{2.64}$$

where

$$B^0(t) = \sum_{i=1}^I \sum_{j\in\mathcal{N}_i} \int_0^t \int_{\Gamma_{i,j}} \frac{1}{\alpha_{i,j}+\alpha_{j,i}} (g_{i,j})^2,$$

for $g_{i,j}$ the initial guess on $\Gamma_{i,j}$. From the definition of E^k, since $\delta_- > 0$, we have

$$\sum_{k=1}^K \sum_{i=1}^I \phi_- \|c_i^k(t)\|_{\Omega_i}^2 \leq B^0(t) + C \sum_{k=1}^K \sum_{i=1}^I \int_0^t \|c_i^k(s)\|_{\Omega_i}^2 ds.$$

Thus, by applying Gronwall's lemma, we obtain for any $K > 0$ and a.e. $t \in (0,T)$

$$\sum_{k=1}^K \sum_{i=1}^I \|c_i^k(t)\|_{\Omega_i}^2 \leq e^{\frac{CT}{\phi_-}} \frac{B^0(T)}{\phi_-}. \tag{2.65}$$

This along with (2.64) implies

$$\sum_{k=1}^K \sum_{i=1}^I 2\delta_- \int_0^t \|\boldsymbol{r}_i^k(s)\|_{\Omega_i}^2 ds \leq (1 + \frac{CT}{\phi_-} e^{\frac{CT}{\phi_-}}) B^0(T), \quad \forall K > 0. \tag{2.66}$$

The inequalities (2.65), (2.66) imply that the sequence c_i^k tends to 0 in $L^\infty\left(0,T;L^2\left(\Omega_i\right)\right)$ and $\boldsymbol{r}_i^k$ converges to 0 in $L^2\left(0,T;\boldsymbol{L^2(\Omega_i)}\right)$ for each $i \in 1,\ldots,I$

as $k \to \infty$.
To show convergence in higher norms, we differentiate the first and the second equations of (2.62) with respect to t, then take $\mu_i = \partial_t c_i^k$ and $\boldsymbol{\nu}_i = \partial_t \boldsymbol{r}_i^k$ and add the resulting equations together. We see that (after bounding the left hand side using the assumptions on ϕ and $\boldsymbol{D}$)

$$\frac{\phi_-}{2}\frac{d}{dt}\|\partial_t c_i^k\|_{\Omega_i}^2 + \delta_-\|\partial_t \boldsymbol{r}_i^k\|_{\Omega_i}^2 \leq \sum_{j\in\mathcal{N}_i}\int_{\Gamma_{i,j}} \partial_t c_i^k(-\partial_t \boldsymbol{r}_i^k\cdot\boldsymbol{n}_i).$$

We proceed as in the previous argument with the use of Robin boundary conditions after differentiating with respect to t

$$-\partial_t \boldsymbol{r}_i^k\cdot\boldsymbol{n}_i + \alpha_{i,j}\partial_t c_i^k = -\partial_t \boldsymbol{r}_j^{k-1}\cdot\boldsymbol{n}_i + \alpha_{i,j}\partial_t c_j^{k-1}, \text{ on } \Gamma_{i,j}\times(0,T), \forall j\in\mathcal{N}_i.$$

We then obtain, for all $k>0$

$$\tilde{E}^k(t) + \tilde{B}^k(t) \leq \tilde{B}^{k-1}(t) + C\sum_{i=1}^{I}\int_0^t \|\partial_t c_i^k(s)\|_{\Omega_i}^2 ds.$$

where

$$\tilde{E}^k(t) = \sum_{i=1}^{I}\left(\phi_-\|\partial_t c_i^k(t)\|_{\Omega_i}^2 + 2\delta_-\int_0^t \|\partial_t \boldsymbol{r}_i^k(s)\|_{\Omega_i}^2 ds\right),$$
$$\tilde{B}^k(t) = \sum_{i=1}^{I}\sum_{j\in\mathcal{N}_i}\int_0^t\int_{\Gamma_{i,j}} \frac{1}{\alpha_{i,j}+\alpha_{j,i}}\left(-\partial_t \boldsymbol{r}_j^k\cdot\boldsymbol{n}_i + \alpha_{i,j}\partial_t c_j^k\right)^2.$$

Now, as before, we sum over the iterates for any $K>0$ and apply Gronwall's lemma to obtain for any $K>0$ and a.e. $t\in(0,T)$

$$\sum_{k=1}^{K}\sum_{i=1}^{I}\|\partial_t c_i^k(t)\|_{\Omega_i}^2 \leq e^{\frac{CT}{\phi_-}}\frac{\tilde{B}^0(T)}{\phi_-}, \quad \text{with } \tilde{B}^0(t) = \sum_{i=1}^{I}\sum_{j\in\mathcal{N}_i}\int_0^t\int_{\Gamma_{i,j}}\frac{1}{\alpha_{i,j}+\alpha_{j,i}}(\partial_t g_{i,j})^2. \tag{2.67}$$

This along with (2.65) shows that the sequence c_i^k converges to 0 in $W^{1,\infty}(0,T;L^2(\Omega_i)$ as $k\to\infty$, for $i = 1, \ldots, I$.
Now we choose $\mu_i = \operatorname{div}\boldsymbol{r}_i^k$ in the first equation of (2.62) to obtain for a.e. $t\in(0,T)$

$$\|\operatorname{div}\boldsymbol{r}_i^k\|_{\Omega_i}^2 = -\left(\partial_t c_i^k, \operatorname{div}\boldsymbol{r}_i^k\right)_{\Omega_i} \leq \|\partial_t c_i^k\|_{\Omega_i}\|\operatorname{div}\boldsymbol{r}_i^k\|_{\Omega_i}.$$

or

$$\|\operatorname{div}\boldsymbol{r}_i^k\|_{\Omega_i} \leq \|\partial_t c_i^k\|_{\Omega_i} \quad \forall t\in(0,T).$$

Hence, by (2.67) we have

$$\|\operatorname{div}\boldsymbol{r}_i^k\|_{L^\infty(0,T;L^2(\Omega_i))} \to 0 \text{ as } k\to\infty. \tag{2.68}$$

This shows that the sequence $\boldsymbol{r}_i^k$ converges to 0 in $L^2\left(0,T;H(\operatorname{div},\Omega_i)\right)$. Moreover, it follows from the definition of $\tilde{E}^k$ and (2.67) that

$$\sum_{k=1}^{K}\sum_{i=1}^{I} 2\delta_-\int_0^t \|\partial_t \boldsymbol{r}_i^k(s)\|_{\Omega_i}^2 ds \leq (1+\frac{CT}{\phi_-}e^{\frac{CT}{\phi_-}})\tilde{B}^0(T), \quad \forall K>0.$$

So that the sequence $\partial_t \boldsymbol{r}_i^k$ also converges to 0 in $L^2(0,T;\boldsymbol{L^2(\Omega_i)})$. □

2.4 Nonconforming time discretizations and projections in time

One of the main advantages of Method 1 or Method 2 is that because these methods are global in time, they enable the use of independent time discretizations in the subdomains. At the space-time interface, data is transferred from one space-time subdomain to a neighboring subdomain by using a suitable projection.

We consider semi-discrete problems in time with nonconforming time grids. Let $\mathscr{T}_1$ and $\mathscr{T}_2$ be two possibly different partitions of the time interval $(0,T)$ into subintervals (see Figure 2.2). We denote by J_m^i the time interval $(t_m^i, t_{m-1}^i]$ and by $\Delta t_m^i := (t_m^i - t_{m-1}^i)$ for $m = 1,\dots,M_i$ and $i = 1,2$, where for simplicity of exposition we have again supposed that we have only two subdomains. We use the lowest order discontinuous Galerkin method [61, 17, 108], which is a modified backward Euler method. The same idea can be generalized to higher order methods. We denote by

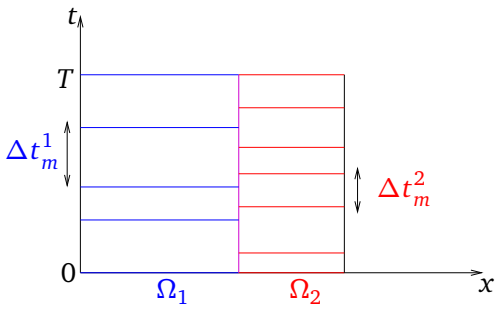

Figure 2.2: Nonconforming time grids in the subdomains.

$P_0(\mathscr{T}_i, W)$ the space of piecewise constant functions in time on grid $\mathscr{T}_i$ with values in W, where $W = H_{00}^{\frac{1}{2}}(\Gamma)$ for Method 1 and $W = L^2(\Gamma)$ for Method 2:

$$P_0(\mathscr{T}_i, W) = \left\{\psi : (0,T) \to W, \psi \quad \text{is constant on } J_m^i, \ \forall m = 1,\dots,M_i\right\}. \tag{2.69}$$

In order to exchange data on the space-time interface between different time grids, we define the following L^2 projection Π_{ji} from $P_0(\mathscr{T}_i, W)$ onto $P_0(\mathscr{T}_j, W)$ (see [48, 61]) : for $\psi \in P_0(\mathscr{T}_i, W)$, $\Pi_{ji}\psi|_{J_m^j}$ is the average value of ψ on J_m^j, for $m = 1,\dots,M_j$:

$$\Pi_{ji}\left(\psi\right)|_{J_m^j} = \frac{1}{|J_m^j|}\sum_{l=1}^{M_i}\int_{J_m^j \cap J_l^i} \psi. \tag{2.70}$$

We use the algorithm described in [50] for effectively performing this projection. With these tools, we are now able to weakly enforce the transmission conditions over the time intervals.

We still denote by $(c_i, \boldsymbol{r}_i)$, for $i = 1,2$, the solution of the problem semi-discrete in time corresponding to problem (2.53) or (2.59).

2.4.1 For Method 1

As there is only one unknown λ on the interface, we need to choose λ piecewise constant in time on one grid, either $\mathscr{T}_1$ or $\mathscr{T}_2$. For instance, let $\lambda \in P_0(\mathscr{T}_2, H_{00}^{\frac{1}{2}}(\Gamma))$ and take $c_2 = \Pi_{22}(\lambda) = \mathrm{Id}(\lambda)$. The weak continuity of the concentration in time across the

interface is fulfilled by letting

$$c_1 = \Pi_{12}(\lambda) \in P_0(\mathscr{T}_1, H_{00}^{\frac{1}{2}}(\Gamma)).$$

The semi-discrete (nonconforming in time) counterpart of the flux continuity in the second equation of (2.47) is weakly enforced by integrating it over each time interval J_m^2 of grid $\mathscr{T}_2$: $\forall m = 1, ..., M_2$,

$$\int_{J_m^2} \Big(\Pi_{21}\big(\boldsymbol{r}_1(\Pi_{12}(\lambda), f, c_0) \cdot \boldsymbol{n}_1\big) + \Pi_{22}\big(\boldsymbol{r}_2(\Pi_{22}(\lambda), f, c_0) \cdot \boldsymbol{n}_2\big) \Big)\, dt = 0, \text{ on } \Gamma. \quad (2.71)$$

Remark 2.16. *Obviously one could choose λ to be constant in time on yet another grid (neither $\mathscr{T}_1$ nor $\mathscr{T}_2$), and this can be useful in some applications (e.g. flow in porous media with fractures).*

2.4.2 For Method 2

In Method 2, there are two interface unknowns representing the Robin terms from each subdomain. Thus we let $\xi_i \in P_0(\mathscr{T}_i, L^2(\Gamma))$, for $i = 1, 2$. The semi-discrete in time counterpart of (2.48) is weakly enforced as follows:

$$\begin{aligned}
&\int_{J_m^1} \Big(\xi_1 - \Pi_{12}\big(-\boldsymbol{r}_2(\xi_2, f, c_0) \cdot \boldsymbol{n}_1 + \alpha_{1,2} c_2(\xi_2, f, c_0)\big) \Big) dt = 0, \text{ on } \Gamma, \ \forall m = 1, \dots, M_1, \\
&\int_{J_m^2} \Big(-\Pi_{21}\big(-\boldsymbol{r}_1(\xi_1, f, c_0) \cdot \boldsymbol{n}_2 + \alpha_{2,1} c_1(\xi_1, f, c_0)\big) + \xi_2 \Big) dt = 0, \text{ on } \Gamma, \ \forall m = 1, \dots, M_2,
\end{aligned} \quad (2.72)$$

where $\big(c_i(\xi_i, f, c_0), \boldsymbol{r}_i(\xi_i, f, c_0)\big)$, $i = 1, 2$, is the solution to (2.59).

Remark 2.17. *For conforming time grids, the two schemes defined by applying GMRES for the two interface problems* (2.71) *and* (2.72) *respectively converge to the same monodomain solution. In the nonconforming case, due to the use of different projection operators, the two schemes yield different solutions at convergence. In Section 2.5, we will study and compare the errors in time for the two methods.*

As in Subsection 2.3.2.1, we consider the semi-discrete OSWR algorithm associated with (2.72) using Jacobi iterations and prove that this algorithm converges to the nonconforming solution (see problem (2.74) below).

2.4.2.1 The semi-discrete, nonconforming in time, OSWR algorithm

We consider a decomposition of Ω into I non-overlapping subdomains ϕ_i and use the same notation as in Subsection 2.3.2.1. We denote by $\mathscr{T}_i$ the time partition in subdomain ϕ_i. Using the DG method of order zero and the projections as well as the notation introduced above, we write the semi-discrete problem of the OSWR algorithm (2.61)

as follows: at k^{th} iteration, we solve, for $m = 1, \ldots, M_i$ and $i = 1, \ldots, I$,

$$\begin{aligned}
&\phi_i \left(c_i^{k,m} - c_i^{k,m-1} \right) + \Delta t_m^i \operatorname{div} \boldsymbol{r}_i^{k,m} &&= \int_{J_m^i} f \, dt, && \text{in } \Omega_i, \\
&\Delta t_m^i \left(\nabla c_i^{k,m} + \boldsymbol{D}_i^{-1} \boldsymbol{r}_i^{k,m} \right) &&= 0, && \text{in } \Omega_i, \\
&\Delta t_m^i \left(-\boldsymbol{r}_i^{k,m} \cdot \boldsymbol{n}_i + \alpha_{i,j} c_i^{k,m} \right) && && \\
&\qquad = \int_{J_m^i} \Pi_{ij} \left(-\boldsymbol{r}_j^{k-1} \cdot \boldsymbol{n}_i + \alpha_{i,j} c_j^{k-1} \right) dt, && \text{on } \Gamma_{i,j}, \forall j \in \mathcal{N}_i, &&
\end{aligned} \tag{2.73}$$

where $c_i^{k,m} := c_{i|J_m^i}^k$, $\boldsymbol{r}_i^{k,m} := \boldsymbol{r}_{i|J_m^i}^k$, for $m = 1, \ldots, M_i$ and $i = 1, \ldots, I$. The third equation of (2.73) is obtained by performing Jacobi iterations for (2.72).

We show in the following theorem that as k tends to infinity the sequence of problem (2.73) converges to the solution of

$$\begin{aligned}
&\phi_i \left(c_i^m - c_i^{m-1} \right) + \Delta t_m^i \operatorname{div} \boldsymbol{r}_i^m \, dt &&= \int_{J_m^i} f \, dt, && \text{in } \Omega_i, \\
&\Delta t_m^i \left(\nabla c_i^m + \boldsymbol{D}_i^{-1} \boldsymbol{r}_i^m \right) &&= 0, && \text{in } \Omega_i, \\
&\Delta t_m^i \left(-\boldsymbol{r}_i^m \cdot \boldsymbol{n}_i + \alpha_{i,j} c_i^m \right) && && \\
&\qquad = \int_{J_m^i} \Pi_{ij} \left(-\boldsymbol{r}_j \cdot \boldsymbol{n}_i + \alpha_{i,j} c_j \right) dt, && \text{on } \Gamma_{i,j}, \forall j \in \mathcal{N}_i. &&
\end{aligned} \tag{2.74}$$

Theorem 2.18. *Assume that $\alpha_{i,j} = \alpha_{j,i}$ for $i = 1, \ldots, I$, $j \in \mathcal{N}_i$. Then*

1. *Problem* (2.74) *has a unique solution $(c_i, \boldsymbol{r}_i) \in P_0(\mathcal{T}_i; L^2(\Omega_i)) \times P_0(\mathcal{T}_i; \mathcal{H}(\operatorname{div}, \Omega_i))$, where $P_0(\mathcal{T}_i; W)$ is defined as in* (2.69) *for $W = L^2(\Omega_i)$ or $W = \mathcal{H}(\operatorname{div}, \Omega_i))$, $\forall i = 1, \ldots, I$.*

2. *Algorithm* (2.73)*, initialized by $(g_{i,j})$ in $P_0\left(\mathcal{T}_i; L^2\left(\Gamma_{i,j}\right)\right)$, $i = 1, \ldots, I$, $j \in \mathcal{N}_i$, defines a unique sequence of iterates*

$$(c_i^k, \boldsymbol{r}_i^k) \in P_0(\mathcal{T}_i; L^2(\Omega_i)) \times P_0(\mathcal{T}_i; \mathcal{H}(\operatorname{div}, \Omega_i)),$$

for $i = 1, \ldots, I$, that converges to the solution of problem (2.74).

Proof. The proof is carried out in several steps: we first derive the enery estimates as in the proof of Theorem 2.15, then we prove the convergence of algorithm (2.73); finally the well-posedness of problem (2.74) is shown.

As the equations are linear, we take $f = 0$ and $c_0 = 0$. We multiply the first and the second equations of (2.73) by $c_i^{k,m}$ and $\boldsymbol{r}_i^{k,m}$ respectively, integrate over ϕ_i then add two resulting equations and use (2.63) to obtain

$$\begin{aligned}
&(\phi_i c_i^{k,m}, c_i^{k,m})_{\Omega_i} - (\phi_i c_i^{k,m-1}, c_i^{k,m})_{\Omega_i} + \Delta t_m^i (\boldsymbol{D}_i^{-1} \boldsymbol{r}_i^{k,m}, \boldsymbol{r}_i^{k,m})_{\Omega_i} \\
&\qquad + \sum_{j \in \mathcal{N}_i} \Delta t_m^i \int_{\Gamma_{i,j}} \frac{1}{2\left(\alpha_{i,j} + \alpha_{j,i}\right)} \left(-\boldsymbol{r}_i^{k,m} \cdot \boldsymbol{n}_i - \alpha_{j,i} c_i^{k,m} \right)^2 \\
&\leq \sum_{j \in \mathcal{N}_i} \Delta t_m^i \int_{\Gamma_{i,j}} \frac{1}{2\left(\alpha_{i,j} + \alpha_{j,i}\right)} \left(-\boldsymbol{r}_i^{k,m} \cdot \boldsymbol{n}_i + \alpha_{i,j} c_i^{k,m} \right)^2 + \frac{\Delta t_m^i}{2} \int_{\Gamma_{i,j}} \left(\alpha_{j,i} - \alpha_{i,j} \right) \left(c_i^{k,m} \right)^2 ds.
\end{aligned} \tag{2.75}$$

Note that c_i^k and $\boldsymbol{r}_i^k$ are piecewise constant on each time interval J_m^i. Using the assumptions about ϕ and $\boldsymbol{D}$ and the inequality $a^2 - ab \geq \frac{1}{2}(a^2 - b^2)$ for the first two terms of (2.75), we obtain

$$\begin{aligned}\phi_- \left(\|c_i^{k,m}\|_{\Omega_i}^2 - \|c_i^{k,m-1}\|_{\Omega_i}^2 \right) + 2\delta_- \int_{J_m^i} \|\boldsymbol{r}_i^k(s)\|_{\Omega_i}^2 ds \\ + \sum_{j\in\mathcal{N}_i} \int_{J_m^i} \int_{\Gamma_{i,j}} \frac{1}{\alpha_{i,j}+\alpha_{j,i}} \left(-\boldsymbol{r}_i^k \cdot \boldsymbol{n}_i - \alpha_{j,i} c_i^k\right)^2 \\ \leq \sum_{j\in\mathcal{N}_i} \int_{J_m^i} \int_{\Gamma_{i,j}} \frac{1}{\left(\alpha_{i,j}+\alpha_{j,i}\right)} \left(-\boldsymbol{r}_i^k \cdot \boldsymbol{n}_i + \alpha_{i,j} c_i^k\right)^2 + \int_{J_m^i} \int_{\Gamma_{i,j}} \left(\alpha_{j,i} - \alpha_{i,j}\right) \left(c_i^k\right)^2 ds,\end{aligned} \tag{2.76}$$

for $i = 1, \ldots, I$, $m = 1, \ldots, M_i$.

Because of the global in time projection Π_{ij}, we can not use Gronwall's lemma as in the continuous case. Thus, we assume that $\alpha_{i,j} = \alpha_{j,i}$, $\forall i \in 1, \ldots, I$, $j \in \mathcal{N}_i$ to cancel the last term. Now summing (2.76) over the sub-intervals J_n^i in $(0, t_m^i]$, as $c_i^k(0) = 0$ we have

$$\begin{aligned}\phi_- \|c_i^{k,m}\|_{\Omega_i}^2 + 2\delta_- \int_0^{t_m^i} \|\boldsymbol{r}_i^k(s)\|_{\Omega_i}^2 ds + \sum_{j\in\mathcal{N}_i} \int_0^{t_m^i} \int_{\Gamma_{i,j}} \frac{1}{\alpha_{i,j}+\alpha_{j,i}} \left(-\boldsymbol{r}_i^k \cdot \boldsymbol{n}_i - \alpha_{j,i} c_i^k\right)^2 \\ \leq \sum_{j\in\mathcal{N}_i} \int_0^{t_m^i} \int_{\Gamma_{i,j}} \frac{1}{\left(\alpha_{i,j}+\alpha_{j,i}\right)} \left(-\boldsymbol{r}_i^k \cdot \boldsymbol{n}_i + \alpha_{i,j} c_i^k\right)^2.\end{aligned} \tag{2.77}$$

Substituting the third equation of (2.73) into (2.77) and as Π_{ij} is an L^2 projection we obtain

$$\begin{aligned}\phi_- \|c_i^{k,m}\|_{\Omega_i}^2 + 2\delta_- \int_0^{t_m^i} \|\boldsymbol{r}_i^k(s)\|_{\Omega_i}^2 ds + \sum_{j\in\mathcal{N}_i} \int_0^{t_m^i} \int_{\Gamma_{i,j}} \frac{1}{\alpha_{i,j}+\alpha_{j,i}} \left(-\boldsymbol{r}_i^k \cdot \boldsymbol{n}_i - \alpha_{j,i} c_i^k\right)^2 \\ \leq \sum_{j\in\mathcal{N}_i} \int_0^{t_m^i} \int_{\Gamma_{i,j}} \frac{1}{\alpha_{i,j}+\alpha_{j,i}} \left(\Pi_{ij}\left(-\boldsymbol{r}_j^{k-1} \cdot \boldsymbol{n}_i + \alpha_{i,j} c_j^{k-1}\right)\right)^2 \\ \leq \sum_{j\in\mathcal{N}_i} \int_0^{t_m^i} \int_{\Gamma_{i,j}} \frac{1}{\alpha_{i,j}+\alpha_{j,i}} \left(-\boldsymbol{r}_j^{k-1} \cdot \boldsymbol{n}_i + \alpha_{i,j} c_j^{k-1}\right)^2.\end{aligned}$$

Now we sum over all subdomains and define for $k \geq 1$

$$B_m^k = \sum_{i=1}^{I} \sum_{j\in\mathcal{N}_i} \int_0^{t_m^i} \int_{\Gamma_{i,j}} \frac{1}{\alpha_{i,j}+\alpha_{j,i}} \left(-\boldsymbol{r}_j^k \cdot \boldsymbol{n}_i + \alpha_{i,j} c_j^k\right)^2.$$

Then we have, for all $k > 0$,

$$\phi_- \|c_i^{k,m}\|_{\Omega_i}^2 + 2\delta_- \int_0^{t_m^i} \|\boldsymbol{r}_i^k(s)\|_{\Omega_i}^2 ds + B_m^k \leq B_m^{k-1}. \tag{2.78}$$

We sum over the iterates k to obtain that $\|c_i^{k,m}\|_{\Omega_i}^2$ and $\int_0^{t_m^i} \|\boldsymbol{r}_i^k(s)\|_{\Omega_i}^2 ds$ converge to 0 as $k \to \infty$ for $m = 1, \ldots, M_i$ and $i = 1, \ldots, I$.

Now we multiply the first equation of (2.73) by $\nabla \cdot \boldsymbol{r}_i^{k,m}$ and integrate over Ω_i to obtain

$$\begin{aligned} \Delta t_m^i \|\nabla \cdot \boldsymbol{r}_i^{k,m}\|_{\Omega_i}^2 &= -\left(\omega_i (c_i^{k,m} - c_i^{k,m-1}), \nabla \cdot \boldsymbol{r}_i^{k,m}\right)_{\Omega_i} \\ &\leq \omega_- \|c_i^{k,m} - c_i^{k,m-1}\|_{\Omega_i} \|\nabla \cdot \boldsymbol{r}_i^{k,m}\|_{\Omega_i}, \end{aligned} \tag{2.79}$$

which implies that $\|\nabla \cdot \boldsymbol{r}_i^{k,m}\|_{\Omega_i}$ converges to 0 as $k \to \infty$ for $m = 1, \ldots, M_i$ and $i = 1, \ldots, I$.

To prove the well-posedness of a solution to problem (2.74), one has to show only the uniqueness of the solution as (2.74) is a square discrete system. This is obtained by noting that (2.78) and (2.79) still hold without the superscript k. □

Remark 2.19. *The proof can be extended to higher order DG methods (see [62]) using a technique introduced in [87] to rewrite the DG formulation in another way with a reconstruction operator. Since only the lowest order DG method is considered here, a simpler proof without using such a technique was given.*

2.5 Numerical results

In this section, we carry out numerical experiments in 2D (using MATLAB) to investigate the performance of the two methods presented above. We consider $\boldsymbol{D} = d\boldsymbol{I}$ isotropic and constant on each subdomain, where $\boldsymbol{I}$ is the 2D identity matrix. Consequently, we may denote by d_i, the diffusion coefficient in the subdomains. For the spatial discretization, we use mixed finite elements with the lowest order Raviart-Thomas spaces on rectangles (for details about the subdomain solver, see Appendix B).

We consider in the first test problem (see Section 2.5.1) a homogeneous case with a decomposition into two subdomains. The convergence and asymptotic behaviors of the two methods will be studied. In the second test problem (see Section 2.5.2), we consider the two subdomain case with discontinuous coefficients. We vary the jumps in the diffusion coefficients and we see how it affects the convergence speed. We also analyze the behavior of the error versus the time steps in the nonconforming case. In the last test problem (see Section 2.5.3), suggested by ANDRA [1] as a first step towards repository simulations, we consider several subdomains. We observe how both methods handle this application with the strong heterogeneity and long time computations.

Remark 2.20. *The numerical results presented for Method 2 are done with optimized two-sided Robin parameters. We refer to Appendix A.2 for details of how to calculated these optimized parameters.*

Remark 2.21. *One iteration of Method 1 with the preconditioner costs twice as much as one iteration of Method 2 (in terms of number of subdomain solves). Thus to compare the convergence of the two methods with GMRES, in the sequel we show the error in the concentration c and the vector field $\boldsymbol{r}$ versus the number of subdomain solves (instead of the number of iterations).*

[1] The French agency for nuclear waste management

2.5.1 A test case with a homogeneous medium

The computational domain Ω is the unit square, and the final time is $T = 1$. The porosity is $\phi = 1$ and the diffusion coefficient $d = 0.02$. We split Ω into two nonoverlapping subdomains $\Omega_1 = (0, 0.5) \times (0, 1)$ and $\Omega_2 = (0.5, 1) \times (0, 1)$. For the spatial discretization, we use a uniform rectangular mesh with size $\Delta x = 1/200$. For the time discretization, we use conforming time grids with $\Delta t_1 = \Delta t_2 = 1/200$.

We consider the error equations, i.e. $f = 0$, $c_0 = 0$ and homogeneous boundary conditions, and use a random initial guess on the space-time interface. We stop the iteration when the errors (both in c and $\boldsymbol{r}$) are less than 10^{-6} as depicted in Figure 2.3 (left). We observe that the two methods work well and Method 1 converges very fast compared to Method 2. The errors in c (in red (Method 1) and blue (Method 2)) and the errors in $\boldsymbol{r}$ (in magenta (Method 1) and green (Method 2)) are in the same order of magnitude.

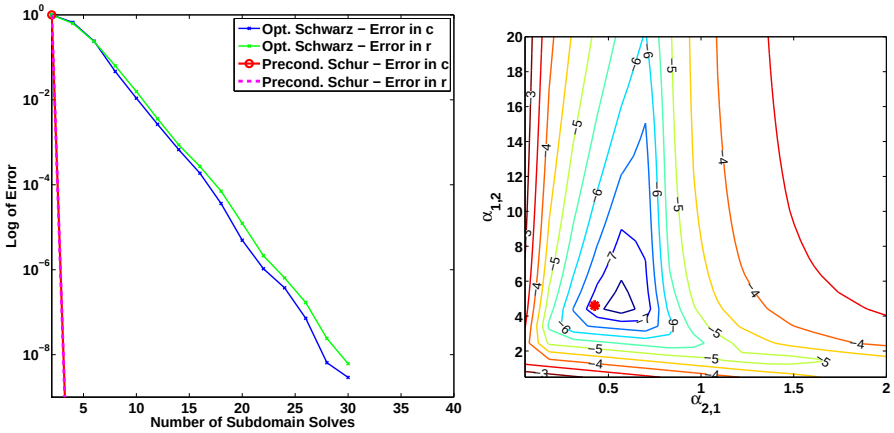

Figure 2.3: Left: Convergence curves with GMRES. Right: Level curves for the error in the vector field (in logarithmic scale) for various values of the parameters $\alpha_{1,2}$ and $\alpha_{2,1}$, where the red star shows the optimized parameters.

To verify the performance of the optimized parameters we vary $\alpha_{1,2}$ and $\alpha_{2,1}$ and plot the logarithmic scale of error in the concentration after 24 Jacobi iterations in Figure 2.3 (right). We see that the pair of optimized two-sided Robin parameters (the red star), computed by numerically minimizing the continuous convergence factor (see Appendix A.2.1), is located close to those giving the smallest error after the same number of iterations.

Table 2.1 shows the number of subdomain solves (for different algorithms) required to reach a reduction of 10^{-6} of the errors in the concentration and in the vector field (in square brackets) when refining the mesh in space and in time, with $\Delta x^2/\Delta t = \text{const}$. We observe that the convergence of Method 1 is independent of the mesh (due to the use of the preconditioner), while that of Method 2 is slightly dependent on the mesh. The latter is obtained because the optimization depends on the mesh size $h = \max h_i$ and the time step $\Delta t = \max \Delta t_i$ (see Appendix A), i.e. the optimized parameters serve in some sense as a preconditioner (see [12]). For Method 2, GMRES gives faster convergence speed than Jacobi but it does not improve the asymptotic results by a square root as it does in the case of elliptic problems [44]. This has been pointed out and analyzed in [98] and one should use the convolution Krylov subspace methods

[86] for dynamic systems to accelerate the convergence at the same degree as in the case of stationary problems [43] .

Δx	Δt	Method 1	Method 2	
		GMRES	GMRES	Jacobi
1/10	1/100	4 [4]	14 [15]	17 [18]
1/20	1/400	4 [4]	17 [18]	21 [23]
1/40	1/800	4 [4]	21 [22]	24 [27]
1/80	1/6400	4 [4]	25 [26]	28 [31]

Table 2.1: Number of subdomain solves needed to reach a reduction of 10^{-6} of the errors for different algorithms, and for different values of the discretization parameters Δx and Δt.

2.5.2 A test case with a heterogeneous medium

The computational domain Ω is again the unit square, and the final time is $T = 1$. We decompose Ω into 2 nonoverlapping subdomains as in Subsection 2.5.1. The porosity is $\phi_1 = \phi_2 = 1$, the diffusion coefficients are d_1 and d_2 in Ω_1 and Ω_2 respectively ($d_1 \neq d_2$). We fix $d_2 = 0.2$ and vary d_1 as shown in Table 2.2. We let $\mathfrak{D}$ denote the diffusion ratio d_2/d_1. For the spatial discretization, we use a uniform rectangular mesh with size $\Delta x_1 = \Delta x_2 = 1/200$. For the time discretization, we use nonconforming time grids with Δt_1 and Δt_2, given in Table 2.2, adapted to different diffusion ratios.

$\mathfrak{D}$	d_1	$1/\Delta t_1$	d_2	$1/\Delta t_2$
10	0.02	150	0.2	200
100	0.002	50	0.2	200
1000	0.0002	20	0.2	200

Table 2.2: Diffusion coefficients and corresponding nonconforming time steps.

As in the first test case, we analyze the convergence behavior of each method. We solve a problem with $c_0 = 0$ and $f = 0$ (thus $c = 0$ and $\boldsymbol{r} = 0$). We start with a random initial guess on the space-time interface and plot the error (in logarithmic scale) in the $L^2(0,T;L^2(\Omega))$-norm of the concentration c and the vector field $\boldsymbol{r}$, versus the number of subdomain solves. We stop the iteration when the errors (both in c and $\boldsymbol{r}$) are less than 10^{-6}. In Figure 2.4, the convergence of the two methods (with GMRES) for different diffusion ratios is shown. We see that both methods work well. Method 1 (Schur) converges faster than Method 2 (Schwarz) for small diffusion ratios $\mathfrak{D}$. However, when $\mathfrak{D}$ is increased, they are comparable. We also observe that the errors in c and $\boldsymbol{r}$ are nearly the same for Method 2 while the error in $\boldsymbol{r}$ is greater than the error in c for Method 1. Both methods handle the heterogeneities efficiently. To obtain such a good performance, we have used the following formula for calculating the weights in (2.54) (see [89])

$$\sigma_i = \left(\frac{d_i}{d_1 + d_2}\right)^2, \quad i = 1,2.$$

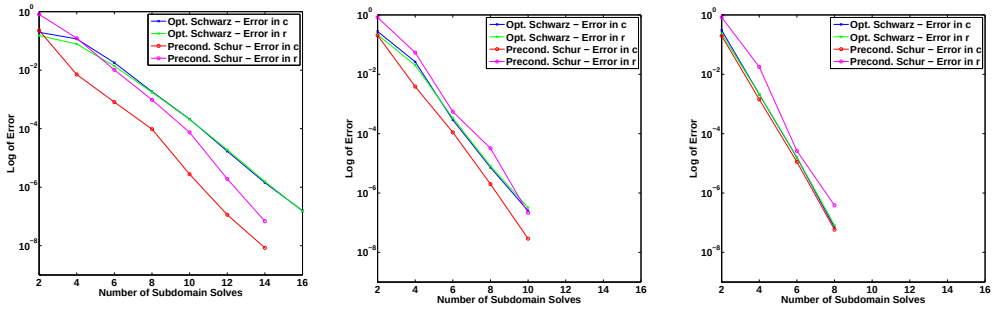

$\mathfrak{D} = 10$ $\mathfrak{D} = 100$ $\mathfrak{D} = 1000$

Figure 2.4: Convergence curves for different diffusion ratios: errors in c for Method 1 (red) and Method 2 (blue); errors in $\boldsymbol{r}$ for Method 1 (magenta) and Method 2 (green).

Consider now the case with $\mathfrak{D} = 10$. For Method 2, we vary Robin parameters $\alpha_{1,2}$ and $\alpha_{2,1}$ and plot the logarithmic scale of the residual after 20 Jacobi iterations in Figure 2.5. We again see that the pair of optimized Robin parameters (the red star) is located close to those giving the smallest residual after the same number of iterations.

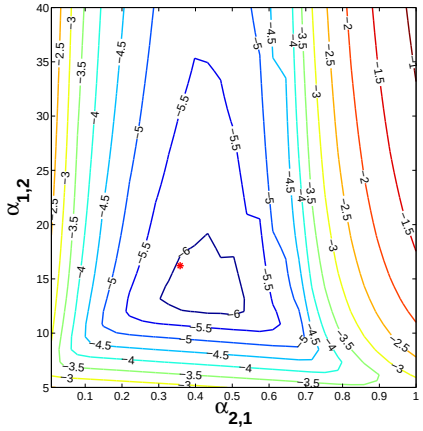

Figure 2.5: Level curves for the residual (in logarithmic scale) after 20 Jacobi iterations for various values of the parameters $\alpha_{1,2}$ and $\alpha_{2,1}$. The red star shows the optimized parameters computed by numerically minimizing the continuous convergence factor.

As in the first test case, we show in Table 2.3 the number of subdomain solves needed to reach a reduction of 10^{-6} of the errors in the concentration and in the vector field (in square brackets) when refining the mesh in space and in time, with $\Delta x^2/\Delta t =$ const. We observe that for discontinuous coefficients, the convergence of Method 1 is again independent of the mesh size while that of Method 2 is almost independent of the discretizations, especially when the diffusion ratio is large. Just as in the homogeneous case, for Method 2, GMRES does not improve either the convergence speed or the asymptotic results.

Next, we analyze the accuracy in time of the two methods with nonconforming time steps. We impose an inital condition $c_0 = \exp\left((x-0.55)^2 + 0.5(y-0.5)^2\right)$ together with a zero source term $f = 0$. We consider four initial time grids (for Δt_c and Δt_f

Δx	Δt	$\mathfrak{D} = 10$			$\mathfrak{D} = 100$		
		Method 1	Method 2		Method 1	Method 2	
		GMRES	GMRES	Jacobi	GMRES	GMRES	Jacobi
1/10	1/100	14 [14]	11 [11]	13 [12]	10 [10]	8 [9]	9 [10]
1/20	1/400	14 [14]	13 [13]	14 [14]	10 [12]	9 [9]	9 [9]
1/40	1/800	12 [14]	14 [14]	15 [16]	10 [10]	9 [9]	10 [10]
1/80	1/6400	12 [14]	15 [16]	16 [16]	10 [10]	10 [10]	10 [10]

Table 2.3: Number of subdomain solves needed to reach a reduction of 10^{-6} of the errors for different algorithms , and for different values of the discretization parameters Δx and Δt.

given), which we then refine several times by a factor of 2:

- Time grid 1 (fine-fine): conforming with $\Delta t_1 = \Delta t_2 = \Delta t_f$.
- Time grid 2 (coarse-fine): nonconforming with $\Delta t_1 = \Delta t_c$ and $\Delta t_2 = \Delta t_f$.
- Time grid 3 (fine-coarse): nonconforming with $\Delta t_1 = \Delta t_f$ and $\Delta t_2 = \Delta t_c$.
- Time grid 4 (coarse-coarse): conforming with $\Delta t_1 = \Delta t_2 = \Delta t_c$.

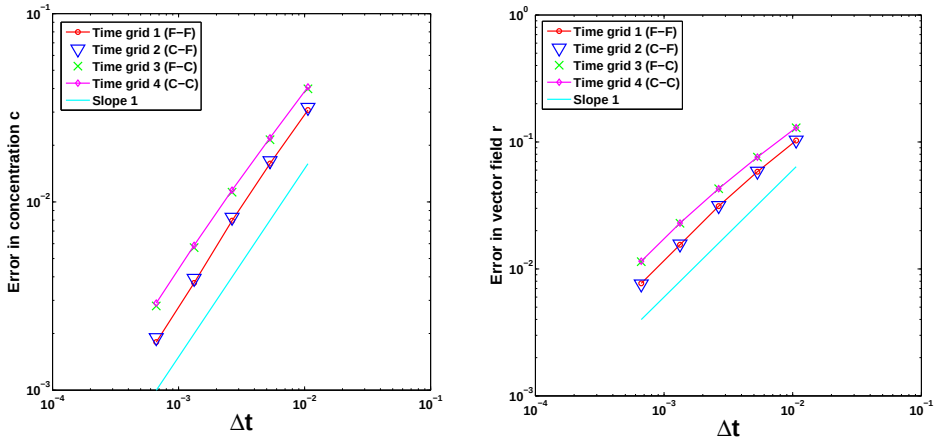

Figure 2.6: Errors in c (left) and $\boldsymbol{r}$ (right) in logarithmic scales between the reference and the multidomain solutions versus the time step for $\mathfrak{D} = 10$.

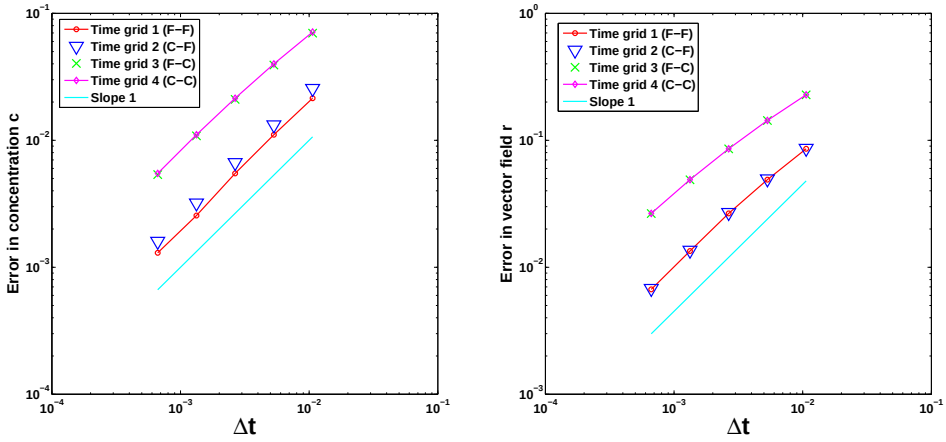

Figure 2.7: Errors in c (left) and $\boldsymbol{r}$ (right) in logarithmic scales between the reference and the multidomain solutions versus the time step for $\mathfrak{D} = 100$.

In space, we fix a conforming rectangular mesh and we compute a reference solution by solving problem (2.4) directly on a very fine time grid, with $\Delta t = \Delta t_f/2^6$. The converged multidomain solution is such that the relative residual is smaller than 10^{-11}. We show in Figures 2.6 and 2.7 the errors in the $L^2(0,T;L^2(\Omega))$-norms of the concentration c and the vector field $\boldsymbol{r}$ versus the time step $\Delta t = \max(\Delta t_c, \Delta t_f)$ for different diffusion ratios. We only give the results for Method 1 because the curves for Method 2 look exactly the same. For $\mathfrak{D} = 10$, we take $\Delta t_c = 1/94$ and $\Delta t_f = 1/128$; for $\mathfrak{D} = 100$, we take $\Delta t_c = 1/40$ and $\Delta t_f = 1/160$ (for $\mathfrak{D} = 1000$, the same results hold for $\Delta t_c = 1/16$ and $\Delta t_f = 1/160$ but we don't present them here). We first observe that first order convergence is preserved in the nonconforming case. Moreover, the errors obtained in the nonconforming case (Time grid 2, in blue) are nearly the same as in the finer conforming case (Time grid 1, in red). This means that nonconforming time grids preserve the accuracy in time of the solution and one should refine the time step where the solution varies most (i.e. where the diffusion coefficient is larger).

2.5.3 A porous medium test case

In this subsection, we consider a simplified version of a problem simulating contaminant transport in and around a nuclear waste repository site. The test case is described in Figure 2.8, where the repository is shown in red and the clay layer in yellow. The domain is a 3950m by 140m rectangle and the repository is a centrally located 2950m by 10m rectangle. The initial condition is $c_0 = 0$. We impose homogeneous Dirichlet conditions on top and bottom, and homogeneous Neumann conditions on the left and right hand sides. We decompose Ω into 9 subdomains as depicted in Figure 2.9 with Ω_5 representing the repository. The porosity is $\phi_5 = 0.2$ and $\phi_i = 0.05$, $i \neq 5$. The diffusion coefficients are $d_5 = 2\,10^{-9}$ m^2/s and $d_i = 5\,10^{-12}$ m^2/s, $i \neq 5$. So the diffusion ratio is $\mathfrak{D} = 400$.

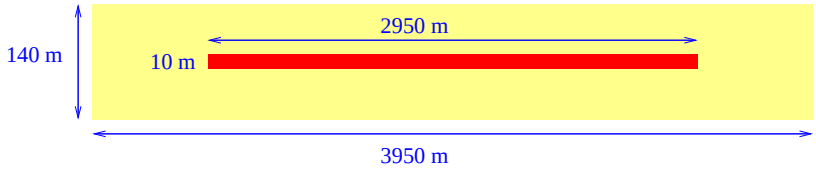

Figure 2.8: Geometry of the domain.

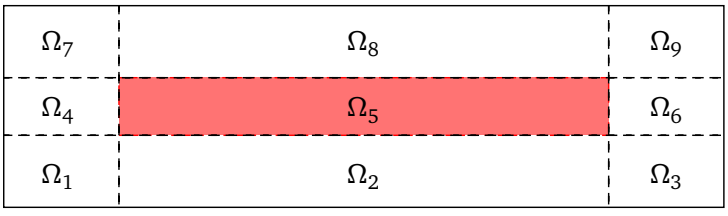

Figure 2.9: The decomposition into 9 subdomains (blow up in the y-direction).

For the spatial discretization, we use a non-uniform but conforming rectangular mesh with a finer discretization in the repository (a uniform mesh with 600 points in the x direction and 30 points in the y direction) and a coarser discretization in

the clay layer (the mesh size progressively increases with distance from the repository by a factor of 1.05). For the time discretization, we use nonconforming time grids with $\Delta t_5 = 2000$ years and $\Delta t_i = 10,000$ years, $i \neq 5$. For this application, we are interested in the long-term behavior of the repository, say over one million years. Thus, we test the performance of the two methods for a "short" time interval ($T = 200,000$ years) and for a longer time interval ($T = 1,000,000$ years). The same time steps, Δt_i, are used for both cases. As in the first test problem, we analyze the convergence results by solving a problem with $f = 0$. For Method 2, as we have a small, thin object embedded in a large area, it has been shown in [60, 75] that it is important to derive an adapted optimization for Robin parameters. Thus, we consider two different optimization techniques: the classical one (Opt. 1, see Appendix A.2.1) as used in the first test problem, and an adapted version (Opt. 2, see Appendix A.2.2) where we take into account the dimension of the subdomains.

In Figure 2.10 we compare the errors in the concentration c (on the left) and in the vector field $\boldsymbol{r}$ (on the right) both over a shorter time interval (on top) and over a longer time interval (on bottom) where GMRES is used in all cases as the iterative solver: Method 1 (red), Method 2 with Opt. 1 (blue) and Method 2 with Opt. 2 (green). They are comparable and perform well in the case of multiple subdomains. We also note that the longer the time interval, the larger the number of subdomain solves needed to converge to a given tolerance (here 10^{-6}). Thus, the use of time windows (see [17, 62]) could considerably improve the performance of all the algorithms, especially with an adapted choice of the initial guess on the interface based on the solution on the previous time window. In Figure 2.11, we plot the errors in the concentration c over different time intervals for Method 2: GMRES with Opt. 1 (continuous blue), GMRES with Opt. 2 (continuous green), Jacobi iteration with Opt. 1 (dashed blue) and Jacobi iteration with Opt. 2 (dashed green) (the errors in the vector field $\boldsymbol{r}$ behave similarly). We observe that GMRES converges faster than Jacobi iteration, especially for the long time interval. Further, with Jacobi iteration, unlike with GMRES, only Opt. 2 is able to handle the long time interval.

Next we consider the problem over the long time interval, $T = 1,000,000$ years, and with the source term defined as follows: $f = 0$ in the clay layer and

$$f = \begin{cases} 10^{-5}\,\mathrm{s}^{-1} & \text{if } t \leq 10^5 \text{ years}, \\ 0 & \text{if } t > 10^5 \text{ years}, \end{cases} \qquad \text{in the repository.} \tag{2.80}$$

The discretizations in space and in time (nonconforming) are the same as above. We verify the performance of Method 1 and Method 2 (with Opt. 2) using GMRES and zero initial guess on the space-time interfaces. The tolerance of the iteration is 10^{-6}. In Figure 2.12, the evolution of the solution at different times is depicted (both methods give similar results). As time goes on and under the effect of diffusion, the contaminant slowly migrates from the repository to the surrounding area. Moreover, its concentration c increases until injection stops (i.e. after 100,000 years) and then decreases. In Figure 2.13 the relative residuals for each method versus the number of subdomain solves are shown, as the monodomain solution with nonconforming grids is unknown. Both methods work well and we observe that Method 1 converges linearly while Method 2 initially converges extremely rapidly, the convergence becoming linear after the first few iterations.

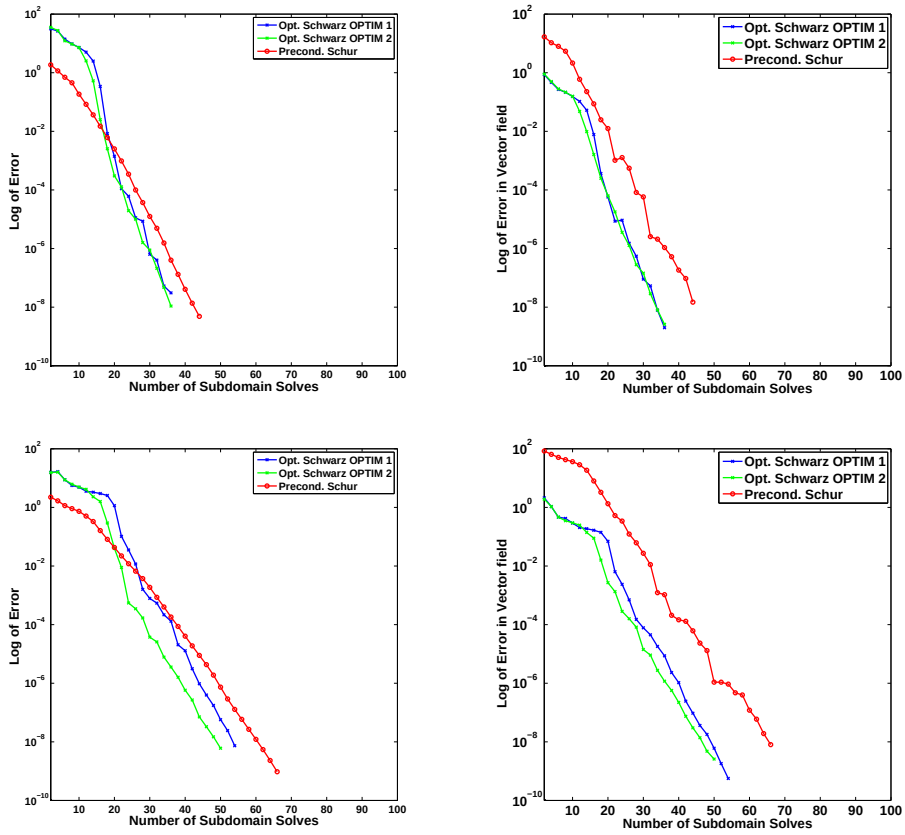

Figure 2.10: Convergence curves for different time intervals with GMRES: error in c (on the left) and error in $\boldsymbol{r}$ (on the right), for short time $T = 200,000$ years (on top) and for long time $T = 1,000,000$ years (on bottom).

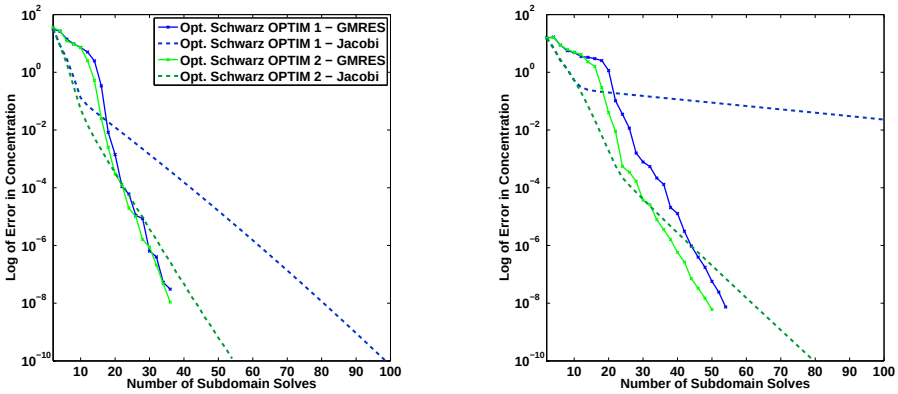

Figure 2.11: Convergence curves for Method 2 using GMRES and Jacobi iteration: for short time $T = 200,000$ years (on the left) and for long time $T = 1,000,000$ years (on the right).

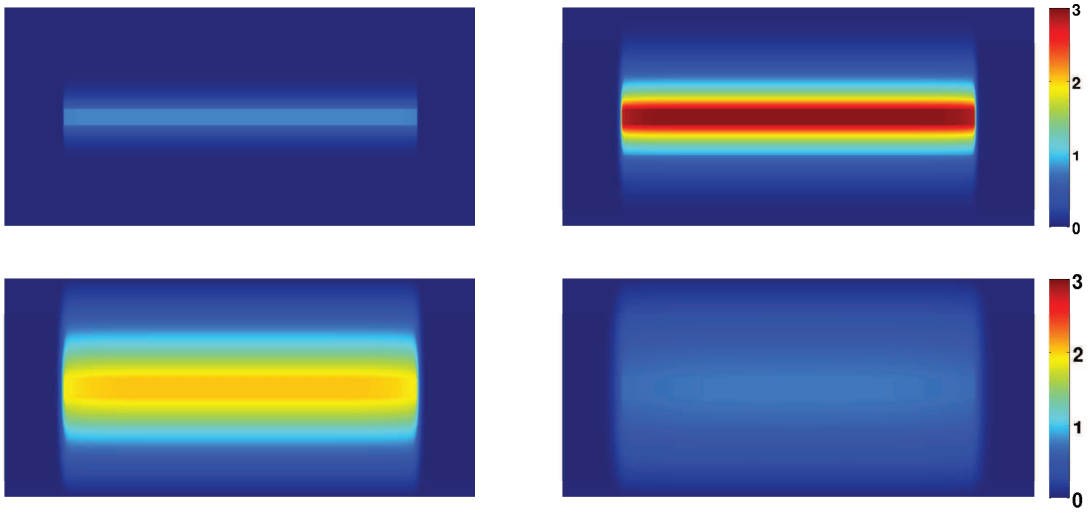

Figure 2.12: Snapshots of the multidomain solution after 20,000 years (top left), 100 000 years (top right), 200 000 years (bottom left), and 1,000,000 years (bottom right), with a blow up in the y-direction.

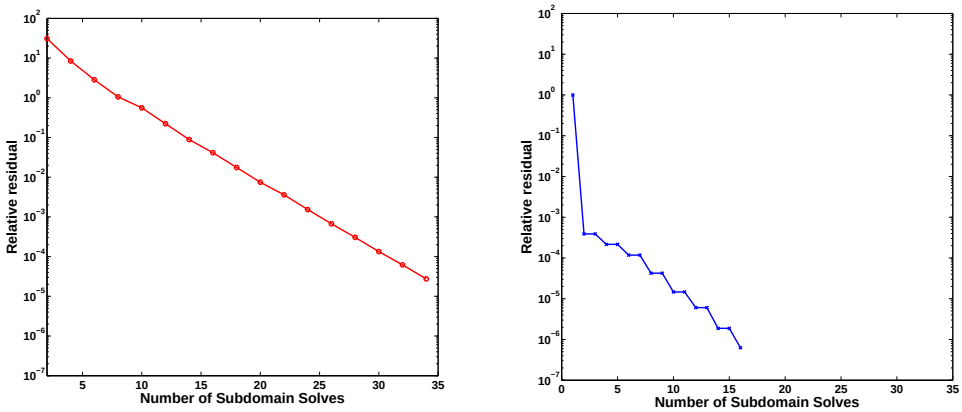

Figure 2.13: The relative residuals in logarithmic scales using GMRES for Method 1 (on the left) and Method 2 (with Opt. 2) (on the right).

Conclusion

We have given mixed formulations for two different interface problems for the diffusion equation, one using the time-dependent Steklov-Poincaré operator and the other using OSWR with Robin transmission conditions on the space-time interfaces between subdomains. The subdomain problems with Dirichlet and Robin boundary conditions are proved to be well-posed. Nonconforming time grids are considered and a suitable projection in time is employed to exchange information between subdomains on the space-time interface. Convergence proofs of the continuous and semi-discrete OSWR algorithms in mixed form are given. Numerical results for 2D problems using mixed finite elements (with the lowest order Raviart-Thomas spaces on rectangles) for discretization in space and the lowest order discontinuous Galerkin method for discretization in time are presented. We have analyzed numerically the performance of the two methods for three test cases, the first two are academic with two subdomains and the last one is more realistic with several subdomains. We have observed that Method 1 (with the Neumann-Neumann preconditioner and averaging weights) and Method 2 (with optimized Robin parameters) handle well the heterogeneity and nonconforming time grids, both efficiently preserving the accuracy in time of the solution. Asymptotically, their convergence is almost independent of the discretizations. The two methods are also well-adapted for the simulation of diffusive contaminant transport in and around a repository with a special geometry and long time computations. In particular, for Method 2 we have shown that an adapted optimization technique to compute the optimized parameters is necessary if Jacobi iteration is used. We have pointed out the possible advantage for efficiency of using time windows for problems with long time intervals. This will be considered in the next chapter.

Chapter 3

Space-time domain decomposition for advection-diffusion problems

Contents

3.1 A model problem and operator splitting 54

3.2 Domain decomposition with operator splitting 56

3.2.1 Method 1: An extension of the time-dependent Steklov-Poincaré operator approach 60

3.2.2 Method 2: An extension of the Optimized Schwarz Waveform Relaxation approach 64

3.3 Nonconforming time discretizations 67

3.4 Numerical results 69

3.4.1 Test case 1: Piecewise constant coefficients 69

3.4.2 Test case 2: Rotating velocity 77

3.4.3 Test case 3: A near-field simulation 79

3.4.4 Test case 4: A simulation for a surface, nuclear waste storage . . . 85

In this chapter, we present extensions of the two methods introduced in the previous chapter to the coupled advection-diffusion problem. We use operator splitting to treat differently the advection equation and the diffusion equation: the former is approximated with the explicit Euler method in time and with an upwind, cell-centered finite volume method in space, while the latter is approximated with the implicit Euler method in time and with a mixed finite element method in space. This chapter consists of two main parts. In the first part, we derive the discrete multidomain problem in operator splitting context and define two discrete, interface problems, extensions of the methods, Method 1 and Method 2, analyzed in Chapter 2. For Method 1, a generalized Neumann-Neumann preconditioner is given. We describe how we handle the nonconforming time grids (for advection and diffusion time steps) using the L^2 projection defined in Chapter 2. In the second part, we carry out numerical experiments for various test cases, both academic and more realistic prototypes for nuclear waste disposal simulation, to investigate and compare the behavior of the two methods.

3.1 A model problem and operator splitting

In this section, we define our model problem and the corresponding discrete problem. For an open, bounded domain Ω of $\mathbb{R}^d$ $(d = 2,3)$ with Lipschitz boundary $\partial\Omega$ and some fixed time $T > 0$, consider the linear advection-diffusion problem written in mixed form:

$$\begin{aligned} \phi\,\partial_t c + \operatorname{div}(\boldsymbol{u}c + \boldsymbol{r}) &= f \quad \text{in } \Omega \times (0,T), \\ \nabla c + \boldsymbol{D}^{-1}\boldsymbol{r} &= 0 \quad \text{in } \Omega \times (0,T), \\ c &= 0 \quad \text{on } \partial\Omega \times (0,T), \\ c(\cdot,0) &= c_0 \quad \text{in } \Omega. \end{aligned} \tag{3.1}$$

Recall (see Chapter 1) that c is the concentration of a contaminant dissolved in a fluid, f the source term, ϕ the porosity, $\boldsymbol{u}$ the Darcy velocity (assumed to be given and time-independent) and $\boldsymbol{D}$ a symmetric time independent diffusion tensor. For simplicity, we have imposed homogeneous Dirichlet boundary conditions. The analysis presented in the following can be generalized to other types of boundary conditions.

One of the advantages of the time splitting approach [68] is that one can use different numerical time schemes for the advection and diffusion. It has been shown that treating the advection explicitly can significantly reduce the numerical diffusion (see, e.g., [27]). In the sequel, we use a first-order in time splitting method for solving problem (3.1): the advection equation is approximated by the forward Euler method and the diffusion equation by the backward Euler method. The resulting scheme is first-order accurate in time, $O(\Delta t)$ (see, e.g., [29], [6, Chapter 2, p.14–32]). In the context of local mass conservative approximations, we consider an upwind, cell-centered finite volume method for the advection equation, and a mixed finite element method for the diffusion equation.

In the following, we write the fully discrete problem associated with such discretization techniques. For that purpose, we first introduce the discretizations in space and in time.

Let $\mathscr{K}_h$ be a finite element partition of Ω into rectangles for simplicity, we suppose $\Omega \subset \mathbb{R}^2$). We use the lowest order Raviart-Thomas (or Nédélec in three dimensions) mixed finite element spaces $M_h \times \Sigma_h \subset L^2(\Omega) \times H(\operatorname{div},\Omega)$ (see, e.g., [22, 104] and Appendix B). For $\Omega \subset \mathbb{R}^2$ and for rectangular elements, these spaces have the form

$$\begin{aligned} M_h &= \left\{\mu \in L^2(\Omega) : \mu_{|K} = \text{const}, K \in \mathscr{K}_h\right\}, \\ \Sigma_h &= \left\{\boldsymbol{v} \in H(\operatorname{div},\Omega) : \boldsymbol{v}_{|K} = \left(a_K + b_K x, c_K + d_K y\right), (a_K, b_K, c_K, d_K) \in \mathbb{R}^4, K \in \mathscr{K}_h\right\}. \end{aligned}$$

The degrees of freedom of $c_h \in M_h$ correspond to the average values of c_h on the elements $K \in \mathscr{K}_h$, and those of $\boldsymbol{r}_h$ correspond to the values of the flux $\boldsymbol{r}_h \cdot \boldsymbol{n}_E$ across the edges E of K, where $\boldsymbol{n}_E$ is a previously chosen unit normal vector to E.

For the time discretization (see Figure 3.1), we consider, for simplicity, a uniform partition of $(0,T)$ into N subintervals $\left(t^n, t^{n+1}\right)$ with length $\Delta t = t^{n+1} - t^n$ for $n = 0,\ldots,N-1$ with $t^0 = 0$ and $t^N = T$ (the derivation can be easily generalized to the case of nonuniform partitions). In order to satisfy the CFL condition required for the explicit scheme used for the advection equation without imposing that condition on the diffusion equation, we consider sub-time steps for the advection part:

$$\Delta t_a = \Delta t / L, \text{ for some } L \geq 1,$$

and

$$t^{n,l} = l\Delta t_a + t^n, \text{ for } l = 0,\dots,L,\ n = 0,\dots,N-1.$$

Note that $t^{n,0} = t^n$ and $t^{n,L} = t^{n+1}$.

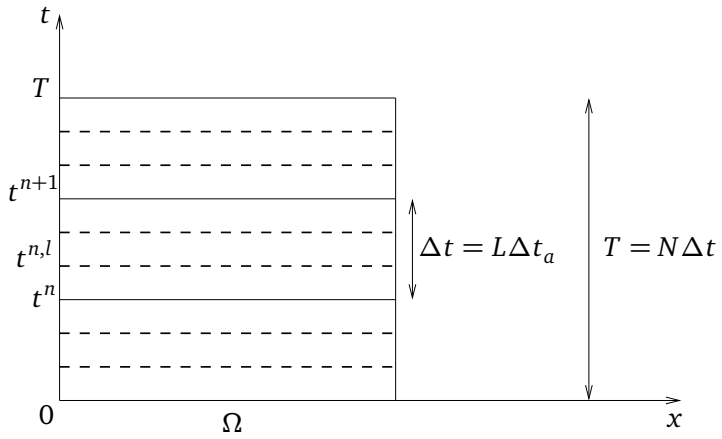

Figure 3.1: A uniform partition in time with different time steps for advection and diffusion.

The operator splitting algorithm is initialized by defining c_h^0 to be the L^2 projection of c_0 onto M_h:

$$c_{h|K}^0 := \frac{1}{\text{meas}(K)} \int_K c_0,\ \forall K \in \mathscr{K}_h.$$

(For convenience of notation, we also write $c_h^{0,0}$ for c_h^0).

Using the advection equation, we calculate $c_h^{n,l}$, the approximation of $c(t^{n,l})$, for $n = 0,\dots,N-1$, $l = 1,\dots,L$ and then using the diffusion equation we calculate c_h^{n+1} and $\boldsymbol{r}_h^{n+1}$, approximations of $c(t^{n+1})$ and $\boldsymbol{r}(t^{n+1})$ respectively, for $n = 0,\dots,N-1$.

As we use an upwind scheme for the advection equation, to calculate $c_h^{n,l+1}$ for $n = 0,\dots,N-1$, $l = 0,\dots,L-1$, in addition to the value $c_h^{n,l}$, we will need an upwind value $\hat{c}_h^{n,l}$ of the concentration on each edge of the grid. This upwind value is defined by

$$\left(\hat{c}_h^{n,l}\right)_{|E} = \begin{cases} \bullet \text{ the given Dirichlet boundary data (in our case 0) if } E \text{ is on the boundary } \partial\Omega \text{ and the average value of } \boldsymbol{u}\cdot\boldsymbol{n}_\Omega \text{ over } E \text{ is negative (i.e., fluid entering } \Omega \text{ through } E), \text{ where } \boldsymbol{n}_\Omega \text{ is the outward normal to } \partial\Omega, \\ \bullet \text{ the value of } c_h^{n,l} \text{ on } K \text{ if } E \text{ is an edge of } K \text{ and the average value of } \boldsymbol{u}\cdot\boldsymbol{n}_K \text{ over } E \text{ is nonnegative (fluid exiting } K \text{ through } E), \text{ where } \boldsymbol{n}_K \text{ is the outward normal to } \partial K. \\ \text{(Note that if the average value of } \boldsymbol{u}\cdot\boldsymbol{n}_K \text{ over } E \text{ is 0, it makes no difference which of the neighboring value is assigned).} \end{cases} \tag{3.2}$$

In Figure 3.2, we show some examples where the upwind value is defined specifically.

The operator splitting algorithm is defined by:

For given $c_h^n \in M_h$, first solve the advection equation, for $l = 0, \ldots, L-1$:

$$\int_K \phi \frac{c_h^{n,l+1} - c_h^{n,l}}{\Delta t_a} + \sum_{E \subset \partial K} \int_E \hat{c}_h^{n,l} \left(\boldsymbol{u} \cdot \boldsymbol{n}_K\right) = 0, \quad \forall K \in \mathscr{K}_h. \tag{3.3}$$

The solution generated after these L advection steps is $c_h^{n,L}$.

Next, we solve the diffusion equation (recall that the test functions for the first equation are just linear combinations of the characteristic functions on the elements $K \in \mathscr{K}_h$):

$$\begin{aligned} \int_K \phi \frac{c_h^{n+1} - c_h^{n,L}}{\Delta t} + \int_K \operatorname{div} \boldsymbol{r}_h^{n+1} &= \int_K f(t^{n+1}), \quad \forall K \in \mathscr{K}_h, \\ \int_\Omega \boldsymbol{D}^{-1} \boldsymbol{r}_h^{n+1} \cdot \boldsymbol{v} - \int_\Omega c_h^{n+1} \operatorname{div} \boldsymbol{v} &= 0, \qquad \forall \boldsymbol{v} \in \Sigma_h, \end{aligned} \tag{3.4}$$

The solution generated at this step is $\left(c_h^{n+1}, \boldsymbol{r}_h^{n+1}\right)$.

Thus, we end up with the algorithm as follows:

For $n = 0, \ldots, N-1$,

1. define $c_h^{n,0} = c_h^n$, where $c_{h|K}^0 := \dfrac{1}{\operatorname{meas}(K)} \displaystyle\int_K c_0, \ \forall K \in \mathscr{K}_h$,
2. for $l = 0, \ldots, L-1$,
   (a) define the upwind value $\hat{c}_h^{n,l}$ (cf. (3.2)),
   (b) solve the advection equation (3.3) with $c_h^{n,l}$ and obtain $c_h^{n,l+1}$,
3. solve the diffusion equation (3.4) with $c_h^{n,L}$ and obtain c_h^{n+1} and $\boldsymbol{r}_h^{n+1}$.

Remark 3.1. *Due to the upwind scheme, for the advection equation, we need to impose Dirichlet conditions only on the inflow boundary of Ω (i.e. where the fluid enters Ω).*

In the next section, we consider the domain decomposition approach for solving problem (3.3)-(3.4). An equivalent multidomain problem adapted to the splitting approach will be formulated and from that we will derive two global-in-time domain decomposition methods.

3.2 Domain decomposition with operator splitting

For simplicity, we consider a conforming decomposition of Ω into two non-overlapping subdomains Ω_1 and Ω_2 (the analysis can be generalized to the case of many subdomains). Note that the partition $\mathscr{K}_{h,i}$ of subdomain Ω_i, $i = 1, 2$, is a subset of $\mathscr{K}_h$. We denote by $\Gamma := \partial\Omega_1 \cap \partial\Omega_2$ the interface between the subdomains, and denote by $\mathscr{G}_h$ the set of edges (or faces) of elements of $\mathscr{K}_h$ that lie on Γ. For $i = 1, 2$, let $\boldsymbol{n}_i$ denote the unit outward pointing vector field on $\partial\Omega_i$, and for any scalar, vector or tensor valued function ψ defined on Ω, let ψ_i denote the restriction of ψ to Ω_i.

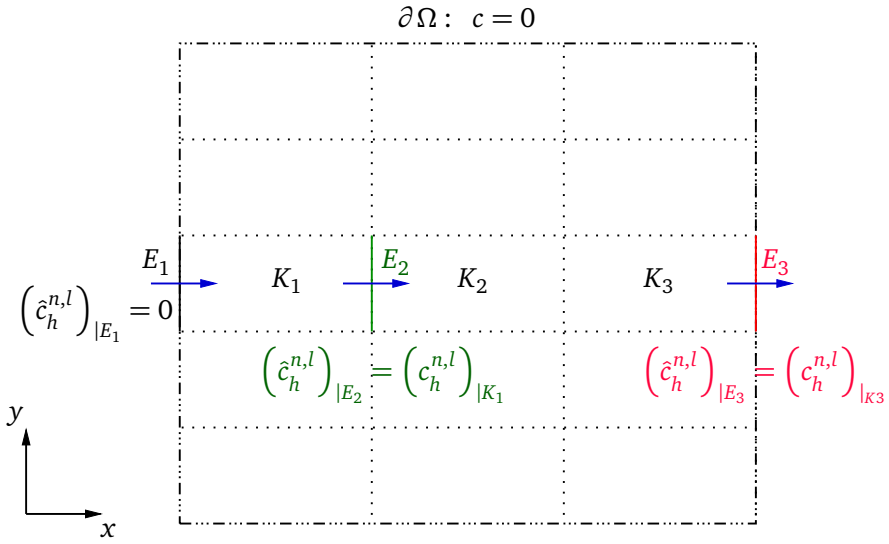

Figure 3.2: An illustration of the upwind concentration defined in the context of cell-centered finite volumes, the arrows represent the direction of the normal flux across the edges, $\int_E \boldsymbol{u}\cdot\boldsymbol{n}$, with $\boldsymbol{n} = (1,0)$.

As noted in Remark 3.1 only the inflow boundary (not the whole boundary) is important for an upwind scheme, we then define the set of the inflow boundary edges on the interface for each subdomain:

$$\mathscr{G}_{h,i}^{\text{in}} := \left\{ E \in \mathscr{G}_h : \int_E \boldsymbol{u}_i \cdot \boldsymbol{n}_i < 0 \right\}, \ \text{for } i = 1,2.$$

Thus

$$\mathscr{G}_{h,1}^{\text{in}} \cap \mathscr{G}_{h,2}^{\text{in}} = \emptyset, \ \text{and} \ \mathscr{G}_{h,1}^{\text{in}} \cup \mathscr{G}_{h,2}^{\text{in}} = \mathscr{G}_h.$$

Since we have split apart advection equation and diffusion equation, and treat them with different numerical schemes, it is natural to have separate transmission conditions for the advection part and for the diffusion part when domain decomposition is used. In the following, we will write the advection and diffusion equations associated with each subdomain Ω_i, and derive the transmission conditions on the space-time interface which are needed to obtain a formulation equivalent to the monodomain problem (3.3)-(3.4).

With this aim, we denote by $M_{h,i}$ and $\Sigma_{h,i}$, $i = 1,2$, the restrictions of the mixed finite element spaces M_h to Ω_i and Σ_h to Ω_i respectively. To define the transmission conditions, we introduce the following interface space

$$\Lambda_h := \left\{ \lambda \in L^2(\Gamma) : \lambda_{|E} = \text{const}, \ \forall E \in \mathscr{G}_h \right\}.$$

Because conforming discretization in space is used, we have

$$\Lambda_h = \Sigma_{h,i} \cdot \boldsymbol{n}_i \,|_\Gamma, \ i = 1,2.$$

Now, for $i = 1,2$, and for given $c_{h,i}^n$, the advection equation in Ω_i is defined for $l = 0, \ldots, L-1$, by

$$\int_K \phi_i \frac{c_{h,i}^{n,l+1} - c_{h,i}^{n,l}}{\Delta t_a} + \sum_{E \subset \partial K} \int_E \hat{c}_{h,i}^{n,l} (\boldsymbol{u}\cdot\boldsymbol{n}_K) \quad = 0, \quad \forall K \in \mathscr{K}_{h,i}, \tag{3.5}$$

with $c_{h,i}^{n,0} = c_{h,i}^{n}$.

Because of the decomposition, the upwind value of $c_{h,i}^{n,l}$ on edges on the interface Γ may not depend only on the element values $c_{h,i}^{n,l}$ inside subdomain Ω_i. In particular, if $\mathscr{G}_{h,i}^{\text{in}} \neq \emptyset$ (i.e. there is fluid flowing in Ω_i through some part of Γ), then the upwind concentration $\hat{c}_{h,i}^{n,l}$ on the edge $E \in \mathscr{G}_{h,i}^{\text{in}}$ is defined by the concentration value of the element in the neighboring subdomain (see Figure 3.3):

$$\left(\hat{c}_{h,i}^{n,l}\right)_{|E} = \left(c_{h,j}^{n,l}\right)_{|K_E}, \ \forall E \in \mathscr{G}_{h,i}^{\text{in}}, \tag{3.6}$$

where K_E necessarily in $\mathscr{K}_{h,j}$, $j = 3 - i$, is the element has E as an edge.

Equation (3.6) serves as a Dirichlet boundary condition on $E \in \mathscr{G}_{h,i}^{\text{in}}$ and it defines the transmission condition for the advection equation.

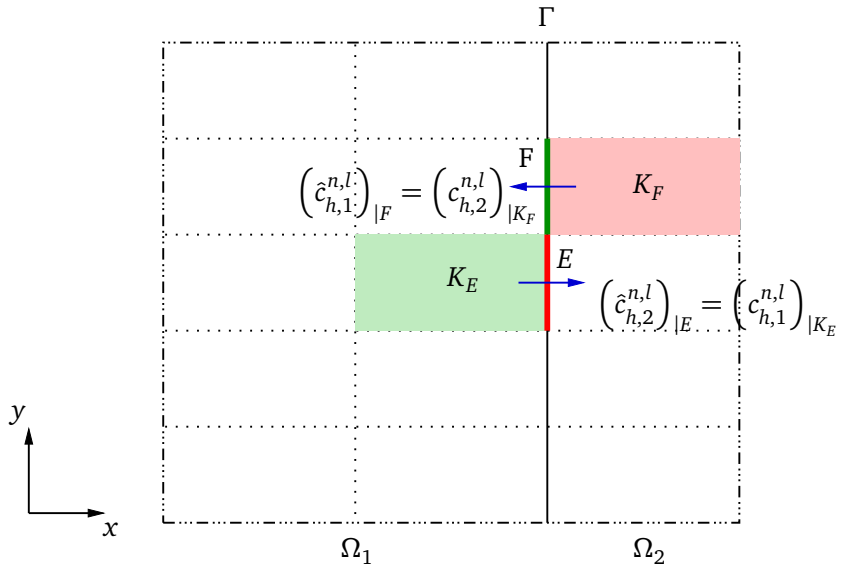

Figure 3.3: An illustration of the upwind concentration in the context of domain decomposition, the arrows represent the direction of the normal flux across the edges (for a fixed normal vector $\boldsymbol{n} = (1, 0)$).

Now for the diffusion equation, with data $c_{h,i}^{n,L}$ generated by the advection step, we solve:

$$\begin{aligned} \int_K \phi_i \frac{c_{h,i}^{n+1} - c_{h,i}^{n,L}}{\Delta t} + \int_K \operatorname{div} \boldsymbol{r}_{h,i}^{n+1} &= \int_K f(t^{n+1}), \quad \forall K \in \mathscr{K}_{h,i}, \\ \int_{\Omega_i} \boldsymbol{D}_i^{-1} \boldsymbol{r}_{h,i}^{n+1} \cdot \boldsymbol{v} - \int_{\Omega_i} c_{h,i}^{n+1} \operatorname{div} \boldsymbol{v} - \int_\Gamma \lambda_{h,i}^{n+1} (\boldsymbol{v} \cdot \boldsymbol{n}) &= 0, \qquad \forall \boldsymbol{v} \in \Sigma_{h,i}, \end{aligned} \tag{3.7}$$

where $\lambda_{h,i}^{n+1} \in \Lambda_h$, $i = 1, 2$, is the Lagrange multiplier (see, e.g., [22, 104]) representing "the trace" of the concentration $c_{h,i}^{n+1}$ on the interface Γ. We need to introduce $\lambda_{h,i}$ since the concentration approximation $c_{h,i}$ is defined on the elements only (this is of course not the case if one considers the continuous problem (see Chapter 2)).

As in the pure diffusion problem (cf. Chapter 2), the transmission conditions for the diffusion equation consist of the equality between the concentration and the conservation of the normal diffusive flux across the interface:

$$\begin{aligned} \int_E \lambda_{h,1}^{n+1} &= \int_E \lambda_{h,2}^{n+1}, \\ \int_E \left(\boldsymbol{r}_{h,1}^{n+1} \cdot \boldsymbol{n}_1 + \boldsymbol{r}_{h,2}^{n+1} \cdot \boldsymbol{n}_2 \right) &= 0, \end{aligned} \qquad \forall E \in \mathscr{G}_h. \tag{3.8}$$

The multidomain problem is defined by

For $n = 0, \ldots, N-1$,

1. for $i = 1, 2$, define $c_{h,i}^{n,0} = c_{h,i}^n$, where $\left(c_{h,i}^0\right)_{|K} := \dfrac{1}{\text{meas}(K)} \displaystyle\int_K c_0, \ \forall K \in \mathscr{K}_{h,i}$,
2. for $l = 0, \ldots, L-1$,
   (a) define the upwind concentration $\hat{c}_{h,i}^{n,l}$, $i = 1, 2$, in each subdomain using the transmission condition (3.6),
   (b) solve the advection equation (3.5) in each subdomain with $c_{h,i}^{n,0}$ known and obtain $c_{h,i}^{n,L}$, $i = 1, 2$,
3. solve the diffusion equation (3.7) in each subdomain together with the transmission conditions (3.8), with $c_{h,i}^{n,L}$ known and obtain $c_{h,i}^{n+1}$ and $\boldsymbol{r}_{h,i}^{n+1}$ for $i = 1, 2$.

To show the equivalence between this multidomain problem and the monodomain problem (3.3)-(3.4) is straightforward.

Alternatively, and equivalently to (3.8), one may impose Robin transmission conditions (for the diffusion equation), for all $E \in \mathscr{G}_h$ and $n = 0, \ldots, N-1$:

$$\begin{aligned} \int_E \left(-\boldsymbol{r}_{h,1}^{n+1} \cdot \boldsymbol{n}_1 + \alpha_{1,2} \lambda_{h,1}^{n+1} \right) &= \int_E \left(-\boldsymbol{r}_{h,2}^{n+1} \cdot \boldsymbol{n}_1 + \alpha_{1,2} \lambda_{h,2}^{n+1} \right), \\ \int_E \left(-\boldsymbol{r}_{h,2}^{n+1} \cdot \boldsymbol{n}_2 + \alpha_{2,1} \lambda_{h,2}^{n+1} \right) &= \int_E \left(-\boldsymbol{r}_{h,1}^{n+1} \cdot \boldsymbol{n}_2 + \alpha_{2,1} \lambda_{h,1}^{n+1} \right), \end{aligned} \tag{3.9}$$

where $\alpha_{1,2}$ and $\alpha_{2,1}$ are two positive constants. The first method that we consider is based on (3.5), (3.7) together with the "natural" transmission conditions (3.6), (3.8) while the second method is based on (3.5), (3.7) together with Robin transmission conditions (3.6), (3.9). For both methods the multidomain problem is formulated as a problem posed on the space-time interface via the use of interface operators.

Remark 3.2. *As pointed out above, with the upwind scheme, the solution of the advection equation in a subdomain depends not only on the information in the subdomain and on its boundary, but also on information coming from the neighboring subdomain, while for the diffusion equation the solution is local to the subdomain as in the pure diffusion case. However, since we use operator splitting, we do not need to be concerned about the problem of a slow convergence of the OSWR algorithm as has been observed when a fully implicit scheme and an upwind scheme for the advection are used [57]. With operator splitting we obtain separate transmission conditions for the advection part and for the*

diffusion part. In fact, we observe numerically (see Section 3.4) that the convergence is governed by the Robin transmission conditions associated with the diffusion equation and the optimized Robin parameters significantly improve the convergence of the algorithm (for both advection-dominated and diffusion-dominated problems). In our observations, the advection plays no role in the rate of convergence.

Remark 3.3. *As the advection and the diffusion equations are treated separately, the formulations of the diffusion equation corresponding to Method 1 and Method 2 will be derived just as in Chapter 2. The formulation for the advection equation will be the same for both methods.*

In the multidomain context, the formulation of the advection step can be expressed more simply by defining an upwind operator $\mathscr{U}_{h,i}$, $i = 1, 2$, which associates to a set of concentration values on each element of $\mathscr{K}_{h,i}$ and on each edge of $\mathscr{G}_h$, a value on each edge of an element of $K \in \mathscr{K}_{h,i}$. These latter values will be the upwind values. So if we denote by $\mathscr{E}_{h,i}$ the set of edges of elements of $\mathscr{K}_{h,i}$ and by $N_{h,i}$ the space of functions on the union of the edges in $\mathscr{E}_{h,i}$ that are constant on each edge, we may define $\mathscr{U}_{h,i}$ as follows

$$\mathscr{U}_{h,i} : M_{h,i} \times \Lambda_h \to N_{h,i}$$

$$\left(\mathscr{U}_{h,i}\right)_{|_E} = \begin{cases} 0 & \text{if } E \subset \left(\partial\Omega_i \cap \Omega\right) \text{ and the average value of } \boldsymbol{u}\cdot\boldsymbol{n}_i \text{ over } E \\ & \text{is negative,} \\ \left(c_{h,j}\right)_{|K} & \text{if } E \in \mathscr{G}_{h,i}^{\text{in}} \text{ where } K \text{ is the element in } \mathscr{K}_{h,j} \text{ having } E \text{ as an} \\ & \text{edge, for } j = 3 - i, \\ \left(c_{h,i}\right)_{|K} & \text{otherwise, where } K \text{ is the element in } \mathscr{K}_{h,i} \text{ having } E \text{ as an} \\ & \text{edge and having the average value of } \boldsymbol{u}\cdot\boldsymbol{n}_K \text{ over } E \text{ is non-} \\ & \text{negative.} \end{cases} \tag{3.10}$$

In the following,using operator splitting we derive discrete, interface problems for the advection-diffusion equation (3.1), which are extensions of the discrete counterparts of the interface problems (2.51) and (2.57) derived for the diffusion problem in the previous chapter.

3.2.1 Method 1: An extension of the time-dependent Steklov-Poincaré operator approach

To define the interface problem for Method 1, we introduce solution operators $\mathscr{D}_i$, $i = 1, 2$, where $\mathscr{D}_i$ associates to an $L^2(0,T;L^2(\Omega_i))$ source term f together with $H^1_*(\Omega_i)$ (cf. (2.49)) initial data c_0 and discrete boundary data $\left(\lambda_a, \lambda\right)$ given on $\Gamma \times (0,T)$, the solution of the discrete advection-diffusion problem in $\Omega_i \times (0,T)$ that we define below (problem (3.11)-(3.12)). In our notation, $\lambda_a \in \Lambda^{N\times L}$ and $\lambda \in \Lambda^N$ represent the Dirichlet boundary data for the advection equation and for the diffusion equation respectively:

$$\lambda_a = \left(\lambda_{h,a}^{n,l}\right)_{n=0,\ldots,N-1,\ l=0,\ldots,L-1} \quad \text{and} \quad \lambda = \left(\lambda_h^{n+1}\right)_{n=0,\ldots,N-1}.$$

Using the upwind operator (3.10), the subdomain problem is defined, for given $\left(\lambda_a, \lambda, f, c_0\right)$, by:

For $n = 0, \ldots, N-1$,

1. define $c_{h,i}^{n,0} = c_{h,i}^n$, where $\left(c_{h,i}^0\right)_{|K} := \dfrac{1}{\text{meas}(K)} \displaystyle\int_K c_0,\ \forall K \in \mathscr{K}_{h,i}$,

2. for $l = 0, \ldots, L-1$,

   (a) define the upwind values

   $$\hat{c}_{h,i}^{n,l} = \mathscr{U}_{h,i}\left(c_{h,i}^{n,l}, \lambda_{h,a}^{n,l}\right),$$

   (b) solve the advection equation

   $$\int_K \phi_i \frac{c_{h,i}^{n,l+1} - c_{h,i}^{n,l}}{\Delta t_a} + \sum_{E \subset \partial K} \int_E \hat{c}_{h,i}^{n,l} (\boldsymbol{u} \cdot \boldsymbol{n}_K) = 0, \quad \forall K \in \mathscr{K}_{h,i}, \tag{3.11}$$

   with $c_{h,i}^{n,l}$ known and obtain $c_{h,i}^{n,l+1}$,

3. solve the diffusion equation

$$\begin{aligned} \int_K \phi_i \frac{c_{h,i}^{n+1} - c_{h,i}^{n,L}}{\Delta t} + \int_K \operatorname{div} \boldsymbol{r}_{h,i}^{n+1} &= \int_K f(t^{n+1}), \qquad \forall K \in \mathscr{K}_{h,i}, \\ \int_{\Omega_i} \boldsymbol{D}_i^{-1} \boldsymbol{r}_{h,i}^{n+1} \cdot \boldsymbol{\nu} - \int_{\Omega_i} c_{h,i}^{n+1} \operatorname{div} \boldsymbol{\nu} &= \int_\Gamma \lambda_h^{n+1} (\boldsymbol{\nu} \cdot \boldsymbol{n}_i), \quad \forall \boldsymbol{\nu} \in \Sigma_{h,i}. \end{aligned} \tag{3.12}$$

   with $c_{h,i}^{n,L}$ known and obtain $(c_{h,i}^{n+1}, \boldsymbol{r}_{h,i}^{n+1})$.

The operator $\mathscr{D}_i$ is now defined by

$$\begin{aligned} \mathscr{D}_i : \Lambda_h^{N\times L} \times \Lambda_h^N \times L^2(0,T; L^2(\Omega_i)) \times H_*^1(\Omega_i) &\to \left(N_{h,i}\right)^{N\times L} \times \left(M_{h,i}\right)^N \times \left(\Sigma_{h,i}\right)^N \\ (\lambda_a, \lambda, f, c_0) &\mapsto \left(\hat{c}_{h,i}^{\Delta t, \Delta t_a}, c_{h,i}^{\Delta t}, \boldsymbol{r}_{h,i}^{\Delta t}\right), \end{aligned}$$

where $\hat{c}_{h,i}^{\Delta t, \Delta t_a} = \left(\hat{c}_{h,i}^{n,l}\right)_{n=0,\ldots,N-1,\, l=0,\ldots,L-1}$ and $\left(c_{h,i}^{\Delta t}, \boldsymbol{r}_{h,i}^{\Delta t}\right) = \left(c_{h,i}^n, \boldsymbol{r}_{h,i}^n\right)_{n=1,\ldots,N}$.

We remark that as the advection is approximated explicitly, in the definition of $\mathscr{D}_i$ we have extracted the upwind values $\hat{c}_{h,i}^{n,l}$ for $l = 0, \ldots, L-1$ (instead of $l = 1, \ldots, L$) for each n, $n = 0, \ldots, N-1$.

For the problem on the interface, we will need as input from the subdomain problems the first component $\hat{c}_{h,i}^{\Delta t, \Delta t_a}$ of the output of $\mathscr{D}_i$ (for the advection step) and the values of the third component $\boldsymbol{r}_{h,i}^{\Delta t}$ (for the diffusion step). In fact, we need only the values of $\hat{c}_{h,i}^{\Delta t, \Delta t_a}$ associated with edges E in $\mathscr{G}_{h,i}^{\text{in}}$ ($j = 3-i$) and values of $\boldsymbol{r}_{h,i}^{\Delta t}$ associated with edges E in $\mathscr{G}_h$. Thus we define the two projection operators $\mathscr{H}_i$ and $\mathscr{F}_i$ as follows

$$\begin{aligned} \mathscr{H}_i : \left(N_{h,i}\right)^{N\times L} \times \left(M_{h,i}\right)^N \times \left(\Sigma_{h,i}\right)^N &\to (\Lambda_h)^{N\times L} \\ \left(\hat{c}_{h,i}^{\Delta t, \Delta t_a}, c_{h,i}^{\Delta t}, \boldsymbol{r}_{h,i}^{\Delta t}\right) &\mapsto \begin{cases} 0, & \forall E \in \mathscr{G}_{h,i}^{\text{in}}, \\ \left(\hat{c}_{h,i}^{\Delta t, \Delta t_a}\right)_{|E}, & \forall E \in \mathscr{G}_{h,j}^{\text{in}}, \text{ with } j = 3-i, \end{cases} \end{aligned}$$

and

$$\begin{aligned}\mathscr{F}_i : \left(N_{h,i}\right)^{N\times L} \times \left(M_{h,i}\right)^{N} \times \left(\Sigma_{h,i}\right)^{N} &\to \left(\Lambda_h\right)^{N} \\ \left(\hat{c}_{h,i}^{\Delta t,\Delta t_a}, c_{h,i}^{\Delta t}, \boldsymbol{r}_{h,i}^{\Delta t}\right) &\mapsto \left(\boldsymbol{r}_{h,i}^{\Delta t}\cdot\boldsymbol{n}_i\right)_{|E},\ \forall E\in\mathscr{G}_h.\end{aligned}$$

With these operators, we can rewrite the transmission condition (3.6) for the advection equation equivalently as

$$\begin{aligned}\int_{t^{n,l}}^{t^{n,l+1}}\int_E \lambda_a - \mathscr{H}_1\mathscr{D}_1(\lambda_a,\lambda,f,c_0) &= 0, \quad \forall E\in\mathscr{G}_{h,1}^{\text{in}},\\ \int_{t^{n,l}}^{t^{n,l+1}}\int_E \lambda_a - \mathscr{H}_2\mathscr{D}_2(\lambda_a,\lambda,f,c_0) &= 0, \quad \forall E\in\mathscr{G}_{h,2}^{\text{in}},\\ \forall n=0,\dots,N-1,\ \forall l=0,\dots,L-1,&\end{aligned}$$

or

$$\begin{aligned}\int_{t^{n,l}}^{t^{n,l+1}}\int_E \lambda_a - \mathscr{H}_1\mathscr{D}_1(\lambda_a,\lambda,f,c_0) - \mathscr{H}_2\mathscr{D}_2(\lambda_a,\lambda,f,c_0) = 0,\\ \forall E\in\mathscr{G}_h,\ \forall n=0,\dots,N-1,\ \forall l=0,\dots,L-1.\end{aligned} \tag{3.13}$$

Since we have imposed a Dirichlet condition on Γ in (3.12) for the diffusion equation, the first equation of (3.8) is satisfied and (3.8) reduces to the flux equality, which is equivalent to

$$\begin{aligned}\int_{t^n}^{t^{n+1}}\int_E \mathscr{F}_1\mathscr{D}_1(\lambda_a,\lambda,f,c_0) - \mathscr{F}_2\mathscr{D}_2(\lambda_a,\lambda,f,c_0) = 0,\\ \forall E\in\mathscr{G}_h,\ \forall n=0,\dots,N-1.\end{aligned} \tag{3.14}$$

Note that the composite operator $\mathscr{F}_i\mathscr{D}_i$, $i=1,2$, is a Steklov-Poincaré (Dirichlet-to-Robin) type operator. Equation (3.14) together with (3.13) forms an interface problem, equivalent to problem (3.5) - (3.7) - (3.6) - (3.8):

Find $\left(\lambda_a,\lambda\right)\in(\Lambda_h)^{N\times L}\times(\Lambda_h)^N$ such that

$$\begin{aligned}\int_{t^{n,l}}^{t^{n,l+1}}\int_E \lambda_a - \mathscr{H}_1\mathscr{D}_1(\lambda_a,\lambda,f,c_0) - \mathscr{H}_2\mathscr{D}_2(\lambda_a,\lambda,f,c_0) &= 0,\\ \int_{t^n}^{t^{n+1}}\int_E \mathscr{F}_1\mathscr{D}_1(\lambda_a,\lambda,f,c_0) + \mathscr{F}_2\mathscr{D}_2(\lambda_a,\lambda,f,c_0) &= 0,\\ \forall E\in\mathscr{G}_h,\ \forall n=0,\dots,N-1,\ \forall l=0,\dots,L-1,&\end{aligned} \tag{3.15}$$

or equivalently

$$\begin{aligned}&\text{Find } \left(\lambda_a,\lambda\right)\in(\Lambda_h)^{N\times L}\times(\Lambda_h)^N \text{ such that}\\ &\mathscr{S}\begin{pmatrix}\lambda_a\\ \lambda\end{pmatrix} = \begin{pmatrix}\hat{\chi}\\ \chi\end{pmatrix},\end{aligned} \tag{3.16}$$

where

$$\mathscr{S}\begin{pmatrix}\lambda_a\\ \lambda\end{pmatrix} = \begin{pmatrix}\displaystyle\int_{t^{n,l}}^{t^{n,l+1}}\int_E \lambda_a - \sum_{i=1}^{2}\mathscr{H}_i\mathscr{D}_i(\lambda_a,\lambda,0,0)\\ \displaystyle\int_{t^n}^{t^{n+1}}\int_E -\sum_{i=1}^{2}\mathscr{F}_i\mathscr{D}_i(\lambda_a,\lambda,0,0)\end{pmatrix}_{E\in\mathscr{G}_h,\, n=0,\dots,N-1,\, l=0,\dots,L-1}$$

and

$$\begin{pmatrix} \hat{\chi} \\ \chi \end{pmatrix} = \begin{pmatrix} \int_{t^{n,l}}^{t^{n,l+1}} \int_E \sum_{i=1}^{2} \mathscr{H}_i \mathscr{D}_i(0,0,f,c_0) \\ \int_{t^n}^{t^{n+1}} \int_E \sum_{i=1}^{2} \mathscr{F}_i \mathscr{D}_i(0,0,f,c_0) \end{pmatrix}_{E\in\mathscr{G}_h,\, n=0,\dots,N-1,\, l=0,\dots,L-1}.$$

System (3.16) can be solved iteratively by using a Krylov method (e.g. GMRES): the right hand side is computed only once by solving problem (3.11)-(3.12) in each subdomain with $\lambda_a = 0$ and $\lambda = 0$; then for a pair of vectors (η_a, η) given in $(\Lambda_h)^{N\times L}\times(\Lambda_h)^N$, the matrix vector product is obtained, at each Krylov iteration, by solving subdomain problem (3.11)-(3.12) with $\lambda_a = \eta_a$, $\lambda = \eta$ and with $f = 0$ and $c_0 = 0$, and extracting the correct traces on the interface.

Following the same idea as in Section 2.3.1 we apply a generalized Neumann-Neumann preconditioner. With this aim, we define the solution operator $\mathscr{N}_i$, $i = 1, 2$:

$$\begin{aligned} \mathscr{N}_i : \left(\Lambda_h\right)^{N\times L} \times \left(\Lambda_h\right)^N &\to \left(N_{h,i}\right)^{N\times L} \times \left(M_{h,i}\right)^N \times \left(\Sigma_{h,i}\right)^N \\ (\lambda_a, \varphi) &\mapsto \left(\hat{c}_{h,i}^{\Delta t,\Delta t_a}, c_{h,i}^{\Delta t}, \boldsymbol{r}_{h,i}^{\Delta t}\right), \end{aligned}$$

where

$$\hat{c}_{h,i}^{\Delta t,\Delta t_a} = \left(\hat{c}_{h,i}^{n,l}\right)_{n=0,\dots,N-1,\, l=0,\dots,L-1} \text{ and } \left(c_{h,i}^{\Delta t}, \boldsymbol{r}_{h,i}^{\Delta t}\right) = \left(c_{h,i}^{n}, \boldsymbol{r}_{h,i}^{n}\right)_{n=1,\dots,N}$$

are the solution of the subdomain problem that consists of solving, for $n = 0,\dots,N-1$,

- the advection equation: for $l = 0,\dots,L-1$,

$$\begin{aligned} \int_K \phi_i \frac{c_{h,i}^{n,l+1} - c_{h,i}^{n,l}}{\Delta t_a} + \sum_{E\subset\partial K} \int_E \hat{c}_{h,i}^{n,l}(\boldsymbol{u}\cdot\boldsymbol{n}_K) &= 0, && \forall K \in \mathscr{K}_{h,i}, \\ \hat{c}_{h,i}^{n,l} &= \mathscr{U}_{h,i}\left(c_{h,i}^{n,l}, \lambda_{h,a}^{n,l}\right), \end{aligned}$$

  with $c_{h,i}^{n,0} := c_{h,i}^{n}$ where $c_{h,i}^{0} := 0$,

- and the diffusion equation

$$\begin{aligned} \int_K \phi_i \frac{c_{h,i}^{n+1} - c_{h,i}^{n,L}}{\Delta t} + \int_K \operatorname{div} \boldsymbol{r}_{h,i}^{n+1} &= 0, && \forall K \in \mathscr{K}_{h,i}, \\ \int_{\Omega_i} \boldsymbol{D}_i^{-1} \boldsymbol{r}_{h,i}^{n+1}\cdot\boldsymbol{\nu} - \int_{\Omega_i} c_{h,i}^{n+1} \operatorname{div}\boldsymbol{\nu} &= 0, && \forall \boldsymbol{\nu} \in \Sigma_{h,i}^0, \\ \int_E \boldsymbol{r}_{h,i}^{n+1}\cdot\boldsymbol{n}_i &= \int_E \varphi^{n+1}, && \forall E \in \mathscr{G}_h, \end{aligned}$$

  where $\Sigma_{h,i}^0$ is introduced to treat the Neumann boundary condition on the interface and is defined by

$$\Sigma_{h,i}^0 = \left\{\boldsymbol{\nu} \in \Sigma_{h,i} : \boldsymbol{\nu}\cdot\boldsymbol{n}_{|E} = 0,\ \forall E \in \mathscr{G}_h\right\}.$$

In order to define a (pseudo-)inverse operator of $\mathscr{F}_i\mathscr{D}_i,\ i=1,2$, we need to introduce the trace operator

$$\begin{aligned}\mathrm{Tr}_i : \left(N_{h,i}\right)^{N\times L}\times\left(M_{h,i}\right)^{N}\times\left(\Sigma_{h,i}\right)^{N} &\to \left(\Lambda_h\right)^N\\ \left(\hat{c}_{h,i}^{\Delta t,\Delta t_a}, c_{h,i}^{\Delta t}, \boldsymbol{r}_{h,i}^{\Delta t}\right), &\mapsto \underline{\lambda}\end{aligned}$$

where $\underline{\lambda}=\left(\underline{\lambda}_h^n\right)_{n=1,\dots,N}$ stands for the trace of the concentration on the interface and is defined by

$$\int_E \underline{\lambda}_h^n(\boldsymbol{v}_E\cdot\boldsymbol{n}_i)=\int_{\Omega_i}\boldsymbol{D}_i^{-1}\boldsymbol{r}_{h,i}^n\cdot\boldsymbol{v}_E-\int_{\Omega_i}c_{h,i}^n\mathrm{div}\,\boldsymbol{v}_E,\ \ \forall E\in\mathscr{G}_h,\ n=1,\dots,N,$$

for $\boldsymbol{v}_E\in\Sigma_{h,i}$ such that $\left(\boldsymbol{v}_E\right)_{|K}=0$ for all $K\in\mathscr{K}_{h,i}$ that do not share the edge E.

The generalized Neumann-Neumann preconditioner for (3.16) is defined as

$$\begin{aligned}\int_{t^{n,l}}^{t^{n,l+1}}\int_E \mathscr{S}\lambda_a-\sum_{i=1}^{2}\mathscr{H}_i\mathscr{N}_i(\mathscr{S}\lambda_a,\mathscr{S}\lambda) &= \int_{t^{n,l}}^{t^{n,l+1}}\int_E \hat{\chi}-\sum_{i=1}^{2}\mathscr{H}_i\mathscr{N}_i(\hat{\chi},\chi),\\ \int_{t^{n}}^{t^{n+1}}\int_E \sum_{i=1}^{2}\sigma_i\mathrm{Tr}_i\mathscr{N}_i(\mathscr{S}\lambda_a,\mathscr{S}\lambda) &= \int_{t^{n}}^{t^{n+1}}\int_E \sum_{i=1}^{2}\sigma_i\mathrm{Tr}_i\mathscr{N}_i(\hat{\chi},\chi),\\ \forall E\in\mathscr{G}_h,\ \ \forall n=0,\dots,N-1,\ \ \forall l=0,\dots,L-1.&\end{aligned}\tag{3.17}$$

Here the composite operator $\mathrm{Tr}_i\mathscr{N}_i,\ i=1,2$, is a Neuman-to-Dirichlet type operator (which is the inverse operator of $\mathscr{F}_i\mathscr{D}_i,\ i=1,2$) and $\sigma_i:\Lambda_h\to[0,1], i=1,2$, are weights such that $\sigma_1+\sigma_2=1$. As in the case of pure diffusion problems (see Chapter 2), if $\boldsymbol{D}_i=d_i\mathbf{I}, i=1,2$, then

$$\sigma_i:=\frac{d_i}{d_1+d_2}.$$

3.2.2 Method 2: An extension of the Optimized Schwarz Waveform Relaxation approach

As in Method 1, we first define several operators needed to define the interface problem for this method. Let $\mathscr{R}_i,\ i=1,2$, be the solution operator which depends on the two Robin parameters $\alpha_{i,j},\ i=1,2,\ j=3-i$:

$$\begin{aligned}\mathscr{R}_i : \left(\Lambda_h\right)^{N\times L}\times\left(\Lambda_h\right)^{N}\times L^2(0,T;L^2(\Omega_i))\times H^1_*(\Omega_i)&\\ \to \left(\Lambda_h\right)^N\times\left(N_{h,i}\right)^{N\times L}\times\left(M_{h,i}\right)^{N}\times\left(\Sigma_{h,i}\right)^{N}&\\ \left(\lambda_a,\xi,f,c_0\right) \mapsto \left(\xi,\hat{c}_{h,i}^{\Delta t,\Delta t_a}, c_{h,i}^{\Delta t}, \boldsymbol{r}_{h,i}^{\Delta t}\right),&\end{aligned}$$

where

- $\lambda_a=\left(\lambda_{h,a}\right)_{n=0,\dots,N-1,\ l=0,\dots,L-1}$ represents Dirichlet boundary data on the interface for the advection equation (just as in Method 1).

- $\xi=\left(\xi_h^n\right)_{n=1,\dots,N}$ represents the Robin boundary data (instead of Dirichlet data as in Method 1) on the interface for the diffusion equation. Here we include ξ in the output of $\mathscr{D}_i$ as in the pure diffusion case (see Subsection 2.3.2) in order to calculate Robin data transmitted to the neighboring subdomain.

- $\hat{c}_{h,i}^{\Delta t,\Delta t_a} = \left(\hat{c}_{h,i}^{n,l}\right)_{n=0,\dots,N-1,\, l=0,\dots,L-1}$ and $\left(c_{h,i}^{\Delta t}, \boldsymbol{r}_{h,i}^{\Delta t}\right) = \left(c_{h,i}^{n}, \boldsymbol{r}_{h,i}^{n}\right)_{n=1,\dots,N}$ are the solution of the subdomain problem, for given (λ_a, ξ, f, c_0) :

For $n = 0, \dots, N-1$,

1. define $c_{h,i}^{n,0} = c_{h,i}^{n}$, where $\left(c_{h,i}^{0}\right)_{|K} := \dfrac{1}{\mathrm{meas}(K)} \displaystyle\int_K c_0,\ \forall K \in \mathscr{K}_{h,i}$,

2. for $l = 0, \dots, L-1$,

   (a) define the upwind values

   $$\hat{c}_{h,i}^{n,l} = \mathscr{U}_{h,i}\left(c_{h,i}^{n,l}, \lambda_{h,a}^{n,l}\right),$$

   (b) solve the advection equation

   $$\int_K \phi_i \frac{c_{h,i}^{n,l+1} - c_{h,i}^{n,l}}{\Delta t_a} + \sum_{E \subset \partial K} \int_E \hat{c}_{h,i}^{n,l} (\boldsymbol{u} \cdot \boldsymbol{n}_K) = 0, \quad \forall K \in \mathscr{K}_{h,i}, \tag{3.18}$$

   with $c_{h,i}^{n,l}$ known and obtain $c_{h,i}^{n,l+1}$,

3. solve the diffusion equation

$$\begin{aligned}
\int_K \phi_i \frac{c_{h,i}^{n+1} - c_{h,i}^{n,L}}{\Delta t} + \int_K \operatorname{div} \boldsymbol{r}_{h,i}^{n+1} &= \int_K f(t^{n+1}), \quad \forall K \in \mathscr{K}_{h,i}, \\
\int_{\Omega_i} \boldsymbol{D}_i^{-1} \boldsymbol{r}_{h,i}^{n+1} \cdot \boldsymbol{v} - \int_{\Omega_i} c_{h,i}^{n+1} \operatorname{div} \boldsymbol{v} + \frac{1}{\alpha_{i,j}} \int_\Gamma (\boldsymbol{r}_{h,i}^{n+1} \cdot \boldsymbol{n}_i)(\boldsymbol{v} \cdot \boldsymbol{n}_i) &= \\
-\frac{1}{\alpha_{i,j}} \int_\Gamma \xi_h^{n+1} (\boldsymbol{v} \cdot \boldsymbol{n}_i), &\quad \forall \boldsymbol{v} \in \Sigma_{h,i}.
\end{aligned} \tag{3.19}$$

   with $c_{h,i}^{n,L}$ known and obtain $(c_{h,i}^{n+1}, \boldsymbol{r}_{h,i}^{n+1})$.

As stated in Remark 3.3, the advection step for Method 1 and Method 2 are the same. So we define the projection operator $\widetilde{\mathscr{H}_i}$, $i = 1, 2$, similar to the operator $\mathscr{H}_i$ in Method 1, but now take the second component of the output of $\mathscr{R}_i$:

$$\begin{aligned}
\widetilde{\mathscr{H}_i} : \left(\Lambda_h\right)^N \times \left(N_{h,i}\right)^{N \times L} \times \left(M_{h,i}\right)^N \times \left(\Sigma_{h,i}\right)^N &\to \left(\Lambda_h\right)^{N \times L} \\
\left(\xi, \hat{c}_{h,i}^{\Delta t,\Delta t_a}, c_{h,i}^{\Delta t}, \boldsymbol{r}_{h,i}^{\Delta t}\right) &\mapsto \begin{cases} 0, & \forall E \in \mathscr{G}_{h,i}^{\mathrm{in}}, \\ \left(\hat{c}_{h,i}^{\Delta t,\Delta t_a}\right)_{|E}, & \forall E \in \mathscr{G}_{h,j}^{\mathrm{in}},\ j = 3 - i, \end{cases}
\end{aligned}$$

Next, for the Robin transmission conditions (3.9) of the diffusion equation, we need the following interface operators defined for $i = 1, 2$, with $j = 3 - i$,

$$\begin{aligned}
&\mathscr{B}_i : \left(\Lambda_h\right)^N \times \left(N_{h,i}\right)^{N \times L} \times \left(M_{h,i}\right)^N \times \left(\Sigma_{h,i}\right)^N \to \left(\Lambda_h\right)^N \\
&\left(\xi, \hat{c}_{h,j}^{\Delta t,\Delta t_a}, c_{h,j}^{\Delta t}, \boldsymbol{r}_{h,j}^{\Delta t}\right) \mapsto \left(-\boldsymbol{r}_{h,j} \cdot \boldsymbol{n}_i + \frac{\alpha_{i,j}}{\alpha_{j,i}} (\xi + \boldsymbol{r}_{h,j} \cdot \boldsymbol{n}_j)\right)_{|E},\ \forall E \in \mathscr{G}_h.
\end{aligned}$$

The transmission condition (3.6) for the advection part leads to

$$\int_{t^{n,l}}^{t^{n,l+1}} \int_E \lambda_a - \widetilde{\mathscr{H}_1}\mathscr{R}_1(\lambda_a,\xi_1,f,c_0) - \widetilde{\mathscr{H}_2}\mathscr{R}_2(\lambda_a,\xi_2,f,c_0) = 0, \quad \forall E \in \mathscr{G}_h,\ \forall n = 0,\dots,N-1,\ \forall l = 0,\dots,L-1. \tag{3.20}$$

The transmission conditions (3.9) for the diffusion equation lead to

$$\begin{aligned} &\int_{t^n}^{t^{n+1}} \int_E \xi_1 - \mathscr{B}_1\mathscr{R}_2(\lambda_a,\xi_2,f,c_0) = 0, \\ &\int_{t^n}^{t^{n+1}} \int_E \xi_2 - \mathscr{B}_2\mathscr{R}_1(\lambda_a,\xi_1,f,c_0) = 0, \end{aligned} \quad \forall E \in \mathscr{G}_h,\ \forall n = 0,\dots,N-1. \tag{3.21}$$

Note that the composite operator $\mathscr{B}_i\mathscr{R}_i$, $i = 1,2$, is a discrete Robin-to-Robin type operator. Equation (3.21) together with (3.20) forms an interface problem, equivalent to problem (3.5) - (3.7) - (3.6) - (3.9), as follows

Find $(\lambda_a,\xi_1,\xi_2) \in (\Lambda_h)^{N\times L} \times (\Lambda_h)^N \times (\Lambda_h)^N$ such that

$$\begin{aligned} &\int_{t^{n,l}}^{t^{n,l+1}} \int_E \lambda_a - \widetilde{\mathscr{H}_1}\mathscr{R}_1(\lambda_a,\xi_1,f,c_0) - \widetilde{\mathscr{H}_2}\mathscr{R}_2(\lambda_a,\xi_2,f,c_0) &&= 0, \\ &\int_{t^n}^{t^{n+1}} \int_E \xi_1 - \mathscr{B}_1\mathscr{R}_2(\lambda_a,\xi_2,f,c_0) &&= 0, \\ &\int_{t^n}^{t^{n+1}} \int_E \xi_2 - \mathscr{B}_2\mathscr{R}_1(\lambda_a,\xi_1,f,c_0) &&= 0, \end{aligned} \tag{3.22}$$

$$\forall E \in \mathscr{G}_h,\ \forall n = 0,\dots,N-1,\ \forall l = 0,\dots,L-1,$$

or equivalently,

$$\mathscr{S}_R \begin{pmatrix} \hat{\lambda} \\ \xi_1 \\ \xi_2 \end{pmatrix} = \chi_R, \tag{3.23}$$

where

$$\mathscr{S}_R \begin{pmatrix} \hat{\lambda} \\ \xi_1 \\ \xi_2 \end{pmatrix} = \begin{pmatrix} \displaystyle\int_{t^{n,l}}^{t^{n,l+1}} \int_E \lambda_a - \sum_{i=1}^{2} \widetilde{\mathscr{H}_i}\mathscr{R}_i(\lambda_a,\xi_i,0,0) \\ \displaystyle\int_{t^n}^{t^{n+1}} \int_E \xi_1 - \mathscr{B}_1\mathscr{R}_2(\lambda_a,\xi_2,0,0) \\ \displaystyle\int_{t^n}^{t^{n+1}} \int_E \xi_2 - \mathscr{B}_2\mathscr{R}_1(\lambda_a,\xi_1,0,0) \end{pmatrix}_{E\in\mathscr{G}_h,\ n=0,\dots,N-1,\ l=0,\dots,L-1}$$

and

$$\chi_R = \begin{pmatrix} \displaystyle\int_{t^{n,l}}^{t^{n,l+1}} \int_E \sum_{i=1}^{2} \widetilde{\mathscr{H}_i}\mathscr{R}_i(0,0,f,c_0) \\ \displaystyle\int_{t^n}^{t^{n+1}} \int_E \mathscr{B}_1\mathscr{R}_2(0,0,f,c_0) \\ \displaystyle\int_{t^n}^{t^{n+1}} \int_E \mathscr{B}_2\mathscr{R}_1(0,0,f,c_0) \end{pmatrix}_{E\in\mathscr{G}_h,\ n=0,\dots,N-1,\ l=0,\dots,L-1}.$$

System (3.23) can be solved iteratively using Jacobi iterations, which corresponds to the discrete "splitting" OSWR algorithm) or a Krylov method such as GMRES: the right hand side is computed by solving subdomain problem (3.18)-(3.19) with $\lambda_a = 0$ and $\xi = 0$; then for a given vector (η_a, ξ_1, ξ_2) in $(\Lambda_h)^{N\times L} \times (\Lambda_h)^N \times (\Lambda_h)^N$, the matrix vector product is obtained (at each iteration) by solving problem (3.18)-(3.19) in $\Omega_i \times (0,T)$, $i = 1,2$, with $\lambda_a = \eta_a$, $\xi = \xi_i$, and with $f = 0$ and $c_0 = 0$.

Remark 3.4. *Due to the use of the splitting method, we have formulated a generalization of the OSWR method in which the Robin parameters only act on the diffusion equation as in the case of pure diffusion problems. The advection term is now like a source term for the diffusion equation. Thus the optimized Robin parameters $\alpha_{i,j}$, $i = 1,2$, $j = 3 - i$, are calculated in the same way as for the pure diffusion case (see Appendix A.2.1). Consequently, the advection coefficient is not taken into account in the computation of the optimized parameters. This may be an advantage of using operator splitting because we don't need to handle variable coefficients due to the velocity field, as one does for a fully implicit scheme (see, e.g, [61, 62]. In Section 3.4, we study numerically the impact of the optimized parameters on the convergence behavior, especially for advection-dominated problems.*

As the interface problem derived above for each method is global in time, one may use different time steps for different subdomains as in the case of pure diffusion problems (see Section 2.4). In the next section, we describe how we enforce the transmission conditions over such nonconforming time grids.

3.3 Nonconforming time discretizations

Let $\mathcal{T}_1$ and $\mathcal{T}_2$ be two different uniform partitions of the time interval $(0,T)$ into N_1 and N_2 sub-intervals respectively with lengths Δt_1 and Δt_2, respectively (see Figure 3.4). The sub-time step for the advection in each subdomain is defined by

$$\Delta t_i = L_i \Delta t_{i,a},\ i = 1,2,$$

and we denote by $\mathcal{T}_i^a$, $i = 1,2$, the corresponding partition in time for the advection. We denote by $P_0(\mathcal{T}_i, \Lambda_h)$ the space of piecewise constant functions in time on grid $\mathcal{T}_i$ with values in Λ_h. Then define Π_{ij} the average-valued projection from $P_0(\mathcal{T}_j, \Lambda_h)$ to $P_0(\mathcal{T}_i, \Lambda_h)$ (see (2.70)), and Π_{ij}^a from $P_0(\mathcal{T}_j^a, \Lambda_h)$ to $P_0(\mathcal{T}_i^a, \Lambda_h)$.

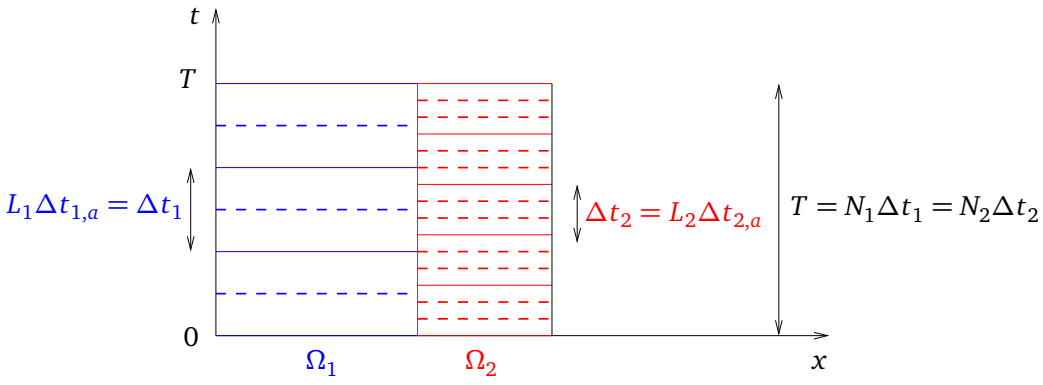

Figure 3.4: Nonconforming time grids in the subdomains.

As pointed out earlier, due to the use of the splitting method the interface problem for either Method 1 or Method 2 consists of an equation imposing the transmission condition for the advection problem and one or more imposing the transmission conditions for the diffusion problem. The latter can be enforced in time in a way similar to that of the pure diffusion problem (see Section 2.4). For the advection transmission condition, as there is only one unknown λ_a on the interface, one needs to choose λ_a to be piecewise constant in time on either the grid $\mathscr{T}_1^a$ or $\mathscr{T}_2^a$. This is the case for both methods.

For Method 1 We choose λ_a and λ to be piecewise constant in time on the advection and diffusion time grids respectively. For instance, let $\lambda_a \in P_0(\mathscr{T}_2^a, \Lambda_h)$ and $\lambda \in P_0(\mathscr{T}_2, \Lambda_h)$. Then the interface problem (3.15) is rewritten as

$$\begin{aligned}
&\text{Find } (\lambda_a, \lambda) \in (\Lambda_h)^{N_2 \times L_2} \times (\Lambda_h)^N \text{ such that} \\
&\int_{t_2^{n,l}}^{t_2^{n,l+1}} \int_E \lambda_a - \Pi_{21}^a \left(\mathscr{H}_1 \mathscr{D}_1(\Pi_{12}^a(\lambda_a), \Pi_{12}(\lambda), f, c_0) \right) - \mathscr{H}_2 \mathscr{D}_2(\lambda_a, \lambda, f, c_0) \quad = 0, \\
&\int_{t_2^n}^{t_2^{n+1}} \int_E \Pi_{21} \left(\mathscr{F}_1 \mathscr{D}_1(\Pi_{12}^a(\lambda_a), \Pi_{12}(\lambda), f, c_0) \right) - \mathscr{F}_2 \mathscr{D}_2(\lambda_a, \lambda, f, c_0) \quad = 0,
\end{aligned} \tag{3.24}$$

for $\forall E \in \mathscr{G}_h$ and $\forall n = 0, \ldots, N_2 - 1$, $\forall l = 0, \ldots, L_2 - 1$.

For Method 2 We choose λ_a to be piecewise constant in time on one grid, for instance, $\mathscr{T}_2^a$. For the two Robin terms ξ_1 and ξ_2, we use the same technique as in Subsection 2.4.2. The interface problem (3.22) is then rewritten as

$$\begin{aligned}
&\text{Find } (\lambda_a, \xi_1, \xi_2) \in (\Lambda_h)^{N_2 \times L_2} \times (\Lambda_h)^{N_1} \times (\Lambda_h)^{N_2} \text{ such that} \\
&\int_{t_2^{n,l}}^{t_2^{n,l+1}} \int_E \lambda_a - \Pi_{21}^a \left(\widetilde{\mathscr{H}_1} \mathscr{R}_1(\Pi_{12}^a(\lambda_a), \xi_1, f, c_0) - \widetilde{\mathscr{H}_2} \mathscr{R}_2(\lambda_a, \xi_2, f, c_0) \right) \quad = 0, \\
&\int_{t_1^m}^{t_1^{m+1}} \int_E \xi_1 - \Pi_{12} \left(\mathscr{B}_1 \mathscr{R}_2(\lambda_a, \xi_2, f, c_0) \right) \quad = 0, \\
&\int_{t_2^n}^{t_2^{n+1}} \int_E \xi_2 - \Pi_{21} \left(\mathscr{B}_2 \mathscr{R}_1(\Pi_{12}^a(\lambda_a), \xi_1, f, c_0) \right) \quad = 0,
\end{aligned} \tag{3.25}$$

for $\forall E \in \mathscr{G}_h$, $\forall m = 0, \ldots, N_1 - 1$, and $\forall n = 0, \ldots, N_2 - 1$, $\forall l = 0, \ldots, L_2 - 1$.

For conforming time grids, the two schemes defined by performing GMRES on the two interface problems (3.24) and (3.25) respectively converge to the same monodomain solution; while for the nonconforming case, these two schemes yield different solutions at convergence due to the use of different projection operators (this is also the case for pure diffusion problems studied in Chapter 2). In the next section we will carry out numerical experiments to investigate and compare the errors in time of the two methods.

3.4 Numerical results

We present 2D, numerical experiments (carried out using MATLAB) to illustrate the performance of the two methods formulated in the previous sections. We consider an isotropic diffusion matrix $\boldsymbol{D}_i = d_i \boldsymbol{I}$, where $\boldsymbol{I}$ is the 2D identity matrix. In Subsection 3.4.1, a simple test case with two subdomains is studied. The coefficients are constant in the subdomains and can be continuous or discontinuous across the interface. We verify the convergence behavior of the two methods for different Péclet numbers and check that the nonconforming time grids preserve the accuracy in time of the solution. Then in Subsection 3.4.2, we consider a test case with a rotating velocity and discontinuous diffusion coefficients (and also with two subdomains). We investigate how the two methods handle the variable coefficients, especially when the advection is dominant. Different time steps for the advection equation and for the diffusion equation are considered in this case.

In Subsection 3.4.3 we consider a test case that is a prototype for a nuclear waste repository simulation, in which the subdomains involved have different length scales (from 1m to 100m) and different physical properties. In particular, the advection field is governed by Darcy's law (and thus is variable), and the diffusion coefficients are discontinuous. The convergence of the two methods for a decomposition into 9 subdomains is studied, and we analyze numerically the error in time when nonconforming grids are used. Time windows are employed to approximate the solution over long time intervals. In Subsection 3.4.4, a test case for the simulation of the transport around a surface nuclear waste storage site is considered. In this case, the geometry of the domain is quite complex and layers with highly different physical properties are present. The domain is decomposed into 6 subdomains and time windows are also used.

As in the pure diffusion problem (see Remark 2.21), to compare the convergence of Method 1 and Method 2 with GMRES, we show the error in c and in $\boldsymbol{r}$ versus the number of subdomain solves (instead of the number of iterations as one iteration of Method 1 with the preconditioner costs twice as much as one iteration of Method 2).

3.4.1 Test case 1: Piecewise constant coefficients

The computational domain Ω is the unit square, and the final time is $T = 1$. We split Ω into two nonoverlapping subdomains $\Omega_1 = (0, 0.5) \times (0, 1)$ and $\Omega_2 = (0.5, 1) \times (0, 1)$. Homogeneous Dirichlet boundary conditions are imposed on $\partial\Omega$, the initial condition is

$$c_0(x, y) = xy(x-1)(y-1)\exp(-100((x-0.2)^2 + (y-0.2)^2)), \tag{3.26}$$

and the source term is

$$f(x, y, t) \;=\; \exp(-100((x-0.2)^2 + (y-0.2)^2)). \tag{3.27}$$

The porosity is $\phi_1 = \phi_2 = \phi = 1$. The diffusion and advection coefficients, d_i and $\boldsymbol{u}_i$ for $i = 1, 2$, are constant in each subdomain. These coefficients can be continuous or discontinuous across the interface. In the following we consider each of the two cases.

3.4.1.1 A case with continuous coefficients

The advection field is $\boldsymbol{u}_1 = \boldsymbol{u}_2 = \boldsymbol{u} = (1, 1)$, and the diffusion coefficient is $d_1 = d_2 = d$, where d is successively 1 then 0.1 and then 0.01. The corresponding global Péclet

numbers,

$$\mathrm{Pe}_G := \frac{H\,|\,\boldsymbol{u}\,|}{d},$$

where H is the size of the domain (in this case $H = 1$), are $\sqrt{2}$ then $10\sqrt{2}$ and then $100\sqrt{2}$ respectively. This range of the Péclet numbers covers most common cases one may deal with in practice. For the spatial discretization, we use a uniform rectangular mesh with size $\Delta x_1 = \Delta x_2 = \Delta x = 1/100$. For the time discretization, we use conforming time grids with $\Delta t_1 = \Delta t_2 = \Delta t = 1/100$. The advection time step is equal to the diffusion time step, $\Delta t_{a,i} = \Delta t$, $i = 1, 2$. The CFL condition in this case is $\Delta t_{\mathrm{CFL}} \leq 0.01$.

We first check that for the two methods, the multidomain solution computed at each iteration of GMRES converges to the monodomain solution on the same mesh in space and in time. We start with a zero initial guess on the space-time interface and compute the error in the $L^2(0,T;L^2(\Omega))$-norm of the difference between the multidomain solution and the monodomain solution at each iteration. For $d = 0.01$, we show in Figure 3.5 the error in the concentration c (left) and in the diffusive velocity $\boldsymbol{r}$ (right) versus the number of subdomain solves for Method 1 with the generalized Neumann-Neumann preconditioner (red, triangle) and Method 2 (blue, x-mark). We observe that the error tends to zero as the iteration increases, which implies that the two methods work well and confirms the theoretical equivalence between the multidomain formulation and the monodomain formulation. Furthermore, we see that Method 2 converges much faster than Method 1.

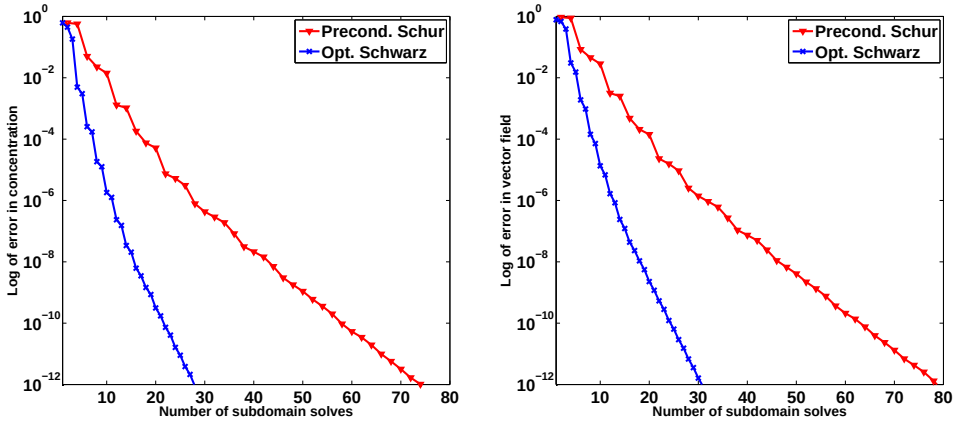

Figure 3.5: $L^2 - L^2$ error in c (left) and in $\boldsymbol{r}$ (right) in logarithmic scale of the difference between the multidomain and the monodomain solutions versus the number of subdomain solves for $\mathrm{Pe_G} = 100\sqrt{2}$.

We now analyze the convergence behavior of each method and study the effect of the preconditioner on the convergence of Method 1. We solve a problem with $c_0 = 0$ and $f = 0$ (thus $c = 0$ and $\boldsymbol{r} = 0$). We start with a random initial guess on the space-time interface. We compute the errors in the $L^2(0,T;L^2(\Omega))$-norm of the concentration c and the diffusive velocity $\boldsymbol{r}$, and stop the iteration (of GMRES) when the errors are less than 10^{-6}. We show in Figures 3.6, 3.7 and A2Fig:Test1ContConvergencePe100 the convergence of different algorithms for different Péclet numbers $\mathrm{Pe_G} = \sqrt{2}$, $\mathrm{Pe_G} = 10\sqrt{2}$ and $\mathrm{Pe_G} = 100\sqrt{2}$ respectively. Three algo-

rithms are considered: Method 1 with no preconditioner (magenta, circle), Method 1 with the preconditioner (red, triangle) and Method 2 (blue, x-mark). We observe that for Method 1, the preconditioner works well in the case of small Pe_G. The larger Pe_G, the slower the convergence of Method 1 with the preconditioner while inversely, the faster the convergence of Method 1 with no preconditioner. For Method 2, the convergence speed does not significantly change with the Péclet number. Method 1 with the preconditioner is comparable with Method 2 when diffusion is dominant. When advection is dominant, Method 2 converges faster than Method 1 (at least by about a factor of 2). The errors in c and in $\boldsymbol{r}$ behaves quite similarly.

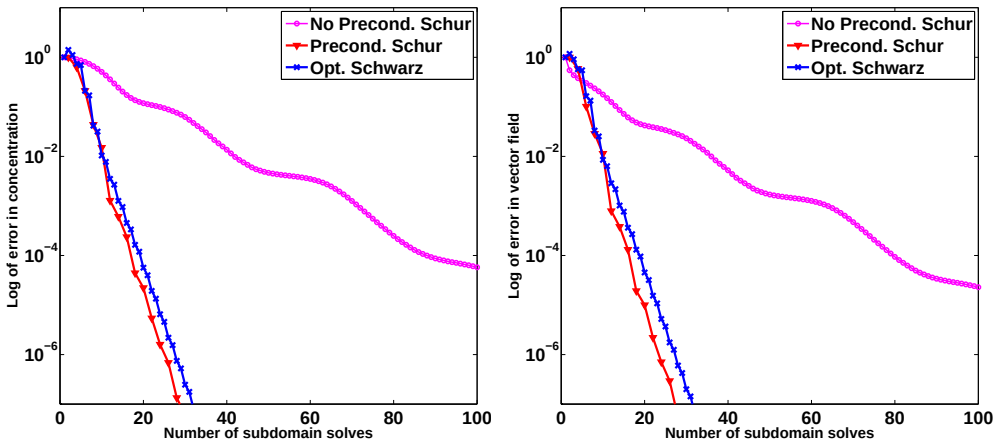

For $\mathrm{Pe}_G = \sqrt{2}$.

Figure 3.6: Convergence curves with GMRES for $\mathrm{Pe}_G = \sqrt{2}$: $L^2 - L^2$ error in the concentration c (left) and in the vector field $\boldsymbol{r}$ (right).

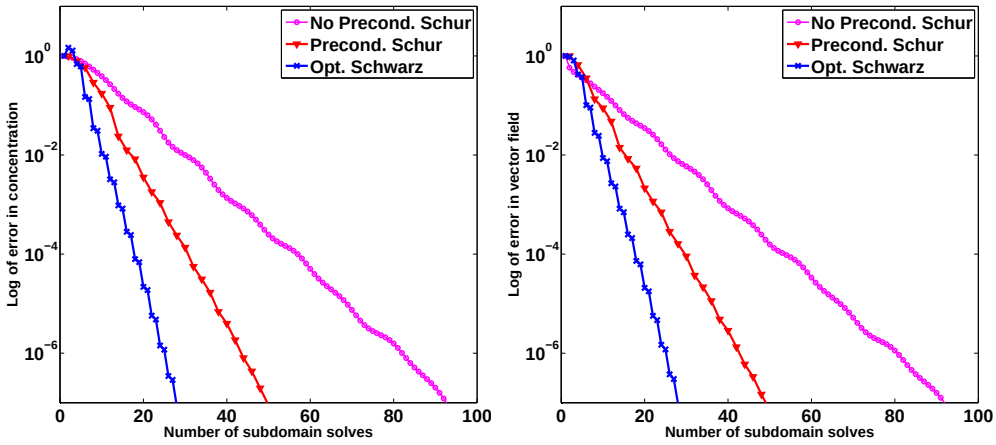

For $\mathrm{Pe}_G = 10\sqrt{2}$.

Figure 3.7: Convergence curves with GMRES for $\mathrm{Pe}_G = 10\sqrt{2}$: $L^2 - L^2$ error in the concentration c (left) and in the vector field $\boldsymbol{r}$ (right).

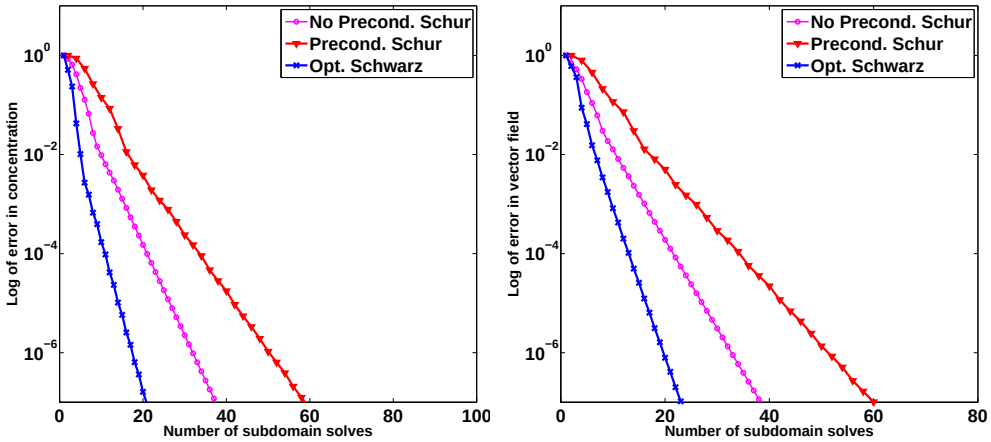

For $\mathrm{Pe}_G = 100\sqrt{2}$.

Figure 3.8: Convergence curves with GMRES for $\mathrm{Pe}_G = 1000\sqrt{2}$: $L^2 - L^2$ error in the concentration c (left) and in the vector field $\boldsymbol{r}$ (right).

We now fix $d = 0.01$ so that $\mathrm{Pe}_G = 100\sqrt{2}$. In order to check the performance of the optimized parameters, we show in Figure 3.9 the error in the concentration (in logarithmic scale) for various values of the parameters $\alpha_{1,2}$ and $\alpha_{2,1}$ after 20 Jacobi iterations. We see that the pair of optimized Robin parameters (red star), computed by numerically minimizing the continuous convergence factor, is located close to those giving the smallest error after the same number of iterations.

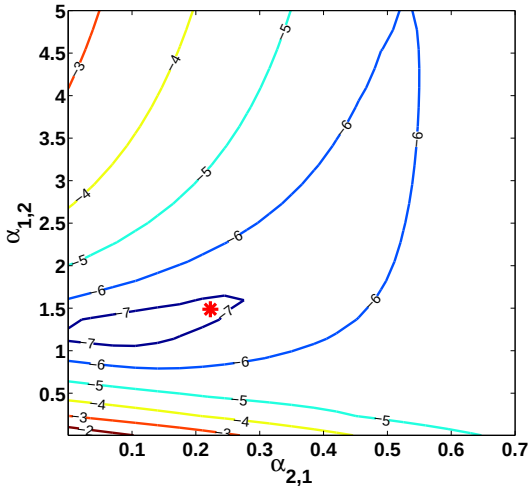

Figure 3.9: For $\mathrm{Pe}_G = 100\sqrt{2}$: Level curves for the error in the concentration (in logarithmic scale) after 20 Jacobi iterations for various values of the parameters $\alpha_{1,2}$ and $\alpha_{2,1}$, where the red star shows the optimized two-sided Robin parameters.

In the sense of efficiency, it is important for a domain decomposition algorithm to be weakly dependent on the mesh size (space and time), i.e. the number of iterations (or subdomain solves) does not increase considerably when the mesh size decreases. Thus, in Table 3.1, we count the number of subdomain solves required to reach a reduction

of 10^{-6} in the error in the concentration c and in the diffusive velocity r (in square brackets) of the different algorithms when refining the mesh in space and in time with $\Delta x/\Delta t = \text{const}$. We see that the convergence of Method 1 with the preconditioner is independent of the mesh size, while that with no preconditioner increases significantly. This is a well-known result for elliptic problems [88, 89, 28], but we haven't developed an analysis of the generalized Neumann- Neumann preconditioner for time-dependent problems. For Method 2, the convergence has a very weak dependence on the mesh size, which is obtained by the fact that the optimized parameters plays a role of a preconditioner (as it does for the pure diffusion equation, see Chapter 2). We also observe that for Method 2, GMRES does not improve the convergence speed compared to Jacobi iterations. This is also the case for pure diffusion problems (see Chapter 2), and thus the convolution Krylov subspace method [86], adapted to time-dependent systems, is an alternative that one could use in order to obtain the same acceleration in the convergence speed as in the case of stationary problems.

Δx	No Precond. Schur	Precond. Schur	Opt. Schwarz	
			GMRES	Jacobi
1/50	26 [27]	52 [54]	18 [18]	20 [20]
1/100	33 [33]	52 [52]	18 [20]	18 [21]
1/200	43 [43]	54 [52]	18 [20]	20 [22]
1/400	61 [59]	54 [52]	20 [22]	20 [25]

Table 3.1: For $\text{Pe}_G = 100\sqrt{2}$: Number of subdomain solves needed to reach a reduction of 10^{-6} in the error for the different algorithms , and for different values of the discretization parameters.

With the aim of analyzing the accuracy in time of the various methods when non-conforming time steps are used, we consider now $c_0 \neq 0$ and $f \neq 0$ defined in (3.26) and (3.27) respectively. We consider four initial time grids, which we then refine four times by a factor of 2,

- Time grid 1 (fine-fine): conforming with $\Delta t_1 = \Delta t_2 = T/125$.
- Time grid 2 (fine-coarse): nonconforming with $\Delta t_1 = T/125$ and $\Delta t_2 = T/100$.
- Time grid 3 (coarse-fine): nonconforming with $\Delta t_1 = T/100$ and $\Delta t_2 = T/125$.
- Time grid 4 (coarse-coarse): conforming with $\Delta t_1 = \Delta t_2 = T/100$.

The advection time step in each subdomain is such that $\Delta t_i = \Delta t_{a,i}, i = 1,2$. In space, we fix a conforming rectangular mesh and we compute a reference solution by solving problem (3.3)-(3.4) directly on a very fine time grid, with $\Delta t = \Delta t_a = T/(125 \times 2^6)$. The converged multidomain solution is such that the relative residual is smaller than 10^{-11}. We show in Figure 3.10 the error in the $L^2(0,T;L^2(\Omega))$-norm of the concentration c and of the vector field $\boldsymbol{r}$ versus the length of the maximum time step, $\max_i \Delta t_i$. We only give the results for Method 2 because the curves for Method 1 look exactly the same. We observe that first order convergence is preserved in the nonconforming case and the errors obtained in the nonconforming cases (Time grid 2, in blue and Time grid 3, in green) lie in between the errors in the fine and coarse conforming cases (Time grid 1, in red and Time grid 4, in magenta). Furthermore, the error in the concentration obtained in the nonconforming case (Time grid 2, in blue)

are very close to the errors in the finer conforming case (Time grid 1, in red). So for the continuous coefficient case, depending on the physics of the problem, nonconforming time grids may preserve the accuracy in time of the solution in the concentration (not in the diffusive velocity).

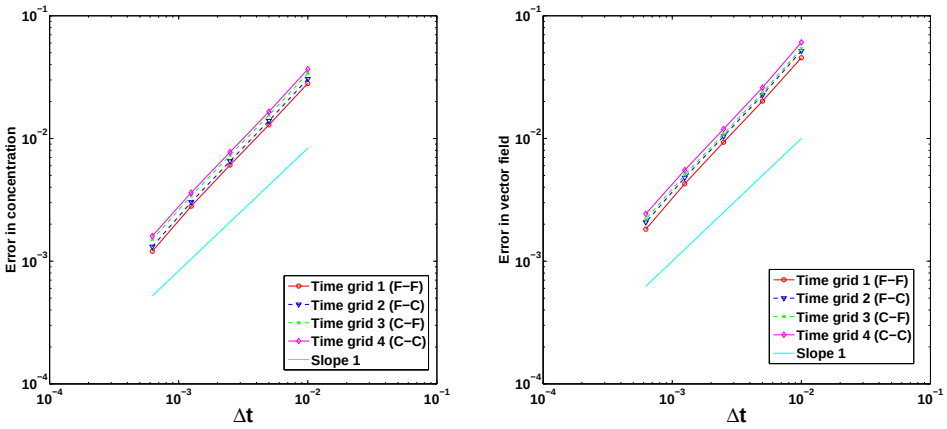

Figure 3.10: For $\mathrm{Pe}_G = 100\sqrt{2}$: $L^2 - L^2$ error in c (left) and in $\boldsymbol{r}$ (right) in logarithmic scale of the difference between the reference and the multidomain solutions versus the size of the time step.

3.4.1.2 A case with discontinuous coefficients

The advection and diffusion coefficients, $\boldsymbol{u}_i$ and $d_i, i = 1, 2$, given in Table 3.2, are constant in each subdomain but discontinuous across the interface. The global Péclet number and the CFL condition in each subdomain are also shown. We use nonconforming time grids $\Delta t_1 \neq \Delta t_2$, but equal advection and diffusion time steps, $\Delta t_{a,i} = \Delta t_i, i = 1, 2$. In space, we use a uniform rectangular mesh with size $\Delta x_1 = \Delta x_2 = \Delta x = 1/100$. As in the continuous coefficient case, we analyze the convergence behavior of each

	$\boldsymbol{u}_i$	d_i	Pe_G	Δt_i	dt_{CFL}	$\Delta t_{a,i}$
Ω_1	$(0.5, 1)$	0.02	≈ 10	$1/100$	$1/100$	$1/100$
Ω_2	$(0.5, 0.1)$	0.002	≈ 100	$1/75$	$1/50$	$1/75$

Table 3.2: Data for the discontinuous test case.

method with $c_0 = 0$ and $f = 0$. Figure 3.11 shows the error (in logarithmic scale) in the $L^2(0, T; L^2(\Omega))$-norm of the concentration c and of the vector field $\boldsymbol{r}$, versus the number of subdomain solves using GMRES with a random initial guess. Again we see that for advection-dominated problems, the preconditioner for Method 1 does not work well and Method 2 converges much faster than Method 1, by about a factor of 2.6 (with no preconditioner) and a factor of 3.3 (with the preconditioner) for both errors in c and $\boldsymbol{r}$.

Figure 3.12 shows the error in the diffusive flux $\boldsymbol{r}$ (in logarithmic scale) for various values of the parameters $\alpha_{1,2}$ and $\alpha_{2,1}$ after 15 Jacobi iterations. We observe that, for discontinuous coefficients, the pair of optimized parameters (red star) is also located close to the optimal numerical values after the same number of iterations.

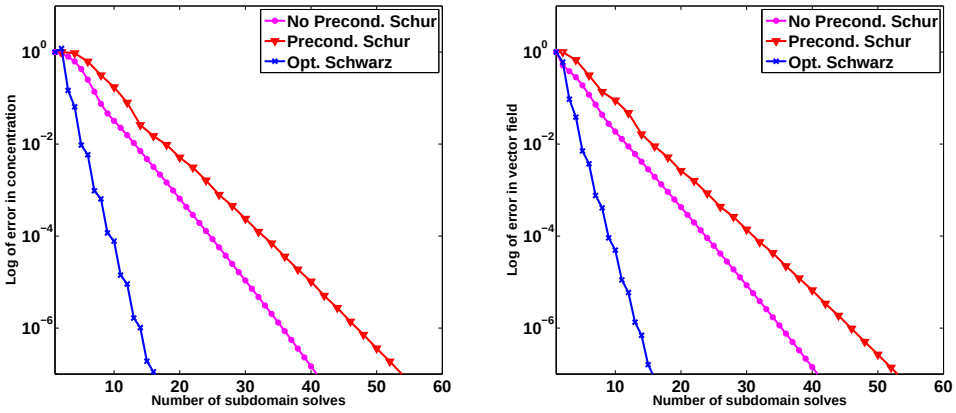

Figure 3.11: For discontinuous coefficients: Convergence curves for the different algorithms using GMRES: $L^2 - L^2$ error in c (left) and in $\boldsymbol{r}$ (right).

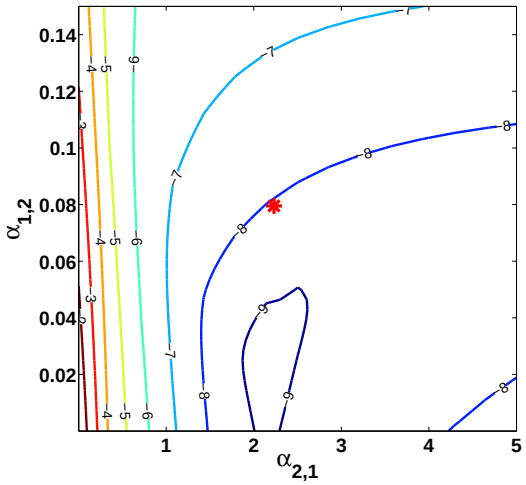

Figure 3.12: For discontinuous coefficients: Level curves for the error in $\boldsymbol{r}$ after 15 Jacobi iterations for various values of $\alpha_{1,2}$ and $\alpha_{2,1}$.

In Table 3.3, the number of subdomain solves needed to reach a reduction of 10^{-6} in the error in the concentration c and in the vector field $\boldsymbol{r}$ (in square brackets) when refining the mesh in space and in time with the ratio of Δx to Δt constant is shown. We see that for discontinuous coefficients and nonconforming time grids, the convergence of Method 1 with the Neumann-Neumann preconditioner is slightly dependent on the mesh size, while that with no preconditioner increases fairly rapidly with decreasing mesh size. For Method 2, the convergence is almost independent of the mesh size and again, the use of GMRES, instead of Jacobi iterations, does not improve significantly the convergence speed. We see that the convergence of Method 2 is very fast.

For the analysis of the accuracy in time of the multidomain solution when nonconforming time grids are used, we consider $c_0 \neq 0$ and $f \neq 0$ defined in (3.26) and (3.27) respectively. We consider four initial time grids which are then refined four times by a factor of 2,

- Time grid 1 (fine-fine): conforming with $\Delta t_1 = \Delta t_2 = T/136$.

Δx	No Precond. Schur	Precond. Schur	Opt. Schwarz	
			GMRES	Jacobi
1/50	25 [25]	40 [40]	13 [13]	14 [14]
1/100	36 [36]	48 [46]	15 [14]	16 [15]
1/200	52 [50]	54 [52]	15 [15]	17 [16]
1/400	76 [72]	58 [54]	16 [15]	18 [17]

Table 3.3: For discontinuous coefficients: Number of subdomain solves required to reach a reduction of 10^{-6} in the error for the different algorithms , and for different values of the discretization parameters.

- Time grid 2 (fine-coarse): nonconforming with $\Delta t_1 = T/136$ and $\Delta t_2 = T/100$.
- Time grid 3 (coarse-fine): nonconforming with $\Delta t_1 = T/100$ and $\Delta t_2 = T/136$.
- Time grid 4 (coarse-coarse): conforming with $\Delta t_1 = \Delta t_2 = T/100$.

As in the case with continuous coefficients, we take the same time step for the advection and the diffusion: $\Delta t_i = \Delta t_{a,i}, i = 1,2$, and a reference solution is computed on a very fine time grid, with $\Delta t = \Delta t_a = T/(136\times 2^6)$ (note that in space, the conforming mesh is fixed). In Figure 3.13 the error in the concentration c and of the vector field $\boldsymbol{r}$ versus the length of the maximum time step, $\max_i \Delta t_i$ is shown. Here we give the results for Method 1 (instead of Method 2 as for the continuous test case) since the error in time given by the two methods can't be distinguished on the figure. We observe that: firstly, first order convergence in time is preserved in the nonconforming cases; secondly, the errors obtained in the nonconforming cases are in between the errors obtained in the conforming coarse and conforming fine grids (which is reasonable); thirdly, the errors obtained in the nonconforming case (Time grid 2, in blue, with a finer time step in Ω_1, where the advection and diffusion coefficients are larger) are very close to the errors in the finer conforming case (Time grid 1, in red). Thus using nonconforming grids can adapt the time steps in the subdomains and limit the computational cost locally, while preserving almost the same accuracy as in the finer conforming case.

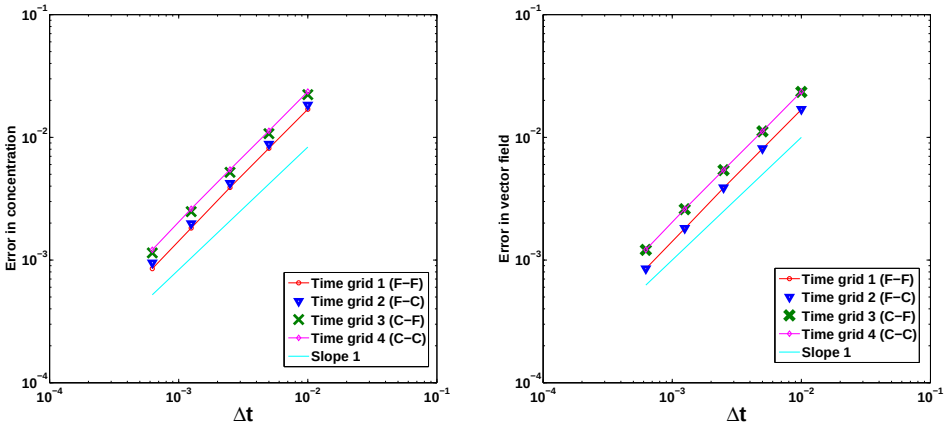

Figure 3.13: For discontinuous coefficients: $L^2 - L^2$ error in c (left) and in $\boldsymbol{r}$ (right) in logarithmic scale of the difference between the reference and the multidomain solutions versus the size of the time step.

3.4.2 Test case 2: Rotating velocity

The computational domain Ω is $(0,2)^2$ and the final time is $T = 1$. We split Ω into two nonoverlapping subdomains $\Omega_1 = (0,0.7) \times (0,2)$ and $\Omega_2 = (0.7,2) \times (0,2)$. The porosity is constant in each subdomain and discontinuous across the interface, $\phi_1 = 1, \phi_2 = 0.1$, and the advection coefficient is the rotating velocity field (see Figure 3.14)

$$\boldsymbol{u} = \big(-\sin(\pi/2(y-1))\cos(\pi/2(x-1)), \cos(\pi/2(y-1))\sin(\pi/2(x-1))\big)\,.$$

The diffusion coefficient is constant in each subdomain. We consider the two cases shown in Table 3.14 . For the spatial discretization, we use a uniform rectangular mesh with size $\Delta x_1 = \Delta x_2 = \Delta x = 1/100$. The maximum local Péclet number in each subdomain is shown in Table 3.14. For the time discretization, we use nonconforming time grids

$$\Delta t_1 = 1/100 \text{ and } \Delta t_2 = 1/75,$$

and the advection time steps are such that

$$\Delta t_i = 10\Delta t_{a,i}, \text{ for } i = 1,2,$$

(which satisfies the CFL condition in each subdomain, $\Delta t^1_{\text{CFL}} \leq 0.02$ in Ω_1 and $\Delta t^2_{\text{CFL}} \leq 0.002$ in Ω_2).

	d_1	$Pe_{L,1}$	d_2	$Pe_{L,2}$
Advection-dominated	0.01	1.9995	0.007	2.8564
Diffusion-dominated	0.1	0.19995	0.07	0.28564

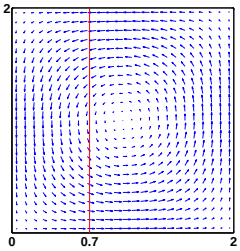

Figure 3.14: Left: Diffusion coefficient and corresponding maximum local Péclet number in each subdomain; Right: The rotating velocity field.

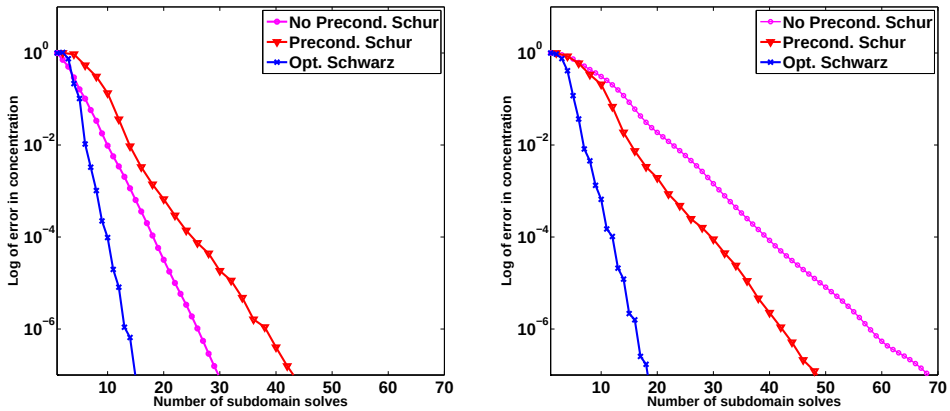

Figure 3.15: For rotating velocity: $L^2 - L^2$ error in the concentration c for the different algorithms using GMRES: the advection-dominated case (left) and the diffusion-dominated case (right).

As in the first test problem, we first analyze the convergence behavior by solving a problem with $c_0 = 0$ and $f = 0$ (thus $c = 0$ and $\boldsymbol{r} = 0$). We start with a random initial guess on the space-time interface and compute the errors (in logarithmic scale) in the $L^2(0,T;L^2(\Omega))$-norm of the concentration c and the vector field $\boldsymbol{r}$, versus the number of subdomain solves. We stop the iteration when the errors are less than 10^{-6}. In Figure 3.15 we show the errors in the concentration c of the different algorithms for the advection-dominated (left) and diffusion-dominated (right) cases (the errors in the vector field $\boldsymbol{r}$ behave in a same way as the errors in the concentration). We observe results similar to those obtained for the previous test cases: for Method 1, the Neumann-Neumann preconditioner considerably improves the convergence speed when the diffusion is dominant but deteriorates it when the advection is dominant; Method 2 converges much faster than Method 1 with or without the preconditioner, it is at least by a factor of 2 (for the advection-dominated case) and of 2.5 (for the diffusion-dominated case). In Figure 3.16, we show the error in the concentration (in logarithmic scale) for various values of the parameters $\alpha_{1,2}$ and $\alpha_{2,1}$ after 15 Jacobi iterations for the advection-dominated case. We see again that the pair of optimized parameters (red star) is located close to the small error zone.

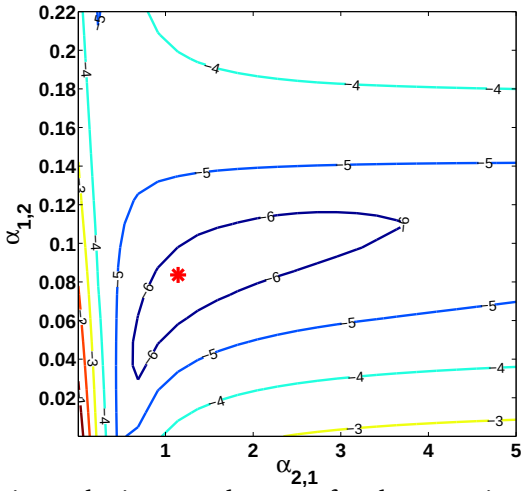

Figure 3.16: For rotating velocity: Level curves for the error in the concentration (in logarithmic scale) after 15 Jacobi iterations for various values of the parameters $\alpha_{1,2}$ and $\alpha_{2,1}$, where the red star the optimized Robin parameters.

Next, we analyze the accuracy in time when nonconforming time grids are used. Toward this end, we consider the advection-dominated case and impose an initial condition

$$c_0(x,y) \;=\; 0.5xy(x-2)(y-2)\exp(-100((x-0.2)^2+(y-0.5)^2)).$$

Four initial time grids, which are then refined 4 times by a factor of 2, are considered

- Time grid 1 (fine-fine): conforming with $\Delta t_1 = \Delta t_2 = T/128$.
- Time grid 2 (fine-coarse): nonconforming with $\Delta t_1 = T/128$ and $\Delta t_2 = T/94$.
- Time grid 3 (coarse-fine): nonconforming with $\Delta t_1 = T/94$ and $\Delta t_2 = T/128$.
- Time grid 4 (coarse-coarse): conforming with $\Delta t_1 = \Delta t_2 = T/94$.

Unlike the first test case, here we consider different time steps for the advection and the diffusion: $\Delta t_i = 10\,\Delta t_{a,i}$, $i = 1,2$. A reference solution is again computed on a very fine time grid, with $\Delta t = 10\Delta t_a = T/(128 \times 2^6)$ (the mesh in space is fixed for the monodomain and multidomain problems). We consider the multidomain solution to have converged when the relative residual is smaller than 10^{-11}. Figure 3.17 shows the error in c and in $\boldsymbol{r}$ versus the size of the time step, $\max_i \Delta t_i$. We observe that for this case with variable coefficients, first order convergence is also preserved in the nonconforming case and the nonconforming time grids preserve the accuracy in time of the solution.

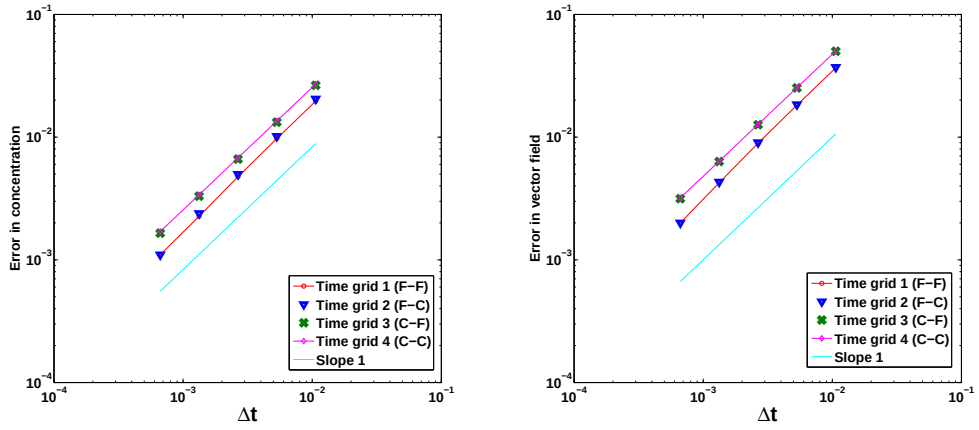

Figure 3.17: For rotating velocity: $L^2 - L^2$ error in c (left) and in $\boldsymbol{r}$ (right) in logarithmic scale of the difference between the reference and the multidomain solutions versus the size of the time step for the advection-dominated case.

3.4.3 Test case 3: A near-field simulation

We consider a simplified test case [53] for the simulation of the transport of a contaminant in a near field around a nuclear waste repository site. The domain of calculation is a 10m by 100m rectangle and the repository is a centrally located unit square (see Figure 3.18 with a blow-up in the $x-$ direction for visualization purpose). The repository consists of the EDZ (Excavation Damaged Zone) and the vitrified waste. The final time is $T_f = 2\,10^{11}$s ($\approx$ 20000 years). The coefficients for the simulation are given in Table 3.4. The advection field is governed by the (time-independent) Darcy flow equation together with the law of mass conservation

$$\begin{aligned} \boldsymbol{u} &= -K\nabla p \quad \text{in } \Omega, \\ \operatorname{div} \boldsymbol{u} &= 0 \quad \text{in } \Omega, \end{aligned}$$

No flow boundary is imposed horizontally and a pressure gradient is imposed vertically with $p = 100$ Pa on bottom and $p = 0$ on top.

The source term is $f = 0$ and an initial condition c_0 is defined by

$$c_0 = \begin{cases} 1, & \text{in the red box (containing the vitrified waste),} \\ 0, & \text{elsewhere.} \end{cases} \tag{3.28}$$

Boundary conditions of the tranport problem are homogeneous Dirichlet conditions on top and bottom, and homogeneous Neumann conditions on the left and right hand sides.

Material	Permeability K (m/s)	Porosity ϕ	Diffusion coefficient d (m^2/s)
Host rock	10^{-13}	0.06	$6\,10^{-13}$
EDZ	$5\,10^{-11}$	0.20	$2\,10^{-11}$
Vitrified waste	10^{-8}	0.10	10^{-11}

Table 3.4: Data for flow and transport problems.

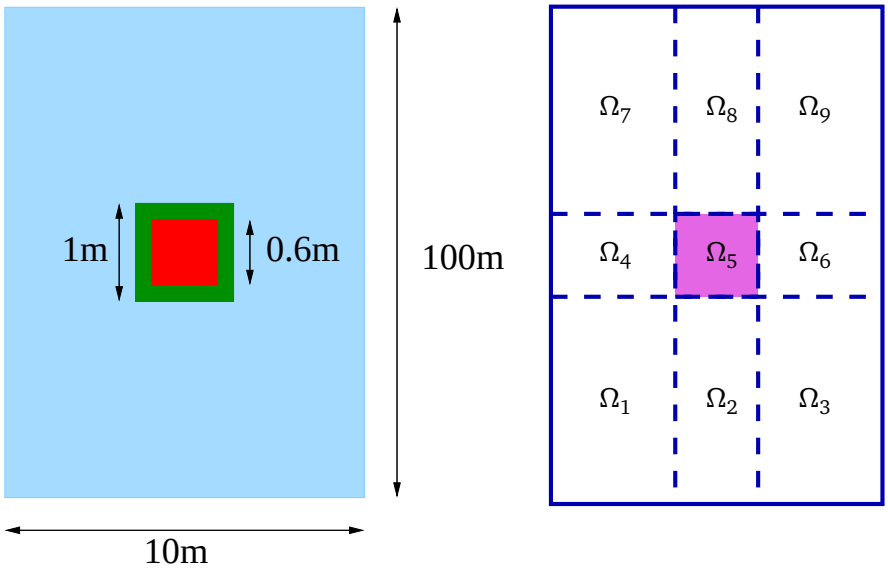

Figure 3.18: The domain of calculation and its decomposition.

For the spatial discretization (for both the flow and transport equations), we use a non-uniform but conforming rectangular mesh with a finer discretization in the repository (a uniform mesh with 10 points in each direction) and a coarser discretization in the host rock (the mesh size progressively increases with distance from the repository by a factor of 1.05). The Darcy flow is approximated by using mixed finite elements. Figure 3.19 shows a zoom of the velocity field around the repository. The maximum local Péclet number in this test case is 0.0513, thus it is a diffusion-dominated problem. The time step due to the CFL condition is large as the velocity field is very small (of order of 10^{-13} m/s), $\Delta t_{\text{CFL}} = 0.075\ T_f$ in the repository and $\Delta t_{\text{CFL}} = 0.125\ T_f$ elsewhere. We decompose Ω into 9 subdomains as depicted in Figure 3.18 with Ω_5 representing the repository. For the time discretization, we use nonconforming time grids (with a finer time step in the repository) and equal diffusion and advection time steps $\Delta t_i = \Delta t_{a,i}, \forall i$.

As observed in the second test case of Chapter 2, the longer the time interval the slower the convergence. In addition, for a fixed time step Δt, it is more costly to approximate the solution for a longer time interval than for a shorter time interval. Thus we use time windows (see Appendix for this test case. We divide $(0, T_f)$ into 200 time windows with size $T = 10^9$s. We will first analyze the convergence behavior as well as the accuracy in time of the multidomain solution with nonconforming grids

for the first time window, $(0, T)$. The time steps are $\Delta t_5 = \Delta t_{a,5} = T/500$, and $\Delta t_i = \Delta t_{a,i} = T/100$, $i \neq 5$.

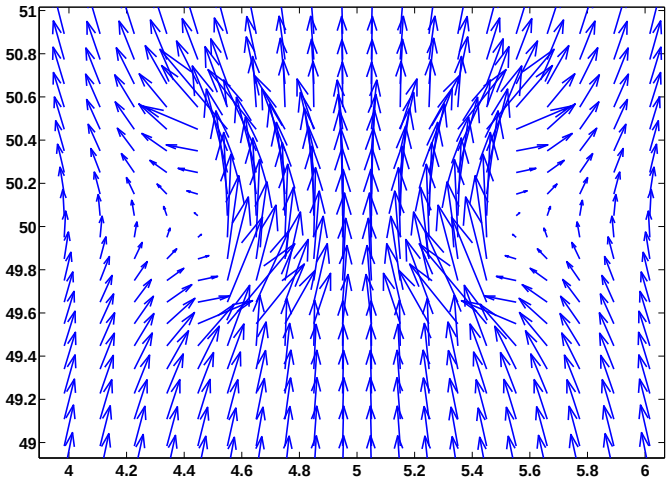

Figure 3.19: Darcy flow.

To analyze the convergence behavior of each method, as in the previous test cases, we solve a problem with $c_0 = 0$ (thus $c = 0$ and $\boldsymbol{r} = 0$). We start with a random initial guess on the space-time interface and stop the iteration when the errors both in the concentration c and in the vector field $\boldsymbol{r}$ are less than 10^{-6} (Figure 3.20). We see that Method 1 with the preconditioner significantly improves the convergence speed compared to the case with no preconditioner, which makes it and Method 2 comparable. This is because the diffusion is dominant in this case. The errors in c and $\boldsymbol{r}$ behave quite similarly.

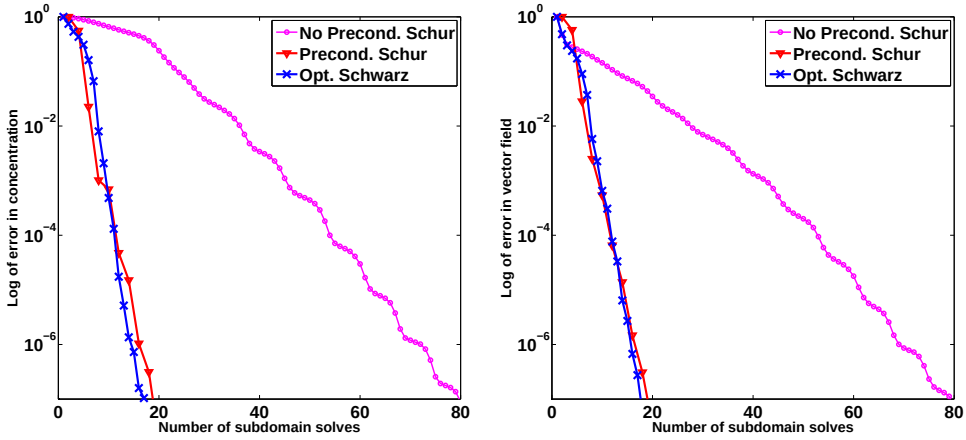

Figure 3.20: Convergence curves using GMRES: errors in c (on the left) and error in $\boldsymbol{r}$ (on the right).

Consider now the initial condition $c_0 \neq 0$ defined in (3.28). We check if the non-conforming time grids preserve the accuracy in time. We consider four initial time grids, which we then refine 4 times by a factor of 2,

- Time grid 1 (conforming fine): $\Delta t_i = T/250$, $\forall i$.

- Time grid 2 (nonconforming, fine in the repository): $\Delta t_5 = T/250$ and $\Delta t_i = T/50$, $\forall i \neq 5$.
- Time grid 3 (nonconforming, coarse in the repository): $\Delta t_5 = T/50$ and $\Delta t_i = T/250$,$\forall i \neq 5$.
- Time grid 4 (conforming coarse): $\Delta t_i = T/50$, $\forall i$.

Note that the advection time steps are equal to the diffusion time steps. The time steps are then refined several times by a factor of 2. In space, we fix a conforming rectangular mesh and we compute a reference solution on a very fine time grid, with $\Delta t = \Delta t_a = T/(250 \times 2^6)$. Figure 3.21 shows the error in the $L^2(0,T;L^2(\Omega))$-norm of the concentration c and of the vector field $\boldsymbol{r}$ versus the length of the maximum time step, $\max_i \Delta t_i$. We observe that first order convergence is preserved in the nonconforming case and the errors obtained in the nonconforming case with a fine time step in the repository (Time grid 2, in blue) are nearly the same as in the finer conforming case (Time grid 1, in red). Thus the use of nonconforming grids (where the ratio of the fine time step to the coarse time step is 5) preserves the accuracy in time of the monodomain scheme.

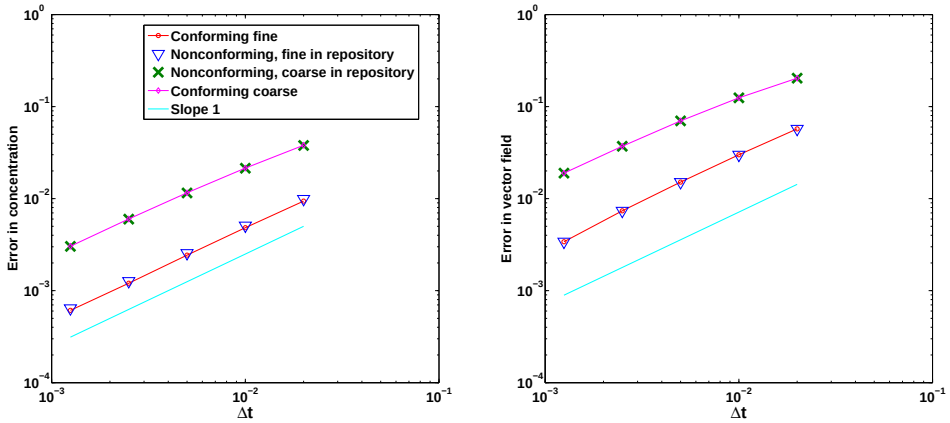

Figure 3.21: Errors in c (left) and $\boldsymbol{r}$ (right) in logarithmic scales between the reference and the multidomain solutions versus the time step.

Next we test how the two methods work in practice, where the exact solution is unknown and one can only rely on the relative residual at each iteration of GMRES to know whether he should stop the iterations and compute the corresponding multidomain solution. Consider the time grid defined at the beginning, $\Delta t_5 = T/500$, $\Delta t_i = T/100$, $i \neq 5$ and $\Delta t_i = \Delta t_{a,i}$ for $T = 10^9$s. We use GMRES for Method 1 (with the Neumann-Neumann preconditioner) and Method 2, and then compute the $L^2(0,T;L^2(\Omega))$ error of the difference between the multidomain solution and a reference solution computed on a very fine time grid, $\Delta t = \Delta t_a = T/(500 \times 2^2)$. We show in Figure 3.22 the relative residuals for each method versus the number of subdomain solves, and in Figure 3.23 the corresponding errors in c (left) and $\boldsymbol{r}$ (right) . We see that Method 2 converges faster than Method 1 and that the scheme errors in c and $\boldsymbol{r}$ are obtained for both methods when the relative residual is less than 10^{-3}; typically after 10 subdomain solves for Method 1 and 6 subdomain solves for Method 2.

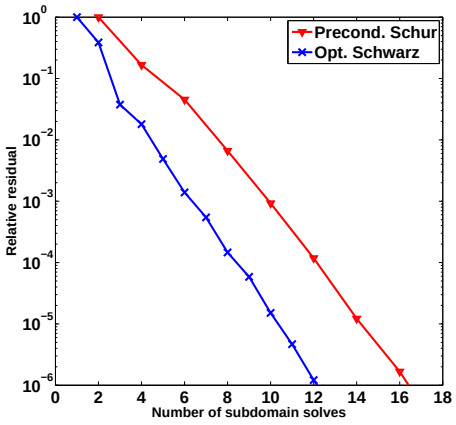

Figure 3.22: Relative residuals of GMRES for Method 1 (with the Neumann-Neumann preconditioner) and Method 2.

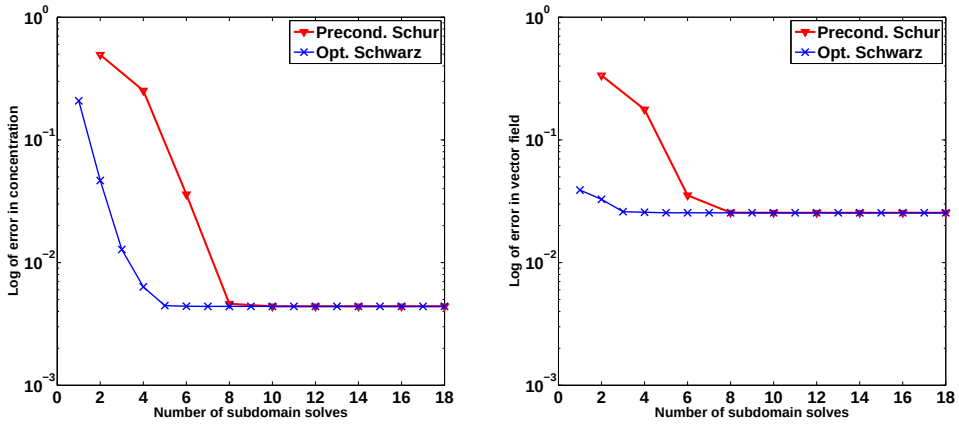

Figure 3.23: $L^2 - L^2$ error in c(left) and in $\boldsymbol{r}$ (right) in logarithmic scales between the reference and the multidomain solutions.

We now use time windows where the initial guess of the $(N+1)^{\text{th}}$ time window is calculated from the information at the final time of the N^{th} time window (see Appendix C), which helps reduce considerably the number of iterations required to reach the same tolerance compared with an arbitrary initial guess. Since the size of the time windows is uniform, we can use the same optimized parameters for all time windows for Method 2. In each time window, we stop the iterations when the relative residual is less than 10^{-3}. From the observation above, the maximum number of iterations in each time window is not greater than 5 (equivalent to 10 subdomain solves) for Method 1 (with the Neumann-Neumann preconditioner) and is not greater than 5 (equivalent to 5 subdomain solves) for Method 2. Figure 3.24 show the concentration in the repository (left) and in the host rock (right) after 1 ($\approx$ 100 years), 50 ($\approx$ 5000 years), 100 ($\approx$ 10000 years) and 200 ($\approx$ 20000 years) time windows respectively. We use different color scales for the solution in the repository to see clearly the effect of the advection field, while we use same color scales for the solution in the host rock to see the spreading of the contaminant in time. The concentration field behaves as expected and the migration of the radionuclide from the repository to the surrounding medium takes

place very slowly.

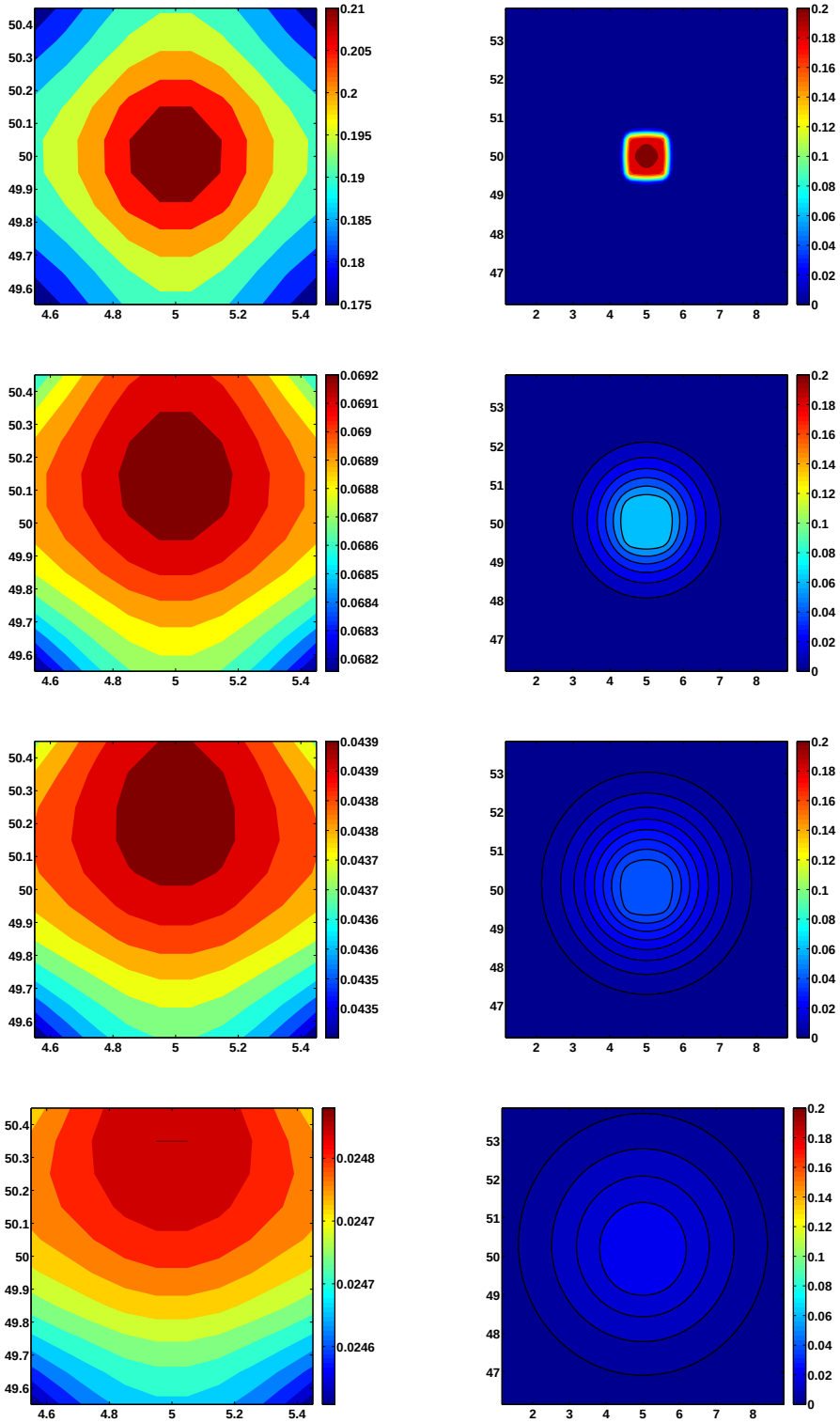

Figure 3.24: Snapshots of the concentration in the repository (left) and in the host rock (right) after approximately 100 years, 5000 years, 10000 years and 20000 years respectively

3.4.4 Test case 4: A simulation for a surface, nuclear waste storage

We consider a test case designed by ANDRA for a surface storage of short half-life nuclear waste. The computational domain is depicted in Figure 3.25 with different physical zones, where the waste is stored in square boxes ("dechet" zone). The properties of these zones are given in Table 3.5. Note that in our calculation, we use the effective diffusion, defined by $d_{\text{eff}} = \phi \times d_{\text{m}}$. The advection field is governed by Darcy's law together with the law of mass conservation

$$\begin{aligned} \boldsymbol{u} &= -K\nabla h \quad \text{in } \Omega, \\ \operatorname{div} \boldsymbol{u} &= 0 \quad \text{in } \Omega. \end{aligned}$$

Dirichlet conditions are imposed on top, $h = 10$m and on bottom $h = 9.998$m of the domain and no flow boundary on the left and right sides.

The final time is $T_f = 500$ years. The source term is $f = 0$ and the initial condition is such that

$$c_0 = \begin{cases} 1, & \text{in "dechet1" and "dechet2",} \\ 0, & \text{elsewhere.} \end{cases}$$

Boundary conditions of the transport problem are homogeneous Dirichlet conditions on top and bottom, and homogeneous Neumann conditions on the left and right hand sides.

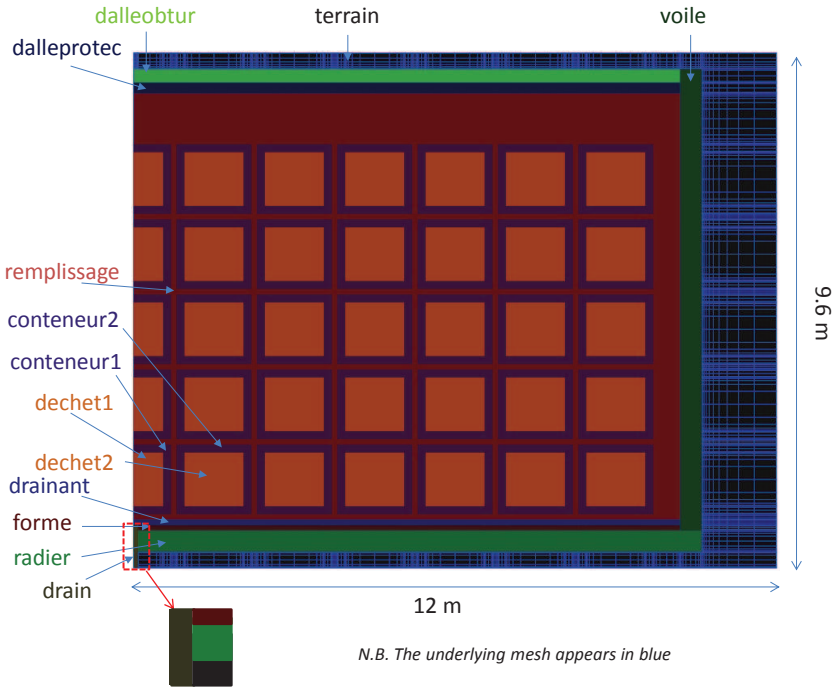

Figure 3.25: The geometry of the test case.

For the spatial discretization (for both the flow and transport equations), we use a non-uniform rectangular mesh, shown in Figure 3.25 in blue, with 171 cells in the $x-$direction and 158 cells in the $y-$direction (see Appendix D for more details about the discretization). The mesh size is $\Delta x \approx 0.42$m. The hydraulic head is approximated by mixed finite elements and is shown in Figure 3.26 (left). We decompose the domain into 6 rectangular subdomains in a way such that the black zone ("terrain") is separated

Zone	Hydraulic conductivity K (m/year)	Porosity ϕ	Molecular diffusion d_m (m^2/year)
terrain	94608	0.30	1
radier	$3.1536\,10^{-4}$	0.15	$6.31\,10^{-5}$
forme	$3.1536\,10^{-3}$	0.20	$1.58\,10^{-3}$
drainant	94608	0.30	$5.36\,10^{-2}$
voile	$3.1536\,10^{-3}$	0.20	$1.58\,10^{-3}$
remplissage	5045.76	0.30	$5.36\,10^{-2}$
dalleprotec	$3.1536\,10^{-3}$	0.20	$1.58\,10^{-3}$
dalleobtur	$3.1536\,10^{-3}$	0.20	$1.58\,10^{-3}$
drain	94608	0.30	1
conteneur1/conteneur2	$3.1536\,10^{-4}$	0.12	$4.47\,10^{-4}$
dechet1/dechet2	$3.1536\,10^{-4}$	0.30	$1.37\,10^{-3}$

Table 3.5: Data for flow and transport problems.

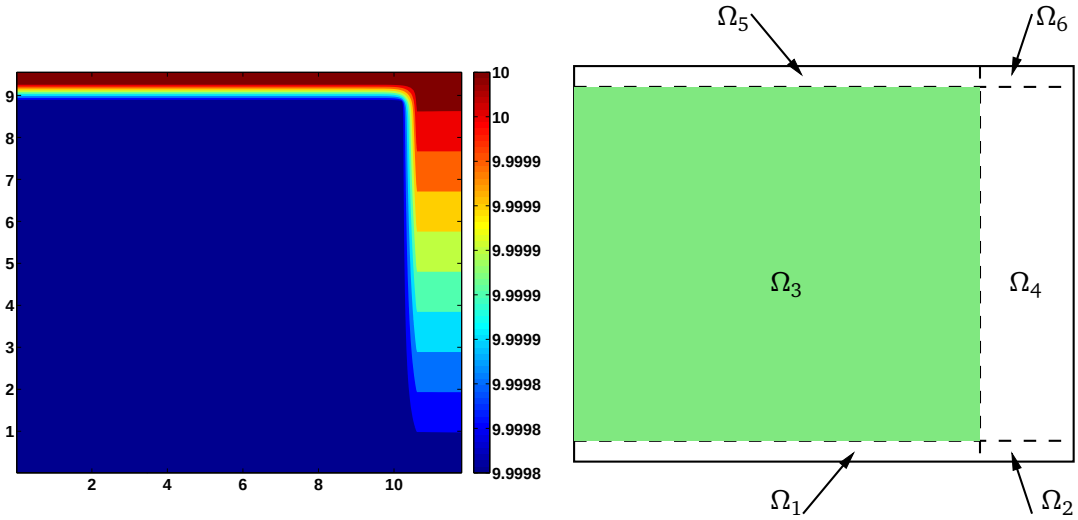

Figure 3.26: The hydraulic head field and the decomposition of the domain.

from the rest and subdomain Ω_3 includes the "dallerobtur", "voile", "radier" and a part of "drain" zones (see Figure 3.26 (right)). The transport is dominated by diffusion in subdomain Ω_3 (the maximum of the local Péclet number $\mathrm{Pe}_L \approx 0.0032$) and is dominated by advection (with $\mathrm{Pe}_L \approx 2.75$). The time steps due to the CFL condition are $\Delta t_{a,3} \leq 0.6551$ year and very small elsewhere, $\Delta t_{a,i} \leq 6.0874\,10^{-5}$ year, $\forall i \neq 3$.

As in test case 3, we use time windows with size $T = 10$ years. We consider the first time window, $(0, T)$ and use nonconforming time grids with $\Delta t_{d,3} = 0.1$ (year) and $\Delta t_{d,i} = 0.5$ year, $\forall i \neq 3$. The advection steps, satisfying the CFL conditions, are $\Delta t_{a,3} = \Delta t_{d,3}$ and $\Delta t_{a,i} = 825 \Delta t_{d,i}$, $\forall i \neq 3$. We use a zero initial guess on the space-time interface, and perform GMRES for Method 1 (with Neumann-Neumann preconditioner) and Method 2. We compute the errors of the difference between the multidomain solution and a reference solution computed with a very fine, conforming time grid. We show in Figure 3.27 the relative residuals for each method versus the number of subdomain solves, and in Figure 3.28 the corresponding errors in c and $\boldsymbol{r}$ (note that the scales between the errors in c and $\boldsymbol{r}$ are different). We observe that the

convergence of Method 2 is much faster than Method 1. The error due to the schemes in c and $\boldsymbol{r}$ are obtained for both methods when the relative residual is less than 10^{-2}.

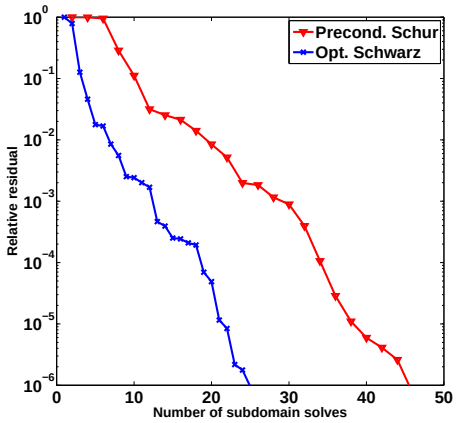

Figure 3.27: Relative residuals of GMRES for Method 1 (with the Neumann-Neumann preconditioner) and Method 2.

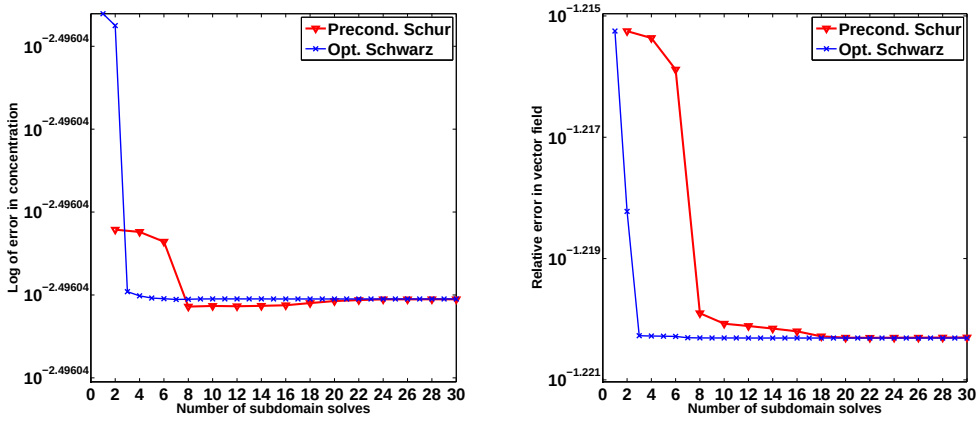

Figure 3.28: $L^2 - L^2$ error in c (left) and in $\boldsymbol{r}$ (right) in logarithmic scales between the reference and the multidomain solutions.

Next, we run the two methods for 50 time windows and stop the iterations in each time window when the relative residual is less than 10^{-2}. From the observation above, the maximum number of iterations in each time window is not greater than 10 (equivalent to 20 subdomain solves) for Method 1 (with the Neumann-Neumann preconditioner) and is not greater than 8 (equivalent to 8 subdomain solves) for Method 2. Figures 3.29 shows the concentration field after 2 (20 years), 5 (50 years), 35 (350 years) and 50 (500 years) time windows respectively. We see that the radionuclide escapes from the waste packages and slowly migrates into the surrounding area. Due to the specific design of the storage and under the effect of advection, the radionuclide tends to move toward the bottom right corner.

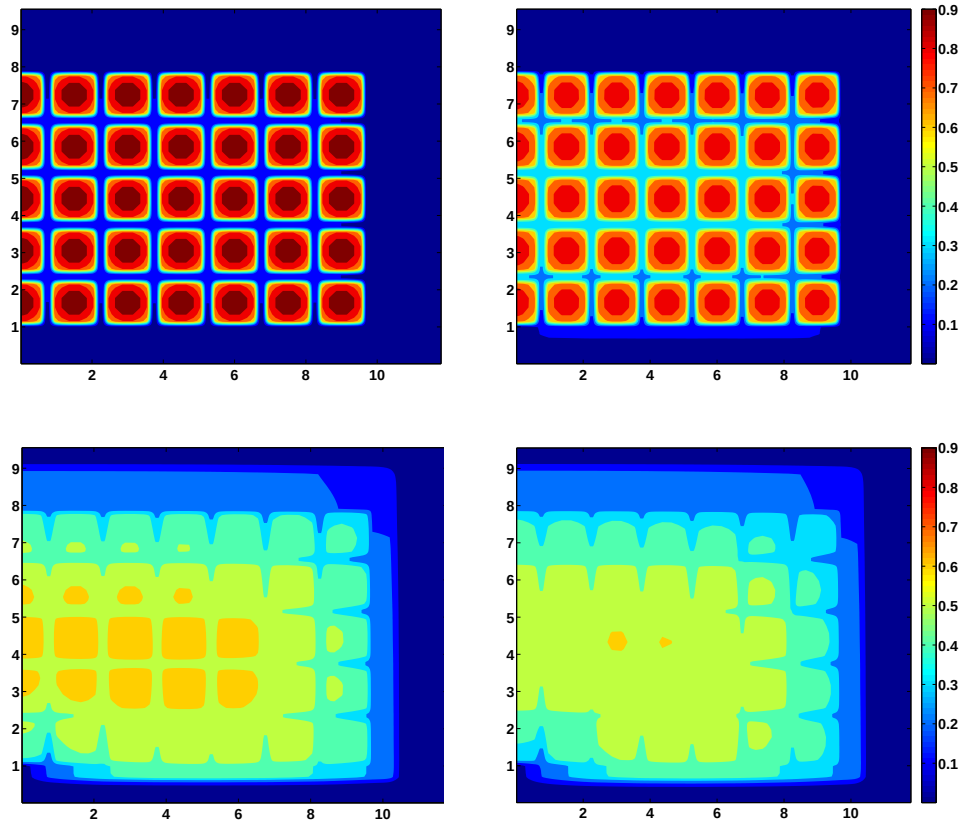

Figure 3.29: Snapshots of the concentration after 20 years, 50 years, 350 years and 500 years respectively.

Conclusion

In the context of operator splitting, we have extended the two methods derived in the previous section for the pure diffusion problem to the heterogeneous advection-diffusion problem. Two discrete interface problems corresponding to the generalized time-dependent Steklov-Poincaré operator and OSWR approach have been formulated in a way such that they are equivalent to the discrete monodomain problem and that they enable different advection and diffusion time steps in the subdomains. For Method 1, a generalized Neumann-Neumann preconditioner is considered and is validated for different test cases in 2D experiments. Numerical results show that Method 2 outperforms Method 1 (with or without preconditioner) in terms of subdomain solves needed to reach a fixed error reduction in the solution (by a factor of 2 to 2.5 in our test cases). Due to the use of the optimized Robin parameters, Method 2 is robust in the sense that it handles well and consistently both the advection-dominated and diffusion-dominated problems. Method 1 with the Neumann-Neumann preconditioner works well and converges faster than without preconditioner when the diffusion is dominant and it also efficiently deals with the case with large jumps in the diffusion coefficients. When the advection is dominant, the Neumann-Neumann preconditioner converges slower than when there is no preconditioner. However, asymptotically the convergence of the Neumann-Neumann preconditioned Method 1 has a weak depen-

dence on the mesh size of the discretizations while that of Method 1 with no preconditioner significantly depends on the mesh size. For Method 2, because of the optimized parameters, which play in some sense the role of a preconditioner, the convergence is weakly dependent on the discretization parameters. In addition, both methods preserve the accuracy in time when nonconforming time steps are used, both for two subdomains and for multiple subdomains: the error of the nonconforming time grid (with finer time steps in the zones where the solution varies most, i.e. with larger advection and diffusion coefficients) is close to that of the conforming fine grid.

Two test cases for the simulation of nuclear waste disposal are implemented using nonconforming time grids and time windows. As the geometry of the computational domain is complex and the physical coefficients are highly variable, we consider multiple subdomains. For this application where the diffusion is dominant, the Neumann-Neumann preconditioned Method 1 and Method 2 work well but Method 2 converges faster than Method 1. We also observe that with an adapted initial guess calculated from the previous time window, one performs only a few iterations in each time window to reach the scheme error.

Chapter 4

Extension to Ventcell transmission conditions

Contents

4.1 Stationary problems 92
4.1.1 Multidomain formulation with Ventcell transmission conditions . . 93
4.1.2 Equivalence between the multidomain and the monodomain problems 94
4.1.3 Well-posedness of the Ventcell boundary value problem 96
4.1.4 An interface problem 99
4.1.5 Numerical results 100
4.2 Time-dependent diffusion problems 103
4.2.1 Multidomain formulation with Ventcell transmission conditions . . 104
4.2.2 Well-posedness of the Ventcell boundary value problem 105
4.2.3 A space-time interface problem 108
4.2.4 Nonconforming discretization in time 109
4.2.5 Numerical results 110
4.3 Time-dependent advection-diffusion problems 116
4.3.1 An extension of the OSWR with Ventcell transmission conditions and operator splitting 116
4.3.2 Nonconforming time discretizations 120
4.3.3 Some comments on the approach with Ventcell transmission conditions and operator splitting 120

In the previous chapters, we have studied the Optimized Schwarz Waveform Relaxation (OSWR) method with optimized Robin transmission conditions in a mixed formulation. Robin transmission conditions result from approximations by zero order polynomials of the optimal interface operators (here "optimal" means that these operators lead to convergence of the algorithm in a number of iterations equal to the number of subdomains (see, e.g., [97, 72, 44, 48] and Appendix A.2). The convergence of the OSWR algorithm can be improved by using higher order approximations, such as Ventcell transmission conditions [62, 73]. The optimized transmission conditions were originally introduced for stationary problems in [97, 72] and analyzed in [44], namely

Optimized Schwarz methods, and were considered in the primal formulation only. In this chapter, we study the Optimized Schwarz and OSWR methods with Ventcell transmission conditions in the context of mixed formulations. The chapter consists of three sections treating the stationary problem, the time-dependent diffusion problem and the advection-diffusion problem, respectively. For each of these three problems, the multidomain formulation with Ventcell transmission conditions in mixed form is derived; the equivalence between the multidomain problem and the original problem is proved and an interface problem is formulated and solved iteratively using Jacobi iterations or GMRES. For the stationary and time-dependent diffusion problems, the proofs of the well-posedness of the subdomain problems with Ventcell boundary conditions are given. For the advection-diffusion problem, we use operator splitting to treat the advection and the diffusion separately as was done in Chapter 3. For time-dependent problems, we consider nonconforming time grids to take advantage of this global-in-time method. Numerical experiments (for two subdomains) for different test cases are presented for the stationary problem and the time-dependent diffusion problem to study the performance of the Optimized Schwarz and OSWR methods with Ventcell transmission conditions and (for the diffusion problem) to compare it with the two methods analyzed in Chapter 2.

4.1 Stationary problems

For an open, bounded domain $\Omega \subset \mathbb{R}^d$ $(d = 2, 3)$ with Lipschitz boundary $\partial\Omega$, consider a model for single phase flow in porous media written in mixed form:

$$\begin{aligned} \operatorname{div} \boldsymbol{u} &= f \quad \text{in } \Omega, \\ \boldsymbol{K}^{-1}\boldsymbol{u} + \nabla p &= 0 \quad \text{in } \Omega, \\ p &= 0 \quad \text{on } \partial\Omega. \end{aligned} \tag{4.1}$$

Recall (see Chapter 1) that p is the pressure, $\boldsymbol{u}$ the Darcy velocity, f the source term and $\boldsymbol{K}$ a symmetric, positive definite, time independent hydraulic conductivity (or permeability) tensor. For the sake of simplicity, we have imposed homogeneous Dirichlet condition on the boundary, other types of boundary conditions can be treated similarly. The well-posedness of problem (4.1) is well-known (see, e.g., [21, 22, 104]).

Theorem 4.1. *Assume that there exist positive constants K_- and K_+ such that $\varsigma^T \boldsymbol{K}^{-1}(\cdot)\varsigma \geq K_-|\varsigma|^2$, and $|\boldsymbol{K}(\cdot)\varsigma| \leq K_+|\varsigma|$ a.e. in Ω and $\forall \varsigma \in \mathbb{R}^d$. If f is in $L^2(\Omega)$, problem* (4.1) *has a unique weak solution*

$$(p, \boldsymbol{u}) \in L^2(\Omega) \times H(div, \Omega).$$

In the following, we consider a nonoverlapping decomposition of Ω and formulate a multidomain problem equivalent to problem (4.1), in which Ventcell transmission conditions are used. This type of transmission conditions involves not only the normal flux and the pressure trace on the interface (as in zero order (Robin) transmission conditions), but also the tangential divergence of the flux on the interface.

4.1.1 Multidomain formulation with Ventcell transmission conditions

For simplicity, we consider a decomposition of Ω into two nonoverlapping subdomains, Ω_1 and Ω_2, separated by an interface Γ:

$$\Omega_1 \cap \Omega_2 = \emptyset; \quad \Gamma = \partial\Omega_1 \cap \partial\Omega_2 \cap \Omega, \quad \Omega = \Omega_1 \cup \Omega_2 \cup \Gamma.$$

The same analysis can be extended to the case of many subdomains in bands. For $i = 1,2$, let $\boldsymbol{n}_i$ denote the unit, outward pointing, vector field on $\partial\Omega_i$, and for any scalar, vector or tensor valued function ψ defined on Ω, let ψ_i denote the restriction of ψ to Ω_i. We use the notation ∇_τ and div_τ for the tangential gradient and divergence respectively, where τ is the tangential unit vector. We denote by $\boldsymbol{K}_{i,\Gamma}$ the tangential component of $\boldsymbol{K}_i$, $i = 1,2$, restricted to Γ. A multidomain formulation equivalent to problem (4.1) is obtained by solving in each subdomain the following problem

$$\begin{aligned} \mathrm{div}\,\boldsymbol{u}_i &= f \quad \text{in } \Omega_i, \\ \boldsymbol{K}_i^{-1}\boldsymbol{u}_i + \nabla p_i &= 0 \quad \text{in } \Omega_i, \\ p_i &= 0 \quad \text{on } \left(\partial\Omega_i \cap \partial\Omega\right), \end{aligned}$$

together with the transmission conditions

$$\begin{aligned} p_1 &= p_2, \\ \boldsymbol{u}_1 \cdot \boldsymbol{n}_1 + \boldsymbol{u}_2 \cdot \boldsymbol{n}_2 &= 0, \end{aligned} \quad \text{on } \Gamma. \tag{4.2}$$

Under sufficient regularity, one may replace (4.2) by the Ventcell transmission conditions, which were introduced and analyzed for primal formulations in [96, 71, 74]:

$$\begin{aligned} -\boldsymbol{u}_1 \cdot \boldsymbol{n}_1 + \alpha_{1,2}\, p_1 + \beta_{1,2}\, \mathrm{div}_\tau\left(-\boldsymbol{K}_{2,\Gamma}\nabla_\tau p_1\right) &= -\boldsymbol{u}_2 \cdot \boldsymbol{n}_1 + \alpha_{1,2}\, p_2 + \\ &\quad \beta_{1,2}\, \mathrm{div}_\tau\left(-\boldsymbol{K}_{2,\Gamma}\nabla_\tau p_2\right), \quad \text{on } \Gamma, \\ -\boldsymbol{u}_2 \cdot \boldsymbol{n}_2 + \alpha_{2,1}\, p_2 + \beta_{2,1}\, \mathrm{div}_\tau\left(-\boldsymbol{K}_{1,\Gamma}\nabla_\tau p_2\right) &= -\boldsymbol{u}_1 \cdot \boldsymbol{n}_2 + \alpha_{2,1}\, p_1 + \\ &\quad \beta_{2,1}\, \mathrm{div}_\tau\left(-\boldsymbol{K}_{1,\Gamma}\nabla_\tau p_1\right), \quad \text{on } \Gamma, \end{aligned} \tag{4.3}$$

where $\alpha_{i,j}$ and $\beta_{i,j}$, $i = 1,2$, $j = 3 - i$, are positive constants. The transmission conditions (4.3) are derived in such a way that they are equivalent to the original ones given in (4.2) (see Subsection 4.1.2 for the proof). However, the convergence rate of the iterative algorithm used to solve the multidomain problem depends on the parameter $\alpha_{i,j}$ and $\beta_{i,j}$ used in the transmission conditions (4.3). These parameters then may be chosen to optimize the convergence factor. See [72, 71] and Appendix A.1 for details of the derivation of Ventcell transmission conditions and of how to compute the optimized parameters $\alpha_{i,j}$ and $\beta_{i,j}$.

In order to handle Ventcell transmission conditions in mixed form (where higher regularity required for the second order term), we introduce Lagrange multipliers on the interface Γ: $p_{i,\Gamma}, i = 1,2$, representing the pressure trace p_i on Γ and a vector field $\boldsymbol{u}_{\Gamma,i} := \boldsymbol{K}_{j,\Gamma}\nabla_\tau p_{i,\Gamma}$, $i = 1,2, j = 3 - i$. We use the notation $\boldsymbol{u}_{\Gamma,i}$ instead of $\boldsymbol{u}_{i,\Gamma}$ to insist that $\boldsymbol{u}_{\Gamma,i}$ is NOT the tangential component of a trace of $\boldsymbol{u}_i$ on the interface. In fact $\boldsymbol{u}_{\Gamma,i}$ is used as an artificial tool for convergence purposes (it does not have a particular

physical meaning). We rewrite (4.3) defined on Γ as follows

$$\begin{aligned}
-\boldsymbol{u}_1\cdot\boldsymbol{n}_1+\alpha_{1,2}\,p_{1,\Gamma}+\beta_{1,2}\,\mathrm{div}_\tau\,\boldsymbol{u}_{\Gamma,1} &= -\boldsymbol{u}_2\cdot\boldsymbol{n}_1+\alpha_{1,2}\,p_{2,\Gamma}+\beta_{1,2}\,\mathrm{div}_\tau\,\left(\boldsymbol{K}_{2,\Gamma}\boldsymbol{K}_{1,\Gamma}^{-1}\boldsymbol{u}_{\Gamma,2}\right),\\
-\boldsymbol{u}_2\cdot\boldsymbol{n}_2+\alpha_{2,1}\,p_{2,\Gamma}+\beta_{2,1}\,\mathrm{div}_\tau\,\boldsymbol{u}_{\Gamma,2} &= -\boldsymbol{u}_1\cdot\boldsymbol{n}_2+\alpha_{2,1}\,p_{1,\Gamma}+\beta_{2,1}\,\mathrm{div}_\tau\,\left(\boldsymbol{K}_{1,\Gamma}\boldsymbol{K}_{2,\Gamma}^{-1}\boldsymbol{u}_{\Gamma,1}\right),\\
\boldsymbol{K}_{2,\Gamma}^{-1}\,\boldsymbol{u}_{\Gamma,1}+\nabla_\tau p_{1,\Gamma} &= 0,\\
\boldsymbol{K}_{1,\Gamma}^{-1}\,\boldsymbol{u}_{\Gamma,2}+\nabla_\tau p_{2,\Gamma} &= 0.
\end{aligned} \tag{4.4}$$

The corresponding multidomain problem consists of solving in the subdomains the problem, for $i=1,2,\ j=3-i$:

$$\begin{aligned}
\mathrm{div}\,\boldsymbol{u}_i &= f && \text{in } \Omega_i,\\
\boldsymbol{K}_i^{-1}\boldsymbol{u}_i+\nabla p_i &= 0 && \text{in } \Omega_i,\\
p_i &= 0 && \text{on } \left(\partial\Omega_i\cap\partial\Omega\right),\\
-\boldsymbol{u}_i\cdot\boldsymbol{n}_i+\alpha_{i,j}\,p_{i,\Gamma}+\beta_{i,j}\,\mathrm{div}_\tau\,\boldsymbol{u}_{\Gamma,i} &= -\boldsymbol{u}_j\cdot\boldsymbol{n}_i+\alpha_{i,j}\,p_{j,\Gamma}+\beta_{i,j}\,\mathrm{div}_\tau\,(\boldsymbol{K}_{j,\Gamma}\boldsymbol{K}_{i,\Gamma}^{-1}\boldsymbol{u}_{\Gamma,j}) && \text{on } \Gamma,\\
\boldsymbol{K}_{j,\Gamma}^{-1}\,\boldsymbol{u}_{\Gamma,i}+\nabla_\tau p_{i,\Gamma} &= 0 && \text{on } \Gamma,\\
p_{i,\Gamma} &= 0 && \text{on } \partial\Gamma.
\end{aligned} \tag{4.5}$$

This can be seen as a coupling problem between a $d-$dimensional PDE in the subdomain Ω_i and a $(d-1)-$dimensional PDE on the interface Γ, and both PDEs are written in mixed form. In the following, we prove that under a suitable regularity hypothesis the multidomain formulation (4.5) is equivalent to the monodomain formulation (4.1) and that the subdomain problem of (4.5) is well-posed. Then we derive an interface problem associated with this multidomain formulation.

4.1.2 Equivalence between the multidomain and the monodomain problems

To prove the equivalence between monodomain problem (4.1) and multidomain problem (4.5), we need to write their variational formulations. With this aim, we introduce the following space (as was used in the Robin case, see Subsection 2.2):

$$\mathscr{H}_\Gamma(\mathrm{div}\,,\Omega_i):=\left\{\boldsymbol{v}\in H(\mathrm{div},\Omega_i):\boldsymbol{v}\cdot\boldsymbol{n}_{i|\Gamma}\in L^2(\Gamma)\right\},\ i=1,2.$$

Then variational forms of the monodomain and multidomain problems are respectively as follows:

Find $(p,\boldsymbol{u})\in L^2(\Omega)\times H(\mathrm{div}\,,\Omega)$ such that

$$(\mathrm{div}\,\boldsymbol{u},\mu)_\Omega=(f,\mu)_\Omega \qquad \forall\mu\in L^2(\Omega), \tag{4.6a}$$

$$(\boldsymbol{K}^{-1}\boldsymbol{u},\boldsymbol{v})_\Omega-(\mathrm{div}\,\boldsymbol{v},p)_\Omega=0 \qquad \forall\boldsymbol{v}\in H(\mathrm{div}\,,\Omega). \tag{4.6b}$$

Find $(p_i,\boldsymbol{u}_i,p_{i,\Gamma},\boldsymbol{u}_{\Gamma,i})\in L^2(\Omega_i)\times\mathscr{H}_\Gamma(\mathrm{div}\,,\Omega_i)\times L^2(\Gamma)\times H(\mathrm{div}_\tau\,,\Gamma)$ such that

$$(\mathrm{div}\,\boldsymbol{u}_i,\mu)_{\Omega_i}=(f,\mu)_{\Omega_i}, \qquad \forall\mu\in L^2(\Omega_i), \tag{4.7a}$$

$$(\boldsymbol{K}_i^{-1}\boldsymbol{u}_i,\boldsymbol{v})_{\Omega_i}-(\mathrm{div}\,\boldsymbol{v},p_i)_{\Omega_i}+(\boldsymbol{v}\cdot\boldsymbol{n}_i,p_{i,\Gamma})_\Gamma=0, \qquad \forall\boldsymbol{v}\in\mathscr{H}_\Gamma(\mathrm{div}\,,\Omega_i), \tag{4.7b}$$

$$\begin{aligned}
&(-\boldsymbol{u}_i\cdot\boldsymbol{n}_i,\mu_\Gamma)_\Gamma+(\alpha_{i,j}\,p_{i,\Gamma},\mu_\Gamma)_\Gamma+(\beta_{i,j}\,\mathrm{div}_\tau\,\boldsymbol{u}_{\Gamma,i},\mu_\Gamma)_\Gamma=\\
&(-\boldsymbol{u}_j\cdot\boldsymbol{n}_i,\mu_\Gamma)_\Gamma+(\alpha_{i,j}\,p_{j,\Gamma},\mu_\Gamma)_\Gamma+\left(\beta_{i,j}\,\mathrm{div}_\tau\,(\boldsymbol{K}_{j,\Gamma}\boldsymbol{K}_{i,\Gamma}^{-1}\boldsymbol{u}_{\Gamma,j}),\mu_\Gamma\right)_\Gamma, \forall\mu_\Gamma\in L^2(\Gamma),
\end{aligned} \tag{4.7c}$$

$$(\boldsymbol{K}_{j,\Gamma}^{-1}\,\boldsymbol{u}_{\Gamma,i},\boldsymbol{v}_\Gamma)_\Gamma-(\mathrm{div}_\tau\,\boldsymbol{v}_\Gamma,p_{i,\Gamma})_\Gamma=0, \qquad \forall\boldsymbol{v}_\Gamma\in H(\mathrm{div}_\tau\,,\Gamma), \tag{4.7d}$$

for $i=1,2,\ j=3-i$.

The multidomain problem (4.7) is equivalent to the monodomain problem (4.6) in a sense made explicitly in the following two theorems:

Theorem 4.2. *Let $(p,\boldsymbol{u})$ be the solution of problem* (4.6). *If p and $\boldsymbol{u}$ are sufficiently regular, then $(p_i,\boldsymbol{u}_i,p_{i,\Gamma},\boldsymbol{u}_{\Gamma,i})$, defined by*

$$\begin{array}{rcrcl} p_i := & p_{|\Omega_i}, & \boldsymbol{u}_i & := & \boldsymbol{u}_{|\Omega_i}, \\ p_{i,\Gamma} := & p_{|\Gamma}, & \boldsymbol{u}_{\Gamma,i} & := & \boldsymbol{K}_{\Gamma,j}\nabla_\tau p_{i,\Gamma}, \end{array} \qquad \text{for } i=1,2,$$

is the solution of (4.7).

Proof. The proof of this theorem is obvious. □

Theorem 4.3. *Assume that*

$$(p_i,\boldsymbol{u}_i,p_{i,\Gamma},\boldsymbol{u}_{\Gamma,i}) \in L^2(\Omega_i)\times\mathscr{H}_\Gamma(div\,,\Omega_i)\times L^2(\Gamma)\times H(div_\tau\,,\Gamma)$$

is the solution to (4.7), *for $i=1,2$. Define $p\in L^2(\Omega)$ and $\boldsymbol{u}\in\boldsymbol{L^2(\Omega)}$ by*

$$p_{|\Omega_i} := p_i,\ \boldsymbol{u}_{|\Omega_i} := \boldsymbol{u}_i,\ \text{for } i=1,2, \tag{4.8}$$

then $\boldsymbol{u}\in H(div\,,\Omega)$ and $(p,\boldsymbol{u})$ is the solution to (4.6).

Proof. We first sum $(4.7a)_{|i=1}$ and $(4.7a)_{|i=2}$ for a test function $\mu\in L^2(\Omega)$ and sum $(4.7b)_{|i=1}$ and $(4.7b)_{|i=2}$ for a test function $\boldsymbol{v}\in\boldsymbol{C^\infty(\Omega)}$ to obtain

$$\sum_{i=1}^{2}(\operatorname{div}\boldsymbol{u}_i,\mu)_{\Omega_i} = \sum_{i=1}^{2}(f,\mu)_{\Omega_i}, \qquad \forall\mu\in L^2(\Omega), \tag{4.9a}$$

$$(\boldsymbol{K}^{-1}\boldsymbol{u},\boldsymbol{v})_\Omega - (\operatorname{div}\boldsymbol{v},p)_\Omega + (\boldsymbol{v}\cdot\boldsymbol{n}_1,[p_\Gamma])_\Gamma = 0, \qquad \forall\boldsymbol{v}\in\boldsymbol{C^\infty(\Omega)}, \tag{4.9b}$$

where $[p_\Gamma] := p_{1,\Gamma} - p_{2,\Gamma}$ is the jump of p across Γ. Then there remains to show that $\boldsymbol{u}\in H(\operatorname{div}\,,\Omega)$ and thus (4.6a) holds, and that the third term on the left hand side of (4.9b) vanishes and thus (4.6b) holds for test functions $\boldsymbol{v}\in\boldsymbol{C^\infty(\Omega)}$. That (4.6b) holds for test functions $\boldsymbol{v}\in H(\operatorname{div}\,,\Omega)$ then follows from the density of $\boldsymbol{C^\infty(\Omega)}$ in $H(\operatorname{div}\,,\Omega)$ (see [103, p. 209]). Hence it suffices to show that *(i)* $[\boldsymbol{u}\cdot\boldsymbol{n}] := \boldsymbol{u}_1\cdot\boldsymbol{n}_{1|\Gamma} + \boldsymbol{u}_2\cdot\boldsymbol{n}_{2|\Gamma} = 0$, which together with the fact that $\boldsymbol{u}_i\in H(\operatorname{div}\,,\Omega_i)$, $i=1,2$, implies that $\boldsymbol{u}\in H(\operatorname{div}\,,\Omega)$; and that *(ii)* $[p_\Gamma]=0$.

Toward this end, we rewrite equation (4.7c), for $i=1,2$, and for test functions $\mu_\Gamma\in L^2(\Gamma)$, as

$$-([\boldsymbol{u}\cdot\boldsymbol{n}],\mu_\Gamma)_\Gamma + (\alpha_{1,2}\,[p_\Gamma],\mu_\Gamma)_\Gamma + \left(\beta_{1,2}\operatorname{div}_\tau(\boldsymbol{K}_{2,\Gamma}[\![\boldsymbol{u}_\Gamma]\!]),\mu_\Gamma\right)_\Gamma = 0, \tag{4.10a}$$

$$-([\boldsymbol{u}\cdot\boldsymbol{n}],\mu_\Gamma)_\Gamma - (\alpha_{2,1}\,[p_\Gamma],\mu_\Gamma)_\Gamma - \left(\beta_{2,1}\operatorname{div}_\tau(\boldsymbol{K}_{1,\Gamma}[\![\boldsymbol{u}_\Gamma]\!]),\mu_\Gamma\right)_\Gamma = 0, \tag{4.10b}$$

where $[\![\boldsymbol{u}_\Gamma]\!] := \boldsymbol{K}_{2,\Gamma}^{-1}\boldsymbol{u}_{\Gamma,1} - \boldsymbol{K}_{1,\Gamma}^{-1}\boldsymbol{u}_{\Gamma,2}$.

We then subtract (4.10b) from (4.10a) for test functions $\mu_\Gamma\in L^2(\Gamma)$ and subtract $(4.7d)_{|i=2}$ from $(4.7d)_{|i=1}$ for test functions $\boldsymbol{v}_\Gamma\in H(\operatorname{div}_\tau\,,\Gamma)$ to obtain

$$\begin{gathered}(\alpha_{1,2}+\alpha_{2,1})([p_\Gamma],\mu_\Gamma)_\Gamma + \left(\operatorname{div}_\tau\left((\beta_{1,2}\boldsymbol{K}_{2,\Gamma}+\beta_{2,1}\boldsymbol{K}_{1,\Gamma})[\![\boldsymbol{u}_\Gamma]\!]\right),\mu_\Gamma\right)_\Gamma = 0,\ \forall\mu_\Gamma\in L^2(\Gamma), \\ ([\![\boldsymbol{u}_\Gamma]\!],\boldsymbol{v}_\Gamma)_\Gamma - (\operatorname{div}_\tau\boldsymbol{v}_\Gamma,[p_\Gamma])_\Gamma = 0, \quad \forall\boldsymbol{v}_\Gamma\in H(\operatorname{div}_\tau\,,\Gamma).\end{gathered} \tag{4.11}$$

We seek the pair $\left([p_\Gamma],[\![\boldsymbol{u}_\Gamma]\!]\right)\in L^2(\Gamma)\times H(\operatorname{div}_\tau\,,\Gamma)$ as the unique solution (see [22, 104]) of the problem (4.11), which is necessarily the solution $[p_\Gamma]=0$, $[\![\boldsymbol{u}_\Gamma]\!]=0$. That $[\boldsymbol{u}\cdot\boldsymbol{n}]=0$ now follows from either equation of (4.10). □

Next we prove the well-posedness of the subdomain problem with Ventcell boundary conditions.

4.1.3 Well-posedness of the Ventcell boundary value problem

For an open, bounded domain $\mathcal{O} \subset \mathbb{R}^d\,(d=2,3)$ with Lipschitz boundary $\partial\mathcal{O}$, consider the following elliptic problem written in mixed form with Ventcell boundary conditions

$$\begin{aligned} \operatorname{div} \boldsymbol{u}_{\mathcal{O}} &= f_{\mathcal{O}} && \text{in } \mathcal{O}, \\ \boldsymbol{K}^{-1}\boldsymbol{u}_{\mathcal{O}} + \nabla p_{\mathcal{O}} &= 0 && \text{in } \mathcal{O}, \\ -\boldsymbol{u}_{\mathcal{O}}\cdot\boldsymbol{n} + \alpha p_{\partial\mathcal{O}} + \beta \operatorname{div}_\tau \tilde{\boldsymbol{u}}_{\partial\mathcal{O}} &= f_{\partial\mathcal{O}} && \text{on } \partial\mathcal{O}, \\ \tilde{\boldsymbol{K}}^{-1}_{\partial\mathcal{O}}\tilde{\boldsymbol{u}}_{\partial\mathcal{O}} + \nabla_\tau p_{\partial\mathcal{O}} &= 0 && \text{on } \partial\mathcal{O}, \end{aligned} \tag{4.12}$$

where $\boldsymbol{n}$ is the unit, outward pointing, normal vector on $\partial\mathcal{O}$, $\boldsymbol{K}(\cdot) \in \mathbb{R}^{d^2}$ and $\tilde{\boldsymbol{K}}_{\partial\mathcal{O}}(\cdot) \in \mathbb{R}^{(d-1)^2}$ are given, and α and β are positive constants.

In order to write the weak formulation of problem (4.12), we need to define the following Hilbert spaces (see Remark 2.1)

$$\begin{aligned} M &= \left\{\mu = (\mu_{\mathcal{O}}, \mu_{\partial\mathcal{O}}) \in L^2(\mathcal{O}) \times L^2(\partial\mathcal{O})\right\}, \\ \Sigma &= \{\boldsymbol{\nu} = (\boldsymbol{\nu}_{\mathcal{O}}, \tilde{\boldsymbol{\nu}}_{\partial\mathcal{O}}) \in \boldsymbol{L^2(\mathcal{O})} \times \boldsymbol{L^2(\partial\mathcal{O})} : \operatorname{div}\boldsymbol{\nu}_{\mathcal{O}} \in L^2(\mathcal{O}) \text{ and} \\ &\qquad\qquad \beta\operatorname{div}_\tau \tilde{\boldsymbol{\nu}}_{\partial\mathcal{O}} - \boldsymbol{\nu}_{\mathcal{O}}\cdot\boldsymbol{n}_{|\partial\mathcal{O}} \in L^2(\partial\mathcal{O})\}, \end{aligned}$$

equipped with the norms

$$\begin{aligned} \|\mu\|_M^2 &= \|\mu_{\mathcal{O}}\|_{\mathcal{O}}^2 + \|\mu_{\partial\mathcal{O}}\|_{\partial\mathcal{O}}^2, \\ \|\boldsymbol{\nu}\|_\Sigma^2 &= \|\boldsymbol{\nu}_{\mathcal{O}}\|_{\mathcal{O}}^2 + \|\operatorname{div}\boldsymbol{\nu}_{\mathcal{O}}\|_{\mathcal{O}}^2 + \|\tilde{\boldsymbol{\nu}}_{\partial\mathcal{O}}\|_{\partial\mathcal{O}}^2 + \|\beta\operatorname{div}\tilde{\boldsymbol{\nu}}_{\partial\mathcal{O}} - \boldsymbol{\nu}_{\mathcal{O}}\cdot\boldsymbol{n}_{|\partial\mathcal{O}}\|_{\partial\mathcal{O}}^2, \end{aligned}$$

where $\|\cdot\|_{\mathcal{O}}$ and $\|\cdot\|_{\partial\mathcal{O}}$ are the $L^2(\mathcal{O})$ and $L^2(\partial\mathcal{O})-$ norms, respectively. We denote by $(\cdot,\cdot)_{\mathcal{O}}$ and $(\cdot,\cdot)_{\partial\mathcal{O}}$ the inner products of $L^2(\mathcal{O})$ and $L^2(\partial\mathcal{O})$.

Next, define the following bilinear forms (recall that β is a positive constant)

$$\begin{aligned} a: \quad \Sigma\times\Sigma &\longrightarrow \mathbb{R} \\ (\boldsymbol{u},\boldsymbol{\nu}) &\mapsto a(\boldsymbol{u},\boldsymbol{\nu}) = \left(\boldsymbol{K}^{-1}\boldsymbol{u}_{\mathcal{O}}, \boldsymbol{\nu}_{\mathcal{O}}\right)_{\mathcal{O}} + \left(\beta\tilde{\boldsymbol{K}}^{-1}_{\partial\mathcal{O}}\tilde{\boldsymbol{u}}_{\partial\mathcal{O}}, \tilde{\boldsymbol{\nu}}_{\partial\mathcal{O}}\right)_{\partial\mathcal{O}}, \\ b: \quad \Sigma\times M &\longrightarrow \mathbb{R} \\ (\boldsymbol{u},\mu) &\mapsto b(\boldsymbol{u},\mu) = \left(\operatorname{div}\boldsymbol{u}_{\mathcal{O}}, \mu_{\mathcal{O}}\right)_{\mathcal{O}} + \left(\beta\operatorname{div}_\tau\tilde{\boldsymbol{u}}_{\partial\mathcal{O}} - \boldsymbol{u}_{\mathcal{O}}\cdot\boldsymbol{n}_{|\partial\mathcal{O}}, \mu_{\partial\mathcal{O}}\right)_{\partial\mathcal{O}}, \\ c: \quad M\times M &\longrightarrow \mathbb{R} \\ (p,\mu) &\mapsto c(p,\mu) = \left(\alpha p_{\partial\mathcal{O}}, \mu_{\partial\mathcal{O}}\right)_{\partial\mathcal{O}}, \end{aligned}$$

and the linear form

$$\begin{aligned} L_f: \quad M &\longrightarrow \mathbb{R} \\ \mu &\mapsto L_f(\mu) = \left(f_{\mathcal{O}}, \mu_{\mathcal{O}}\right)_{\mathcal{O}} + \left(f_{\partial\mathcal{O}}, \mu_{\partial\mathcal{O}}\right)_{\partial\mathcal{O}}. \end{aligned}$$

With these spaces and forms, the weak form of (4.12) can be written as follows:

$$\begin{aligned} &\text{Find } (p,\boldsymbol{u}) \in M\times\Sigma \text{ such that} \\ &\qquad\begin{aligned} a(\boldsymbol{u},\boldsymbol{\nu}) - b(\boldsymbol{\nu},p) &= 0 && \forall \boldsymbol{\nu}\in\Sigma, \\ -b(\boldsymbol{u},\mu) - c(p,\mu) &= -L_f(\mu) && \forall \mu\in M. \end{aligned} \end{aligned} \tag{4.13}$$

Theorem 4.4. *Assume that there exist positive constants K_- and K_+ such that $\varsigma^T \boldsymbol{K}^{-1}(\cdot)\varsigma \geq K_-|\varsigma|^2$, and $|\boldsymbol{K}(\cdot)\varsigma| \leq K_+|\varsigma|$ a.e. in $\mathscr{O}$ and $\forall \varsigma \in \mathbb{R}^d$; and that $\eta^T \tilde{\boldsymbol{K}}_{\partial\mathscr{O}}^{-1}(\cdot)\eta \geq K_-|\eta|^2$, and $|\tilde{\boldsymbol{K}}_{\partial\mathscr{O}}(\cdot)\eta| \leq K_+|\eta|$ a.e. in $\partial\mathscr{O}$ and $\forall \eta \in \mathbb{R}^{d-1}$.*

If $(f_{\mathscr{O}}, f_{\partial\mathscr{O}})$ is in M then there exists a unique solution $(p, \boldsymbol{u}) \in M \times \Sigma$ of problem (4.13).

Proof. The existence and uniqueness of the solution of (4.13) is a generalization of the classical case (see [22, pp. 47 – 50], [104, pp. 572 – 573]). To prove Theorem 4.4, one has to show that:

- $a(\cdot,\cdot)$, $b(\cdot,\cdot)$ and $c(\cdot,\cdot)$ are continuous on $\Sigma\times\Sigma$, on $\Sigma\times M$ and on $M\times M$ respectively, which is straightforward.
- $a(\cdot,\cdot)$ is positive definite

$$a(\boldsymbol{v},\boldsymbol{v}) > 0,\ \forall \boldsymbol{v} \in \Sigma,\ \boldsymbol{v} \neq 0,$$

  and is $\boldsymbol{V}$-elliptic

$$\inf_{\boldsymbol{v}\in\boldsymbol{V}} \frac{a(\boldsymbol{v},\boldsymbol{v})}{\|\boldsymbol{v}\|^2} \geq C_a > 0,$$

  where $\boldsymbol{V} = \{\boldsymbol{v} \in \Sigma : b(\boldsymbol{v},\mu) = 0,\ \forall \mu \in M\}$.
- $b(\cdot,\cdot)$ satisfies the inf-sup condition:

$$\inf_{\mu\in M} \sup_{\boldsymbol{v}\in\Sigma} \frac{b(\boldsymbol{v},\mu)}{\|\boldsymbol{v}\|_\Sigma \|\mu\|_M} \geq C_b > 0.$$

- $c(\cdot,\cdot)$ is symmetric and positive definite

$$c(\mu,\mu) > 0,\ \forall \mu \in M,\ \mu \neq 0.$$

Firstly we have $c(\mu,\mu) = \alpha\|\mu_{\partial\mathscr{O}}\|^2_{\partial\mathscr{O}} \geq 0$, $\forall \mu \in M$ as $\alpha > 0$. Using the assumptions on the permeability and the coefficient β, one finds

$$\begin{aligned} a(\boldsymbol{v},\boldsymbol{v}) &= \left(\boldsymbol{K}^{-1}\boldsymbol{v}_{\mathscr{O}}, \boldsymbol{v}_{\mathscr{O}}\right)_{\mathscr{O}} + \left(\beta\tilde{\boldsymbol{K}}_{\partial\mathscr{O}}^{-1}\tilde{\boldsymbol{v}}_{\partial\mathscr{O}}, \tilde{\boldsymbol{v}}_{\partial\mathscr{O}}\right)_{\partial\mathscr{O}} \\ &\geq K_-\|\boldsymbol{v}_{\mathscr{O}}\|^2_{\mathscr{O}} + \beta K_-\|\tilde{\boldsymbol{v}}_{\partial\mathscr{O}}\|^2_{\partial\mathscr{O}} \geq 0. \end{aligned}$$

To check that $a(\cdot,\cdot)$ is $\boldsymbol{V}-$elliptic, note that for $\boldsymbol{v} \in \boldsymbol{V}$:

$$\operatorname{div} \boldsymbol{v}_{\mathscr{O}} = 0, \text{ and } \beta \operatorname{div}_\tau \tilde{\boldsymbol{v}}_{\partial\mathscr{O}} = \boldsymbol{v}_{\mathscr{O}} \cdot \boldsymbol{n}_{|\partial\mathscr{O}}.$$

Hence

$$\|\boldsymbol{v}\|^2_\Sigma = \|\boldsymbol{v}_{\mathscr{O}}\|^2_{\mathscr{O}} + \|\tilde{\boldsymbol{v}}_{\partial\mathscr{O}}\|^2_{\partial\mathscr{O}},\ \forall \boldsymbol{v} \in \boldsymbol{V}.$$

Using the assumptions on $\boldsymbol{K}, \tilde{\boldsymbol{K}}_{\partial\mathscr{O}}$ and β we obtain

$$\begin{aligned} a(\boldsymbol{v},\boldsymbol{v}) &= \left(\boldsymbol{K}^{-1}\boldsymbol{v}_{\mathscr{O}}, \boldsymbol{v}_{\mathscr{O}}\right)_{\mathscr{O}} + \left(\beta\tilde{\boldsymbol{K}}_{\partial\mathscr{O}}^{-1}\tilde{\boldsymbol{v}}_{\partial\mathscr{O}}, \tilde{\boldsymbol{v}}_{\partial\mathscr{O}}\right)_{\partial\mathscr{O}} \\ &\geq K_-\|\boldsymbol{v}_{\mathscr{O}}\|^2_{\mathscr{O}} + \beta K_-\|\tilde{\boldsymbol{v}}_{\partial\mathscr{O}}\|^2_{\partial\mathscr{O}} \\ &\geq C_a\|\boldsymbol{v}\|^2_\Sigma, \quad \forall \boldsymbol{v} \in V, \text{ where } C_a = \inf\left\{(1,\beta)K_-\right\}. \end{aligned}$$

To check that $b(\cdot,\cdot)$ satisfies the inf-sup condition, for any given $\mu \in M$ we construct a vector $\boldsymbol{\nu} \in \Sigma$ such that $b(\boldsymbol{\nu},\mu) = \|\mu\|_M^2$ and $\|\boldsymbol{\nu}\|_\Sigma \leq C_b\|\mu\|_M$. Toward this end, we consider the following problem

$$\begin{aligned} -\Delta\phi &= \mu_{\mathscr{O}} \quad \text{in } \mathscr{O}, \\ \frac{\partial\phi}{\partial \boldsymbol{n}} - \beta\Delta_\tau\phi &= \mu_{\partial\mathscr{O}} \quad \text{on } \partial\mathscr{O}, \end{aligned} \tag{4.14}$$

where $\beta > 0$ is a constant and Δ_τ is the Laplace-Beltrami operator. To write the variational formulation of problem (4.14), we introduce the following Hilbert space

$$H^{1,1}(\mathscr{O}) = \{\phi \in H^1(\mathscr{O}) : \phi_{|\partial\mathscr{O}} \in H^1(\partial\mathscr{O})\}, \tag{4.15}$$

equipped with the norm

$$\|\phi\|^2_{H^{1,1}(\mathscr{O})} = \|\phi\|^2_{H^1(\mathscr{O})} + \|\phi\|^2_{H^1(\partial\mathscr{O})}.$$

We define the bilinear form A and the linear form B as follows

$$\begin{array}{rccl} A: & H^{1,1}(\mathscr{O}) \times H^{1,1}(\mathscr{O}) & \longrightarrow & \mathbb{R} \\ & (\phi,\varphi) & \mapsto & a(\phi,\varphi) = \big(\nabla\phi,\nabla\varphi\big)_{\mathscr{O}} + \big(\beta\nabla_\tau\phi,\nabla_\tau\varphi\big)_{\partial\mathscr{O}}, \\ B: & H^{1,1}(\mathscr{O}) & \longrightarrow & \mathbb{R} \\ & \varphi & \mapsto & B(\varphi) = \big(\mu_{\mathscr{O}},\varphi\big)_{\mathscr{O}} + \big(\mu_{\partial\mathscr{O}},\varphi\big)_{\partial\mathscr{O}}. \end{array}$$

The weak formulation of (4.14) is written as

$$\text{Find } \phi \in H^{1,1}(\mathscr{O}) \text{ such that } \quad A(\phi,\varphi) = B(\varphi),\ \forall\varphi \in H^{1,1}(\mathscr{O}). \tag{4.16}$$

Lemma 4.5. *Assume that $\mu = (\mu_{\mathscr{O}},\mu_{\partial\mathscr{O}}) \in M$, then problem* (4.16) *has a unique solution.*

Proof. As $\beta > 0$, one can easily prove that A is coercive. Thus, by applying the Lax-Milgram theorem, we prove the existence and uniqueness of a weak solution ϕ to (4.14). Moreover, there exists a constant $C^* > 0$ such that

$$\|\phi\|_{H^{1,1}(\mathscr{O})} \leq C^*\|\mu\|_M.$$

□

Now, for $\mu = (\mu_{\mathscr{O}},\mu_{\partial\mathscr{O}}) \in M$ let ϕ be the weak solution of (4.14). We define

$$\boldsymbol{\nu}_{\mathscr{O}} = -\nabla\phi \text{ and } \tilde{\boldsymbol{\nu}}_{\partial\mathscr{O}} = -\nabla_\tau\phi_{\partial\mathscr{O}},$$

then

$$\operatorname{div}\boldsymbol{\nu}_{\mathscr{O}} = \mu_{\mathscr{O}} \in L^2(\mathscr{O}) \text{ and } \beta\operatorname{div}_\tau\tilde{\boldsymbol{\nu}}_{\partial\mathscr{O}} - \boldsymbol{\nu}_{\mathscr{O}}\cdot\boldsymbol{n}_{|\partial\mathscr{O}} = \mu_{\partial\mathscr{O}} \in L^2(\partial\mathscr{O}).$$

Hence, $\boldsymbol{\nu} = (\boldsymbol{\nu}_{\mathscr{O}},\tilde{\boldsymbol{\nu}}_{\partial\mathscr{O}}) \in \Sigma$ and $b(\boldsymbol{\nu},\mu) = \|\mu\|_M^2$. Moreover, we have

$$\|\boldsymbol{\nu}\|_\Sigma^2 = \|\mu\|_M^2 + \|\nabla\phi\|^2_{\mathscr{O}} + \|\nabla_\tau\phi\|^2_{\partial\mathscr{O}} \leq (1+C^*)\|\mu\|_M^2.$$

This completes the proof of Theorem 4.4. □

4.1.4 An interface problem

In this subsection, we derive an interface problem associated with the multidomain problem (4.5). With this aim, we define the Ventcell-to-Ventcell operators $\mathscr{S}_i^{\mathrm{VtV}}$ which depend on the parameters $\alpha_{i,j}$ and $\beta_{i,j}$, for $i = 1, 2$, and $j = 3 - i$, as follows

$$\begin{aligned} \mathscr{S}_i^{\mathrm{VtV}} : L^2(\Gamma) \times L^2(\Omega_i) &\to L^2(\Gamma) \\ (\vartheta, f) &\longmapsto \mathscr{S}_i^{\mathrm{VtV}}(\vartheta, f) = -\boldsymbol{u}_i \cdot \boldsymbol{n}_{j|\Gamma} + \alpha_{j,i}\, p_{i,\Gamma} + \beta_{j,i}\, \mathrm{div}_\tau\, (\boldsymbol{K}_{i,\Gamma} \boldsymbol{K}_{j,\Gamma}^{-1} \boldsymbol{u}_{\Gamma,i}), \end{aligned}$$

where $(p_i, \boldsymbol{u}_i, p_{i,\Gamma}, \boldsymbol{u}_{\Gamma,i})$, $i = 1, 2$, is the solution of

$$\begin{aligned} \mathrm{div}\, \boldsymbol{u}_i &= f && \text{in } \Omega_i, \\ \boldsymbol{K}_i^{-1} \boldsymbol{u}_i + \nabla p_i &= 0 && \text{in } \Omega_i, \\ p_i &= 0 && \text{on } \left(\partial\Omega_i \cap \partial\Omega\right), \\ -\boldsymbol{u}_i \cdot \boldsymbol{n}_i + \alpha_{i,j}\, p_{i,\Gamma} + \beta_{i,j}\, \mathrm{div}_\tau\, \boldsymbol{u}_{\Gamma,i} &= \vartheta && \text{on } \Gamma, \\ \boldsymbol{K}_{j,\Gamma}^{-1}\, \boldsymbol{u}_{\Gamma,i} + \nabla_\tau p_{i,\Gamma} &= 0 && \text{on } \Gamma, \\ p_{i,\Gamma} &= 0 && \text{on } \partial\Gamma. \end{aligned} \tag{4.17}$$

The well-posedness of problem (4.17) is given by an extension of Theorem 4.4. The interface problem, corresponding to the Ventcell transmission conditions (4.4), is defined by

$$\begin{aligned} \vartheta_1 &= \mathscr{S}_2^{\mathrm{VtV}}(\vartheta_2, f) \\ \vartheta_2 &= \mathscr{S}_1^{\mathrm{VtV}}(\vartheta_1, f) \end{aligned} \qquad \text{on } \Gamma, \tag{4.18}$$

or equivalently,

$$\boldsymbol{\mathscr{S}_V} \begin{pmatrix} \vartheta_1 \\ \vartheta_2 \end{pmatrix} = \boldsymbol{\chi_V}(f), \quad \text{on } \Gamma, \tag{4.19}$$

where

$$\begin{aligned} \boldsymbol{\mathscr{S}_V} : L^2(\Gamma) \times L^2(\Gamma) &\longrightarrow L^2(\Gamma) \times L^2(\Gamma) \\ \begin{pmatrix} \vartheta_1 \\ \vartheta_2 \end{pmatrix} &\longmapsto \begin{pmatrix} \vartheta_1 - \mathscr{S}_2^{\mathrm{VtV}}(\vartheta_2, 0) \\ \vartheta_2 - \mathscr{S}_1^{\mathrm{VtV}}(\vartheta_1, 0) \end{pmatrix}, \end{aligned}$$

and

$$\begin{aligned} \boldsymbol{\chi_V} : L^2(\Gamma) &\longrightarrow L^2(\Gamma) \times L^2(\Gamma) \\ f &\longmapsto \begin{pmatrix} \mathscr{S}_2^{\mathrm{VtV}}(0, f) \\ \mathscr{S}_1^{\mathrm{VtV}}(0, f) \end{pmatrix}. \end{aligned}$$

One can solve problem (4.19) iteratively using Jacobi iteration or GMRES: the right hand side is computed (only once) by solving problem (4.17) in each subdomain with $\vartheta = 0$; then for a given pair of vectors $(\vartheta_1, \vartheta_2)$, the matrix vector product is obtained (at each iteration) by solving, for $i = 1, 2$, subdomain problem (4.17) in Ω_i with $\vartheta = \vartheta_i$ and with $f = 0$. If one uses Jacobi iteration for solving (4.19), the resulting algorithm is equivalent to the optimized Schwarz algorithm with Ventcell transmission conditions and is written as follows: starting with a given initial guess $g_{i,j}^0$ on Γ for the first iteration,

$$-\boldsymbol{u}_i^0 \cdot \boldsymbol{n}_i + \alpha_{i,j}\, p_{i,\Gamma}^0 + \beta_{i,j}\, \mathrm{div}_\tau\, (\boldsymbol{u}_{\Gamma,i}^0) = g_{i,j}^0,$$

then at the k^{th} iteration, $k = 1, \ldots$, solve in each subdomain the problem

$$\begin{aligned}
\operatorname{div} \boldsymbol{u}_i^k &= f && \text{in } \Omega_i, \\
\boldsymbol{K}_i^{-1}\boldsymbol{u}_i^k + \nabla p_i^k &= 0 && \text{in } \Omega_i, \\
p_i^k &= 0 && \text{on } \left(\partial\Omega_i \cap \partial\Omega\right), \\
-\boldsymbol{u}_i^k \cdot \boldsymbol{n}_i + \alpha_{i,j}\, p_{i,\Gamma}^k + \beta_{i,j}\, \operatorname{div}_\tau\left(\boldsymbol{u}_{\Gamma,i}^k\right) &= -\boldsymbol{u}_j^{k-1} \cdot \boldsymbol{n}_i + \alpha_{i,j}\, p_{j,\Gamma}^{k-1} + \\
& \qquad \beta_{i,j}\, \operatorname{div}_\tau\left(\boldsymbol{K}_{j,\Gamma}\boldsymbol{K}_{i,\Gamma}^{-1}\boldsymbol{u}_{\Gamma,j}^{k-1}\right) && \text{on } \Gamma, \\
\boldsymbol{K}_{j,\Gamma}^{-1}\boldsymbol{u}_{\Gamma,i}^k + \nabla_\tau p_{i,\Gamma}^k &= 0 && \text{on } \Gamma, \\
p_{i,\Gamma}^k &= 0 && \text{on } \partial\Gamma,
\end{aligned} \tag{4.20}$$

for $i = 1, 2$, and $j = 3 - i$.

In the next subsection, we will carry out numerical experiments to study the performance of two algorithms corresponding to Jacobi iterations and GMRES applied to the interface problem (4.19).

4.1.5 Numerical results

We consider a domain $\Omega = (0, \pi)^2$ and its decomposition into two nonoverlapping subdomains $\Omega_1 = \left(0, \frac{\pi}{2}\right) \times (0, \pi)$ and $\Omega_2 = \left(\frac{\pi}{2}, \pi\right) \times (0, \pi)$. The permeability is $\boldsymbol{K} = \mathfrak{K}\boldsymbol{I}$ isotropic and constant on each subdomain, where $\boldsymbol{I}$ is the 2D identity matrix. We take $\mathfrak{K}_1 = 1/\mathscr{K}$ and $\mathfrak{K}_2 = 1$, where $\mathscr{K} = 1, 10$ or 100. The exact solution is

$$p(x, y) = \cos(\pi x)\, \sin(\pi y).$$

For the spatial discretization, we use mixed finite elements (with interface Lagrange multipliers) with the lowest order Raviart-Thomas spaces on rectangles (see Appendix B.5).

Remark 4.6. *In order to handle the discontinuous coefficients, we use the optimized, weighted Ventcell parameters defined by*

$$\begin{aligned}
\alpha_{1,2} &= \mathfrak{K}_2\alpha, \quad & \alpha_{2,1} &= \mathfrak{K}_1\alpha, \\
\beta_{1,2} &= \mathfrak{K}_2\beta, \quad & \beta_{2,1} &= \mathfrak{K}_1\beta.
\end{aligned}$$

Details of how these optimized parameters are calculated are presented in Appendix A.1.

We first verify that the multidomain solution (obtained by solving the interface problem (4.19) with Jacobi iterations or GMRES) converges to the monodomain solution. We start with a zero initial guess and compute the error in the $L^2(\Omega)$-norm of the difference between the multidomain solution and the monodomain solution at each iteration. In Figure 4.1, we show the error in the pressure p (cyan, diamond) and in the velocity $\boldsymbol{u}$ (red, dot) using Jacobi iterations (left) and GMRES (right). We observe that the error tends to zero as the number of iterations increases, which implies that both algorithms work well and the numerical results confirm the theoretical equivalence between the multidomain problem and the monodomain problem.

In order to study the convergence behavior of the optimized Schwarz method with the optimized weighted Ventcell parameters, we consider the error equation, i.e. with $f = 0$ and homogeneous Dirichlet boundary conditions. We start with a random initial guess on the interface and compute the error in the $L^2(\Omega)$-norm of the pressure

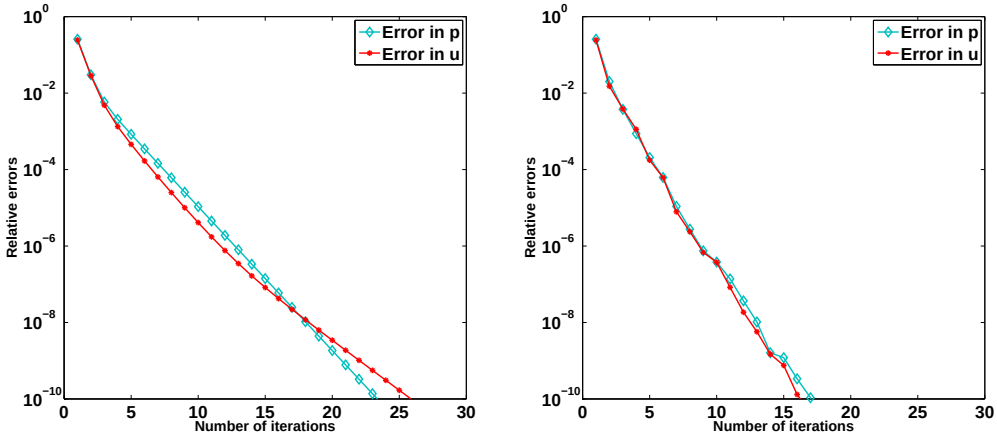

Figure 4.1: L^2 error of the difference between the multidomain solution and the monodomain solution: with Jacobi iterations (left) and GMRES (right).

p and of the velocity $\boldsymbol{u}$. Table 4.1 gives the number of iterations needed to reach an error reduction of 10^{-6} first in p and then in $\boldsymbol{u}$ (in square brackets) when one refines the mesh. Both GMRES and Jacobi iterations are considered. For homogeneous case ($\mathscr{K} = 1$), GMRES significantly improves the convergence speed (by a factor of 2) and also the asymptotic results compared to the Jacobi iteration. These results are consistent with those obtained with primal formulations [44] (where a finite difference scheme is used). As the ratio $\mathscr{K}$ increases, the number of iterations is smaller and GMRES does not greatly accelerate the convergence speed compared to Jacobi iterations. Also for large $\mathscr{K}$, the convergence rate of the algorithms with GMRES or Jacobi are almost independent of the mesh size. This is also the case where a primal formulation and a finite volume method are used [36].

h	$\mathscr{K} = 1$		$\mathscr{K} = 10$		$\mathscr{K} = 100$	
	Jacobi	GMRES	Jacobi	GMRES	Jacobi	GMRES
$\pi/50$	15 [15]	10 [11]	11 [10]	9 [9]	7 [6]	7 [7]
$\pi/100$	17 [18]	11 [12]	11 [10]	9 [9]	7 [6]	7 [7]
$\pi/200$	21 [21]	13 [13]	11 [10]	9 [9]	7 [6]	7 [7]
$\pi/400$	25 [25]	14 [14]	11 [10]	10 [9]	7 [6]	8 [8]
$\pi/800$	29 [29]	15 [16]	13 [12]	10 [10]	7 [6]	8 [8]

Table 4.1: Number of iterations required to reach an error reduction of 10^{-6} in p and in $\boldsymbol{u}$ (in square brackets) for different permeability ratios, and for different values of the discretization parameter h.

Next we verify the performance of the optimized parameters, computed by numerically minimizing the continuous convergence factor (see Appendix A.1). We take $h = \pi/100$, vary α and β, and compute the error in the velocity $\boldsymbol{u}$ after a fixed number of Jacobi iterations for different permeability ratios. The results are shown in Figure 4.2 for $\mathscr{K} = 1$ (# iter = 20 iterations), $\mathscr{K} = 10$ (# iter = 12 iterations) and $\mathscr{K} = 100$ (# iter = 8 iterations) respectively. We see that, in all cases, the optimized weighted Ventcell parameters (the red star) are located close to those giving the smallest error after the same number of iterations.

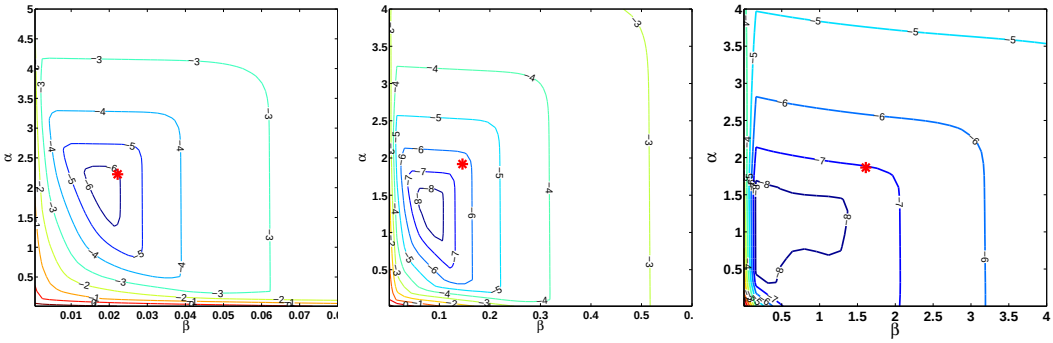

$\mathscr{K} = 1$ ($\#$ iter $=$ 20 iterations) $\mathscr{K} = 10$ ($\#$ iter $=$ 12 iterations) $\mathscr{K} = 100$ ($\#$ iter $=$ 8 iterations)

Figure 4.2: Level curves for the error in the velocity (in logarithmic scale) after some fixed number of Jacobi iterations for various values of the parameters α and β and for different permeability ratios $\mathscr{K}$. The red start shows the optimized parameters.

Finally, we compare the performance of the optimized Schwarz method with Ventcell transmission conditions with that with Robin transmission conditions (i.e. $\beta = 0$). We consider the optimized 2-sided Robin parameters with $\alpha_{1,2} \neq \alpha_{2,1}$ and $\beta_{1,2} = \beta_{2,1} = 0$ (see Appendix A.1 for the calculation of these parameters). Figures 4.3, 4.4 and 4.5 show the error in the pressure versus the number of iterations using Jacobi (on the left) and GMRES (on the right) for different diffusion ratios, $\mathscr{K} = 1$, $\mathscr{K} = 10$ and $\mathscr{K} = 100$ respectively. We see that for the homogeneous case ($\mathscr{K} = 1$), with Jacobi iterations the optimized weighted Ventcell converges significantly faster than the optimized 2-sided Robin (by a factor of 2). As $\mathscr{K}$ increases, the optimized weighted Ventcell and the optimized 2-sided Robin are comparable. With GMRES, the difference in the convergence of the two types of optimized parameters becomes less significant, especially for high diffusion ratios. These results are for a symmetric two subdomain case with a conforming mesh, Ventcell transmission conditions may have a more important effect on the convergence (compared with Robin transmission conditions) when many subdomains and nonmatching grids are considered [73].

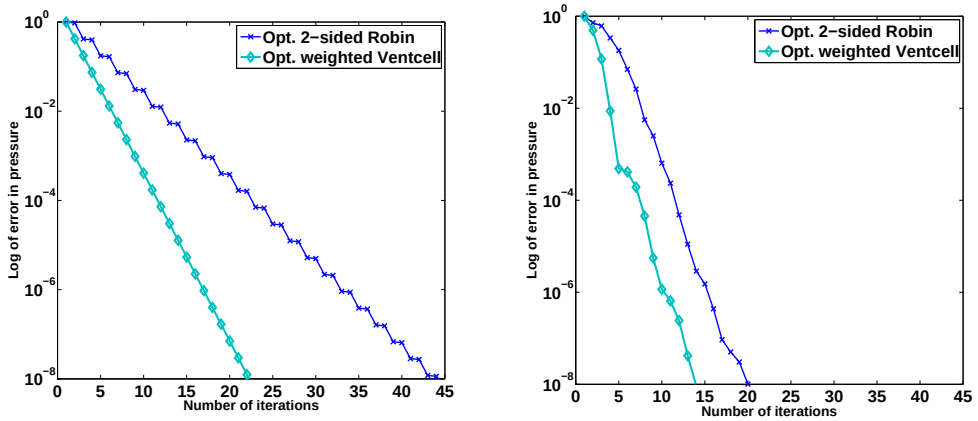

Figure 4.3: L^2 error in the pressure p for $\mathscr{K} = 1$: Jacobi (left) and GMRES (right).

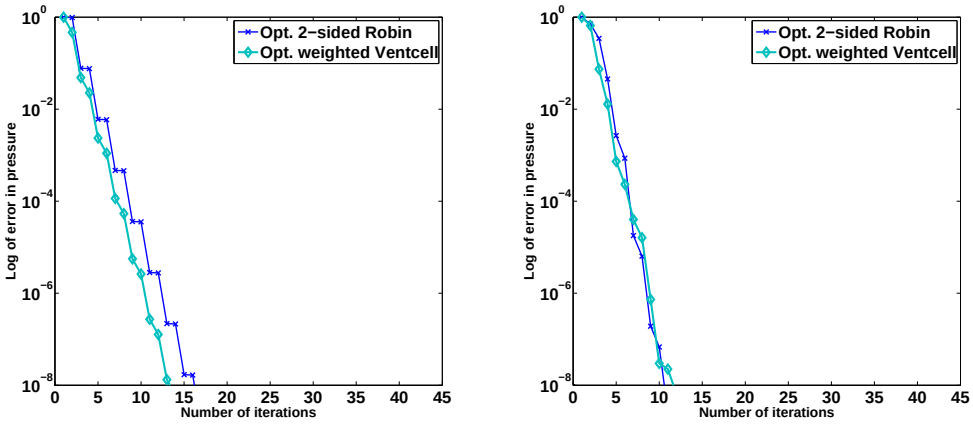

Figure 4.4: L^2 error in the pressure p for $\mathscr{K} = 10$: Jacobi (left) and GMRES (right).

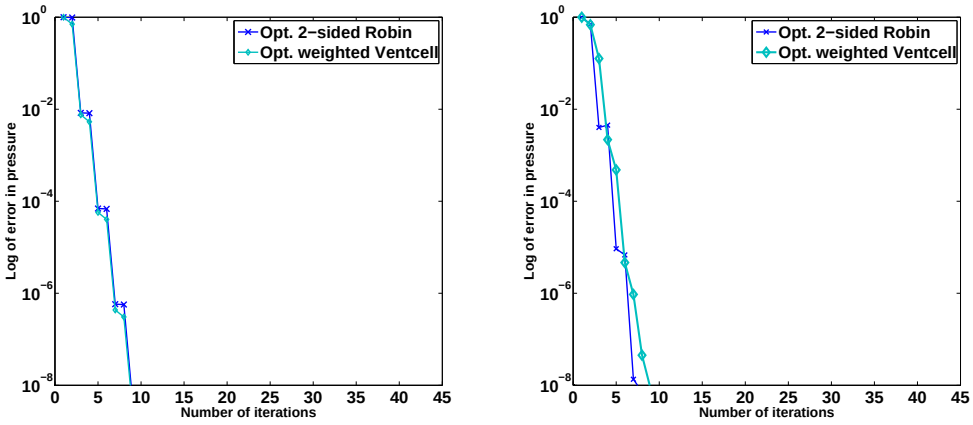

Figure 4.5: L^2 error in the pressure p for $\mathscr{K} = 100$: Jacobi (left) and GMRES (right).

4.2 Time-dependent diffusion problems

We extend the results in the previous section to the case of time-dependent problems. We consider the transient problem for compressible flow of a single phase fluid (cf. Chapter 1) written in mixed form:

$$\begin{aligned} s\partial_t p + \operatorname{div} \boldsymbol{u} &= f && \text{in } \Omega \times (0,T), \\ \boldsymbol{K}^{-1}\boldsymbol{u} + \nabla p &= 0 && \text{in } \Omega \times (0,T), \\ p &= 0 && \text{on } \partial\Omega \times (0,T), \\ p(\cdot,0) &= p_0 && \text{in } \Omega, \end{aligned} \tag{4.21}$$

where $s > 0$ is the storage coefficient, p is the pressure, $\boldsymbol{u}$ the velocity, $\boldsymbol{K}$ a symmetric time independent hydraulic conductivity (or permeability) tensor, f the source term and p_0 an initial condition. As usual, we have imposed homogeneous Dirichlet condition on the boundary for the sake of simplicity.

Remark 4.7. *Problem* (4.21) *can be interpreted as a model problem for diffusion process*

(see Chapter 2):

$$\begin{aligned} \phi\,\partial_t c + div\,\boldsymbol{r} &= f \quad in\ \Omega\times(0,T),\\ \boldsymbol{D}^{-1}\boldsymbol{r} + \nabla c &= 0 \quad in\ \Omega\times(0,T),\\ c &= 0 \quad on\ \partial\Omega\times(0,T),\\ c(\cdot,0) &= c_0 \quad in\ \Omega, \end{aligned} \tag{4.22}$$

(recall that c is the concentration of a contaminant dissolved in a fluid, f the source term, ϕ the porosity and $\boldsymbol{D}$ a symmetric time independent diffusion tensor).

To give a coherent representation of the analysis of this section with that of Section 4.1, we will use the notation (4.21) *for the analysis while we present numerical experiments in context of the formulation* (4.22) *to compare with the results in Chapter 2.*

The well-posedness of problem (4.21) follows from Theorem 2.2 (see Chapter 2). We recall a result concerning the regularity of the solution in the following theorem:

Theorem 4.8. *Assume that s is bounded above and below by positive constants, $0 < s_- \leq s(x) \leq s_+$, and that there exist positive constants K_- and K_+ such that $\varsigma^T\boldsymbol{K}^{-1}(x)\varsigma \geq K_-|\varsigma|^2$, and $|\boldsymbol{K}(x)\varsigma| \leq K_+|\varsigma|$, a.e. $x\in\Omega$ and $\forall\varsigma\in\mathbb{R}^d$. If f is in $L^2(0,T;L^2(\Omega))$ and p_0 in $H_0^1(\Omega)$ then problem* (4.21) *has a unique solution*

$$(p,\boldsymbol{u}) \in H^1(0,T;L^2(\Omega)) \times \left(L^2(0,T;H(\mathrm{div}\,,\Omega)) \cap L^\infty(0,T;\boldsymbol{L^2(\Omega)})\right).$$

In the following, we derive a multidomain formulation associated with problem (4.21) where Ventcell transmission conditions are used on the space-time interface. The difference between this case and the elliptic case is that now these transmission conditions also involve the time derivative of the trace of the pressure on the interface.

4.2.1 Multidomain formulation with Ventcell transmission conditions

For simplicity, we consider a decomposition of Ω into two nonoverlapping subdomains and we use the same notation as introduced in Subsection 4.1.1. Proceeding as in Section 4.1.1, we can reformulate problem (4.21) as a multidomain problem consisting of the subdomain problems, for $i=1,2$, $j=3-i$,

$$\begin{aligned} s_i\partial_t p_i + \mathrm{div}\,\boldsymbol{u}_i &= f && \text{in } \Omega_i\times(0,T),\\ \boldsymbol{K}_i^{-1}\boldsymbol{u}_i + \nabla p_i &= 0 && \text{in } \Omega_i\times(0,T),\\ p_i &= 0 && \text{on } \left(\partial\Omega_i\cap\partial\Omega\right)\times(0,T),\\ -\boldsymbol{u}_i\cdot\boldsymbol{n}_i + \alpha_{i,j}\,p_{i,\Gamma} + \beta_{i,j}\,\left(s_j\partial_t p_{i,\Gamma} + \mathrm{div}_\tau\,\boldsymbol{u}_{\Gamma,i}\right) &= && \\ -\boldsymbol{u}_j\cdot\boldsymbol{n}_i + \alpha_{i,j}\,p_{j,\Gamma} + \beta_{i,j}\,\left(s_j\partial_t p_{j,\Gamma} + \mathrm{div}_\tau\,(\boldsymbol{K}_{j,\Gamma}\boldsymbol{K}_{i,\Gamma}^{-1}\boldsymbol{u}_{\Gamma,j})\right) && \text{on } \Gamma\times(0,T),\\ \boldsymbol{K}_{j,\Gamma}^{-1}\,\boldsymbol{u}_{\Gamma,i} + \nabla_\tau p_{i,\Gamma} &= 0 && \text{on } \Gamma\times(0,T),\\ p_{i,\Gamma} &= 0 && \text{on } \partial\Gamma\times(0,T),\\ p_i(\cdot,0) &= p_0 && \text{in } \Omega_i\times(0,T),\\ p_{i,\Gamma}(\cdot,0) &= p_{0|\Gamma} && \text{on } \Gamma. \end{aligned} \tag{4.23}$$

where $\alpha_{i,j}$ and $\beta_{i,j}$, $i=1,2$, $j=3-i$, are positive constants (see Appendix A.2 for details concerning how these constants are used to optimize the convergence factor).

Remark 4.9. *As in the elliptic case, under suitable regularity hypotheses the multidomain problem* (4.23) *with Ventcell transmission conditions is equivalent to the monodomain problem* (4.21)*. It is simple to extend the demonstration of Theorem 4.3 to the case of the problem considered here.*

In the following, we prove the well-posedness of the subdomain problem (4.23) with Ventcell boundary conditions. We then reformulate the multidomain problem as a space-time interface problem, which is used in the numerical experiments to investigate the performance of the OSWR method with Ventcell transmission conditions.

4.2.2 Well-posedness of the Ventcell boundary value problem

For an open, bounded domain $\mathcal{O} \subset \mathbb{R}^d$ $(d = 2, 3)$ with Lipschitz boundary $\partial\mathcal{O}$ and for some $T > 0$, consider the following time-dependent problem in mixed form

$$\begin{aligned}
s\partial_t p_{\mathcal{O}} + \operatorname{div} \boldsymbol{u}_{\mathcal{O}} &= f && \text{in } \mathcal{O} \times (0,T),\\
\boldsymbol{K}^{-1}\boldsymbol{u}_{\mathcal{O}} + \nabla p_{\mathcal{O}} &= 0 && \text{in } \mathcal{O} \times (0,T),\\
-\boldsymbol{u}_{\mathcal{O}} \cdot \boldsymbol{n} + \alpha p_{\partial\mathcal{O}} + \beta\left(\tilde{s}\partial_t p_{\partial\mathcal{O}} + \operatorname{div}_\tau\left(\tilde{\boldsymbol{u}}_{\partial\mathcal{O}}\right)\right) &= f_{\partial\mathcal{O}} && \text{on } \partial\mathcal{O} \times (0,T),\\
\tilde{\boldsymbol{K}}^{-1}_{\partial\mathcal{O}}\tilde{\boldsymbol{u}}_{\partial\mathcal{O}} + \nabla_\tau p_{\partial\mathcal{O}} &= 0 && \text{on } \partial\mathcal{O} \times (0,T),\\
p_{\mathcal{O}}(\cdot,0) &= p_0 && \text{in } \mathcal{O} \times (0,T),\\
p_{\partial\mathcal{O}}(\cdot,0) &= p_{0|\partial\mathcal{O}} && \text{on } \partial\mathcal{O},
\end{aligned} \tag{4.24}$$

where $\boldsymbol{n}$ is the unit, outward pointing, normal vector on $\partial\mathcal{O}$; $\boldsymbol{K}(\cdot) \in \mathbb{R}^{d^2}$, $\tilde{\boldsymbol{K}}_{\partial\mathcal{O}}(\cdot) \in \mathbb{R}^{(d-1)^2}$ and $s, \tilde{s} > 0$ are given functions defined on $\mathcal{O}$ and $\partial\mathcal{O}$ respectively; α and β are positive constants.

To write the variational formulation of (4.24), we use the Hilbert spaces M and Σ as well as the bilinear forms a, b and c, and the linear form L_f defined in Subsection 4.1.3. Furthermore, we define

$$\begin{aligned}
c_s : \quad M \times M &\longrightarrow \mathbb{R}\\
(p,\mu) &\mapsto c_s(p,\mu) = \left(sp_{\mathcal{O}}, \mu_{\mathcal{O}}\right)_{\mathcal{O}} + \left(\tilde{s}p_{\partial\mathcal{O}}, \mu_{\partial\mathcal{O}}\right)_{\partial\mathcal{O}}.
\end{aligned}$$

The weak form of (4.24) can be written as follows:

For a.e. $t \in (0,T)$, find $\left(p(t), \boldsymbol{u}(t)\right) \in M \times \Sigma$ such that

$$\begin{aligned}
a(\boldsymbol{u},\boldsymbol{v}) - b(\boldsymbol{v},p) &= 0 && \forall \boldsymbol{v} \in \Sigma,\\
b(\boldsymbol{u},\mu) + c(p,\mu) + c_s(\partial_t p,\mu) &= L_f(\mu) && \forall \mu \in M.
\end{aligned} \tag{4.25}$$

together with the initial conditions

$$\begin{aligned}
p_{\mathcal{O}}(\cdot,0) &= p_0 && \text{in } \mathcal{O},\\
p_{\partial\mathcal{O}}(\cdot,0) &= p_{0|\partial\mathcal{O}} && \text{in } \partial\mathcal{O}.
\end{aligned} \tag{4.26}$$

Theorem 4.10. *Assume that s and $\tilde{s}$ are bounded above and below by positive constants, $0 < s_- \le s(\cdot) \le s_+$ a.e. in $\mathcal{O}$ and $0 < s_- \le \tilde{s}(x) \le s_+$ a.e. in $\partial\mathcal{O}$, and that there exist positive constants K_- and K_+ such that $\varsigma^T \boldsymbol{K}^{-1}(\cdot)\varsigma \ge K_-|\varsigma|^2$, and $|\boldsymbol{K}(\cdot)\varsigma| \le K_+|\varsigma|$ a.e. in $\mathcal{O}$ and $\forall \varsigma \in \mathbb{R}^d$; and that $\eta^T \tilde{\boldsymbol{K}}^{-1}_{\partial\mathcal{O}}(\cdot)\eta \ge K_-|\eta|^2$, and $|\tilde{\boldsymbol{K}}_{\partial\mathcal{O}}(\cdot)\eta| \le K_+|\eta|$ a.e. in $\partial\mathcal{O}$ and $\forall \eta \in \mathbb{R}^{d-1}$.*

If $(f_{\mathcal{O}}, f_{\partial\mathcal{O}})$ is in $L^2(0,T;M)$ and p_0 in $H^{1,1}(\mathcal{O})$ (cf. (4.15)) then there exists a unique solution $(p,\boldsymbol{u}) \in M \times \Sigma$ of problem (4.25).

As in the Dirichlet and Robin boundary condition case (see Chapter 2), we use Galerkin's method and a priori estimates to prove Theorem 4.10. These estimates are given by the following lemma:

Lemma 4.11. *Assume that f is in $L^2(0,T;M)$ and p_0 in $H^{1,1}(\mathscr{O})$ then the following estimate holds*

$$\|p\|_{L^\infty(0,T;M)} + \|\partial_t p\|_{L^2(0,T;M)} + \|\boldsymbol{u}\|_{L^2(0,T;\Sigma)} \leq C\left(\|f\|_{L^2(0,T;M)} + \|p_0\|_{H^{1,1}(\mathscr{O})}\right).$$

Remark 4.12. *The proof of Lemma 4.11 is given in the infinite dimensional setting but some technical points (those involving $\boldsymbol{r}$ at time $t = 0$) can only be defined by their finite dimensional Galerkin approximations (as was done in detail for Dirichlet and Robin boundary conditions in Sections 2.1 and 2.2 respectively). The results presented below have to be understood in that sense.*

Proof. We prove this lemma by deriving successively the estimates on p, $\partial_t p$ and $\boldsymbol{u}$.

- In order to obtain an estimate on p, we take $p(t) \in M$ and $\boldsymbol{u}(t) \in \Sigma$ as the test functions in (4.25) and add

$$a(\boldsymbol{u},\boldsymbol{u}) + c(p,p) + c_s(\partial_t p, p) = L_f(p).$$

Using the definitions of a, c and c_s, and the assumptions on the storage coefficient and the permeability tensor as well as the Cauchy-Schwarz inequality, we obtain

$$\frac{s_-}{2}\frac{d}{dt}\|p\|_M^2 + \alpha\|p_{\partial\mathscr{O}}\|_{\partial\mathscr{O}}^2 + K_-\|\boldsymbol{u}\|_{\boldsymbol{M}}^2 \leq \frac{1}{2}\left(\|f\|_M^2 + \|p\|_M^2\right), \tag{4.27}$$

where $\boldsymbol{M} := \left\{\boldsymbol{v} = (\boldsymbol{v}_{\mathscr{O}}, \tilde{\boldsymbol{v}}_{\partial\mathscr{O}}) \in \boldsymbol{L^2(\mathscr{O})} \times \boldsymbol{L^2(\partial\mathscr{O})}\right\}$ and $\|\boldsymbol{v}\|_{\boldsymbol{M}}^2 = \|\boldsymbol{v}_{\mathscr{O}}\|_{\mathscr{O}}^2 + \|\tilde{\boldsymbol{v}}_{\partial\mathscr{O}}\|_{\partial\mathscr{O}}^2$. Integrate (4.27) over $(0,t)$ for $t \in (0,T]$, we find

$$s_-\|p(t)\|_M^2 + 2\alpha\int_0^t \|p_{\partial\mathscr{O}}\|_{\partial\mathscr{O}}^2 + 2K_-\int_0^t \|\boldsymbol{u}\|_{\boldsymbol{M}}^2 \leq s_-\|p_0\|_M^2 + \|f\|_{L^2(0,T;M)}^2 + \int_0^t \|p\|_M^2.$$

Using Gronwall's lemma, we obtain

$$\|p\|_{L^\infty(0,T;M)}^2 \leq C\left(\|p_0\|_M^2 + \|f\|_{L^2(0,T;M)}^2\right), \tag{4.28}$$

and consequently,

$$\|\boldsymbol{u}\|_{L^2(0,T;\boldsymbol{M})}^2 \leq C\left(\|p_0\|_M^2 + \|f\|_{L^2(0,T;M)}^2\right). \tag{4.29}$$

- Now to derive an estimate on $\partial_t p$, we differentiate the first equation of (4.25) with respect to t and take $\boldsymbol{u}$ as a test function:

$$a(\partial_t \boldsymbol{u}, \boldsymbol{u}) - b(\boldsymbol{u}, \partial_t p) = 0. \tag{4.30}$$

Next, take $\partial_t p$ as a test function in the second equation of (4.25), we have

$$c(\partial_t p, p) + c_s(\partial_t p, \partial_t p) + b(\boldsymbol{u}, \partial_t p) = L_f(\partial_t p). \tag{4.31}$$

Now adding (4.30) and (4.31), we obtain

$$a(\partial_t \boldsymbol{u}, \boldsymbol{u}) + c(\partial_t p, p) + c_s(\partial_t p, \partial_t p) = L_f(\partial_t p),$$

thus

$$s_-\|\partial_t p\|_M^2 + \frac{\alpha}{2}\frac{d}{dt}\|p_{\partial\mathscr{O}}\|_{\partial\mathscr{O}}^2 + \frac{K_-}{2}\frac{d}{dt}\|\boldsymbol{u}\|_{\boldsymbol{M}}^2 \leq \frac{1}{2}\|f\|_M^2 + \frac{1}{2}\|\partial_t p\|_M^2.$$

Integrating this inequality over $(0,t)$ for $t \in (0,T]$

$$s_-\int_0^t \|\partial_t p\|_M^2 + \alpha\|p_{\partial\mathscr{O}}(t)\|_{\partial\mathscr{O}}^2 + K_-\|\boldsymbol{u}(t)\|_{\boldsymbol{M}}^2 \leq \|f\|_{L^2(0,T;M)}^2 + \alpha\|p_{0|\partial\mathscr{O}}\|_{\partial\mathscr{O}}^2 + K_-\|\boldsymbol{u}(0)\|_{\boldsymbol{M}}^2. \tag{4.32}$$

There only remains to bound the term $K_-\|\boldsymbol{u}(0)\|_{\boldsymbol{M}}^2$. Toward this end, we use the first equation of (4.25) with $\boldsymbol{v} = \boldsymbol{u}$ and for $t = 0$

$$\begin{aligned} K_-\|\boldsymbol{u}(0)\|_{\boldsymbol{M}}^2 &\leq \left(\operatorname{div}\boldsymbol{u}_{\mathscr{O}}(0), p_0\right)_{\mathscr{O}} + \left(\beta\operatorname{div}_\tau \tilde{\boldsymbol{u}}_{\partial\mathscr{O}}(0) - \boldsymbol{u}_{\mathscr{O}}(0)\cdot\boldsymbol{n}, p_0\right)_{\partial\mathscr{O}}, \\ &\leq -\left(\boldsymbol{u}_{\mathscr{O}}(0), \nabla p_0\right)_{\mathscr{O}} - \beta\left(\tilde{\boldsymbol{u}}_{\partial\mathscr{O}}(0), \nabla_\tau p_0\right)_{\partial\mathscr{O}}, \\ &\leq \frac{K_-}{2}\|\boldsymbol{u}(0)\|_{\boldsymbol{M}}^2 + \frac{\beta}{2K_-}\|p_0\|_{H^{1,1}(\mathscr{O})}. \end{aligned}$$

Substituting this into (4.32), we obtain

$$s_-\int_0^t \|\partial_t p\|_M^2 + \alpha\|p_{\partial\mathscr{O}}(t)\|_{\partial\mathscr{O}}^2 + K_-\|\boldsymbol{u}(t)\|_{\boldsymbol{M}}^2 \leq C\left(\|f\|_{L^2(0,T;M)}^2 + \|p_0\|_{H^{1,1}(\mathscr{O})}\right).$$

Thus

$$\|\partial_t p\|_{L^2(0,T;M)}^2 \leq C\left(\|f\|_{L^2(0,T;M)}^2 + \|p_0\|_{H^{1,1}(\mathscr{O})}\right). \tag{4.33}$$

- Finally, to obtain an estimate for $\boldsymbol{u} \in \Sigma$, because of (4.29) there only remains to estimate the terms $\|\operatorname{div}\boldsymbol{u}_{\mathscr{O}}\|_{\mathscr{O}}^2$ and $\|\beta\operatorname{div}_\tau \tilde{\boldsymbol{u}}_{\partial\mathscr{O}} - \boldsymbol{u}_{\mathscr{O}}\cdot\boldsymbol{n}\|_{\partial\mathscr{O}}^2$. For that purpose, take $(q_{\mathscr{O}}, q_{\partial\mathscr{O}}) = \left(\operatorname{div}\boldsymbol{u}_{\mathscr{O}}, \beta\operatorname{div}_\tau \tilde{\boldsymbol{u}}_{\partial\mathscr{O}} - \boldsymbol{u}_{\mathscr{O}}\cdot\boldsymbol{n}_{|\partial\mathscr{O}}\right)$ as the test function in the second equation of (4.25), we have

$$\begin{aligned} &\|\operatorname{div}\boldsymbol{u}_{\mathscr{O}}\|_{\mathscr{O}}^2 + \|\beta\operatorname{div}_\tau \tilde{\boldsymbol{u}}_{\partial\mathscr{O}} - \boldsymbol{u}_{\mathscr{O}}\cdot\boldsymbol{n}\|_{\partial\mathscr{O}}^2 \\ &\quad = (f_{\mathscr{O}} - s\partial_t p_{\mathscr{O}}, \operatorname{div}\boldsymbol{u}_{\mathscr{O}})_{\mathscr{O}} + (f_{\partial\mathscr{O}} - \alpha p_{\partial\mathscr{O}} - \tilde{s}\partial_t p_{\partial\mathscr{O}}, \beta\operatorname{div}_\tau \tilde{\boldsymbol{u}}_{\partial\mathscr{O}} - \boldsymbol{u}_{\mathscr{O}}\cdot\boldsymbol{n})_{\partial\mathscr{O}}, \\ \leq &\left(\frac{1}{2}\|f_{\mathscr{O}} - s\partial_t p_{\mathscr{O}}\|_{\mathscr{O}}^2 + \frac{1}{2}\|\operatorname{div}\boldsymbol{u}_{\mathscr{O}}\|_{\mathscr{O}}^2\right) + \frac{1}{2}\|f_{\partial\mathscr{O}} - \alpha p_{\partial\mathscr{O}} - \tilde{s}\partial_t p_{\partial\mathscr{O}}\|_{\partial\mathscr{O}}^2 + \frac{1}{2}\|\beta\operatorname{div}_\tau \tilde{\boldsymbol{u}}_{\partial\mathscr{O}} - \boldsymbol{u}_{\mathscr{O}}\cdot\boldsymbol{n}\|_{\partial\mathscr{O}}^2, \end{aligned}$$

then

$$\|\operatorname{div}\boldsymbol{u}_{\mathscr{O}}\|_{\mathscr{O}}^2 + \|\beta\operatorname{div}_\tau \tilde{\boldsymbol{u}}_{\partial\mathscr{O}} - \boldsymbol{u}_{\mathscr{O}}\cdot\boldsymbol{n}\|_{\partial\mathscr{O}}^2 \leq \|f\|_M^2 + \alpha\|p\|_M^2 + s_+\|\partial_t p\|_M^2.$$

Using (4.28) and (4.33), we obtain

$$\int_0^T \left(\|\operatorname{div}\boldsymbol{u}_{\mathscr{O}}\|_{\mathscr{O}}^2 + \|\beta\operatorname{div}_\tau \tilde{\boldsymbol{u}}_{\partial\mathscr{O}} - \boldsymbol{u}_{\mathscr{O}}\cdot\boldsymbol{n}\|_{\partial\mathscr{O}}^2\right) \leq C\left(\|f\|_{L^2(0,T;M)}^2 + \|p_0\|_{H^{1,1}(\mathscr{O})}\right).$$

This along with (4.29) gives the estimate for $\|\boldsymbol{u}\|_{L^2(0,T;\Sigma)}$, which completes the proof of the lemma.

The proof of Theorem 4.10 is then completed as was done for Theorem 2.2 (see Chapter 2). □

4.2.3 A space-time interface problem

In this subsection, we derive an interface formulation associated with the multidomain problem (4.23). With this aim, we introduce the spaces

$$\Theta := L^2(0,T;L^2(\Gamma)),$$

and

$$H^{1,1}_*(\Omega_i) := \left\{ q \in H^1(\Omega_i) : q_{|\partial\Omega_i\cap\partial\Omega} = 0 \text{ and } q_{|\Gamma} \in H^1(\Gamma) \right\},\ i = 1,2. \tag{4.34}$$

The time-dependent Ventcell-to-Ventcell operator $\mathscr{S}_i^{\mathrm{VtV}}$, which depends on the parameters $\alpha_{i,j}$ and $\beta_{i,j}$, $i = 1,2$, $j = 3-i$, is defined as

$$\begin{aligned}
&\mathscr{S}_i^{\mathrm{VtV}} : \Theta \times L^2(0,T;L^2(\Omega_i)) \times H^{1,1}_*(\Omega_i) \to \Theta \\
&(\vartheta, f, p_0) \longmapsto \mathscr{S}_i^{\mathrm{VtV}}(\vartheta, f, p_0) = -\boldsymbol{u}_i \cdot \boldsymbol{n}_{j|\Gamma} + \alpha_{j,i}\, p_{i,\Gamma} + \beta_{j,i} \left(s_i \partial_t p_{i,\Gamma} + \mathrm{div}_\tau \left(\boldsymbol{K}_{i,\Gamma} \boldsymbol{K}_{j,\Gamma}^{-1} \boldsymbol{u}_{\Gamma,i} \right) \right),
\end{aligned} \tag{4.35}$$

where $(p_i, \boldsymbol{u}_i, p_{i,\Gamma}, \boldsymbol{u}_{\Gamma,i}), i = 1,2$, is the solution of

$$\begin{aligned}
s_i \partial_t p_i + \mathrm{div}\, \boldsymbol{u}_i &= f && \text{in } \Omega_i \times (0,T), \\
\boldsymbol{K}_i^{-1} \boldsymbol{u}_i + \nabla p_i &= 0 && \text{in } \Omega_i \times (0,T), \\
p_i &= 0 && \text{on } \left(\partial\Omega_i \cap \partial\Omega\right) \times (0,T), \\
-\boldsymbol{u}_i \cdot \boldsymbol{n}_i + \alpha_{i,j}\, p_{i,\Gamma} + \beta_{i,j} \left(s_j \partial_t p_{i,\Gamma} + \mathrm{div}_\tau\, \boldsymbol{u}_{\Gamma,i} \right) &= \vartheta && \text{on } \Gamma \times (0,T), \\
\boldsymbol{K}_{j,\Gamma}^{-1}\, \boldsymbol{u}_{\Gamma,i} + \nabla_\tau p_{i,\Gamma} &= 0 && \text{on } \Gamma \times (0,T), \\
p_{i,\Gamma} &= 0 && \text{on } \partial\Gamma \times (0,T), \\
p_i(\cdot,0) &= p_0 && \text{in } \Omega_i \times (0,T), \\
p_{i,\Gamma}(\cdot,0) &= p_{0|\Gamma} && \text{on } \Gamma.
\end{aligned} \tag{4.36}$$

The well-posedness of problem (4.36) is guaranteed by an extension of Theorem 4.10. The space-time interface problem, corresponding to the Ventcell transmission conditions, is defined by

$$\begin{aligned}
\vartheta_1 &= \mathscr{S}_2^{\mathrm{VtV}}(\vartheta_2, f, p_0) \\
\vartheta_2 &= \mathscr{S}_1^{\mathrm{VtV}}(\vartheta_1, f, p_0)
\end{aligned} \qquad \text{on } \Gamma \times (0,T), \tag{4.37}$$

or equivalently,

$$\boldsymbol{\mathscr{S}_V} \begin{pmatrix} \vartheta_1 \\ \vartheta_2 \end{pmatrix} = \boldsymbol{\chi_V}(f, p_0), \quad \text{on } \Gamma \times (0,T), \tag{4.38}$$

where

$$\begin{aligned}
\boldsymbol{\mathscr{S}_V} : \Theta \times \Theta &\longrightarrow \Theta \times \Theta \\
\begin{pmatrix} \vartheta_1 \\ \vartheta_2 \end{pmatrix} &\longmapsto \begin{pmatrix} \vartheta_1 - \mathscr{S}_2^{\mathrm{VtV}}(\vartheta_2, 0, 0) \\ \vartheta_2 - \mathscr{S}_1^{\mathrm{VtV}}(\vartheta_1, 0, 0) \end{pmatrix},
\end{aligned}$$

and

$$\begin{aligned}
\boldsymbol{\chi_V} : L^2(0,T;L^2(\Omega)) \times H^{1,1}_*(\Omega_i) &\longrightarrow \Theta \times \Theta \\
(f, p_0) &\longmapsto \begin{pmatrix} \mathscr{S}_2^{\mathrm{VtV}}(0, f, p_0) \\ \mathscr{S}_1^{\mathrm{VtV}}(0, f, p_0) \end{pmatrix}.
\end{aligned}$$

Problem (4.38) can be solved iteratively using Jacobi iteration or GMRES. The former choice yields an algorithm equivalent to the OSWR algorithm with Ventcell transmission conditions and is written as follows: starting with a given initial guess $g_{i,j}^0$ on

$\Gamma \times (0,T)$ for the first iteration,

$$-\boldsymbol{u}_i^0 \cdot \boldsymbol{n}_i + \alpha_{i,j}\, p_{i,\Gamma}^0 + \beta_{i,j} \left(s_j \partial_t p_{i,\Gamma}^0 + \mathrm{div}_\tau \left(\boldsymbol{K}_{j,\Gamma} \boldsymbol{K}_{i,\Gamma}^{-1} \boldsymbol{u}_{\Gamma,i}^0 \right) \right) = g_{i,j}^0,$$

then at the k^{th} iteration, $k = 1, \ldots,$ solve in each subdomain the problem, for $i = 1,2,\ j = 3-i$:

$$\begin{aligned}
s_i \partial_t p_i^k + \mathrm{div}\, \boldsymbol{u}_i^k &= f && \text{in } \Omega_i \times (0,T),\\
\boldsymbol{K}_i^{-1} \boldsymbol{u}_i^k + \nabla p_i^k &= 0 && \text{in } \Omega_i \times (0,T),\\
p_i^k &= 0 && \text{on } \left(\partial\Omega_i \cap \partial\Omega\right) \times (0,T),\\
-\boldsymbol{u}_i^k \cdot \boldsymbol{n}_i + \alpha_{i,j}\, p_{i,\Gamma}^k + \beta_{i,j} \left(s_j \partial_t p_{i,\Gamma}^k + \mathrm{div}_\tau\, \boldsymbol{u}_{\Gamma,i}^k \right) &= \\
-\boldsymbol{u}_j^{k-1} \cdot \boldsymbol{n}_i + \alpha_{i,j}\, p_{j,\Gamma}^{k-1} + \beta_{i,j} \left(s_j \partial_t p_{j,\Gamma}^{k-1} + \mathrm{div}_\tau \left(\boldsymbol{K}_{j,\Gamma} \boldsymbol{K}_{i,\Gamma}^{-1} \boldsymbol{u}_{\Gamma,j}^{k-1} \right) \right) && \text{on } \Gamma \times (0,T),\\
\boldsymbol{K}_{j,\Gamma}^{-1}\, \boldsymbol{u}_{\Gamma,i}^k + \nabla_\tau p_{i,\Gamma}^k &= 0 && \text{on } \Gamma \times (0,T),\\
p_{i,\Gamma}^k &= 0 && \text{on } \partial\Gamma \times (0,T),\\
p_i^k(\cdot,0) &= p_0 && \text{in } \Omega_i \times (0,T),\\
p_{i,\Gamma}^k(\cdot,0) &= p_{0|\Gamma} && \text{on } \Gamma.
\end{aligned} \tag{4.39}$$

Remark 4.13. *The proof of the convergence of algorithm* (4.39) *is more complicated than in the Robin case (see Subsection 2.3.2.1). The counterpart of algorithm* (4.39) *in primal form was proved to converge in [62] and one should be able to obtain the same results with mixed formulations. However, we haven't had time to pursue that here.*

As in the case with Robin transmission conditions (see Chapter 2), the interface problem with Ventcell transmission conditions, problem (4.38), is defined on the whole time interval $(0,T)$, where its left and right hand sides are computed by solving the subdomain problems in each subdomain over $(0,T)$. Thus one may use different time steps in the subdomains and then exchange the interface data over the whole time interval using the projections introduced in Section 2.4.

4.2.4 Nonconforming discretization in time

We consider semi-discrete problems in time with nonconforming time grids. Let $\mathcal{T}_1$ and $\mathcal{T}_2$ be two possibly different partitions of the time interval $(0,T)$ into sub-intervals (see Figure 4.6). We denote by J_m^i the time interval $(t_m^i, t_{m-1}^i]$ and by $\Delta t_m^i := (t_m^i - t_{m-1}^i)$ for $m = 1, \ldots, M_i$ and $i = 1,2$. For the approximation in time, we use the lowest order discontinuous Galerkin method as in Chapter 2. We denote by $P_0(\mathcal{T}_i, L^2(\Gamma))$, $i = 1,2$, the space of piecewise constant functions in time on grid $\mathcal{T}_i$ with values in $L^2(\Gamma)$:

$$P_0(\mathcal{T}_i, L^2(\Gamma)) := \left\{ \theta : (0,T) \to W,\ \theta \ \text{ is constant on } J_m^i,\ \forall m = 1, \ldots, M_i \right\}.$$

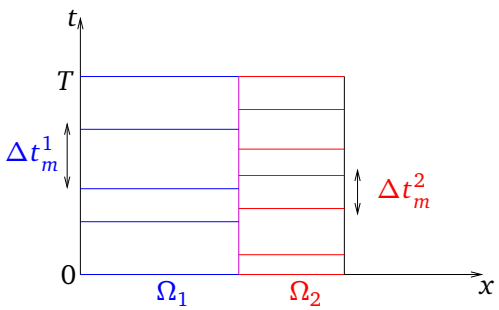

Figure 4.6: Nonconforming time grids in the subdomains.

The semi-discrete-in-time counterpart of the Ventcell-to-Ventcell operator (4.35), which is still denoted by $\mathscr{S}_i^{\mathrm{VtV}}$, is defined by

$$\begin{aligned}\mathscr{S}_i^{\mathrm{VtV}} : P_0(\mathscr{T}_i, L^2(\Gamma)) \times L^2(0,T;L^2(\Omega_i)) \times H^{1,1}_*(\Omega_i) &\to P_0(\mathscr{T}_i, L^2(\Gamma)) \\ (\vartheta, f, p_0) &\longmapsto \mathscr{S}_i^{\mathrm{VtV}}(\vartheta, f, p_0),\end{aligned}$$

with

$$\mathscr{S}_i^{\mathrm{VtV}}(\vartheta, f, p_0) := -\boldsymbol{u}_i^m \cdot \boldsymbol{n}_{j|\Gamma} + \alpha_{j,i}\, p_{i,\Gamma}^m + \beta_{j,i} \left(s_i \frac{p_{i,\Gamma}^m - p_{i,\Gamma}^{m-1}}{\Delta t_i^m} + \mathrm{div}_\tau \left(\boldsymbol{K}_{i,\Gamma} \boldsymbol{K}_{j,\Gamma}^{-1} \boldsymbol{u}_{\Gamma,i}^m \right) \right), \quad \forall m = 1, \ldots, M_i.$$

To exchange the interface data on nonconforming time grids, we use the L^2 projection Π_{ji} from the space $P_0(\mathscr{T}_i, L^2(\Gamma))$ onto $P_0(\mathscr{T}_j, L^2(\Gamma))$ (see Chapter 2), defined by

$$\Pi_{ji}(\theta)\,|_{J_m^j} = \frac{1}{|J_m^j|} \sum_{l=1}^{M_i} \int_{J_m^j \cap J_l^i} \theta, \quad \forall m = 1, \ldots, M_j. \tag{4.40}$$

With this projection, the semi-discrete in time counterpart of (4.37) is weakly enforced over each time sub-interval, in the same way as was done for the Robin transmission conditions (Subsection 2.4.2):

$$\begin{aligned}\int_\Gamma \int_{J_m^1} \vartheta_1 - \Pi_{12} \left(\mathscr{S}_2^{\mathrm{VtV}}(\vartheta_2, f, p_0) \right) dt = 0, \quad \forall m = 1, \ldots, M_1, \\ \int_\Gamma \int_{J_m^2} \vartheta_2 - \Pi_{21} \left(\mathscr{S}_1^{\mathrm{VtV}}(\vartheta_1, f, p_0) \right) dt = 0, \quad \forall m = 1, \ldots, M_2.\end{aligned}$$

In the next subsection, we study the numerical behavior of the method with Ventcell transmission conditions with nonconforming time grids. We compare it with the two algorithms introduced and analyzed in Chapter 2.

4.2.5 Numerical results

As stated in Remark 4.7, we now change the notation and consider the diffusion problem as follows:

$$\begin{aligned}\phi\, \partial_t c + \mathrm{div}\, \boldsymbol{r} &= f, && \text{in } \Omega \times (0,T), \\ \nabla c + \boldsymbol{D}^{-1} \boldsymbol{r} &= 0, && \text{in } \Omega \times (0,T), \\ c(\cdot, 0) &= c_0, && \text{in } \Omega, \\ c &= 0, && \partial\Omega \times (0,T).\end{aligned} \tag{4.41}$$

We consider the first two test cases of Section 2.5 for homogeneous and heterogeneous media respectively. Recall that the computational domain Ω is a unit square which is decomposed into two nonoverlapping subdomains $\Omega_1 = (0, 0.5) \times (0,1)$ and $\Omega_2 = (0.5, 1) \times (0,1)$, and the final time is $T = 1$. The porosity is $\phi_1 = \phi_2 = 1$ and the diffusion is an isotropic tensor, $\boldsymbol{D}_i = d_i \boldsymbol{I}, i = 1, 2$, where $\boldsymbol{I}$ is the 2D identity matrix. The diffusion coefficient $d_i, i = 1, 2$, is assumed to be constant in each subdomain. The source term is $f = 0$, and an initial condition is

$$c_0 = \exp\left((x - 0.55)^2 + 0.5(y - 0.5)^2 \right). \tag{4.42}$$

Just as in the stationary case (see Subsection 4.1.5), for the discretization in space we use mixed finite elements (with Lagrange multipliers on the space-time interface) with the lowest Raviart-Thomas spaces on rectangles (cf. Appendix B.5). We refer to Appendix A.2.1 for the calculation of the optimized two-sided Robin and weighted Ventcell parameters used for the numerical results in this section.

Remark 4.14. *To compare the convergence behavior of Ventcell transmission conditions with the two methods presented in Chapter 2, we will use GMRES and plot the error in the concentration c and in the vector field $\boldsymbol{r}$ versus the number of subdomain solves (instead of the number of iterations) (see Remark 2.21). However, a more appropriate comparison would be considered after (such as using CPU time) since the cost per subdomain solve corresponding to Ventcell boundary conditions is more costly than that of Robin conditions (due to the introduction of Lagrange multipliers on the interface).*

4.2.5.1 A test case with a homogeneous medium

The diffusion coefficient is continuous across the interface, $d_1 = d_2 = 0.02$. The mesh and the time grids are conforming in the subdomains, and $\Delta x_1 = \Delta x_2 = \Delta x = 1/200$ and $\Delta t_1 = \Delta t_2 = \Delta t = 1/200$. We first verify that the multidomain solution converges to the monodomain solution as the number of iterations increases. We start with a zero initial guess on the interface and compute, at each iteration of GMRES, the error in the $L^2(0,T;L^2(\Omega))$-norm of the difference between the multidomain solution and the monodomain solution. Figure 4.7 shows that the error goes to zero when the number of iterations goes to infinity, which confirms the theoretical equivalence between the multidomain problem and the monodomain problem.

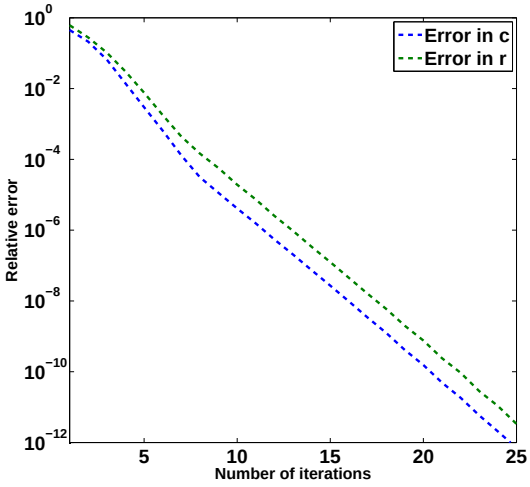

Figure 4.7: $L^2 - L^2$ error in the concentration c and in the vector field $\boldsymbol{r}$ of the difference between the multidomain solution and the monodomain solution, using optimized Ventcell parameters.

Next, we analyze the convergence behavior of the method with Ventcell transmission conditions and compare it with the two methods analyzed in Chapter 2. We consider the error equation, i.e. $c_0 = 0$, and use a random initial guess on the space-time interface. In Figure 4.8, we plot the error in the concentration c and the vector field $\boldsymbol{r}$ versus the number of subdomain solves for the different algorithms (using GMRES):

Method 1 with Neumann-Neumann preconditioner, Method 2 with optimized 2-sided Robin parameters and Method 2 with optimized weighted Ventcell. We see that the optimized weighted Ventcell improves the convergence of the optimized two-sided, but it is still slower than that of the preconditioned Method 1. For pure diffusion problems and with continuous coefficients, it seems that the preconditioned Method 1 is the best choice.

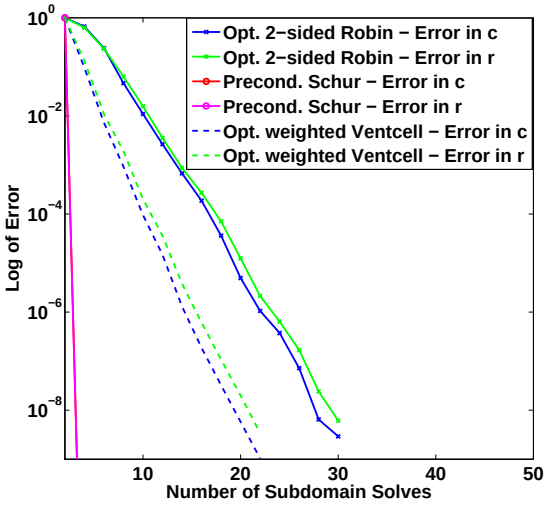

Figure 4.8: $L^2 - L^2$ error in the concentration c and in the vector field $\boldsymbol{r}$ with GMRES for the different algorithms.

To check the performance of the optimized parameters, we plot the error in the concentration after 14 Jacobi iterations for various values of α and β as depicted in Figure 4.9. We see that optimized weighted Ventcell parameters (the red star), which are calculated by numerically minimizing the convergence factor (see Appendix A.2), are not far from the zone giving the small errors after the same number of iterations .

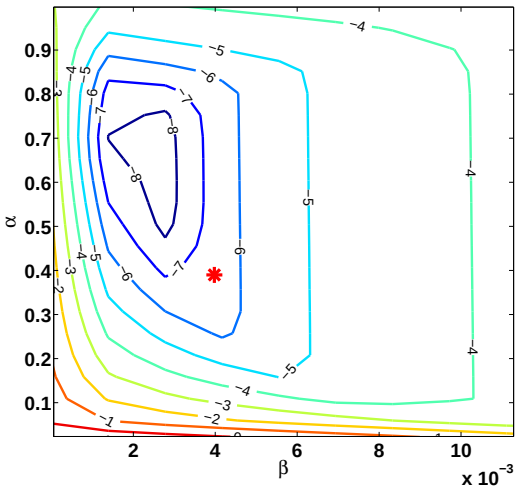

Figure 4.9: Level curves for the error in the vector field for various values of α and β, where the red star shows the optimized Ventcell parameters.

To study the asymptotic behavior of the algorithm with Ventcell transmission conditions, we show in Table 4.2 the number of subdomain solves needed to reach an error reduction of 10^{-6} first in c and then in $\boldsymbol{r}$ (in square brackets) when refining the mesh in space and in time, with the ratio of Δx^2 to Δt constant. We observe that the convergence has a weak dependence on the mesh size of the spatial and time discretizations. In contrast to the stationary case, GMRES does not improve the convergence speed compared to Jacobi iterations, which is similar to the case of optimized Robin parameters (see Subsection 2.5.1). This is explained by the fact that GMRES is not well-adapted to dynamic systems and, as mentioned in Chapters 2 and 3, a convolution-based approach (see, e.g., [98, 86]) should be considered instead.

Δx	Δt	Jacobi	GMRES
1/10	1/100	14 [19]	14 [17]
1/20	1/400	14 [22]	15 [20]
1/40	1/1600	15 [25]	16 [24]
1/80	1/6400	16 [29]	17 [27]

Table 4.2: Number of subdomain solves needed to reach an error reduction of 10^{-6} for continuous coefficients, using optimized Ventcell parameters.

4.2.5.2 A test case with a heterogeneous medium

We consider the case in which the diffusion coefficients are discontinuous across the interface: $d_1 \neq d_2$. These coefficients are shown in Table 4.3, together with the nonconforming time discretizations in the subdomains adapted to different diffusion ratios $\mathfrak{D} = d_2/d_1$. For the spatial discretization, we use a conforming rectangular mesh with $\Delta x_1 = \Delta x_2 = \Delta x = 1/200$.

$\mathfrak{D}$	d_1	$1/\Delta t_1$	d_2	$1/\Delta t_2$
10	0.02	150	0.2	200
100	0.002	50	0.2	200
1000	0.0002	20	0.2	200

Table 4.3: Diffusion coefficients and corresponding nonconforming time steps.

As in the first test case, we compare the convergence behavior of the different algorithms by solving the error equation, i.e. $c_0 = 0$. We start with a random initial guess and compute the error in c and in $\boldsymbol{r}$ at each iteration of GMRES. The results are depicted in Figure 4.10 for $\mathfrak{D} = 10$, $\mathfrak{D} = 100$ and $\mathfrak{D} = 1000$ respectively. We observe results similar to those obtained in the stationary case with discontinuous coefficients: the larger the diffusion ratio, the smaller the difference between the optimized weighted Ventcell and optimized 2-sided Robin. Consequently, for large $\mathfrak{D}$ the convergence of three algorithms - the preconditioned Method 1, Method 2 with optimized Robin parameters and Method 2 with optimized weighted Ventcell parameters - are comparable.

In order to check the performance of the optimized parameter, in Figure 4.11 we plot the error in the vector field after 12 Jacobi iterations for various values of α and β for ratio $\mathfrak{D} = 10$. We observe that with discontinuous coefficients, the optimization

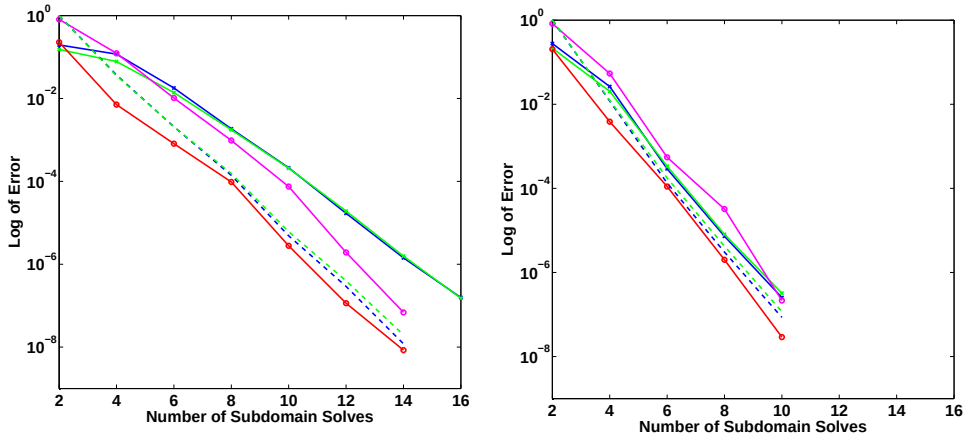

$\mathfrak{D} = 10.$ $\mathfrak{D} = 100.$

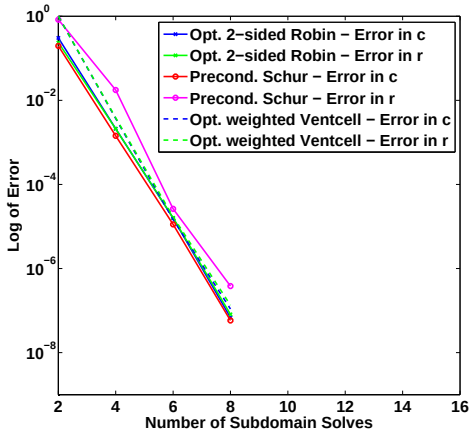

$\mathfrak{D} = 1000.$

Figure 4.10: $L^2 - L^2$ error in the concentration c and in the vector field $\boldsymbol{r}$ with GMRES for the different algorithms and different diffusion ratios (the same legend applies to all three subfigures).

works well since the optimized parameters are located very close to the zone with smallest errors.

To verify the asymptotic behavior of Method 2 with optimized weighted Ventcell parameters, we show in Table 4.4 the number of subdomain solves required to reach a reduction of 10^{-6} of the errors in the concentration and in the vector field (in square brackets) when refining the mesh in space and in time, with $\Delta x^2/\Delta t = \text{const}$. We observe that the convergence of the optimized weighted Ventcell is almost independent of the discretizations for different diffusion ratios and as in the stationary case, GMRES does not improve either the convergence speed or the asymptotic results compared to Jacobi iterations.

Next, we check that Ventcell transmission conditions with nonconforming time grids preserve the accuracy in time. We use the initial condition $c_0 \neq 0$ defined in (4.42). We consider four initial time grids (for Δt_c and Δt_f given), which we then refine several times by a factor of 2:

- Time grid 1 (fine-fine): conforming with $\Delta t_1 = \Delta t_2 = \Delta t_f$.
- Time grid 2 (coarse-fine): nonconforming with $\Delta t_1 = \Delta t_c$ and $\Delta t_2 = \Delta t_f$.

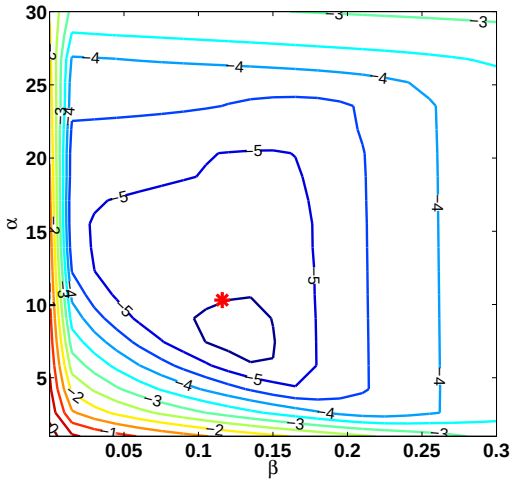

Figure 4.11: Level curves for the error in $\boldsymbol{r}$ after 12 Jacobi iterations for various values of the parameters α and β. The red star shows the optimized parameters.

Δx	Δt	$\mathfrak{D} = 10$		$\mathfrak{D} = 100$	
		Jacobi	GMRES	Jacobi	GMRES
1/10	1/100	11 [10]	9 [9]	8 [8]	7 [7]
1/20	1/400	12 [12]	10 [10]	9 [8]	9 [9]
1/40	1/1600	12 [12]	11 [11]	9 [8]	9 [9]
1/80	1/6400	12 [12]	11 [12]	10 [10]	9 [9]

Table 4.4: Number of subdomain solves needed to reach an error reduction of 10^{-6} for different diffusion ratios, using optimized weighted Ventcell parameters.

- Time grid 3 (fine-coarse): nonconforming with $\Delta t_1 = \Delta t_f$ and $\Delta t_2 = \Delta t_c$.
- Time grid 4 (coarse-coarse): conforming with $\Delta t_1 = \Delta t_2 = \Delta t_c$.

For $\mathfrak{D} = 10$, we take $\Delta t_c = 1/94$ and $\Delta t_f = 1/128$; for $\mathfrak{D} = 100$, we take $\Delta t_c = 1/40$ and $\Delta t_f = 1/160$. In space, we fix a conforming rectangular mesh and we compute a reference solution by solving problem (4.41) directly on a very fine time grid, with $\Delta t = \Delta t_f / 2^6$. The converged multidomain solution is such that the relative residual is smaller than 10^{-11}.

Figure 4.12 shows the error in the $L^2(0,T;L^2(\Omega))$-norm of the concentration c versus the maximum length of the time steps, $\max_i \Delta t_i$, for $\mathfrak{D} = 10$ (left) and $\mathfrak{D} = 100$ (right). We see that for both cases Method 2 with optimized Ventcell parameters with nonconforming grids preserves the accuracy in time of the solution: firstly, the error with nonconforming time steps is in between that of the conforming coarse and conforming fine time steps; secondly, first-order convergence of the scheme is obtained for nonconforming grids; thirdly, the error for Time grid 2 (nonconforming with a finer time step in Ω_2 where the diffusion coefficient is larger) is close to that of Time grid 1 (conforming fine).

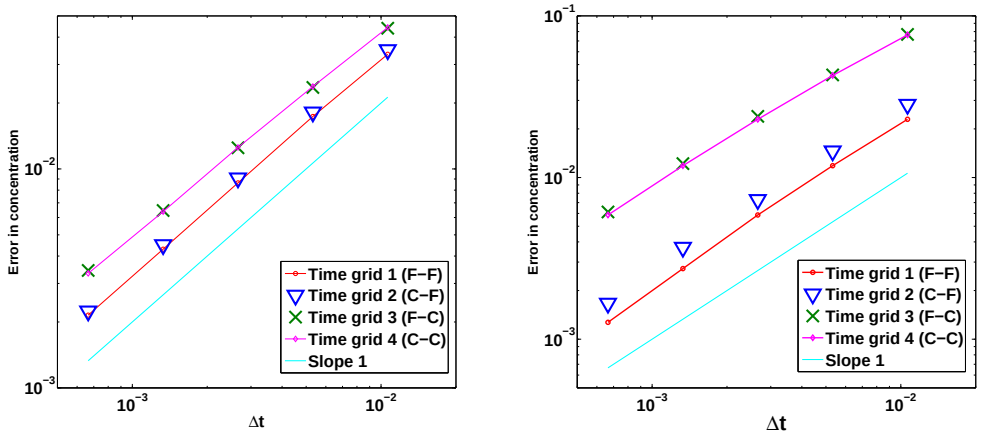

Figure 4.12: $L^2 - L^2$ error in c of the difference between the reference and the multidomain solutions versus the time step size for $\mathfrak{D} = 10$ (left) and $\mathfrak{D} = 100$ (right), using Ventcell transmission conditions.

4.3 Time-dependent advection-diffusion problems

As in the Robin case, we extend the OSWR method with Ventcell transmission conditions (derived in the previous section) to the advection-diffusion problem (cf. (3.1)) written in mixed form:

$$\begin{aligned} \phi\partial_t c + \operatorname{div}(\boldsymbol{u}c + \boldsymbol{r}) &= f && \text{in } \Omega \times (0,T), \\ \boldsymbol{D}^{-1}\boldsymbol{r} + \nabla c &= 0 && \text{in } \Omega \times (0,T), \\ c &= 0 && \text{on } \partial\Omega \times (0,T), \\ c(\cdot,0) &= c_0 && \text{in } \Omega. \end{aligned} \tag{4.43}$$

We use operator splitting as in the previous chapter to treat differently the advection and the diffusion equations. Details about the discretizations in space and in time, the derivation of the monodomain problem and its associated multidomain problem in the operator splitting context, and the corresponding notation can be found in Sections 3.1 and 3.2. Here we only point out the differences when Ventcell transmission conditions are used and then formulate the interface problem for this case.

4.3.1 An extension of the OSWR with Ventcell transmission conditions and operator splitting

Recall that due to operator splitting, the transmission conditions consists of one equation (cf. (3.6)) for the advection steps and two equations (cf. (3.8)) for the diffusion step. The Ventcell transmission conditions can be used only for the latter (as for the Robin case, see Section 3.2) and the former will be treated in the same way as in Chapter 3. Thus we just replace the transmission conditions (3.8) for the diffusion equation by Ventcell transmission conditions (under a suitable regularity hypothesis). To write the discrete Ventcell transmission conditions, we first introduce the following notation: Let

$$M_{h,i} \times \Sigma_{h,i} \subset L^2(\Omega_i) \times H(\operatorname{div}, \Omega_i)$$

be the usual mixed finite element approximation made of Raviart-Thomas (and Nédélec in three dimensions) spaces of lowest order (see, e.g., [22, 104] and Appendix B), and

let

$$\Lambda_h \times \Sigma_{h,\Gamma} \subset L^2(\Gamma) \times H(\mathrm{div}_\tau, \Gamma)$$

be the lowest order Raviart-Thomas mixed finite element space defined on the interface Γ.

The discrete Ventcell transmission conditions, equivalent to (3.8), for the diffusion equation is defined by: for $n = 0, \ldots, N-1$,

$$\begin{aligned}
&\int_E -\boldsymbol{r}_{h,1}^{n+1} \cdot \boldsymbol{n}_1 + \alpha_{1,2} c_{1,\Gamma}^{n+1} + \beta_{1,2} \left(\phi_2 \frac{c_{1,\Gamma}^{n+1} - c_{1,\Gamma}^{n}}{\Delta t} + \mathrm{div}_\tau \, \boldsymbol{r}_{\Gamma,1}^{n+1} \right) = \\
&\quad \int_E -\boldsymbol{r}_{h,2}^{n+1} \cdot \boldsymbol{n}_1 + \alpha_{1,2} c_{2,\Gamma}^{n+1} + \beta_{1,2} \left(\phi_2 \frac{c_{2,\Gamma}^{n+1} - c_{2,\Gamma}^{n}}{\Delta t} + \mathrm{div}_\tau \, (\boldsymbol{D}_{2,\Gamma} \boldsymbol{D}_{1,\Gamma}^{-1} \boldsymbol{r}_{\Gamma,2}^{n+1}) \right), \ \forall E \in \mathscr{G}_h, \\
&\int_E -\boldsymbol{r}_{h,2}^{n+1} \cdot \boldsymbol{n}_2 + \alpha_{2,1} c_{2,\Gamma}^{n+1} + \beta_{2,1} \left(\phi_1 \frac{c_{2,\Gamma}^{n+1} - c_{2,\Gamma}^{n}}{\Delta t} + \mathrm{div}_\tau \, \boldsymbol{r}_{\Gamma,2}^{n+1} \right) = \\
&\quad \int_E -\boldsymbol{r}_{h,1}^{n+1} \cdot \boldsymbol{n}_2 + \alpha_{2,1} c_{1,\Gamma}^{n+1} + \beta_{2,1} \left(\phi_1 \frac{c_{1,\Gamma}^{n+1} - c_{1,\Gamma}^{n}}{\Delta t} + \mathrm{div}_\tau \, (\boldsymbol{D}_{1,\Gamma} \boldsymbol{D}_{2,\Gamma}^{-1} \boldsymbol{r}_{\Gamma,1}^{n+1}) \right), \ \forall E \in \mathscr{G}_h, \\
&\int_\Gamma \boldsymbol{D}_{2,\Gamma}^{-1} \boldsymbol{r}_{\Gamma,1}^{n+1} \cdot \boldsymbol{\nu}_\Gamma - \int_\Gamma c_{1,\Gamma}^{n+1} \mathrm{div}_\tau \, \boldsymbol{\nu}_\Gamma = 0, \quad \forall \boldsymbol{\nu}_\Gamma \in \Sigma_{h,\Gamma}, \\
&\int_\Gamma \boldsymbol{D}_{2,\Gamma}^{-1} \boldsymbol{r}_{\Gamma,2}^{n+1} \cdot \boldsymbol{\nu}_\Gamma - \int_\Gamma c_{2,\Gamma}^{n+1} \mathrm{div}_\tau \, \boldsymbol{\nu}_\Gamma = 0, \quad \forall \boldsymbol{\nu}_\Gamma \in \Sigma_{h,\Gamma},
\end{aligned} \tag{4.44}$$

where $\alpha_{i,j}$ and $\beta_{i,j}$, $i = 1,2$, $j = 3-i$, are positive constants, $c_{i,\Gamma}$, $i = 1,2$, (which is equal to $\lambda_{h,i}^{n+1}$ in (3.8)) represents the trace of the subdomain concentration on the interface. Note that (4.44) is the discrete counterpart of the Ventcell transmission conditions in derived Section 4.2 for pure diffusion problems (cf. (4.23)).

In order to define the interface problem of the method, we introduce the solution operators $\mathscr{V}_i$, $i = 1,2$, which associate to an $L^2(0,T; L^2(\Omega_i))$ source term f together with $H_*^{1,1}(\Omega_i)$ initial data c_0 and discrete boundary data (λ_a, θ) given on $\Gamma \times (0,T)$, the solution of the discrete advection-diffusion problem in $\Omega_i \times (0,T)$ which is defined below (problem (4.45)-(4.46)). Input

$$\lambda_a = \left(\lambda_{h,a}^{n,l} \right)_{n=0,\ldots,N-1,\, l=0,\ldots,L-1} \text{ and } \theta = \left(\theta_h^n \right)_{n=1,\ldots,N}$$

are Dirichlet data for the advection equation and Ventcell data for the diffusion equation respectively.

The initial data $c_0 \in H_*^{1,1}(\Omega_i)$ is discretized by L^2 projections onto $M_{h,i}$ and onto Λ_h:

$$\left(c_{h,i}^0 \right)_{|K} := \frac{1}{\mathrm{meas}(K)} \int_K c_0, \ \forall K \in \mathscr{K}_{h,i} \text{ and } \left(c_{i,\Gamma}^0 \right)_{|E} := \frac{1}{\mathrm{meas}(E)} \int_E c_0, \ \forall E \in \mathscr{G}_h.$$

Then for given $(\lambda_a, \theta, f, c_0)$, the discrete subdomain problem is defined by:

For $n = 0, \ldots, N-1$,

1. initialize $c_{i,\Gamma}^0$ by projecte

2. define $c_{h,i}^{n,0} = c_{h,i}^{n}$,
3. for $l = 0, \dots, L-1$,
   (a) define the upwind values
   $$\hat{c}_{h,i}^{n,l} = \mathscr{U}_{h,i}\left(c_{h,i}^{n,l}, \lambda_{h,a}^{n,l}\right),$$
   (b) solve the advection equation
   $$\int_K \phi_i \frac{c_{h,i}^{n,l+1} - c_{h,i}^{n,l}}{\Delta t_a} + \sum_{E \subset \partial K} \int_E \hat{c}_{h,i}^{n,l} (\boldsymbol{u} \cdot \boldsymbol{n}_K) = 0, \quad \forall K \in \mathscr{K}_{h,i}, \tag{4.45}$$
   with initial data $c_{h,i}^{n,l}$ and obtain $c_{h,i}^{n,l+1}$,
4. solve the diffusion equation
$$\begin{aligned}
\int_K \phi_i \frac{c_{h,i}^{n+1} - c_{h,i}^{n,L}}{\Delta t} + \int_K \operatorname{div} \boldsymbol{r}_{h,i}^{n+1} &= \int_K f(t^{n+1}), && \forall K \in \mathscr{K}_{h,i}, \\
\int_{\Omega_i} \boldsymbol{D}_i^{-1} \boldsymbol{r}_{h,i}^{n+1} \cdot \boldsymbol{v} - \int_{\Omega_i} c_{h,i}^{n+1} \operatorname{div} \boldsymbol{v} + \int_\Gamma c_{i,\Gamma}^{n+1} (\boldsymbol{v} \cdot \boldsymbol{n}_i) &= 0, && \forall \boldsymbol{v} \in \Sigma_{h,i}, \\
\int_E -\boldsymbol{r}_{h,i}^{n+1} \cdot \boldsymbol{n}_i + \alpha_{i,j} c_{i,\Gamma}^{n+1} + \beta_{i,j} \left(\phi_j \frac{c_{\Gamma,i}^{n+1} - c_{\Gamma,i}^{n}}{\Delta t} + \operatorname{div}_\tau \boldsymbol{r}_{\Gamma,i}^{n+1} \right) &= \int_E \vartheta, && \forall E \in \mathscr{G}_h, \\
\int_\Gamma \boldsymbol{D}_{j,\Gamma}^{-1} \boldsymbol{r}_{\Gamma,i}^{n+1} \cdot \boldsymbol{v}_\Gamma - \int_\Gamma c_{\Gamma,i}^{n+1} \operatorname{div}_\tau \boldsymbol{v}_\Gamma &= 0, && \forall \boldsymbol{v}_\Gamma \in \Sigma_{h,\Gamma},
\end{aligned} \tag{4.46}$$
   with initial data $c_{h,i}^{n,L}$ and $c_{i,\Gamma}^{n}$, and obtain $\left(c_{h,i}^{n+1}, \boldsymbol{r}_{h,i}^{n+1}, c_{i,\Gamma}^{n+1}, \boldsymbol{r}_{\Gamma,i}^{n+1}\right)$.

The solution operator $\mathscr{V}_i$, $i = 1, 2$, is now defined by

$$\begin{aligned}
\mathscr{V}_i : \left(\Lambda_h\right)^{N \times L} \times \left(\Lambda_h\right)^N \times L^2(0,T; L^2(\Omega_i)) \times H^{1,1}_*(\Omega_i) & \\
\to \left(N_{h,i}\right)^N \times \left(M_{h,i}\right)^{N \times L} \times \times \left(\Sigma_{h,i}\right)^N \times \left(\Lambda_h\right)^N \times \left(\Sigma_{h,\Gamma}\right)^N & \\
\left(\lambda_a, \vartheta, f, c_0\right) \mapsto \left(\hat{c}_{h,i}^{\Delta t, \Delta t_a}, c_{h,i}^{\Delta t}, \boldsymbol{r}_{h,i}^{\Delta t}, c_{\Gamma,i}^{\Delta t}, \boldsymbol{r}_{\Gamma,i}^{\Delta t}\right), &
\end{aligned}$$

where

$$\hat{c}_{h,i}^{\Delta t, \Delta t_a} = \left(\hat{c}_{h,i}^{n,l}\right)_{n=0,\dots,N-1,\, l=0,\dots,L-1},$$

and

$$\left(c_{h,i}^{\Delta t}, \boldsymbol{r}_{h,i}^{\Delta t}, c_{\Gamma,i}^{\Delta t}, \boldsymbol{r}_{\Gamma,i}^{\Delta t}\right) = \left(c_{h,i}^{n}, \boldsymbol{r}_{h,i}^{n}, c_{\Gamma,i}^{n}, \boldsymbol{r}_{\Gamma,i}^{n}\right)_{n=1,\dots,N}.$$

As in the Robin case, to impose the transmission condition for the advection equation, we define the projection operators $\overline{\mathscr{H}}_i$, $i = 1, 2$, which extract the first component of the output of $\mathscr{V}_i$:

$$\begin{aligned}
\overline{\mathscr{H}}_i : \left(N_{h,i}\right)^{N \times L} \times \left(M_{h,i}\right)^N \times \left(\Sigma_{h,i}\right)^N \times \left(\Lambda_h\right)^N \times \left(\Sigma_{h,\Gamma}\right)^N \to \left(\Lambda_h\right)^{N \times L} & \\
\left(\hat{c}_{h,i}^{\Delta t, \Delta t_a}, c_{h,i}^{\Delta t}, \boldsymbol{r}_{h,i}^{\Delta t}, c_{\Gamma,i}^{\Delta t}, \boldsymbol{r}_{\Gamma,i}^{\Delta t}\right) \mapsto \begin{cases} 0, & \forall E \in \mathscr{G}_{h,i}^{\mathrm{in}}, \\ \left(\hat{c}_{h,i}^{\Delta t, \Delta t_a}\right)_{|E}, & \forall E \in \mathscr{G}_{h,j}^{\mathrm{in}}, \text{ with } j = 3 - i. \end{cases} &
\end{aligned}$$

Now for the diffusion equation, we define the interface operators to transmit Ventcell data between the subdomains

$$\begin{aligned}
&\overline{\mathscr{B}}_i : \left(N_{h,i}\right)^{N\times L} \times \left(M_{h,i}\right)^N \times \left(\Sigma_{h,i}\right)^N \times \left(\Lambda_h\right)^N \times \left(\Sigma_{h,\Gamma}\right)^N \to \left(\Lambda_h\right)^N \\
&\left(\hat{c}_{h,i}^{\Delta t,\Delta t_a}, c_{h,i}^{\Delta t}, \boldsymbol{r}_{h,i}^{\Delta t}, c_{\Gamma,i}^{\Delta t}, \boldsymbol{r}_{\Gamma,i}^{\Delta t}\right) \mapsto \\
&\qquad \left(-\boldsymbol{r}_{h,j}^{\Delta t}\cdot\boldsymbol{n}_i + \alpha_{i,j}c_{j,\Gamma}^{\Delta t} + \beta_{i,j}\left(\phi_j\partial_t c_{j,\Gamma}^{\Delta t} + \mathrm{div}_\tau\left(\boldsymbol{D}_{j,\Gamma}\boldsymbol{D}_{i,\Gamma}^{-1}\boldsymbol{r}_{\Gamma,j}^{\Delta t}\right)\right)\right)_{|E}, \forall E\in\mathscr{G}_h,
\end{aligned}$$

where

$$\partial_t c_{j,\Gamma}^{\Delta t} := \left(\frac{c_{j,\Gamma}^{n+1}-c_{j,\Gamma}^{n}}{\Delta t}\right)_{n=0,\ldots,N-1}.$$

With these operators, the interface problem corresponding to the transmission condition for the advection quation and Ventcell transmission conditions for the diffusion equation is:

$$\begin{aligned}
&\text{Find } \left(\lambda_a,\vartheta_1,\vartheta_2\right)\in\left(\Lambda_h\right)^{N\times L}\times\left(\Lambda_h\right)^N\times\left(\Lambda_h\right)^N \text{ such that}\\
&\int_{t^{n,l}}^{t^{n,l+1}}\int_E \lambda_a - \overline{\mathscr{H}}_1\mathscr{V}_1(\lambda_a,\vartheta_1,f,c_0) - \overline{\mathscr{H}}_2\mathscr{V}_2(\lambda_a,\vartheta_2,f,c_0) \quad = 0,\\
&\int_{t^n}^{t^{n+1}}\int_E \vartheta_1 - \overline{\mathscr{B}}_1\mathscr{V}_2(\lambda_a,\vartheta_2,f,c_0) \quad = 0,\\
&\int_{t^n}^{t^{n+1}}\int_E \vartheta_2 - \overline{\mathscr{B}}_2\mathscr{V}_1(\lambda_a,\vartheta_1,f,c_0) \quad = 0,\\
&\qquad\qquad \forall E\in\mathscr{G}_h,\ \forall n=0,\ldots,N-1,\ \forall l=0,\ldots,L-1.
\end{aligned} \tag{4.47}$$

Note that the composite operator $\overline{\mathscr{B}}_i\mathscr{V}_i$, $i=1,2$, is a discrete Ventcell-to-Ventcell type operator and the last two equations of (4.47) are an extension of the discrete counterpart of the interface problem (4.37) for pure diffusion equations. As usual, we solve (4.47) iteratively using Jacobi iterations or GMRES.

As in all the time-dependent considered, the domain decomposition method is derived globally in time so that different time steps in the subdomains, $\Delta t_1 \neq \Delta t_2$, can be used. In the next subsection, we briefly describe the weakly enforcement of the Ventcell transmission conditions over the time interval with nonconforming time grids in the operator splitting context. In fact, it is done just as in Chapter 3 for Robin transmission conditions.

4.3.2 Nonconforming time discretizations

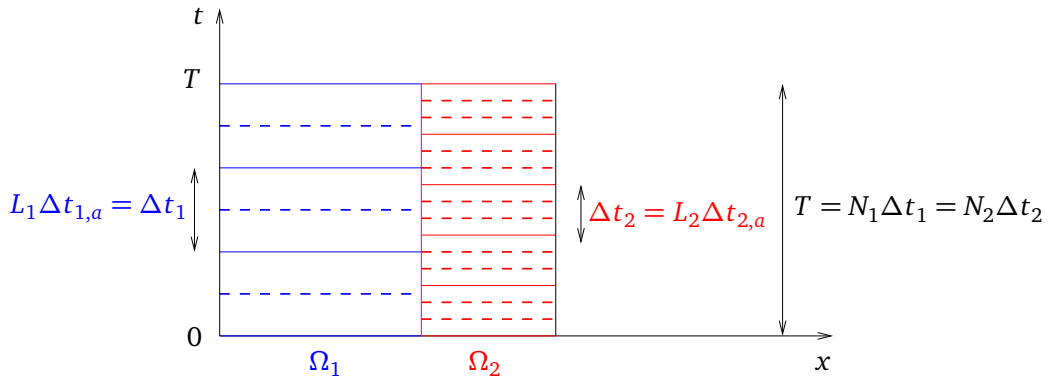

Figure 4.13: Nonconforming time grids in the subdomains.

We first recall notation which was defined earlier in Section 3.3. Let $\mathscr{T}_1$ and $\mathscr{T}_2$ be two different uniform partitions of the time interval $(0,T)$ into N_1 and N_2 sub-intervals respectively with lengths Δt_1 and Δt_2, respectively (see Figure 4.13). The sub-time step for the advection in each subdomain is defined by

$$\Delta t_i = L_i \Delta t_{i,a},\ i = 1,2,$$

and we denote by $\mathscr{T}_i^a,\ i = 1,2$, the corresponding partition in time for the advection. We denote by $P_0(\mathscr{T}_i, \Lambda_h)$ the space of piecewise constant functions in time on grid $\mathscr{T}_i$ with values in Λ_h. Then define Π_{ij} the average-valued projection from $P_0(\mathscr{T}_j, \Lambda_h)$ to $P_0(\mathscr{T}_i, \Lambda_h)$ (see (4.40)), and Π_{ij}^a the projection from $P_0(\mathscr{T}_j^a, \Lambda_h)$ to $P_0(\mathscr{T}_i^a, \Lambda_h)$ as in Section 3.3.

The transmission condition for the advection is weakly enforced in time in a same way as it was done in Section 3.3 and that for the diffusion is handled like in the pure diffusion case (see the previous section, Subsection 4.2.4). In particular, we choose λ_a to be piecewise constant in time on one grid, for instance, $\mathscr{T}_2^a$ and choose ϑ_i to be piecewise constant on grid $\mathscr{T}_i$, problem (4.47) then becomes

Find $(\lambda_a, \vartheta_1, \vartheta_2) \in (\Lambda_h)^{N_2 \times L_2} \times (\Lambda_h)^{N_1} \times (\Lambda_h)^{N_2}$ such that

$$\int_{t_2^{n,l}}^{t_2^{n,l+1}} \int_E \lambda_a - \Pi_{21}^a \left(\overline{\mathscr{H}}_1 \mathscr{V}_1(\Pi_{12}^a(\lambda_a), \vartheta_1, f, c_0) \right) - \overline{\mathscr{H}}_2 \mathscr{V}_2(\lambda_a, \vartheta_2, f, c_0) \quad = 0,$$

$$\int_{t_1^m}^{t_1^{m+1}} \int_E \vartheta_1 - \Pi_{12} \left(\overline{\mathscr{B}}_1 \mathscr{V}_2(\lambda_a, \vartheta_2, f, c_0) \right) \quad = 0,$$

$$\int_{t_2^n}^{t_2^{n+1}} \int_E \vartheta_2 - \Pi_{21} \left(\overline{\mathscr{B}}_2 \mathscr{V}_1(\Pi_{12}^a(\lambda_a), \vartheta_1, f, c_0) \right) \quad = 0,$$

$$\forall E \in \mathscr{G}_h,\ \forall m = 0, \ldots, N_1 - 1, \text{ and } \forall n = 0, \ldots, N_2 - 1,\ \forall l = 0, \ldots, L_2 - 1.$$

4.3.3 Some comments on the approach with Ventcell transmission conditions and operator splitting

Due to operator splitting, on the space-time interface Dirichlet conditions are imposed on the inflow boundary for the advection equation and Ventcell conditions are used

for the diffusion equation only. In some way, we do not completely take advantage of the optimized Ventcell transmission conditions as one could do with a fully implicit scheme (see, e.g. [62]) in which the tangential component of the advection on the interface is also taken into account and thus the optimized parameters depend on the advection field as well. As a result, information exchange is significantly enhanced, especially when advection is dominant. On the other hand, we observe in Section 4.2 that for pure diffusion equations and for a symmetric two subdomains, the convergence of optimized weighted Ventcell and optimized 2-sided Robin is comparable when the diffusion ratio is sufficiently large. Because of the operator splitting, such a result might be true here for the advection-diffusion equation andfor a decomposition into two subdomains (when many subdomains are considered, the Ventcell transmission conditions may significantly improve the convergence compared with the Robin ones [73]) . We thus have not carried out numerical experiments for the algorithm derived this section. However, it could be interesting to compare the performance of such an algorithm with the fully implicit one with Ventcell transmission conditions.

Conclusion

We have formulated in mixed formulations the multidomain problems with Ventcell transmission conditions for three different types of PDEs. For the stationary and the time-dependent diffusion problems, the associated subdomain problems with Ventcell boundary conditions are proved to be well-posed. For each case, an interface problem with two Lagrange multipliers is derived through an introduction of what's called (time dependent) Ventcell-to-Ventcell operators. For time-dependent problems, such an interface problem is defined over the time interval and thus different time steps can be used in the subdomains. Numerical experiments in 2D for the two subdomain case for the elliptic and the time-dependent diffusion equations are shown. For homogeneous problems, the optimized Ventcell parameters improve significantly the convergence speed compared to the optimized 2-sided Robin parameters (by a factor of 2 with Jacobi iterations). For heterogeneous problems, we use the optimized weighted Ventcell parameters adapted to the jumps in the coefficients and we observe that the stronger the heterogeneity the smaller the difference between the convergence of the optimized weight Ventcell and of optimized 2-sided Robin. The results are valid for both stationary and time-dependent diffusion problems, and for conforming spatial discretizations of two symmetric subdomains. We verify for different diffusion ratios that the Ventcell transmission conditions with nonconforming time grids preserve the accuracy in time of the solution. For the advection-diffusion problems, we derive the discrete multidomain formulation in the context of operator splitting and obtain an interface problem in which the Ventcell transmission conditions are used for the diffusion only. The numerical results have not been implemented yet due to a question as to the efficiency of the algorithm (cf. Subsection 4.3.3) as well as for lack of time.

Chapter 5

Application to reduced fracture models

Contents

5.1 The compressible flow model of a single-phase fluid 124
5.2 A reduced fracture model 125
5.2.1 Existence and uniqueness of the solution 127
5.3 Two space-time domain decomposition methods 130
5.3.1 Method 1: Using the time-dependent Steklov-Poincaré operator . . 130
5.3.2 Method 2: Using Optimized Schwarz waveform relaxation 132
5.3.3 Nonconforming discretizations in time 136
5.4 Numerical results 138
5.5 Extension to transport problems 143
5.5.1 A model problem and operator splitting 143
5.5.2 Domain decomposition formulations 147
5.5.3 Nonconforming discretizations in time 151
5.5.4 Some remarks on numerical implementation 153

An ideal place to apply the domain decomposition methods derived in the previous chapters is where there exist fractures and faults-"fast paths". In such a case, the water flow rapidly through these paths while it moves much more slowly through the rock matrix. As a result, the contaminants present in the porous medium may follow the water and they are transported faster than in the case with no fracture. Thus the time scales in the fractures and in the surrounding medium are very different and in the context of simulation, one should use much smaller time steps in the fractures than in the rock matrix. Here we consider the case in which the domain is separated into two matrix subdomains by a fracture. The permeability in the fracture can be larger or smaller than that in the surrounding medium. The former corresponds to a fast pathway and the latter corresponds to a geological barrier. Here we are interested in the "fast path" fracture and we aim to use space-time domain decomposition methods to model flow and transport problems in a porous medium containing such a fracture. A straightforward application of what has been presented in the previous chapters would be then to consider the fracture as a third subdomain and to take smaller time steps

there. We consider instead however a reduced model in which the fracture is treated as an interface between the two subdomains. We first consider the compressible flow for the reduced model and prove its well-posedness using Galerkin's method, then we extend the two methods, the one using the Steklov-Poincaré type operator and the one using the Optimized Schwarz waveform relaxation (OSWR) approach, to handle this model problem. Extension of the former is straightforward while for the latter a new idea is needed. A linear combination between the pressure continuity equation and the fracture problem is used as a transmission condition, and a free parameter is used to accelerate the convergence rate. We write the space-time interface problem for each method and consider the corresponding semi-discrete problem in time where different time discretizations are used. Numerical experiments are carried out to verify the performance of the two methods. We then extend these results to the advection-diffusion problem where we use operator splitting as considered in Chapter 3. We formulate the fully discrete interface problem for each method and discuss the use of nonconforming time grids in this case.

5.1 The compressible flow model of a single-phase fluid

For an open, bounded domain Ω of $\mathbb{R}^d$ ($d = 2,3$) with Lipschitz boundary $\partial\Omega$ and some fixed time $T > 0$, we consider the compressible flow problem written in mixed form as follows

$$\begin{array}{rll} s\partial_t p + \operatorname{div} \boldsymbol{u} & = q & \text{in } \Omega \times (0,T), \\ \boldsymbol{u} & = -\boldsymbol{K}\nabla p & \text{in } \Omega \times (0,T), \\ p & = 0 & \text{on } \partial\Omega \times (0,T), \\ p(\cdot,0) & = p_0 & \text{in } \Omega. \end{array} \tag{5.1}$$

Recall (see Chapter 1) that p is the pressure, $\boldsymbol{u}$ the velocity, q the source term, s the storage coefficient and $\boldsymbol{K}$ a symmetric time independent hydraulic conductivity (or permeability) tensor. As in the earlier chapters, for simplicity we have imposed the homogeneous Dirichlet condition on the boundary.

We suppose that the fracture Ω_f, with variable thickness $\delta(\cdot)$, is a subdomain of Ω and separates Ω into two connected subdomains (see Figure 5.1, left where for visualization purposes the size of δ is shown as being much larger than it is in reality),

$$\Omega \setminus \overline{\Omega}_f = \Omega_1 \cup \Omega_2, \quad \Omega_1 \cap \Omega_2 = \emptyset.$$

Also for simplicity we assume that Ω_f consists of the intersection with Ω of a line or plane γ (depending on whether $d = 2$ or 3), together with the points $\boldsymbol{x} = \boldsymbol{x}_\gamma + s\boldsymbol{n}_\gamma$ where $\boldsymbol{x}_\gamma \in \gamma$, $s \in \left(-\dfrac{\delta(\boldsymbol{x}_\gamma)}{2}, \dfrac{\delta(\boldsymbol{x}_\gamma)}{2}\right)$ and $\boldsymbol{n}_\gamma$ is a unit vector normal to γ. We denote by γ_i the part of the boundary of Ω_i shared with the boundary of the fracture Ω_f:

$$\gamma_i = \left(\partial\Omega_i \cap \partial\Omega_f\right) \cap \Omega, \quad i = 1,2,$$

and we denote by $\boldsymbol{n}_i$ the unit, outward pointing, normal vector field on $\partial\Omega_i$. We use the convention that for any scalar, vector or tensor valued function ϕ defined on Ω, ϕ_i denotes the restriction of ϕ to $\Omega_i, i = 1,2,f$. We rewrite problem (5.1) as the following

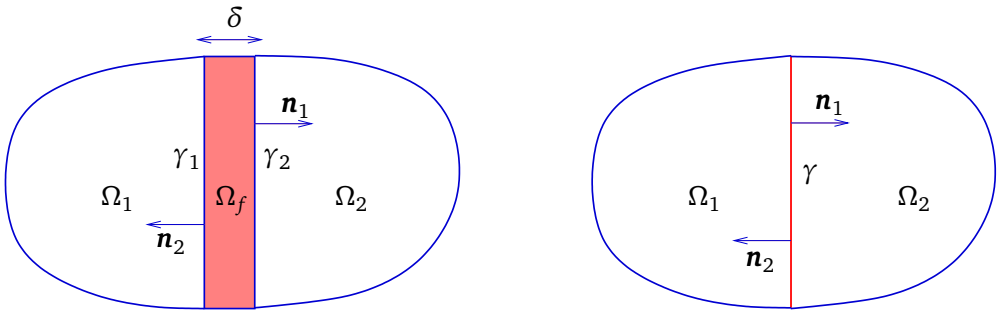

Figure 5.1: Left: The domain Ω with the fracture Ω_f. Right: The domain Ω with the interface-fracture γ.

transmission problem:

$$\begin{array}{rlll} s_i \partial_t p_i + \operatorname{div} \boldsymbol{u}_i & = q_i & \text{in } \Omega_i \times (0,T), & i = 1,2,f, \\ \boldsymbol{u}_i & = -\boldsymbol{K}_i \nabla p_i & \text{in } \Omega_i \times (0,T), & i = 1,2,f, \\ p_i & = 0 & \text{on } \left(\partial\Omega_i \cap \partial\Omega\right) \times (0,T), & i = 1,2,f, \\ p_i & = p_f & \text{on } \gamma_i \times (0,T), & i = 1,2, \\ \boldsymbol{u}_i \cdot \boldsymbol{n}_i & = \boldsymbol{u}_f \cdot \boldsymbol{n}_i & \text{on } \gamma_i \times (0,T), & i = 1,2, \\ p_i(\cdot,0) & = p_{0,i} & \text{in } \Omega_i, & i = 1,2,f. \end{array} \tag{5.2}$$

Modeling flow in porous media with fractures is challenging and requires a multi-scale approach: firstly, the fractures represent strong heterogeneities as they have much higher or much lower permeability than that in the surrounding medium; secondly, the fracture width is much smaller than any reasonable parameter of spatial discretization. Thus one might need to refine the mesh locally around the fractures to tackle the problem, which is well-known to be very computationally costly and is not useful at the macroscopic scale (i.e. when the fractures can be modeled individually). One possible approach is to treat the fractures as $(d-1)-$dimensional interfaces between subdomains (see [10, 5, 40, 92, 8, 110, 42] and the references therein) so that one can avoid refining locally around the fractures. We pointed out that in these reduced fracture models, unlike in some discrete fracture models, the interactions between the fractures and the surrounding porous medium are taken into account. In the next section, we consider a reduced model with a highly permeable fracture, which results in the continuity of the pressure and discontinuity of the normal component of the velocity across the fracture-interface. Then in Section 5.3 we consider a domain decomposition approach for solving the resulting problem. Note that more general reduced models that can handle both large and small permeability fractures [92] introduce more complicated transmission conditions on the fracture-interface (in the form of Robin type conditions), and it is not yet clear how to formulate an associated domain decomposition problem with a parameter that can be optimized.

5.2 A reduced fracture model

In the reduced fracture model, the fracture is treated as an interface γ between subdomains Ω_1 and Ω_2 (see Figure 5.1, right). We use the notation ∇_τ (respectively div_τ) for the tangential gradient (respectively tangential divergence) operators along the

fracture γ. We denote by s_γ and $\boldsymbol{K}_\gamma$ the storage coefficient and the permeability tensor in the fracture. A reduced model [5, 92] consists of the equations in the subdomains

$$\begin{aligned} s_i\partial_t p_i + \operatorname{div} \boldsymbol{u}_i &= q_i && \text{in } \Omega_i \times (0,T), \\ \boldsymbol{u}_i &= -\boldsymbol{K}_i \nabla p_i && \text{in } \Omega_i \times (0,T), \\ p_i &= 0 && \text{on } \left(\partial\Omega_i \cap \partial\Omega\right) \times (0,T), \\ p_i &= p_\gamma && \text{on } \gamma \times (0,T), \\ p_i(\cdot,0) &= p_{0,i} && \text{in } \Omega_i, \end{aligned} \qquad \text{for } i = 1,2, \tag{5.3}$$

and in the fracture

$$\begin{aligned} s_\gamma\partial_t p_\gamma + \operatorname{div}_\tau \boldsymbol{u}_\gamma &= q_\gamma + \left(\boldsymbol{u}_1 \cdot \boldsymbol{n}_{1|\gamma} + \boldsymbol{u}_2 \cdot \boldsymbol{n}_{2|\gamma}\right) && \text{in } \gamma \times (0,T), \\ \boldsymbol{u}_\gamma &= -\boldsymbol{K}_\gamma \delta \nabla_\tau p_\gamma && \text{in } \gamma \times (0,T), \\ p_\gamma &= 0 && \text{on } \partial\gamma \times (0,T), \\ p_\gamma(\cdot,0) &= p_{0,\gamma} && \text{in } \gamma. \end{aligned} \tag{5.4}$$

This model may be derived by averaging across the transversal cross sections of the fracture. It consists of the mass conservation equation and the Darcy equation in the subdomain together with the lower dimensional mass conservation and Darcy equations in the fracture of co-dimension 1. These two systems are coupled: the fracture sees the subdomain through the additional source term in the conservation equation in the fracture (the second term on the right hand side) which represents the difference of the fluid entering the fracture from the subdomain and that exiting through the subdomain. Each subdomain sees the fracture through the Dirichlet boundary condition imposed on the common part of its boundary with the fracture.

In order to prove the well-posedness of problem (5.3)-(5.4) we first write its weak formulation. As before, we use the convention that if V is a space of functions, then we write $\boldsymbol{V}$ for a space of vector functions having each component in V. For an arbitrary domain $\mathcal{O}$, we denote by $(\cdot,\cdot)_{\mathcal{O}}$ the inner product in $L^2(\mathcal{O})$ or $\boldsymbol{L^2(\mathcal{O})}$ and by and $\|\cdot\|_{\mathcal{O}}$ the $L^2(\mathcal{O})-$norm or $\boldsymbol{L^2(\mathcal{O})}$-norm. To write the weak formulation of (5.3)-(5.4), we define the following Hilbert spaces (see Remark 2.1):

$$\begin{aligned} M &= \left\{\mu = (\mu_1,\mu_2,\mu_\gamma) \in L^2(\Omega_1) \times L^2(\Omega_2) \times L^2(\gamma)\right\}, \\ \Sigma &= \{\boldsymbol{\nu} = (\boldsymbol{\nu}_1,\boldsymbol{\nu}_2,\boldsymbol{\nu}_\gamma) \in \boldsymbol{L^2(\Omega_1)} \times \boldsymbol{L^2(\Omega_2)} \times \boldsymbol{L^2(\gamma)} : \operatorname{div} \boldsymbol{\nu}_i \in L^2(\Omega_i), i = 1,2, \\ &\qquad \text{and } \operatorname{div}_\tau \boldsymbol{\nu}_\gamma - \sum_{i=1}^{2} \boldsymbol{\nu}_i \cdot \boldsymbol{n}_{i|\gamma} \in L^2(\gamma)\}, \end{aligned}$$

equipped with the norms

$$\begin{aligned} \|\mu\|_M^2 &= \sum_{i=1}^{2} \|\mu_i\|_{\Omega_i}^2 + \|\mu_\gamma\|_\gamma^2, \\ \|\boldsymbol{\nu}\|_\Sigma^2 &= \sum_{i=1}^{2} \left(\|\boldsymbol{\nu}_i\|_{\Omega_i}^2 + \|\operatorname{div} \boldsymbol{\nu}_i\|_{\Omega_i}^2\right) + \|\boldsymbol{\nu}_\gamma\|_\gamma^2 + \|\operatorname{div}_\tau \boldsymbol{\nu}_\gamma - \sum_{i=1}^{2} \boldsymbol{\nu}_i \cdot \boldsymbol{n}_{i|\gamma}\|_\gamma^2. \end{aligned}$$

We define the following bilinear forms

$$
\begin{aligned}
a: \quad \Sigma \times \Sigma \quad &\longrightarrow \quad \mathbb{R} \\
(\boldsymbol{u},\boldsymbol{v}) \quad &\mapsto \quad a(\boldsymbol{u},\boldsymbol{v}) = \sum_{i=1}^{2} \left(\boldsymbol{K}_i^{-1}\boldsymbol{u}_i, \boldsymbol{v}_i\right)_{\Omega_i} + \left((\boldsymbol{K}_\gamma \delta)^{-1}\boldsymbol{u}_\gamma, \boldsymbol{v}_\gamma\right)_\gamma, \\
b: \quad \Sigma \times M \quad &\longrightarrow \quad \mathbb{R} \\
(\boldsymbol{u},\mu) \quad &\mapsto \quad b(\boldsymbol{u},\mu) = \sum_{i=1}^{2} \left(\operatorname{div} \boldsymbol{u}_i, \mu_i\right)_{\Omega_i} + \left(\operatorname{div}_\tau \boldsymbol{u}_\gamma - \sum_{i=1}^{2} \boldsymbol{u}_i \cdot \boldsymbol{n}_{i|\gamma}, \mu_\gamma\right)_\gamma, \\
c_s: \quad M \times M \quad &\longrightarrow \quad \mathbb{R} \\
(\eta,\mu) \quad &\mapsto \quad c_s(\eta,\mu) = \sum_{i=1}^{2} \left(s_i \eta_i, \mu_i\right)_{\Omega_i} + \left(s_\gamma \eta_\gamma, \mu_\gamma\right)_\gamma,
\end{aligned}
$$

and the linear form

$$
\begin{aligned}
L_q: \quad M \quad &\longrightarrow \quad \mathbb{R} \\
\mu \quad &\mapsto \quad L_q(\mu) = \sum_{i=1}^{2} \left(q_i, \mu_i\right)_{\Omega_i} + \left(q_\gamma, \mu_\gamma\right)_\gamma.
\end{aligned}
$$

With these spaces and forms, the weak form of (5.3)-(5.4) can be written as follows:

$$
\begin{aligned}
&\text{For a.e. } t \in (0,T), \text{ find } p(t) \in M \text{ and } \boldsymbol{u}(t) \in \Sigma \text{ such that} \\
&\qquad\qquad a(\boldsymbol{u},\boldsymbol{v}) - b(\boldsymbol{v},p) = 0 \qquad \forall \boldsymbol{v} \in \Sigma, \\
&\qquad\qquad c_s(\partial_t p,\mu) + b(\boldsymbol{u},\mu) = L_q(\mu) \qquad \forall \mu \in M, \\
&\text{together with the initial conditions}
\end{aligned}
\tag{5.5}
$$

$$
\begin{aligned}
p_i(\cdot,0) &= p_{0,i} \quad \text{in } \Omega_i, \quad i = 1,2, \\
p_\gamma(\cdot,0) &= p_{0,\gamma} \quad \text{in } \gamma.
\end{aligned}
\tag{5.6}
$$

5.2.1 Existence and uniqueness of the solution

We first define the space

$$
H^1_{*,a}(\Omega) := \left\{ \mu = (\mu_1,\mu_2,\mu_\gamma) \in H^1(\Omega_1) \times H^1(\Omega_2) \times H^1_0(\gamma) : \mu_i = 0 \text{ on } \partial\Omega_i \cap \partial\Omega \right\},
$$

equipped with the norm

$$
\|\mu\|^2_{H^1_{*,a}(\Omega)} = \|\mu\|^2_M + \sum_{i=1}^{2} \|\nabla \mu_i\|^2_{\Omega_i} + \|\nabla_\tau \mu_\gamma\|^2_\gamma.
$$

The well-posedness of problem (5.5)-(5.6) is given by the following theorem:

Theorem 5.1. *Assume that there exists four positive constants s_- and s_+, K_- and K_+ such that*

- $s_- \le s_i(x) \le s_+$ *for a.e.* $x \in \Omega_i$, $i = 1,2$,
- $s_- \le s_\gamma(x) \le s_+$ *for a.e.* $x \in \gamma$,
- $\varsigma^T \boldsymbol{K}_i^{-1}(x)\varsigma \ge K_-|\varsigma|^2$, *and* $|\boldsymbol{K}_i(x)\varsigma| \le K_+|\varsigma|$, *for a.e.* $x \in \Omega_i$, $\forall \varsigma \in \mathbb{R}^n$, $i = 1,2$,
- $\eta^T (\boldsymbol{K}_\gamma(x)\delta)^{-1}\eta \ge K_-|\eta|^2$ *and* $|(\boldsymbol{K}_\gamma(x)\delta)^{-1}\eta| \le K_+|\eta|$ *for a.e.* $x \in \gamma$, $\forall \eta \in \mathbb{R}^{n-1}$.

If q is in $L^2(0,T;M)$ and p_0 in $H^1_{*,a}(\Omega)$ then problem (5.5)-(5.6) *has a unique solution*

$$(p,\boldsymbol{u}) \in H^1(0,T;M) \times L^2(0,T;\Sigma).$$

The proof of Theorem 5.1 is quite similar to that of Theorem 4.10. However, we include it here for completeness. We again use Galerkin's method and derive energy estimates to prove the existence and uniqueness of the solution. The energy estimates are given by the following lemma:

Lemma 5.2. *Assume that q is in $L^2(0,T;M)$ and p_0 in $H^1_{*,a}(\Omega)$ then the following estimate holds*

$$\|p\|_{L^\infty(0,T;M)} + \|\partial_t p\|_{L^2(0,T;M)} + \|\boldsymbol{u}\|_{L^2(0,T;\Sigma)} \leq C\left(\|q\|_{L^2(0,T;M)} + \|p_0\|_{H^1_{*,a}(\Omega)}\right).$$

Proof. As usual we proceed by estimating successively p, $\partial_t p$ and $\boldsymbol{u}$.

- Firstly, to derive an estimate for p, we take $p(t) \in M$ and $\boldsymbol{u}(t) \in \Sigma$ as the test functions in (5.5) and add

  $$a(\boldsymbol{u},\boldsymbol{u}) + c_s(\partial_t p, p) = L_q(p).$$

  Using the definitions of a and c_s, and the hypotheses concerning the storage coefficient and the permeability tensor in the subdomains and in the fracture as well as the Cauchy-Schwarz inequality, we obtain

  $$\frac{s_-}{2}\frac{d}{dt}\|p\|_M^2 + K_-\|\boldsymbol{u}\|_{\boldsymbol{M}}^2 \leq \frac{1}{2}\left(\|q\|_M^2 + \|p\|_M^2\right). \tag{5.7}$$

  Now integrate (5.7) over $(0,t)$ for $t \in (0,T]$, we find

  $$s_-\|p(t)\|_M^2 + 2K_-\int_0^t \|\boldsymbol{u}\|_{\boldsymbol{M}}^2 \leq \|p_0\|_M^2 + \|q\|^2_{L^2(0,T;M)} + \int_0^t \|p\|_M^2.$$

  Then we apply Gronwall's lemma to obtain

  $$\|p(t)\|^2_{L^\infty(0,T;M)} \leq C\left(\|p_0\|_M^2 + \|q\|^2_{L^2(0,T;M)}\right),$$

  and consequently,

  $$\|\boldsymbol{u}\|^2_{L^2(0,T;\boldsymbol{M})} \leq C\left(\|p_0\|_M^2 + \|q\|^2_{L^2(0,T;M)}\right). \tag{5.8}$$

- Next, we estimate $\partial_t p$. For this, we differentiate the first equation of (5.5) with respect to t and take $\boldsymbol{u}$ as a test function. This yields

  $$a(\partial_t \boldsymbol{u},\boldsymbol{u}) - b(\boldsymbol{u},\partial_t p) = 0. \tag{5.9}$$

  Then take $\partial_t p$ as a test function in the second equation of (5.5)

  $$c_s(\partial_t p,\partial_t p) + b(\boldsymbol{u},\partial_t p) = L_q(\partial_t p). \tag{5.10}$$

  Now adding (5.9) and (5.10), we obtain

  $$a(\partial_t \boldsymbol{u},\boldsymbol{u}) + c_s(\partial_t p,\partial_t p) = L_q(\partial_t p),$$

or

$$s_-\|\partial_t p\|_M^2 + \frac{K_-}{2}\frac{d}{dt}\|\boldsymbol{u}\|_{\boldsymbol{M}}^2 \leq \frac{1}{2}\|q\|_M^2 + \frac{1}{2}\|\partial_t p\|_M^2.$$

Integrating this inequality over $(0,t)$ for $t \in (0,T]$, we have

$$s_-\int_0^t \|\partial_t p\|_M^2 + K_-\|\boldsymbol{u}(t)\|_{\boldsymbol{M}}^2 \leq \|q\|_{L^2(0,T;M)}^2 + K_-\|\boldsymbol{u}(0)\|_{\boldsymbol{M}}^2. \tag{5.11}$$

There only remains to bound the term $K_-\|\boldsymbol{u}(0)\|_{\boldsymbol{M}}^2$. Toward this end, we use the first equation of (5.5) with $\boldsymbol{v} = \boldsymbol{u}$ and for $t = 0$ (as usual, we assume that the equation is valid at time $t = 0$ in a sense that the analysis is carried out through the construction of finite dimensional approximations of the continuous problem (see Chapter 2)):

$$\begin{aligned} K_-\|\boldsymbol{u}(0)\|_{\boldsymbol{M}}^2 &\leq \sum_{i=1}^2 \left(\operatorname{div}\boldsymbol{u}_i(0), p_{0,i}\right)_{\Omega_i} + \left(\operatorname{div}_\tau \boldsymbol{u}_\gamma(0) - \sum_{i=1}^2 \boldsymbol{u}_i(0)\cdot\boldsymbol{n}_{i|\gamma}, p_{0,\gamma}\right)_\gamma, \\ &\leq -\sum_{i=1}^2 \left(\boldsymbol{u}_i(0), \nabla p_{0,i}\right)_{\Omega_i} - \left(\boldsymbol{u}_\gamma(0), \nabla_\tau p_{0,\gamma}\right)_\gamma, \\ &\leq \frac{K_-}{2}\|\boldsymbol{u}(0)\|_{\boldsymbol{M}}^2 + \frac{1}{2K_-}\|p_0\|_{H^1_{*,a}(\Omega)}. \end{aligned}$$

Substituting this into (5.11), we obtain

$$s_-\int_0^t \|\partial_t p\|_M^2 + K_-\|\boldsymbol{u}(t)\|_{\boldsymbol{M}}^2 \leq C\left(\|q\|_{L^2(0,T;M)}^2 + \|p_0\|_{H^1_{*,a}(\Omega)}\right).$$

Thus

$$\|\partial_t p\|_{L^2(0,T;M)}^2 \leq C\left(\|q\|_{L^2(0,T;M)}^2 + \|p_0\|_{H^1_{*,a}(\Omega)}\right). \tag{5.12}$$

- From (5.8), we only need to derive an estimate for $\operatorname{div}\boldsymbol{u}_i$, $i = 1,2$, and for $\operatorname{div}_\tau \boldsymbol{u}_\gamma - \sum_{i=1}^2 \boldsymbol{u}_i\cdot\boldsymbol{n}_{i|\gamma}$ to complete the proof. With this aim, we take $\left(\mu_1,\mu_2,\mu_\gamma\right) = \left(\operatorname{div}\boldsymbol{u}_1, \operatorname{div}\boldsymbol{u}_2, \operatorname{div}_\tau \boldsymbol{u}_\gamma - \sum_{i=1}^2 \boldsymbol{u}_i\cdot\boldsymbol{n}_{i|\gamma}\right)$ as the test function in the second equation of (5.5), we have

$$\begin{aligned} &\sum_{i=1}^2 \|\operatorname{div}\boldsymbol{u}_i\|_{\Omega_i}^2 + \|\operatorname{div}_\tau \boldsymbol{u}_\gamma - \sum_{i=1}^2 \boldsymbol{u}_i\cdot\boldsymbol{n}_{i|\gamma}\|_\gamma^2 \\ &\qquad = \sum_{i=1}^2 (q_i - s_i\partial_t p_i, \operatorname{div}\boldsymbol{u}_i)_{\Omega_i} + (q_\gamma - s_\gamma\partial_t p_\gamma, \operatorname{div}_\tau \boldsymbol{u}_\gamma - \sum_{i=1}^2 \boldsymbol{u}_i\cdot\boldsymbol{n}_{i|\gamma})_\gamma, \\ &\leq \sum_{i=1}^2 \left(\frac{1}{2}\|q_i - s_i\partial_t p_i\|_{\Omega_i}^2 + \frac{1}{2}\|\operatorname{div}\boldsymbol{u}_i\|_{\Omega_i}^2\right) + \frac{1}{2}\|q_\gamma - s_\gamma\partial_t p_\gamma\|_\gamma^2 + \frac{1}{2}\|\operatorname{div}_\tau \boldsymbol{u}_\gamma - \sum_{i=1}^2 \boldsymbol{u}_i\cdot\boldsymbol{n}_{i|\gamma}\|_\gamma^2, \end{aligned}$$

or

$$\sum_{i=1}^2 \|\operatorname{div}\boldsymbol{u}_i\|_{\Omega_i}^2 + \|\operatorname{div}_\tau \boldsymbol{u}_\gamma - \sum_{i=1}^2 \boldsymbol{u}_i\cdot\boldsymbol{n}_{i|\gamma}\|_\gamma^2 \leq \|q\|_M^2 + s_+\|\partial_t p\|_M^2.$$

Using (5.12), we obtain

$$\int_0^T \left(\sum_{i=1}^{2} \|\mathrm{div}\, \boldsymbol{u}_i\|^2_{\Omega_i} + \|\mathrm{div}_\tau\, \boldsymbol{u}_\gamma - \sum_{i=1}^{2} \boldsymbol{u}_i \cdot \boldsymbol{n}_{i|\gamma}\|^2_\gamma \right) \leq C \left(\|q\|^2_{L^2(0,T;M)} + \|p_0\|_{H_0^{1,*}(\Omega)} \right).$$

This along with (5.8) gives the estimate for $\|\boldsymbol{u}\|_{L^2(0,T;\Sigma)}$, which completes the proof of the lemma.

□

5.3 Two space-time domain decomposition methods

It is natural to apply domain decomposition methods for solving problem (5.2) or problem (5.3) - (5.4), especially since these allow different time steps in the subdomains and in the fracture. For problem (5.2), it is a straightforward application of the methods derived in Chapter 2 while for problem (5.3) - (5.4), we need to derive a different formulation. In the following, we present two global-in-time domain decomposition methods for solving (5.3) - (5.4) based on different transmission conditions. A space-time interface problem is derived for each approach, and it will be solved iteratively using, for instance, GMRES as the system is nonsymmetric.

5.3.1 Method 1: Using the time-dependent Steklov-Poincaré operator

This method is directly derived from the formulation of problem (5.3) - (5.4). To obtain the interface problem for this method, we define the space

$$H^{1,1}_*(\Omega_i) := \left\{ q \in H^1(\Omega_i) : q_{|\partial\Omega_i \cap \partial\Omega} = 0 \text{ and } q_{|\gamma} \in H^1(\gamma) \right\}, i = 1, 2,$$

which was also used in the Ventcell transmission conditions case (4.34). Then we define the following Dirichlet to Neumann operators $\mathscr{S}_i^{\mathrm{DtN}}$, $i = 1, 2$:

$$\begin{aligned} \mathscr{S}_i^{\mathrm{DtN}} : H^1(0,T;L^2(\gamma)) \times L^2(0,T;L^2(\Omega_i)) \times H^1_*(\Omega_i) &\to L^2\left(0,T;L^2(\gamma)\right) \\ \mathscr{S}_i^{\mathrm{DtN}}(\lambda, q, p_0) &= \boldsymbol{u}_i \cdot \boldsymbol{n}_{i|\gamma}, \end{aligned}$$

where, $(p_i, \boldsymbol{u}_i)$, $i = 1, 2$, is the solution of the problem

$$\begin{aligned} s_i \partial_t p_i + \mathrm{div}\, \boldsymbol{u}_i &= q && \text{in } \Omega_i \times (0,T), \\ \boldsymbol{u}_i &= -\boldsymbol{K}_i \nabla p_i && \text{in } \Omega_i \times (0,T), \\ p_i &= 0 && \text{on } \left(\partial\Omega_i \cap \partial\Omega\right) \times (0,T), \\ p_i &= \lambda && \text{on } \gamma \times (0,T), \\ p_i(\cdot,0) &= p_0 && \text{in } \Omega_i. \end{aligned} \tag{5.13}$$

Remark 5.3. *Subdomain problem* (5.17) *with Dirichlet boundary conditions is well-posed (see Chapter 2).*

Problem (5.4) is reduced to an interface problem with one unknown λ

$$\begin{aligned} s_\gamma \partial_t \lambda + \mathrm{div}_\tau\, \boldsymbol{u}_\gamma &= q_\gamma + \sum_{i=1}^{2} \mathscr{S}_i^{\mathrm{DtN}}(\lambda, q_i, p_{0,i}) && \text{in } \gamma \times (0,T), \\ \boldsymbol{u}_\gamma &= -\boldsymbol{K}_\gamma \delta \nabla_\tau \lambda && \text{in } \gamma \times (0,T), \\ \lambda &= 0 && \text{on } \partial\gamma \times (0,T), \\ \lambda(\cdot,0) &= p_{0,\gamma} && \text{in } \gamma. \end{aligned} \tag{5.14}$$

or equivalently

$$\begin{aligned} s_\gamma \partial_t \lambda + \operatorname{div}_\tau \boldsymbol{u}_\gamma - \sum_{i=1}^{2} \mathscr{S}_i^{\mathrm{DtN}}(\lambda,0,0) &= q_\gamma + \sum_{i=1}^{2} \mathscr{S}_i^{\mathrm{DtN}}(0,q_i,p_{0,i}) && \text{in } \gamma\times(0,T),\\ \boldsymbol{u}_\gamma &= -\boldsymbol{K}_\gamma \delta \nabla_\tau \lambda && \text{in } \gamma\times(0,T),\\ \lambda &= 0 && \text{on } \partial\gamma\times(0,T),\\ \lambda(\cdot,0) &= p_{0,\gamma} && \text{in } \gamma. \end{aligned} \tag{5.15}$$

The discrete counterpart of this problem using the discontinuous Galerkin method of order zero for time discretization and mixed finite elements for spatial discretization is of the form

$$\begin{bmatrix} s_\gamma \boldsymbol{I} & \boldsymbol{B} \\ \boldsymbol{B}^T & \boldsymbol{A} \end{bmatrix} \begin{bmatrix} \lambda_h^{n+1} \\ \boldsymbol{U}_{h,\gamma}^{n+1} \end{bmatrix} - \begin{bmatrix} s_\gamma \boldsymbol{I} & 0 \\ 0 & 0 \end{bmatrix} \begin{bmatrix} \lambda_h^{n} \\ \boldsymbol{U}_{h,\gamma}^{n} \end{bmatrix} - \begin{bmatrix} \displaystyle\int_{t^n}^{t^{n+1}} \sum_{i=1}^{2} \mathscr{S}_{h,i}^{\mathrm{DtN}}(\lambda_h,0,0) \\ 0 \end{bmatrix} = \begin{bmatrix} \displaystyle\int_{t^n}^{t^{n+1}} \left(\mathbf{Q}_\gamma + \sum_{i=1}^{2} \mathscr{S}_{h,i}^{\mathrm{DtN}}(0,q_i,p_{0,i}) \right) \\ 0 \end{bmatrix}, \tag{5.16}$$

for $n = 0,\dots,N$, (where N is the number of time intervals of a partition of $(0,T)$), or in compact form (space-time),

$$\overline{\mathscr{S}}\lambda_h = \chi.$$

This problem is solved iteratively as was done in the previous chapters.

To improve the convergence of the iterative algorithm, we will use a preconditioner. We remark that the interface problem is dominated by the second order operator $\left(\operatorname{div}_\tau(\boldsymbol{K}_\gamma \delta\nabla_\tau)\right)$ since the permeability is larger in the fracture and the Steklov-Poincaré is of lower order (first order). Thus the first choice of a preconditioner is $\boldsymbol{P}_{\mathrm{loc}}^{-1}$ defined by taking the discrete counterpart of the operator $\left(\operatorname{div}_\tau(\boldsymbol{K}_\gamma \delta\nabla_\tau)\right)^{-1}$. With the notation in (5.16), we have

$$\boldsymbol{P}_{\mathrm{loc}}^{-1} = \boldsymbol{B}\boldsymbol{A}^{-1}\boldsymbol{B}^T.$$

For elliptic problems, it was shown numerically [7] that this local preconditioner significantly improves the convergence compared with that without preconditioner. Another possibility is to use the Neumann-Neumann preconditioner as employed in Chapter 2 for normal domain decomposition (i.e. without fractures). The preconditioning system is then

$$\boldsymbol{P}_{\mathrm{NN}}^{-1}\varphi = \tilde{\chi},$$

with

$$\boldsymbol{P}_{\mathrm{NN}}^{-1} := \left(\sigma_1 (\mathscr{S}_{h,1}^{\mathrm{DtN}})^{-1} + \sigma_2 (\mathscr{S}_{h,2}^{\mathrm{DtN}})^{-1}\right),$$

where

- $\sigma_i : \Gamma\times(0,T) \to [0,1]$ is such that $\sigma_1+\sigma_2 = 1$. If $\boldsymbol{K}_i = \mathfrak{K}_i \boldsymbol{I}$ and $\mathfrak{K}_i$ is constant in each subdomain then

$$\sigma_i = \frac{\mathfrak{K}_i}{\mathfrak{K}_1+\mathfrak{K}_2}.$$

- $(\mathscr{S}_{h,i}^{\text{DtN}})^{-1}$, $i=1,2$, is the discrete counterpart of the inverse of the operator

$$\mathscr{S}_i^{\text{DtN}} := \mathscr{S}_i^{\text{DtN}}(\cdot,0,0).$$

The continuous (Neumann-to-Dirichlet) operator $(\mathscr{S}_i^{\text{DtN}})^{-1}$ is defined by

$$\begin{aligned}(\mathscr{S}_i^{\text{DtN}})^{-1} : L^2\left(0,T;L^2(\gamma)\right) &\to H^1\left(0,T;L^2(\gamma)\right)\\ \left(\mathscr{S}_i^{\text{DtN}}\right)^{-1}(\varphi) &= p_{i|\gamma},\end{aligned}$$

where, $(p_i,\boldsymbol{u}_i)$, $i=1,2$, is the solution of the problem

$$\begin{aligned} s_i\partial_t p_i + \operatorname{div}\boldsymbol{u}_i &= 0 && \text{in } \Omega_i\times(0,T),\\ \boldsymbol{u}_i &= -\boldsymbol{K}_i\nabla p_i && \text{in } \Omega_i\times(0,T),\\ p_i &= 0 && \text{on } \left(\partial\Omega_i\cap\partial\Omega\right)\times(0,T),\\ -\boldsymbol{u}_i\cdot\boldsymbol{n}_i &= \varphi && \text{on } \gamma\times(0,T),\\ p_i(\cdot,0) &= 0 && \text{in } \Omega_i. \end{aligned} \tag{5.17}$$

In Section 5.4, we will carry out numerical experiments and compare the performance of these two preconditioners.

5.3.2 Method 2: Using Optimized Schwarz waveform relaxation

Instead of imposing Dirichlet boundary conditions on $\gamma\times(0,T)$ and solving the fracture problem in $\gamma\times(0,T)$ as was done for Method 1, we introduce new transmission conditions which combine the equation for continuity of the pressure across the fracture with the flow equations (5.4) in the fracture. These new transmission conditions contain a free parameter which is used to accelerate the convergence. This is an extension of the OSWR method with optimized Robin parameters studied in Chapter 2 in which Robin-to-Robin transmission conditions are considered. Here however, because of the fracture problem, we end up with what we will call Ventcell-to-Robin transmission conditions as presented below.

5.3.2.1 Ventcell-to-Robin transmission conditions

The new transmission conditions are derived by introducing Lagrange multipliers $p_{i,\gamma}$, $i=1,2$, representing the trace on the interface γ of the pressure p_i in each subdomain. As the pressure is continuous across the interface, one finds

$$p_{1,\gamma} = p_{2,\gamma} = p_\gamma, \quad \text{on } \gamma\times(0,T), \tag{5.18}$$

We then rewrite the Darcy equation in the fracture associated with each $p_{i,\gamma}$ as

$$\boldsymbol{u}_{\gamma,i} = -\boldsymbol{K}_\gamma\delta\nabla_\tau p_{i,\gamma}, \quad \text{on } \gamma\times(0,T),\ i=1,2.$$

We have used the notation $\boldsymbol{u}_{\gamma,i}$, $i=1,2$, instead of $\boldsymbol{u}_{i,\gamma}$ to insist on the fact that $\boldsymbol{u}_{\gamma,i}$ is NOT the tangential component of a trace of $\boldsymbol{u}_i$ on γ. In fact, $\boldsymbol{u}_{\gamma,i}$, $i=1,2$, represents the tangential velocity in the fracture:

$$\boldsymbol{u}_{\gamma,1} = \boldsymbol{u}_{\gamma,2} = \boldsymbol{u}_\gamma, \quad \text{on } \gamma\times(0,T),\ i=1,2.$$

With the notation introduced above, the flow equation(5.4) in the fracture can be rewritten, for $i = 1, 2$, and $j = (3 - i)$, as

$$\begin{aligned} -\boldsymbol{u}_i \cdot \boldsymbol{n}_i + s_\gamma \partial_t p_{i,\gamma} + \operatorname{div}_\tau \boldsymbol{u}_{\gamma,i} &= q_\gamma - \boldsymbol{u}_j \cdot \boldsymbol{n}_i, && \text{on } \gamma \times (0,T), \\ \boldsymbol{u}_{\gamma,i} &= -\boldsymbol{K}_\gamma \delta \nabla_\tau p_{i,\gamma}, && \text{on } \gamma \times (0,T), \\ p_{i,\gamma} &= 0 && \text{on } \partial\gamma \times (0,T), \\ p_{i,\gamma}(\cdot,0) &= p_{0,\gamma} && \text{in } \gamma. \end{aligned} \tag{5.19}$$

In the context of domain decomposition, (5.18) and (5.19) are the coupling conditions between the subdomains. Thus, as in the case without a fracture one may take a linear combination of these conditions to obtain equivalent Ventcell-to-Robin transmission conditions:

$$\begin{aligned} -\boldsymbol{u}_1 \cdot \boldsymbol{n}_1 + \alpha p_{1,\gamma} + s_\gamma \partial_t p_{1,\gamma} + \operatorname{div}_\tau \boldsymbol{u}_{\gamma,1} &= -\boldsymbol{u}_2 \cdot \boldsymbol{n}_1 + \alpha p_{2,\gamma} + q_\gamma \\ \boldsymbol{u}_{\gamma,1} &= -\boldsymbol{K}_\gamma \delta \nabla_\tau p_{1,\gamma} \end{aligned} \quad \text{on } \gamma \times (0,T), \tag{5.20}$$

$$\begin{aligned} -\boldsymbol{u}_2 \cdot \boldsymbol{n}_2 + \alpha p_{2,\gamma} + s_\gamma \partial_t p_{2,\gamma} + \operatorname{div}_\tau \boldsymbol{u}_{\gamma,2} &= -\boldsymbol{u}_1 \cdot \boldsymbol{n}_2 + \alpha p_{1,\gamma} + q_\gamma \\ \boldsymbol{u}_{\gamma,2} &= -\boldsymbol{K}_\gamma \delta \nabla_\tau p_{2,\gamma} \end{aligned} \quad \text{on } \gamma \times (0,T), \tag{5.21}$$

together with boundary and initial conditions

$$\begin{aligned} p_{1,\gamma} &= p_{2,\gamma} &&= 0 && \text{on } \partial\gamma \times (0,T), \\ p_{1,\gamma}(\cdot,0) &= p_{2,\gamma}(\cdot,0) &&= p_{0,\gamma} && \text{in } \gamma. \end{aligned} \tag{5.22}$$

Using these transmission conditions, the subdomain problem is obtained by imposing Ventcell boundary conditions on $\gamma \times (0,T)$, $i = 1, 2$, $j = 3 - i$:

$$\begin{aligned} s_i \partial_t p_i + \operatorname{div} \boldsymbol{u}_i &= q && \text{in } \Omega_i \times (0,T), \\ \boldsymbol{u}_i &= -\boldsymbol{K}_i \nabla p_i && \text{in } \Omega_i \times (0,T), \\ -\boldsymbol{u}_i \cdot \boldsymbol{n}_i + \alpha p_{i,\gamma} + s_\gamma \partial_t p_{i,\gamma} + \operatorname{div}_\tau \boldsymbol{u}_{\gamma,i} &= -\boldsymbol{u}_j \cdot \boldsymbol{n}_i + \alpha p_{j,\gamma} + q_\gamma && \text{on } \gamma \times (0,T), \\ \boldsymbol{u}_{\gamma,i} &= -\boldsymbol{K}_\gamma \delta \nabla_\tau p_{i,\gamma} && \text{in } \gamma \times (0,T), \\ p_i &= 0 && \text{on } \left(\partial\Omega_i \cap \partial\Omega\right) \times (0,T), \\ p_{i,\gamma} &= 0 && \text{on } \partial\gamma \times (0,T), \\ p_i(\cdot,0) &= p_0 && \text{in } \Omega_i, \\ p_{i,\gamma}(\cdot,0) &= p_{0,\gamma} && \text{in } \gamma, \end{aligned} \tag{5.23}$$

where the quatity on the right hand side of the third equation is supposed to be known. In the next subsection we prove that problem (5.27) is well-posed.

Remark 5.4. *The subdomain problem of Method 2 corresponding to Ventcell boundary conditions is somewhat more complicated than that of Method 1 (problem* (5.17)*). Consequently, for solving problem* (5.27)*, one needs to introduce Lagrange multipliers on the interface to handle the Ventcell conditions (representing the fracture problem).*

5.3.2.2 Well-posedness of the subdomain problem with Ventcell boundary conditions

For an open, bounded domain $\mathcal{O} \in \mathbb{R}^d$ $(d = 2, 3)$ with Lipschitz boundary $\partial\mathcal{O}$, consider the following time-dependent problem written in mixed form with Dirichlet and

Ventcell boundary conditions

$$\begin{aligned}
s_{\mathscr{O}}\partial_t p_{\mathscr{O}} + \operatorname{div} \boldsymbol{u}_{\mathscr{O}} &= q && \text{in } \mathscr{O}\times(0,T),\\
\boldsymbol{u}_{\mathscr{O}} &= -\boldsymbol{K}_{\mathscr{O}}\nabla p_{\mathscr{O}} && \text{in } \mathscr{O}\times(0,T),\\
-\boldsymbol{u}_{\mathscr{O}}\cdot\boldsymbol{n} + \alpha p_\gamma + s_\gamma\partial_t p_\gamma + \operatorname{div}_\tau \boldsymbol{u}_\gamma &= \theta + q_\gamma && \text{on } \partial\gamma\times(0,T),\\
\boldsymbol{u}_\gamma &= -\boldsymbol{K}_\gamma\delta\nabla_\tau p_\gamma && \text{in } \gamma\times(0,T),\\
p_{\mathscr{O}} &= 0 && \text{on } \left(\partial\mathscr{O}\setminus\gamma\right)\times(0,T),\\
p_\gamma &= 0 && \text{on } \partial\gamma\times(0,T),\\
p_{\mathscr{O}}(\cdot,0) &= p_0 && \text{in } \Omega_i,\\
p_\gamma(\cdot,0) &= p_{0,\gamma} && \text{in } \gamma,
\end{aligned} \tag{5.24}$$

where θ is a given function defined on $\gamma\times(0,T)$. In order to write the weak formulation of (5.24), we need to define the following Hilbert spaces (see Remark 2.1):

$$M = \left\{\mu = (\mu_{\mathscr{O}},\mu_\gamma)\in L^2(\mathscr{O})\times L^2(\gamma)\right\},$$
$$\Sigma = \left\{\boldsymbol{v} = (\boldsymbol{v}_{\mathscr{O}},\boldsymbol{v}_\gamma)\in \boldsymbol{L^2(\mathscr{O})}\times\boldsymbol{L^2(\gamma)} : \operatorname{div}\boldsymbol{v}_{\mathscr{O}}\in H(\operatorname{div},\mathscr{O}) \text{ and } \left(\operatorname{div}_\tau \boldsymbol{v}_\gamma - \boldsymbol{v}_{\mathscr{O}}\cdot\boldsymbol{n}_{|\gamma}\right)\in L^2(\gamma)\right\},$$

equipped with the norms

$$\|\mu\|_M^2 = \|\mu_{\mathscr{O}}\|_{\mathscr{O}}^2 + \|\mu_\gamma\|_\gamma^2,$$
$$\|\boldsymbol{v}\|_\Sigma^2 = \|\boldsymbol{v}_{\mathscr{O}}\|_{\mathscr{O}} + \|\operatorname{div}\boldsymbol{v}_{\mathscr{O}}\|_{\mathscr{O}}^2 + \|\boldsymbol{v}_\gamma\|_\gamma^2 + \|\operatorname{div}_\tau \boldsymbol{v}_\gamma - \boldsymbol{v}_{\mathscr{O}}\cdot\boldsymbol{n}_{|\gamma}\|_\gamma^2.$$

Then we define the bilinear forms

$$\begin{aligned}
a:\quad \Sigma\times\Sigma &\longrightarrow \mathbb{R}\\
(\boldsymbol{u},\boldsymbol{v}) &\mapsto a(\boldsymbol{u},\boldsymbol{v}) = \left(\boldsymbol{K}_{\mathscr{O}}^{-1}\boldsymbol{u}_{\mathscr{O}},\boldsymbol{v}_{\mathscr{O}}\right)_{\mathscr{O}} + \left((\boldsymbol{K}_\gamma\delta)^{-1}\boldsymbol{u}_\gamma,\boldsymbol{v}_\gamma\right)_\gamma,\\
b:\quad \Sigma\times M &\longrightarrow \mathbb{R}\\
(\boldsymbol{u},\mu) &\mapsto b(\boldsymbol{u},\mu) = \left(\operatorname{div}\boldsymbol{u}_{\mathscr{O}},\mu_{\mathscr{O}}\right)_{\mathscr{O}} + \left(\operatorname{div}_\tau \boldsymbol{u}_\gamma - \boldsymbol{u}_{\mathscr{O}}\cdot\boldsymbol{n}_{|\gamma},\mu_\gamma\right)_\gamma,\\
c:\quad M\times M &\longrightarrow \mathbb{R}\\
(\eta,\mu) &\mapsto c(\eta,\mu) = \left(\alpha\eta_\gamma,\mu_\gamma\right)_\gamma,\\
c_s:\quad M\times M &\longrightarrow \mathbb{R}\\
(\eta,\mu) &\mapsto c_s(\eta,\mu) = \left(s_{\mathscr{O}}\eta_{\mathscr{O}},\mu_{\mathscr{O}}\right)_{\mathscr{O}} + \left(s_\gamma\eta_\gamma,\mu_\gamma\right)_\gamma,
\end{aligned}$$

and the linear form

$$\begin{aligned}
L_q:\quad M &\longrightarrow \mathbb{R}\\
\mu &\mapsto L_q(\mu) = \left(q,\mu_{\mathscr{O}}\right)_{\mathscr{O}} + \left(\theta+q_\gamma,\mu_\gamma\right)_\gamma.
\end{aligned}$$

With these spaces and forms, the weak form of (5.24) can be written as follows:

For a.e. $t\in(0,T)$, find $p(t)\in M$ and $\boldsymbol{u}(t)\in\Sigma$ such that

$$\begin{aligned}
a(\boldsymbol{u},\boldsymbol{v}) - b(\boldsymbol{v},p) &= 0 && \forall \boldsymbol{v}\in\Sigma,\\
c_s(\partial_t p,\mu) + c(p,\mu) + b(\boldsymbol{u},\mu) &= L_q(\mu) && \forall \mu\in M,
\end{aligned} \tag{5.25}$$

together with the initial conditions

$$\begin{aligned}
p(\cdot,0) &= p_0 && \text{in } \mathscr{O},\\
p_\gamma(\cdot,0) &= p_{0,\gamma} && \text{in } \gamma.
\end{aligned} \tag{5.26}$$

Next, we define the space

$$H^{1,1}_{*,\gamma}(\mathscr{O}) := \left\{\mu = (\mu_{\mathscr{O}},\mu_\gamma)\in H^1(\Omega)\times H^1(\gamma) : \mu_{\mathscr{O}} = 0 \text{ on } \left(\partial\mathscr{O}\setminus\gamma\right) \text{ and } \mu_\gamma = 0 \text{ on } \partial\gamma\right\},$$

then the well-posedness of problem (5.26) is given by the following theorem:

Theorem 5.5. *Assume that there exist four positive constants s_- and s_+, K_- and K_+*

- $s_- \leq s_{\mathscr{O}}(x) \leq s_+$ *for a.e.* $x \in \mathscr{O}$,
- $s_- \leq s_\gamma(x) \leq s_+$ *for a.e.* $x \in \gamma$,
- $\varsigma^T \boldsymbol{K}_{\mathscr{O}}^{-1}(x)\varsigma \geq K_-|\varsigma|^2$, *and* $|\boldsymbol{K}_i(x)\varsigma| \leq K_+|\varsigma|$, *for a.e.* $x \in \mathscr{O}$, $\forall \varsigma \in \mathbb{R}^n$,
- $\eta^T \boldsymbol{K}_\gamma^{-1}(x)\delta\eta \geq K_-|\eta|^2$ *and* $|(\boldsymbol{K}_\gamma(x)\delta)^{-1}\eta| \leq K_+$ *for a.e.* $x \in \gamma$, $\forall \eta \in \mathbb{R}^{n-1}$.

If q is in $L^2(0,T;M)$, p_0 in $H^{1,1}_{*,\gamma}(\mathscr{O})$ and θ in $L^2(0,T;L^2(\gamma))$ then problem (5.25)-(5.26) *has a unique solution*

$$(p,\boldsymbol{u}) \in H^1(0,T;M) \times L^2(0,T;\Sigma).$$

Proof. The proof of Theorem 5.5 is a simple extension of that of Theorem 4.10. □

5.3.2.3 The interface problem and the convergence factor formula for computing the optimized parameter

As for Method 1, we derive in this subsection the interface problem associated with Ventcell-to-Robin transmission conditions (5.20)-(5.21)-(5.22). With this aim, we define the following Ventcell-to-Robin operator $\mathscr{S}_i^{\mathrm{VtR}}$, which depends on the parameter α, for $i = 1,2$, $j = (3-i)$:

$$\begin{gathered}\mathscr{S}_i^{\mathrm{VtR}} : L^2(0,T;L^2(\gamma)) \times L^2(0,T;L^2(\Omega_i)) \times H^1_*(\Omega_i) \times L^2(0,T;L^2(\gamma)) \times H^1_0(\gamma) \\ \to L^2(0,T;L^2(\gamma)) \\ \mathscr{S}_i^{\mathrm{VtR}}(\theta,q,p_0,q_\gamma,p_{0,\gamma}) = -\boldsymbol{u}_i \cdot \boldsymbol{n}_{j|\gamma} + \alpha p_{i,\gamma},\end{gathered}$$

where, $(p_i,\boldsymbol{u}_i,p_{i,\gamma},\boldsymbol{u}_{\gamma,i})$ is the solution of the subdomain problem with Ventcell boundary conditions

$$\begin{aligned}
s_i\partial_t p_i + \operatorname{div}\boldsymbol{u}_i &= q && \text{in } \Omega_i \times (0,T),\\
\boldsymbol{u}_i &= -\boldsymbol{K}_i\nabla p_i && \text{in } \Omega_i \times (0,T),\\
-\boldsymbol{u}_i\cdot\boldsymbol{n}_i + \alpha p_{i,\gamma} + s_\gamma\partial_t p_{i,\gamma} + \operatorname{div}_\tau \boldsymbol{u}_{\gamma,i} &= \theta + q_\gamma && \text{on } \gamma \times (0,T),\\
\boldsymbol{u}_{\gamma,i} &= -\boldsymbol{K}_\gamma\delta\nabla_\tau p_{i,\gamma} && \text{in } \gamma \times (0,T),\\
p_i &= 0 && \text{on } \left(\partial\Omega_i \cap \partial\Omega\right) \times (0,T),\\
p_{i,\gamma} &= 0 && \text{on } \partial\gamma \times (0,T),\\
p_i(\cdot,0) &= p_0 && \text{in } \Omega_i,\\
p_{i,\gamma}(\cdot,0) &= p_{0,\gamma} && \text{in } \gamma.
\end{aligned} \tag{5.27}$$

The interface problem with two Lagrange multipliers is then

$$\begin{aligned}
\theta_1 &= \mathscr{S}_2^{\mathrm{VtR}}(\theta_2,q_2,p_{0,2},q_\gamma,p_{0,\gamma}) + q_\gamma\\
\theta_2 &= \mathscr{S}_1^{\mathrm{VtR}}(\theta_1,q_1,p_{0,1},q_\gamma,p_{0,\gamma}) + q_\gamma
\end{aligned} \qquad \text{on } \gamma \times (0,T), \tag{5.28}$$

or equivalently

$$\begin{aligned}
\theta_1 - \mathscr{S}_2^{\mathrm{VtR}}(\theta_2,0,0,0,0) &= \mathscr{S}_2^{\mathrm{VtR}}(0,q_2,p_{0,2},q_\gamma,p_{0,\gamma}) + q_\gamma\\
\theta_2 - \mathscr{S}_1^{\mathrm{VtR}}(\theta_1,0,0,0,0) &= \mathscr{S}_1^{\mathrm{VtR}}(0,q_1,p_{0,1},q_\gamma,p_{0,\gamma}) + q_\gamma
\end{aligned} \qquad \text{on } \gamma \times (0,T), \tag{5.29}$$

The discrete counterpart of this problem can be solved iteratively using Jacobi iterations or GMRES. The former choice yields an algorithm equivalent to the OSWR

algorithm for the reduced fracture model (5.3) - (5.4) and is written as follows: starting with a given initial guess $g^0_{i,j}$ on $\gamma \times (0,T)$ for the first iteration,

$$-\boldsymbol{u}^0_i \cdot \boldsymbol{n}_i + \alpha\, p^0_{i,\gamma} + s_\gamma \partial_t p^0_{i,\gamma} + \mathrm{div}_\tau\, \boldsymbol{u}^0_{\gamma,i} - q_\gamma = g^0_{i,j},$$

then at the k^{th} iteration, $k = 1, \ldots$, solve in each subdomain the time-dependent problem, for $i = 1, 2$, $j = (3-i)$,

$$\begin{aligned}
s_i \partial_t p^k_i + \mathrm{div}\, \boldsymbol{u}^k_i &= q_i && \text{in } \Omega_i \times (0,T),\\
\boldsymbol{u}^k_i &= -\boldsymbol{K}_i \nabla p^k_i && \text{in } \Omega_i \times (0,T),\\
-\boldsymbol{u}^k_i \cdot \boldsymbol{n}_i + \alpha p^k_{i,\gamma} + s_\gamma \partial_t p^k_{i,\gamma} + \mathrm{div}_\tau\, \boldsymbol{u}^k_{\gamma,i} &= -\boldsymbol{u}^{k-1}_j \cdot \boldsymbol{n}_i + \alpha p^{k-1}_{j,\gamma} + q_\gamma && \text{on } \gamma \times (0,T),\\
\boldsymbol{u}^k_{\gamma,i} &= -\boldsymbol{K}_{f,\tau} \delta \nabla_\tau p^k_{i,\gamma} && \text{on } \gamma \times (0,T),\\
p^k_i &= 0 && \text{on } \left(\partial\Omega_i \cap \partial\Omega\right) \times (0,T),\\
p^k_{i,\gamma} &= 0 && \text{on } \partial\gamma \times (0,T),\\
p^k_i(\cdot,0) &= p_{0,i} && \text{in } \Omega_i,\\
p^k_{i,\gamma}(\cdot,0) &= p_{0,\gamma} && \text{in } \gamma.
\end{aligned} \tag{5.30}$$

The convergence of algorithm (5.30) depends on the choice of the parameter α. Thus we extend the analysis for the convergence factor of the OSWR algorithm derived in the case without fractures [12, 44] to this algorithm and from that, one can calculate the optimized parameter α. Details about such an analysis and the way to compute α are presented in Appendix A.3.

In our applications, the fracture is assumed to have much larger permeability than the surrounding, which implies that the time step inside the fracture should be very small compared with that of the surrounding matrix subdomains. As either method derived in Subsections 5.3.1 and 5.3.2 is global in time, i.e. the subdomain problem is solved over the whole time interval before the information is exchanged on the space-time interface, we can use different time steps in the fracture and in the rock matrix. In the next subsection, we consider the semi-discrete problem in time with nonconforming time grids.

5.3.3 Nonconforming discretizations in time

Let $\mathscr{T}_1, \mathscr{T}_2$ and $\mathscr{T}_\gamma$ be three different partitions of the time interval $(0,T)$ into subintervals $(t^i_m, t^i_{m-1}]$ for $m = 1, \ldots, M_i$ and $i = 1, 2, \gamma$ (see Figure 5.2). For simplicity, we consider the uniform partitions only, and denote by Δt_i, $i = 1, 2, \gamma$ the corresponding time steps. Assume that $\Delta t_\gamma \ll \Delta t_i$, $i = 1, 2$. We use the lowest order discontinuous Galerkin method [61, 17, 108], which is a modified backward Euler method. The same idea can be generalized to higher order methods. We denote by $P_0(\mathscr{T}_i, L^2(\gamma))$ the space of piecewise constant functions in time on grid $\mathscr{T}_i$ with values in $L^2(\gamma)$:

$$P_0(\mathscr{T}_i, L^2(\gamma)) = \left\{ \psi : (0,T) \to L^2(\gamma), \psi \quad \text{is constant on } J^i_m,\ \forall m = 1, \ldots, M_i \right\}.$$

In order to exchange data on the space-time interface between different time grids, we use L^2 projection $\Pi_{\gamma i}$ from $P_0(\mathscr{T}_i, L^2(\gamma))$ onto $P_0(\mathscr{T}_\gamma, L^2(\gamma))$ as defined in Chapter 2 (see (2.70)): for $\psi \in P_0(\mathscr{T}_i, W)$, $\Pi_{ji}\psi|_{J^j_m}$ is the average value of ψ on J^j_m, for $m = 1, \ldots, M_j$.

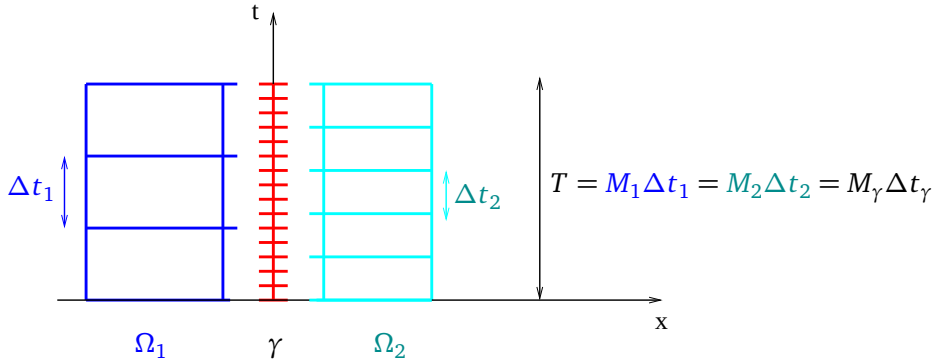

Figure 5.2: Nonconforming time grids in the rock matrix and in the fracture.

For Method 1

The unknown λ on the interface represents the fracture pressure, thus λ is piecewise constant in time on grid $\mathcal{T}_\gamma$. In order to obtain Dirichlet boundary data for solving subdomain problem (5.17), we project λ onto the $\mathcal{T}_i$, for $i = 1, 2$:

$$p_i = \Pi_{i\gamma}(\lambda), \quad \text{on } \gamma,\ i = 1, 2.$$

The semi-discrete counterpart of the interface problem (5.14) is obtained by weakly enforcing the fracture problem over each time sub-interval of $\mathcal{T}_\gamma$ as follows

$$\begin{aligned} s_\gamma\left(\lambda^{m+1} - \lambda^m\right) + \int_{t_\gamma^m}^{t_\gamma^{m+1}} \operatorname{div}_\tau \boldsymbol{u}_\gamma^{m+1} &= \int_{t_\gamma^m}^{t_\gamma^{m+1}} \left(q_\gamma + \sum_{i=1}^{2} \Pi_{\gamma i}\left(\mathscr{S}_i^{\mathrm{DtN}}(\Pi_{i\gamma}(\lambda), q_i, p_{0,i})\right)\right), \\ & && \text{in } \gamma, \\ \boldsymbol{u}_\gamma^{m+1} &= -\boldsymbol{K}_\gamma \delta \nabla_\tau \lambda^{m+1} && \text{in } \gamma, \\ \lambda^{m+1} &= 0 && \text{on } \partial\gamma, \\ \lambda^0 &= p_{0,\gamma} && \text{in } \gamma, \end{aligned} \tag{5.31}$$

for $m = 0, \ldots, M_\gamma - 1$.

For a piecewise constant function φ on the fine grid $\mathcal{T}_\gamma$, the semi-discrete Neumann-Neumann preconditioner (still denoted by $\boldsymbol{P}_{NN}^{-1}$) is defined by:

$$\boldsymbol{P}_{NN}^{-1}\varphi := \sum_{i=1}^{2} \sigma_i \Pi_{\gamma i}\left(\left(\mathscr{S}_i^{DtN}\right)^{-1}\left(\Pi_{1\gamma}(\varphi)\right)\right), \tag{5.32}$$

where we have solved the subdomain problem with Neumann-Neumann data projected from $\mathcal{T}_\gamma$ onto $\mathcal{T}_i$, $i = 1, 2$, then extract the pressure trace on the interface and project backward from $\mathcal{T}_i$ onto $\mathcal{T}_\gamma$. Thus the interface problem is defined on the fracture's time grid.

Remark 5.6. *From* (5.32) *we see that the Neumann-Neumann preconditioner defined by solving the subdomain problems on the coarse grid, thus we indeed enforce the transmission conditions on the coarse grid only. The projection from the coarse to the fine grid does not improve the accuracy in time of the solution in the fracture.*

For Method 2

In Method 2, there are two interface unknowns representing the linear combination of the fracture pressure and some terms from the fracture problem. Thus we let

$\theta_i \in P_0(\mathscr{T}_\gamma, L^2(\Gamma))$, for $i = 1,2$. In order to obtain Ventcell boundary data for solving subdomain problem (5.24), we project θ_i onto the $\mathscr{T}_i$, for $i = 1,2$:

$$-\boldsymbol{u}_i \cdot \boldsymbol{n}_i + \alpha p_i + s_\gamma \partial_t p_i + \mathrm{div}_\tau \, \boldsymbol{u}_\gamma = \Pi_{i\gamma}(\theta_i) + q_\gamma, \quad \text{on } \gamma,\ i = 1,2.$$

Remark 5.7. *This setting is different from the case of usual domain decomposition (without fractures) analyzed in Chapter 2 (see Subsection 2.4.2) where the two interface unknowns represent the Robin data in each subdomain and thus they are chosen to be constant on the associated subdomain's time grid, i.e. $\xi_i \in P_0(\mathscr{T}_i, L^2(\Gamma))$, for $i = 1,2$.*

The semi-discrete in time counterpart of (5.28) is weakly enforced over each time sub-interval of the fracture's time grid as follows:

$$\begin{aligned}
\int_{t_\gamma^m}^{t_\gamma^{m+1}} \theta_1 &= \int_{t_\gamma^m}^{t_\gamma^{m+1}} \Pi_{\gamma 2}\left(\mathscr{S}_2^{\mathrm{VtR}}(\Pi_{2\gamma}(\theta_2), q_2, p_{0,1}, q_\gamma, p_{0,\gamma})\right) + q_\gamma, \\
\int_{t_\gamma^m}^{t_\gamma^{m+1}} \theta_2 &= \int_{t_\gamma^m}^{t_\gamma^{m+1}} \Pi_{\gamma 1}\left(\mathscr{S}_1^{\mathrm{VtR}}(\Pi_{i\gamma}(\theta_1), q_1, p_{0,1}, q_\gamma, p_{0,\gamma})\right) + q_\gamma,
\end{aligned} \qquad \text{on } \gamma, \quad (5.33)$$

for $\forall m = 0, \ldots, M_\gamma - 1$.

Remark 5.8. *We point out that with Method 2 as with Method 1 preconditioned by a Neumann-Neumann preconditioner (cf. Remark 5.6), we can not hope to gain in accuracy in the fracture by using a finer grid there since the fracture problem is actually solved on the coarser time grids of the two subdomains. We will see this in the numerical experiments. Projection onto the fracture grid is only useful for the case when the time grids on Ω_1 and Ω_2 are different and there one could use a master grid and a slave grid.*

5.4 Numerical results

We carry out some preliminary experiments to investigate the numerical performance of the two methods proposed above. We consider the test case pictured in Figure 5.3 where the domain is a rectangle of dimension 2×1 and is divided into two equally sized subdomains by a fracture of width $\delta = 0.001$ parallel to the y axis. The permeability tensor in the subdomains and in the fracture is isotropic: $\boldsymbol{K} = \mathfrak{K}_i \boldsymbol{I}$, $i = 1,2,f$, and $\mathfrak{K}_i$ is assumed to be constant. Here we choose $\mathfrak{K}_1 = \mathfrak{K}_2 = 1$ and $\mathfrak{K}_f = 10^3$ (so that $\mathfrak{K}_f \delta = 1$). A pressure drop of 1 from the bottom to the top of the fracture is imposed: $p = 1$ on bottom and $p = 0$ on top. On the external boundaries of the subdomains a no flow (homogeneous Neumann) boundary condition is imposed except on the lower fifth (length 0.2) of both lateral boundaries where a Dirichlet condition is imposed: $p = 1$ on the right and $p = 0$ on the left. See Figure 5.3.

As in the previous chapter, we consider a uniform rectangular mesh with size $h = 1/100$ and use the lowest order Raviart-Thomas mixed finite element spaces (see Appendix B.5). In time, we fix $T = 0.5$ and use uniform time partitions in the subdomains with time step $\Delta t_i, i = 1,2$, and in the fracture with varying time step Δt_γ. We first consider the case with the same time step throughout the domain, $\Delta t_1 = \Delta t_2 = \Delta t_\gamma = \Delta t = T/300$.

In Figure 5.4 the snapshots of the pressure field and flow field (on a coarse grid for visualization) at different times are shown. The length of the arrows is proportional to

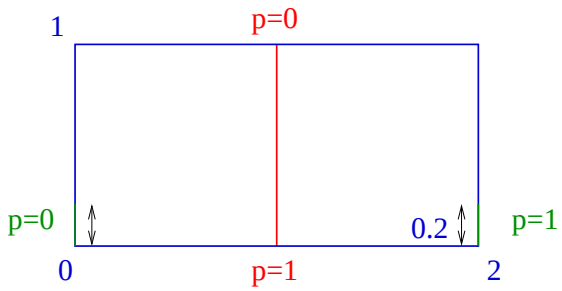

Figure 5.3: Geometry of the test case where the fracture is considered as an interface.

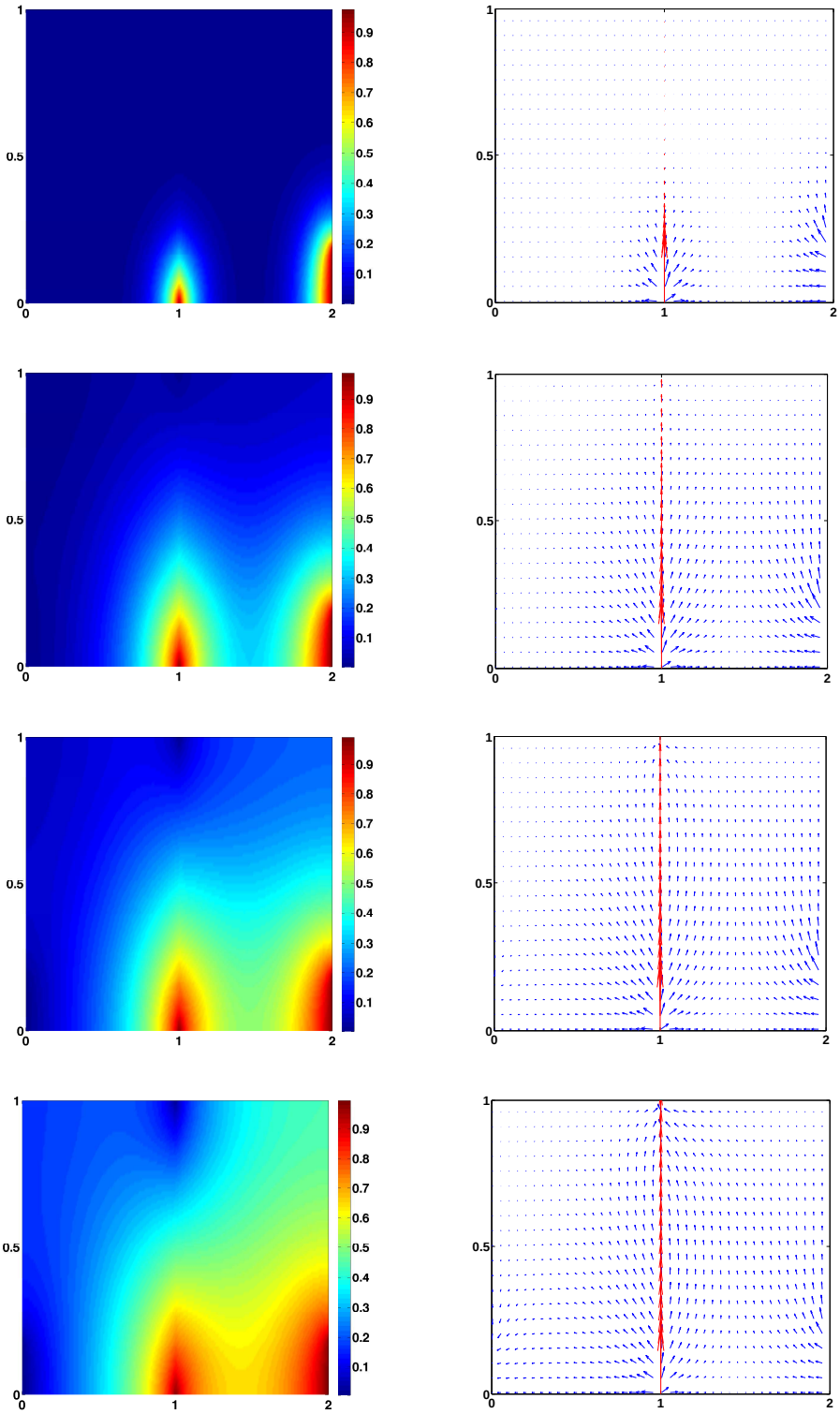

Figure 5.4: Snapshots of the pressure field (left) and flow field (right) at $t = T/300$, $t = T/4$, $t = T/2$ and $t = T$ respectively (from top to bottom).

the magnitude of the velocity and the red arrows represent the flow in the fracture. We see that the flow field is a combination of flow in the fracture and flow going from right to left in the rest of the porous medium and there is actually interaction between them as some fluid is coming out of the fracture and then re-enters it. Since $\mathfrak{K}_f \gg \mathfrak{K}_i, i = 1, 2$, the velocity is much larger in the fracture than in the surrounding medium.

Next, in order to analyze the convergence behavior of Method 1 and Method 2, we consider the problem with homogeneous Dirichlet boundary conditions (i.e., the solution converges to zero). We start with a random initial guess on the space-time interface-fracture and use GMRES as an iterative solver and compute the error in the $L^2(0,T;L^2(\Omega))$-norm for the pressure p and for the velocity $\boldsymbol{u}$. We stop the iteration when the respective error is less than 10^{-6}. We consider four algorithms: Method 1 with no preconditioner, Method 1 with the local preconditioner, Method 1 with the Neumann-Neumann preconditioner and Method 2 with the optimized Robin parameter. As the cost of a subdomain solve for each method is different (see Remark 5.4), in the following we first compare the convergence behavior of these four algorithms in terms of the number of iterations only (though a more appropriate way of comparison should be considered, in particular, using CPU time).

In Figure 5.5, the error curves versus the number of iterations are shown: the error in p (on the left) and in $\boldsymbol{u}$ (on the right). We see that Method 1 with no preconditioner (the blue curves) converges extremely slowly (after 500 iterations, the error, both in p and in $\boldsymbol{u}$, is about 10^{-1}). The performance of Method 1 with the local preconditioner (the green curves) is much improved but still very slow- it requires about 350 iterations to reach an error reduction of 10^{-6}. The Neumann-Neumann preconditioner (the cyan curves) further improves the convergence and one needs about 150 iterations to obtain a similar error reduction. Now Method 2 needs only 6 iterations to reduce the error to 10^{-6} and thus the convergence of Method 2 is much faster than the other algorithms (at least by a factor of 25). This comes from the use of the optimized parameter α. In Figure 5.6, we show the error in $\boldsymbol{u}$ (in logarithmic scale) after 10 Jacobi iterations for various values of α. We see that the optimized Robin parameter (the red star) is located close to those giving the smallest error after the same number of iterations. Also we observe that the convergence can be significantly slower if α is not chosen well.

Next, we study we study the behavior of three of the algorithms when nonconforming time grids are used. For this we use nonhomogeneous boundary conditions as depicted in Figure 5.3. In all cases, we consider equal time steps for the subdomains as they have the same permeability: $\Delta t_1 = \Delta t_2 = \Delta t_m$. We look at three time grids as follows:

- Time grid 1 (conforming coarse): $\Delta t_m = \Delta t_f = T/100$.
- Time grid 2 (nonconforming): $\Delta t_m = T/100$ and $\Delta t_f = T/500$.
- Time grid 3 (conforming fine): $\Delta t_m = \Delta t_f = T/500$.

We start with a zero initial guess on the space-time interface and stop GMRES iterations when the relative residual is less than 10^{-6}. In Figure 5.7 we show the relative residual versus the number of iterations for three schemes: Method 1 with the local preconditioner, Method 1 with the Neumann-Neumann preconditioner and Method 2 with an optimized Robin parameter. We see that Method 2 still performs better

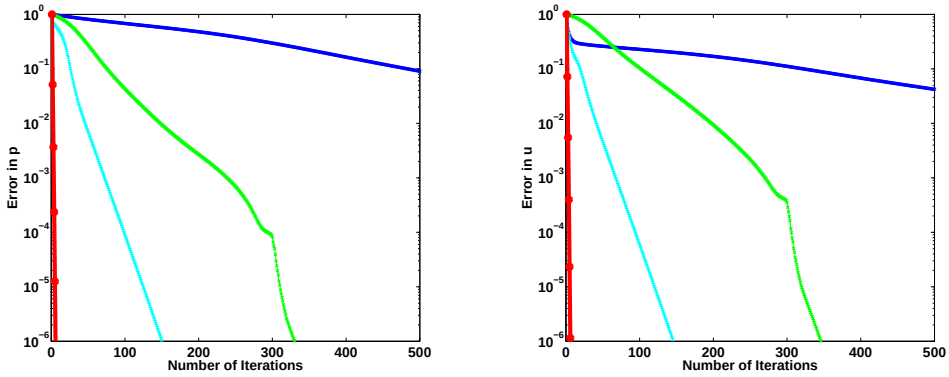

Figure 5.5: Convergence curves for the compressible flow: errors in p (on the left) and in $\boldsymbol{u}$ (on the right) - Method 1 with no preconditioner (blue), Method 1 with local preconditioner (green), Method 1 with Neumann-Neumann preconditioner (cyan) and Method 2 (red).

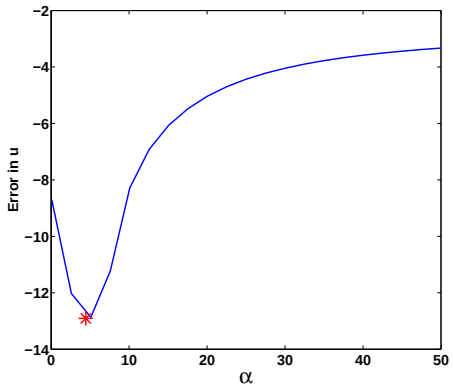

Figure 5.6: L^2 velocity error (in logarithmic scale) after 10 Jacobi iterations for various values of the Robin parameter. The red star shows the optimized parameters computed by numerically minimizing the continuous convergence factor.

than Method 1, and Method 1 with the Neumann-Neumann preconditioner still converges faster than with the local preconditioner. Importantly, both Method 1 with the Neumann-Neumann preconditioner and Method 2 are almost independent of the time grid (the number of iterations does not change with the time grid) while the local preconditioner significantly depends on the time grid. We also notice that the behavior of the three methods in the cases of nonconforming and conforming fine grids are very similar.

Now we analyze the error in time of the three algorithms for each of the three time grids. A reference solution (in time) is obtained by solving problem (5.3) - (5.4) directly on a very fine time grid $\Delta t = T/2000$. The $L^2 - L^2$ error of the difference between the multi-domain and the reference solutions at each iteration are computed. We distinguish two different errors: error in the rock matrix $L^2(0,T;L^2(\Omega_i)), i = 1,2$, and error in the fracture $L^2(0,T;L^2(\gamma))$. Figures 5.8 and 5.9 show the pressure error in the subdomains and in the fracture respectively. We first observe that the error in the subdomains after convergence (Figure 5.8) in the nonconforming case (Time grid

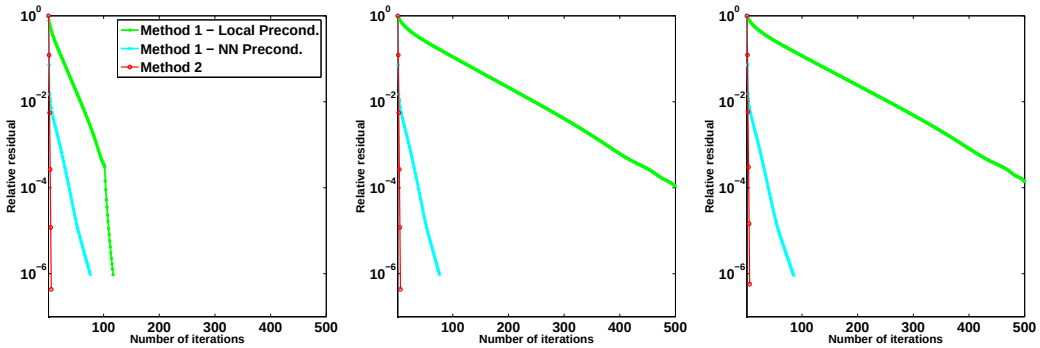

Time grid 1 Time grid 2 Time grid 3

Figure 5.7: Relative residual with GMRES for different time grids: Method 1 with the local preconditioner (green), Method 1 with the Neumann-Neumann preconditioner (cyan) and Method 2 (red).

2) is equal to that in the conforming coarse case (Time grid 1) for all three algorithms. This is as expected as we use the same time step $\Delta t_m = T/100$ in the matrix for both of these grids. However, as already pointed out in Remark 5.8, if one might hope that the error in the fracture (Figure 5.9) in the nonconforming case is close to that in the conforming fine grid case (Time grid 3), this can only be the case for Method 1 with the local preconditioner. Only for this case do we actually solve the fracture problem on the fine grid. For the other algorithms,the fracture error of the nonconforming case is equal to that of the conforming coarse grid instead. None of the methods deteriorates the accuracy because of nonconforming time grids.

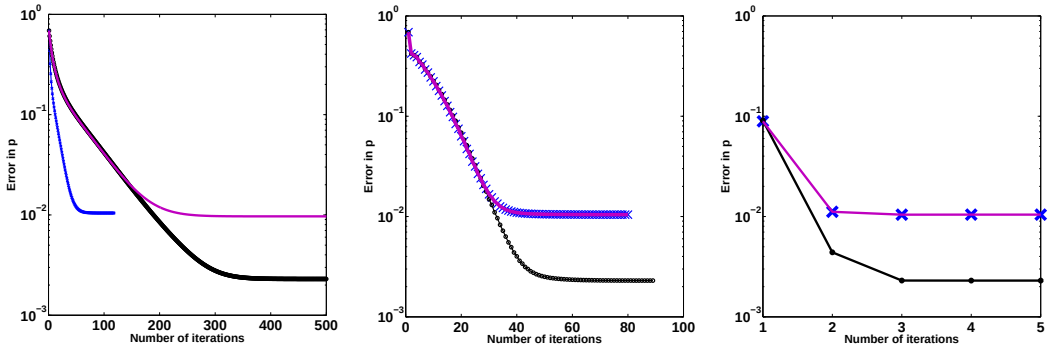

Method 1 - local precond. Method 1 - NN precond. Method 2

Figure 5.8: L^2 pressure error in the rock matrix: Time grid 1 (blue), Time grid 2 (magenta), Time grid 3 (black).

Remark 5.9. *While Method 2 does not make it particularly useful to use a finer time grid in the fracture, it does give a rather remarkable convergence speed. For the advection-diffusion problem of the next subsection with an explicit time scheme for advection, one of if not the main advantage of using smaller time steps in the fracture is to avoid imposing a time step in the two subdomains dictated by the CFL number of the equation in the fracture. Thus we are hopeful that this algorithm will be useful when coupled with the*

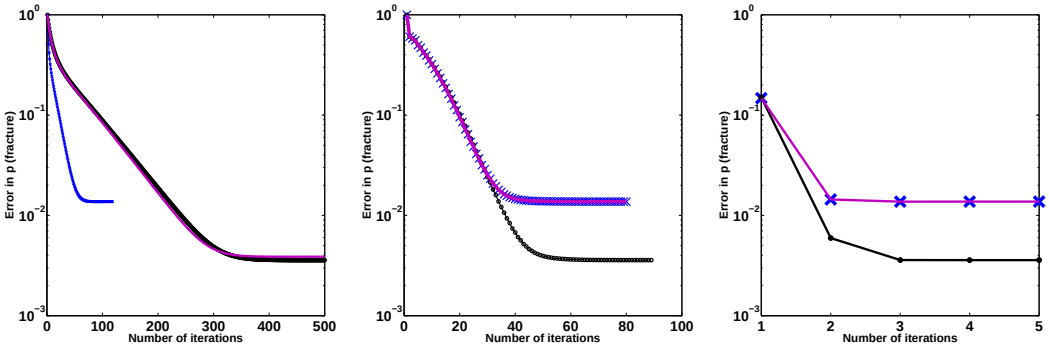

Method 1 - local precond. Method 1 - NN precond. Method 2

Figure 5.9: L^2 pressure error in the fracture: Time grid 1 (blue), Time grid 2 (magenta), Time grid 3 (black).

advection equation simply for the convergence speed that it gives. We add however that we are still pursuing some ideas for modifying this scheme to obtain an algorithm that can take advantage of smaller time steps in the fracture for the diffusion equation.

5.5 Extension to transport problems

We first introduce the model problem and its discretizations using operator splitting. Then we derive extensions of the two methods studied in the previous sections to the advection-diffusion couplings and discuss the use of nonconforming time discretizations in this case.

5.5.1 A model problem and operator splitting

Consider now the linear advection-diffusion problem

$$\begin{aligned} \phi\,\partial_t c + \operatorname{div}(\boldsymbol{u}c + \boldsymbol{r}) &= q_c && \text{in } \Omega \times (0,T), \\ \boldsymbol{r} &= -\boldsymbol{D}\nabla c && \text{in } \Omega \times (0,T), \\ c &= 0 && \text{on } \partial\Omega \times (0,T), \\ c(\cdot,0) &= c_0 && \text{in } \Omega. \end{aligned} \tag{5.34}$$

Here c is the concentration of a contaminant dissolved in a fluid, q_c the source term, ϕ the porosity, $\boldsymbol{u}$ the Darcy velocity (given and time-independent) and $\boldsymbol{D}$ a symmetric time independent diffusion tensor.

Following the same idea as in the previous section, we obtain two models for a fractured porous medium:

- An $n-$dimensional fracture model consists of the following equations

$$\begin{aligned}
\phi_i \partial_t c_i + \operatorname{div}(\boldsymbol{u}_i c_i + \boldsymbol{r}_i) &= q_{c,i} && \text{in } \Omega_i \times (0,T), && i = 1,2,f,\\
\boldsymbol{r}_i &= -\boldsymbol{D}_i \nabla c_i && \text{in } \Omega_i \times (0,T), && i = 1,2,f,\\
c_i &= 0 && \text{on } \left(\partial\Omega_i \cap \partial\Omega\right) \times (0,T), && i = 1,2,f,\\
c_i &= c_f && \text{on } \gamma_i \times (0,T), && i = 1,2,\\
-\boldsymbol{r}_i \cdot \boldsymbol{n}_i - \boldsymbol{u}_i \cdot \boldsymbol{n}_i c_i &= -\boldsymbol{r}_f \cdot \boldsymbol{n}_i - \boldsymbol{u}_f \cdot \boldsymbol{n}_i c_f && \text{on } \gamma_i \times (0,T), && i = 1,2,\\
c_i(\cdot,0) &= c_{0,i} && \text{in } \Omega_i, && i = 1,2,f.
\end{aligned} \tag{5.35}$$

- A co-dimension 1 fracture model consists of the equations in the subdomains

$$\begin{aligned}
\phi_i \partial_t c_i + \operatorname{div}(\boldsymbol{u}_i c_i + \boldsymbol{r}_i) &= q_{c,i} && \text{in } \Omega_i \times (0,T),\\
\boldsymbol{r}_i &= -\boldsymbol{D}_i \nabla c_i && \text{in } \Omega_i \times (0,T),\\
c_i &= 0 && \text{on } \left(\partial\Omega_i \cap \partial\Omega\right) \times (0,T), && \text{for } i = 1,2,\\
c_i &= c_\gamma && \text{on } \gamma \times (0,T),\\
c_i(\cdot,0) &= c_{0,i} && \text{in } \Omega_i,
\end{aligned} \tag{5.36}$$

coupled with the following equation in the $(n-1)-$dimensional fracture

$$\begin{aligned}
\phi_\gamma \partial_t c_\gamma + \operatorname{div}_\tau(\boldsymbol{u}_\gamma c_\gamma + \boldsymbol{r}_\gamma) &= q_{c,\gamma} + \sum_{i=1}^{2} (\boldsymbol{r}_i \cdot \boldsymbol{n}_i + \boldsymbol{u}_i \cdot \boldsymbol{n}_i c_i)_{|\gamma} && \text{in } \gamma \times (0,T),\\
\boldsymbol{r}_\gamma &= -\boldsymbol{D}_\gamma \delta \nabla_\tau c_\gamma && \text{in } \gamma \times (0,T),\\
c_\gamma &= 0 && \text{on } \partial\gamma \times (0,T),\\
c_\gamma(\cdot,0) &= c_{0,\gamma} && \text{in } \gamma.
\end{aligned} \tag{5.37}$$

As in Chapter 3, we use operator splitting to separate the advection and the diffusion terms and treat them with different numerical schemes. Recall that for the time discretization, the advection is approximated with the explicit Euler method (where the sub-time steps are used) and the diffusion with the implicit Euler method. For the spatial discretization, both are approximated with locally mass conservative schemes: the advection with an upwind, cell-center finite volume scheme and the diffusion with a mixed finite element method. In order to write the fully discrete problem corresponding to (5.36), we consider again a uniform partition of $(0,T)$ into N subintervals (t^n, t^{n+1}) of length $\Delta t = t^{n+1} - t^n$, for $n = 0, \ldots, N-1$, and sub-time steps for the advection equation

$$\Delta t_a = \Delta t / L, \text{ for } L \geq 1,$$

and

$$t^{n,l} = l\Delta t_a + t^n, \text{ for } l = 0, \ldots, L, \ n = 0, \ldots, N-1.$$

In space, let $\mathscr{K}_{h,i}$ be a finite element partition of Ω_i, $i = 1,2$, such that $\mathscr{K}_{h,1} \cap \mathscr{K}_{h,2}$ forms a finite element partition of Ω, i.e. such that the two partitions match up at the interface γ. Denote by $\mathscr{G}_h$ the set of edges/faces of elements of $\mathscr{K}_{h,i}$ lying on the interface γ. To perform the upwind scheme for the advection equation, since only the inflow boundary (not the whole boundary) is important, as in Chapter 3 we define

$$\mathscr{G}_{h,i}^{\text{in}} := \left\{ E \in \mathscr{G}_h : \int_E \boldsymbol{u}_i \cdot \boldsymbol{n}_i < 0 \right\}, \text{ for } i = 1,2.$$

For an element $K \in \mathscr{K}_{h,i}$ (respectively an edge E of K), we denote by $\boldsymbol{n}_K$ (respectively $\boldsymbol{n}_E$) the unit, outward normal vector on ∂K (respectively ∂E).

Remark 5.10. *For simplicity, we have used matching grids. This is not necessary, see [41].*

Let

$$M_{h,i} \times \Sigma_{h,i} \subset L^2(\Omega_i) \times H(\mathrm{div}, \Omega_i)$$

be the usual mixed finite element approximation made of Raviart-Thomas (and Nédélec in three dimensions) spaces of lowest order (see, e.g., [22, 104] and Appendix B), and let

$$\Lambda_h \times \Sigma_{h,\gamma} \subset L^2(\gamma) \times H(\mathrm{div}_\tau, \gamma)$$

be the lowest order Raviart-Thomas mixed finite element space defined on the $(d-1)-$dimensional interface γ. Then we define

$$M_h = \bigoplus_{i=1,2} M_{h,i} \oplus \Lambda_h, \quad \Sigma_h = \bigoplus \Sigma_{h,i} \oplus \Sigma_{h,\gamma}.$$

With operator splitting, we use the advection equations in the subdomains and in the fracture to calculate $c_{h,i}^{n,l}$, $i = 1,2$, and $c_{h,\gamma}^{n,l}$, approximations of $c_i(t^{n,l})$ and $c_\gamma(t^{n,l})$ respectively, for $n = 0,\ldots,N-1$, $l = 1,\ldots,L$, and then use the diffusion equations in the subdomain and in the fracture to calculate $\left(c_{h,i}^{n+1}, \boldsymbol{r}_{h,i}^{n+1}\right)$, $i = 1,2$, and $\left(c_{h,\gamma}^{n+1}, \boldsymbol{r}_{h,\gamma}^{n+1}\right)$, approximations of $\left(c_i(t^{n+1}), \boldsymbol{r}_i(t^{n+1})\right)$ and $\left(c_\gamma(t^{n+1}), \boldsymbol{r}_\gamma(t^{n+1})\right)$ respectively, for $n = 0,\ldots,N-1$.

As in all of the advection-diffusion problems we have considered, we use an upwind scheme for the advection equation. Thus, we need to compute the upwind value $\hat{c}_{h,i}^{n,l}$ on each edge of the grid $\mathscr{K}_{h,i}$. Due to the presence of the fracture, which serves as an interface, we make use of the same upwind operator $\mathscr{U}_{h,i}$, $i = 1,2$, defined in (3.10) (see Chapter 3) in the context of domain decomposition. Recall that $\mathscr{U}_{h,i} : M_{h,i} \times \Lambda_h \to N_{h,i}$ where $N_{h,i}$ is the space of functions on the union of the edges of elements of $\mathscr{K}_{h,i}$ that are constant on each edge. We have

$$\hat{c}_{h,i}^{n,l} = \mathscr{U}_{h,i}\left(c_{h,i}^{n,l}, c_{h,\gamma}^{n,l}\right), \text{ for } n = 0,\ldots,N-1,\ l = 0,\ldots,L-1,$$

so that if an edge E lies on γ, i.e. $E \in \mathscr{G}_h$, and if the average value of $\boldsymbol{u}\cdot\boldsymbol{n}_i$ on E is negative (fluid entering Ω_i through E) then

$$\mathscr{U}_{h,i}\left(c_{h,i}^{n,l}, c_{h,\gamma}^{n,l}\right)_{|E} = \left(c_{h,\gamma}^{n,l}\right)_{|E},$$

otherwise $\mathscr{U}_{h,i}$ is defined as before (cf. (3.10)).

Because of the dynamic problem in the fracture, in addition to the upwind values $\hat{c}_{h,i}^{n,l}$ on the edges of the grid, we need to calculate also the upwind value $\hat{c}_{h,\gamma}$ on each end point P of the edges on the fracture:

$$\left(\hat{c}_{h,\gamma}^{n,l}\right)_{|P} = \begin{cases} \bullet \text{ the given Dirichlet boundary data (here 0) if } P \in \partial\gamma \text{ and the fluid enters } \gamma \text{ through } P, \\ \bullet \text{ the value of } c_{h,\gamma}^{n,l} \text{ on } E \text{ if } P \text{ is an end point of } E \text{ and the value of } \boldsymbol{u}\cdot\boldsymbol{n}_E \\ \quad \text{at } P \text{ is nonnegative (i.e. fluid exiting } E \text{ through } P). \end{cases} \tag{5.38}$$

The operator splitting algorithm for problem (5.36)-(5.37) is initialized by defining $c_{h,i}^0$, $i=1,2$, and $c_{h,\gamma}^0$ to be the L^2 projections of $c_{h,i}^0$ onto $M_{h,i}$ and of $c_{h,\gamma}^0$ onto Λ_h respectively:

$$\left(c_{h,i}^0\right)_{|K} := \frac{1}{\text{meas}(K)}\int_K c_{0,i},\ \forall K\in\mathscr{K}_{h,i},\ i=1,2,\ \text{ and }\ \left(c_{h,\gamma}^0\right)_{|E} := \frac{1}{\text{meas}(E)}\int_E c_{0,\gamma},\ \forall E\in\mathscr{G}_h.$$

As before, we also write $c_{h,i}^{0,0}$ for $c_{h,i}^0$ and $c_{h,\gamma}^{0,0}$ for $c_{h,\gamma}^0$.

The algorithm is written as: for $n=0,\dots,N$,

1. define $c_{h,i}^{n,0}=c_{h,i}^n$, $i=1,2$, and $c_{h,\gamma}^{n,0}=c_{h,\gamma}^0$,
2. for $l=0,\dots,L-1$,
   - define the upwind values $\hat{c}_{h,i}^{n,l}$, $i=1,2$, and $\hat{c}_{h,\gamma}^{n,l}$,
   - solve the advection equations in the subdomains and in the fracture

$$\begin{aligned}
\int_K \phi_i\frac{c_{h,i}^{n,l+1}-c_{h,i}^{n,l}}{\Delta t_a} + \sum_{E\subset\partial K}\int_E \hat{c}_{h,i}^{n,l}(\boldsymbol{u}_i\cdot\boldsymbol{n}_K) &= 0,\ \forall K\in\mathscr{K}_{h,i},\ i=1,2,\\
\int_E \phi_\gamma\frac{c_{h,\gamma}^{n,l+1}-c_{h,\gamma}^{n,l}}{\Delta t_a} + \int_{\partial E}\hat{c}_{h,\gamma}^{n,l}(\boldsymbol{u}_\gamma\cdot\boldsymbol{n}_E) &= \int_E\sum_{i=1}^2 \boldsymbol{u}_i\cdot\boldsymbol{n}_i\hat{c}_{h,i}^{n,l},\quad \forall E\in\mathscr{G}_h,
\end{aligned} \tag{5.39}$$

   with $c_{h,i}^{n,l}$, $i=1,2$, known and $c_{h,\gamma}^{n,l}$ and obtain $c_{h,i}^{n,l+1}$, $i=1,2$, and $c_{h,\gamma}^{n,l+1}$.
3. solve the diffusion equations in the subdomains and in the fracture

$$\begin{aligned}
\int_K \phi_i\frac{c_{h,i}^{n+1}-c_{h,i}^{n,L}}{\Delta t} + \int_K \text{div}\,\boldsymbol{r}_{h,i}^{n+1} &= \int_K q_{c,i}(t^{n+1}),\ \forall K\in\mathscr{K}_{h,i},\\
\int_{\Omega_i}\boldsymbol{D}_i^{-1}\boldsymbol{r}_{h,i}^{n+1}\cdot\boldsymbol{\nu} - \int_{\Omega_i} c_{h,i}^{n+1}\text{div}\,\boldsymbol{\nu} + \int_\gamma c_{h,\gamma}^{n+1}(\boldsymbol{\nu}\cdot\boldsymbol{n}_i) &= 0, \qquad \forall\boldsymbol{\nu}\in\Sigma_{h,i},\\
\int_E \phi_\gamma\frac{c_{h,\gamma}^{n+1}-c_{h,\gamma}^{n,L}}{\Delta t} + \int_E \text{div}\,\boldsymbol{r}_{h,\gamma}^{n+1} - \int_E\sum_{i=1}^2 \boldsymbol{r}_{h,i}^{n+1}\cdot\boldsymbol{n}_i &= \int_E q_{c,\gamma}(t^{n+1}),\ \forall E\in\mathscr{G}_h,\\
\int_\gamma(\boldsymbol{D}_\gamma\delta)^{-1}\boldsymbol{r}_{h,\gamma}^{n+1}\cdot\boldsymbol{\nu}_\gamma - \int_\gamma c_{h,\gamma}^{n+1}\text{div}\,\boldsymbol{\nu}_\gamma &= 0, \qquad \forall\boldsymbol{\nu}_\gamma\in\Sigma_{h,\gamma},
\end{aligned} \tag{5.40}$$

   with $c_{h,i}^{n,L}$, $i=1,2$, known and $c_{h,\gamma}^{n,L}$ and obtain $\left(c_{h,i}^{n+1},\boldsymbol{r}_{h,i}^{n+1}\right)$, $i=1,2$, and $\left(c_{h,\gamma}^{n+1},\boldsymbol{r}_{h,\gamma}^{n+1}\right)$.

In the next subsection, we extend the two domain decomposition methods introduced in the previous section to problem (5.39)-(5.40). Since the advection and diffusion equations are split, the interface problem consists of the transmission conditions due to advection and due to diffusion. The latter can be rewritten equivalently as Ventcell transmission conditions as derived in Subsection 5.3.2.

Remark 5.11. *Solving problem* (5.35) *using domain decomposition and operator splitting is a straightforward application of the methods derived in Chapter 3.*

5.5.2 Domain decomposition formulations

Here we derive discrete, interface problems for the advection-diffusion problem (5.36)-(5.37) corresponding to extensions of the discrete counterpart of the interface problems (5.15) and (5.29) derived for the pure diffusion problem (5.3)-(5.4) in the previous section. These extensions are carried out in the context of operator splitting as before. However, unlike in Chapter 3 (cf. Remark 3.3), in this case because of the fracture problem, the formulations for the two methods are different from one another, not only for the diffusion part but also for the advection part.

5.5.2.1 Method 1: an extension of the time-dependent Steklov-Poincaré operator

To define the interface problem for Method 1, we introduce solution operators $\mathscr{D}_i$, $i = 1,2$, where $\mathscr{D}_i$ associates to initial data c_0 on Ω_i, an source term q_c on $\Omega_i \times (0,T)$ and discrete boundary data λ_f given on the discrete counter part of $\gamma \times (0,T)$ the solution of the discrete advection-diffusion subdomain problem on $\Omega_i \times (0,T)$ that will be defined below (problem). In our notation, $\lambda_f \in \Lambda_h^{N\times(L+1)}$; that is $\lambda_h = \left(\lambda_h^{n,l}\right)_{n=0,\ldots,N-1,\ l=0,\ldots,L}$ and for each n, $n = 1,\ldots,N$, we identify λ_h^n with $\lambda_h^{n,0}$

$$\lambda_h^n = \lambda_h^{n,0}.$$

Then for given $\left(\lambda_f, c_0, q_c\right)$, the subdomain problem is defined by:

For $n = 0,\ldots,N-1$,

1. define $c_{h,i}^{n,0} = c_{h,i}^n$, where $\left(c_{h,i}^0\right)_{|K} := \dfrac{1}{\text{meas}(K)} \displaystyle\int_K c_{0,i},\ \forall K \in \mathscr{K}_{h,i}$,

2. for $l = 0,\ldots,L-1$,

   - define the upwind values

   $$\hat{c}_{h,i}^{n,l} = \mathscr{U}_{h,i}\left(c_{h,i}^{n,l}, \lambda_h^{n,l}\right),$$

   - solve the advection equation

   $$\int_K \phi_i \frac{c_{h,i}^{n,l+1} - c_{h,i}^{n,l}}{\Delta t_a} + \sum_{E\subset\partial K} \int_E \hat{c}_{h,i}^{n,l}(\boldsymbol{u}_i \cdot \boldsymbol{n}_K) \quad = 0, \quad \forall K \in \mathscr{K}_{h,i}, \tag{5.41}$$

   with $c_{h,i}^{n,l}$ known and obtain $c_{h,i}^{n,l+1}$.

3. solve the diffusion equations in the subdomain

$$\begin{aligned} \int_K \phi_i \frac{c_{h,i}^{n+1} - c_{h,i}^{n,L}}{\Delta t} + \int_K \operatorname{div} \boldsymbol{r}_{h,i}^{n+1} &= \int_K q_{c,i}(t^{n+1}),\ \forall K \in \mathscr{K}_{h,i}, \\ \int_{\Omega_i} \boldsymbol{D}_i^{-1} \boldsymbol{r}_{h,i}^{n+1} \cdot \boldsymbol{v} - \int_{\Omega_i} c_{h,i}^{n+1} \operatorname{div} \boldsymbol{v} &= -\int_\gamma \lambda_h^{n+1}(\boldsymbol{v}\cdot\boldsymbol{n}_i), \quad \forall \boldsymbol{v} \in \Sigma_{h,i}, \end{aligned} \tag{5.42}$$

   with $c_{h,i}^{n,L}$ known and obtain $\left(c_{h,i}^{n+1}, \boldsymbol{r}_{h,i}^{n+1}\right)$.

The operator $\mathscr{D}_i$, $i = 1,2$, is now defined by

$$\begin{aligned}\mathscr{D}_i : \Lambda_h^{N\times(L+1)} \times L^2(0,T;L^2(\Omega_i)) \times H^1_*(\Omega_i) &\to \left(N_{h,i}\right)^{N\times L} \times \left(M_{h,i}\right)^N \times \left(\Sigma_{h,i}\right)^N \\ \left(\lambda_f, q_c, c_0\right) &\mapsto \left(\hat{c}_{h,i}^{\Delta t,\Delta t_a}, c_{h,i}^{\Delta t}, \boldsymbol{r}_{h,i}^{\Delta t}\right),\end{aligned}$$

where $\hat{c}_{h,i}^{\Delta t,\Delta t_a} = \left(\hat{c}_{h,i}^{n,l}\right)_{n=0,\dots,N-1,\, l=0,\dots,L-1}$ and $\left(c_{h,i}^{\Delta t}, \boldsymbol{r}_{h,i}^{\Delta t}\right) = \left(c_{h,i}^{n}, \boldsymbol{r}_{h,i}^{n}\right)_{n=1,\dots,N}$.

For the problem on the fracture interface, the input needed from the subdomain problem consists of the first and the third components of the output of $\mathscr{D}_i$ restricted to the edges on the fracture, i.e. $E \in \mathscr{G}_h$. So we define the two projection operator $\mathscr{H}_i$ and $\mathscr{F}_i$ as follows:

$$\begin{aligned}\mathscr{H}_i : \left(N_{h,i}\right)^{N\times L} \times \left(M_{h,i}\right)^N \times \left(\Sigma_{h,i}\right)^N &\to \left(\Lambda_h\right)^{N\times L} \\ \left(\hat{c}_{h,i}^{\Delta t,\Delta t_a}, c_{h,i}^{\Delta t}, \boldsymbol{r}_{h,i}^{\Delta t}\right) &\mapsto \left(\hat{c}_{h,i}^{\Delta t,\Delta t_a}\right)_{|E},\ \forall E \in \mathscr{G}_h.\end{aligned}$$

and

$$\begin{aligned}\mathscr{F}_i : \left(N_{h,i}\right)^{N\times L} \times \left(M_{h,i}\right)^N \times \left(\Sigma_{h,i}\right)^N &\to \left(\Lambda_h\right)^N \\ \left(\hat{c}_{h,i}^{\Delta t,\Delta t_a}, c_{h,i}^{\Delta t}, \boldsymbol{r}_{h,i}^{\Delta t}\right) &\mapsto (\boldsymbol{r}_{h,i}^{\Delta t}\cdot\boldsymbol{n}_i)_{|E},\ \forall E \in \mathscr{G}_h.\end{aligned}$$

With these operators, we can write the interface problem, which is the system in the fracture γ, consists of solving, for $n = 0,\dots,N-1$:

- the advection equation: for $l = 0,\dots,L-1$,

$$\begin{aligned}\int_E \phi_\gamma \frac{\lambda_h^{n,l+1} - \lambda_h^{n,l}}{\Delta t_a} + \int_{\partial E} \hat{\lambda}_h^{n,l}(\boldsymbol{u}_\gamma\cdot\boldsymbol{n}_E) &= \frac{1}{\Delta t_a}\int_{t^{n,l}}^{t^{n,l+1}} \int_E \sum_{i=1}^{2} \boldsymbol{u}_i\cdot\boldsymbol{n}_i \mathscr{H}_i\mathscr{D}_i(\lambda_f, q_{c,i}, c_{0,i}), \\ &\qquad \forall E \in \mathscr{G}_h,\end{aligned} \tag{5.43}$$

  where $\lambda_h^{n,0} = \lambda_h^n$, and $\lambda_h^0 := \dfrac{1}{\mathrm{meas}(E)}\displaystyle\int_E c_{0,\gamma},\ \forall E \in \mathscr{G}_h$,

- then the diffusion equation

$$\begin{aligned}\int_E \phi_\gamma \frac{\lambda^{n+1} - \lambda^{n,L}}{\Delta t} + \int_E \mathrm{div}\, \boldsymbol{r}_{h,\gamma}^{n+1} &= \int_E q_{c,\gamma}(t^{n+1}) + \frac{1}{\Delta t}\int_{t^n}^{t^{n+1}} \int_E \sum_{i=1}^{2} \mathscr{F}_i\mathscr{D}_i(\lambda_m, q_{c,i}, c_{0,i}), \\ &\qquad \forall E \in \mathscr{G}_h,\end{aligned} \tag{5.44}$$

$$\int_\gamma (\boldsymbol{D}_\gamma\delta)^{-1}\boldsymbol{r}_{h,\gamma}^{n+1}\cdot\boldsymbol{\nu}_\gamma - \int_\gamma \lambda^{n+1}\mathrm{div}\,\boldsymbol{\nu}_\gamma = 0, \qquad \forall \boldsymbol{\nu}_\gamma \in \Sigma_{h,\gamma}.$$

Note that the composite operator $\mathscr{F}_i\mathscr{D}_i$, $i = 1,2$, is a Steklov-Poincaré (Dirichlet-to-Robin) type operator. The interface problem (5.43)-(5.44) can be written in the form

$$\mathscr{S}\lambda_f = \chi, \tag{5.45}$$

where $\mathscr{S} : \Lambda_h^{N\times(L+1)} \to \Lambda_h^{N\times(L+1)}$ is defined by

$$\mathscr{S}\lambda_f = \left(\begin{array}{l} \displaystyle\int_E \phi_\gamma \frac{\lambda_h^{n,l+1}-\lambda_h^{n,l}}{\Delta t_a} + \int_{\partial E} \hat{\lambda}_h^{n,l}(\boldsymbol{u}_\gamma\cdot\boldsymbol{n}_E) - \frac{1}{\Delta t_a}\int_{t^{n,l}}^{t^{n,l+1}} \int_E \sum_{i=1}^{2} \boldsymbol{u}_i\cdot\boldsymbol{n}_i \mathscr{H}_i\mathscr{D}_i(\lambda_f,0,0) \\ \displaystyle\int_E \phi_\gamma \frac{\lambda_h^{n+1,L}-\lambda_h^{n,L}}{\Delta t} + \int_E \operatorname{div}\boldsymbol{r}_{h,\gamma}^{n+1} - \frac{1}{\Delta t}\int_{t^n}^{t^{n+1}} \int_E \sum_{i=1}^{2} \mathscr{F}_i\mathscr{D}_i(\lambda_f,0,0) \end{array} \right)_{\substack{E\in\mathscr{G}_h \\ n=0,\dots,N-1 \\ l=0,\dots,L-1}}$$

in which $\boldsymbol{r}_{h,\gamma}^{n+1}$ is defined by

$$\int_\gamma (\boldsymbol{D}_\gamma\delta)^{-1}\boldsymbol{r}_{h,\gamma}^{n+1}\cdot\boldsymbol{v}_\gamma - \int_\gamma \lambda_h^{n+1}\operatorname{div}\boldsymbol{v}_\gamma = 0,\ \ \forall \boldsymbol{v}_\gamma\in\Sigma_{h,\gamma},\ \forall n=0,\dots,N-1.$$

and

$$\chi = \left(\begin{array}{l} \displaystyle\frac{1}{\Delta t_a}\int_{t^{n,l}}^{t^{n,l+1}} \int_E \sum_{i=1}^{2} \boldsymbol{u}_i\cdot\boldsymbol{n}_i \mathscr{H}_i\mathscr{D}_i(0,q_{c,i},c_{0,i}) \\ \displaystyle\int_E q_{c,\gamma}(t^{n+1}) + \frac{1}{\Delta t}\int_{t^n}^{t^{n+1}} \int_E \sum_{i=1}^{2} \mathscr{F}_i\mathscr{D}_i(0,q_{c,i},c_{0,i}) \end{array} \right)_{\substack{E\in\mathscr{G}_h \\ n=0,\dots,N-1 \\ l=0,\dots,L-1}}$$

5.5.2.2 Method 2: an extension of the Optimized Schwarz Waveform Relaxation approach

As in the pure diffusion problem (cf. Subsection 5.3.2), for Method 2 the fracture problem is included in the subdomain solves. However, in addition to the diffusion equation in the fracture, here we need to solve also the advection equation in the fracture for each subdomain solve. The formulation associated with the diffusion step is just like in the previous section: we still denote by $\theta\in\Lambda_h^N$ the space-time discrete Robin data transmitted from one subdomain to the neighboring subdomain at each diffusion time step,

$$\theta = \left(\theta_h^n\right),\ n=1,\dots,N.$$

For the advection step, to solve the advection equation in the fracture we need an input data as a source term corresponding to the discrete advective flux from the two subdomains entering or exiting the fracture (the right hand side of the second equation in (5.39)). Thus we introduce an discrete interface unknown $\check{\lambda}\in\Lambda_h^{N\times L}$ defined by

$$\check{\lambda} = \left(\check{\lambda}_h^{n,l}\right),\ n=0,\dots,N-1,\ l=0,\dots,L-1,$$

where

$$\left(\check{\lambda}_h^{n,l}\right)_{|E} := \sum_{i=1}^{2}\int_E \boldsymbol{u}_i\cdot\boldsymbol{n}_i\hat{c}_{h,i}^{n,l},\ \forall E\in\mathscr{G}_h.$$

Now to derive the interface problem for this method, we first define the solution operators $\mathscr{R}_i$, $i=1,2$, by

$$\begin{aligned} \mathscr{R}_i : \left(\Lambda_h\right)^{N\times L}\times\left(\Lambda_h\right)^N\times L^2(0,T;L^2(\Omega_i))\ \times H^1_*(\Omega_i)\times L^2(0,T;L^2(\gamma))\times H^1_0(\gamma) \to \\ \left(N_{h,i}\right)^{N\times L}\times\left(M_{h,i}\right)^N\times\left(\Sigma_{h,i}\right)^N\times(\Lambda)^N\times\left(\Sigma_{h,\gamma}\right)^N \\ \left(\check{\lambda},\theta,q_c,c_0,q_{c,\gamma},c_{0,\gamma}\right)\ \ \mapsto \left(\hat{c}_{h,i}^{\Delta t,\Delta t_a},c_{h,i}^{\Delta t},\boldsymbol{r}_{h,i}^{\Delta t},c_{i,\gamma}^{\Delta t},\boldsymbol{r}_{\gamma,i}^{\Delta t}\right), \end{aligned}$$

where $\hat{c}_{h,i}^{\Delta t,\Delta t_a} = \left(\hat{c}_{h,i}^{n,l}\right)_{n=0,\dots,N-1,\, l=0,\dots,L-1}$
and $\left(c_{h,i}^{\Delta t}, \boldsymbol{r}_{h,i}^{\Delta t}, c_{\gamma,i}^{\Delta t}, \boldsymbol{r}_{\gamma,i}^{\Delta t}\right) = \left(c_{h,i}^{n}, \boldsymbol{r}_{h,i}^{n}, c_{i,\gamma}^{n}, \boldsymbol{r}_{\gamma,i}^{n}\right)_{n=1,\dots,N}$ are the solution of the subdomain problem:

For given $(\check{\lambda}, \theta, q_c, c_0, q_{c,\gamma}, c_{0,\gamma})$, then for $n = 0, \dots, N$:

1. define $c_{h,i}^{n,0} = c_{h,i}^{n}$, $i = 1, 2$, and $c_{\gamma,i}^{n,0} = c_{h,\gamma}^{0}$,
2. for $l = 0, \dots, L-1$,
   - define the upwind values in the subdomain
   $$\hat{c}_{h,i}^{n,l} = \mathscr{U}_{h,i}\left(c_{h,i}^{n,l}, c_{i,\gamma}^{n,l}\right),$$
   and in the fracture $\hat{c}_{h,\gamma}^{n,l}$ (cf. (5.38)),
   - solve the advection equations in the subdomains and in the fracture
   $$\begin{aligned}
   \int_K \phi_i \frac{c_{h,i}^{n,l+1} - c_{h,i}^{n,l}}{\Delta t_a} + \sum_{E \subset \partial K} \int_E \hat{c}_{h,i}^{n,l} (\boldsymbol{u}_i \cdot \boldsymbol{n}_K) &= 0, \qquad \forall K \in \mathscr{K}_{h,i},\ i = 1, 2, \\
   \int_E \phi_\gamma \frac{c_{i,\gamma}^{n,l+1} - c_{i,\gamma}^{n,l}}{\Delta t_a} + \int_{\partial E} \hat{c}_{i,\gamma}^{n,l} (\boldsymbol{u}_\gamma \cdot \boldsymbol{n}_E) &= \int_E \check{\lambda}_h^{n,l}, \quad \forall E \in \mathscr{G}_h,
   \end{aligned} \tag{5.46}$$
   with $c_{h,i}^{n,l}$, $i = 1, 2$, and $c_{i,\gamma}^{n,l}$ known, and obtain $c_{h,i}^{n,l+1}$, $i = 1, 2$, and $c_{i,\gamma}^{n,l+1}$,
3. solve the diffusion equations in the subdomains and in the fracture
$$\begin{aligned}
\int_K \phi_i \frac{c_{h,i}^{n+1} - c_{h,i}^{n,L}}{\Delta t} + \int_K \operatorname{div} \boldsymbol{r}_{h,i}^{n+1} &= \int_K q_{c,i}(t^{n+1}), \quad \forall K \in \mathscr{K}_{h,i}, \\
\int_{\Omega_i} \boldsymbol{D}_i^{-1} \boldsymbol{r}_{h,i}^{n+1} \cdot \boldsymbol{v} - \int_{\Omega_i} c_{h,i}^{n+1} \operatorname{div} \boldsymbol{v} + \int_\gamma c_{i,\gamma}^{n+1} (\boldsymbol{v} \cdot \boldsymbol{n}_i) &= 0, \quad \forall \boldsymbol{v} \in \Sigma_{h,i}, \\
-\int_E \boldsymbol{r}_{h,i}^{n+1} \cdot \boldsymbol{n}_i + \alpha \int_E c_{i,\gamma}^{n+1} + \int_E \phi_\gamma \frac{c_{i,\gamma}^{n+1} - c_{i,\gamma}^{n,L}}{\Delta t} + \int_E \operatorname{div} \boldsymbol{r}_{\gamma,i}^{n+1} &= \int_E \left(\theta_h^{n+1} + q_{c,\gamma}(t^{n+1})\right), \ \forall E \in \mathscr{G}_h, \\
\int_\gamma (\boldsymbol{D}_\gamma \delta)^{-1} \boldsymbol{r}_{\gamma,i}^{n+1} \cdot \boldsymbol{v}_\gamma - \int_\gamma c_{i,\gamma}^{n+1} \operatorname{div} \boldsymbol{v}_\gamma &= 0, \quad \forall \boldsymbol{v}_\gamma \in \Sigma_{h,\gamma},
\end{aligned} \tag{5.47}$$
with $c_{h,i}^{n,L}$, $i = 1, 2$, known and $c_{i,\gamma}^{n,L}$ and obtain $\left(c_{h,i}^{n+1}, \boldsymbol{r}_{h,i}^{n+1}, c_{i,\gamma}^{n+1}, \boldsymbol{r}_{\gamma,i}^{n+1}\right)$.

As in Method 1, to impose the transmission condition for the advection equation, we define the projection operator to extract the first component $\hat{c}_{h,i}^{\Delta t,\Delta t_a}$ of the output of $\mathscr{R}_i$: $\widetilde{\mathscr{H}_i}$, $i = 1, 2$:

$$\begin{aligned}
\widetilde{\mathscr{H}_i} : \left(N_{h,i}\right)^{N\times L} \times \left(M_{h,i}\right)^N \times \left(\Sigma_{h,i}\right)^N \times (\Lambda)^N \times \left(\Sigma_{h,\gamma}\right)^N &\to (\Lambda_h)^{N\times L} \\
\left(\hat{c}_{h,i}^{\Delta t,\Delta t_a}, c_{h,i}^{\Delta t}, \boldsymbol{r}_{h,i}^{\Delta t}, c_{i,\gamma}^{\Delta t}, \boldsymbol{r}_{\gamma,i}^{\Delta t}\right) &\mapsto \left(\hat{c}_{h,i}^{\Delta t,\Delta t_a}\right)_{|E},\ \forall E \in \mathscr{G}_h.
\end{aligned}$$

Now for the Ventcell-to-Robin transmission conditions, we need the following interface operators $\mathscr{B}_i$, $i = 1, 2$, which depend on the Robin parameter α:

$$\begin{aligned}\mathscr{B}_i : \left(N_{h,i}\right)^{N\times L} \times \left(M_{h,i}\right)^{N} \times \left(\Sigma_{h,i}\right)^{N} \times (\Lambda)^{N} \times \left(\Sigma_{h,\gamma}\right)^{N} \quad &\to (\Lambda_h)^N \\ \left(\hat{c}_{h,i}^{\Delta t,\Delta t_a}, c_{h,i}^{\Delta t}, \boldsymbol{r}_{h,i}^{\Delta t}, c_{i,\gamma}^{\Delta t}, \boldsymbol{r}_{\gamma,i}^{\Delta t}\right) \quad &\mapsto (\boldsymbol{r}_{h,i}^{\Delta t}\cdot\boldsymbol{n}_i + \alpha c_{i,\gamma}^{\Delta t})_{|E},\ \forall E \in \mathscr{G}_h.\end{aligned}$$

With these operators, we can write the interface problem for Method 2 as follows

$$\begin{aligned}\int_{t^{n,l}}^{t^{n,l+1}}\int_E \check{\lambda} &= \int_{t^{n,l}}^{t^{n,l+1}}\int_E \sum_{i=1}^{2} \boldsymbol{u}_i\cdot\boldsymbol{n}_i \widetilde{\mathscr{H}_i}\mathscr{R}_i(\check{\lambda}, \theta_i, q_{c,i}, c_{0,i}, q_{c,\gamma}, c_{0,\gamma}),\\
\int_{t^n}^{t^{n+1}}\int_E \theta_1 &= \int_{t^n}^{t^{n+1}}\int_E \left(\mathscr{B}_2\mathscr{R}_2(\check{\lambda}, \theta_2, q_{c,2}, c_{0,2}, q_{c,\gamma}, c_{0,\gamma}) + q_{c,\gamma}(t^{n+1})\right),\\
\int_{t^n}^{t^{n+1}}\int_E \theta_2 &= \int_{t^n}^{t^{n+1}}\int_E \left(\mathscr{B}_1\mathscr{R}_1(\check{\lambda}, \theta_1, q_{c,1}, c_{0,1}, q_{c,\gamma}, c_{0,\gamma}) + q_{c,\gamma}(t^{n+1})\right),\\
&\forall E \in \mathscr{G}_h,\ \forall n = 0,\dots,N-1,\ \forall l = 0,\dots,L-1.\end{aligned} \tag{5.48}$$

Note that the composite operator $\mathscr{B}_i\mathscr{R}_i$, $i = 1, 2$, is the discrete Ventcell-to-Robin operator. As usual, we solve (5.48) using Jacobi iterations or GMRES. The former choice yields an algorithm equivalent to the OSWR algorithm, extended to the reduced fracture model and operator splitting.

As stated in Remark 5.9, we are interested in the case where different advection time steps (maybe also different diffusion time steps for Method 1) are used. In the next step, we explain how to handle these nonconforming grids in this case, using the L^2 projections as in the previous chapters.

5.5.3 Nonconforming discretizations in time

As in Subsection 5.3.3, we consider $\mathscr{T}_i$, $i = 1, 2, \gamma$, three different uniform partitions of the time interval $(0, T)$ with into N_i subintervals with size Δt_i, $i = 1, 2, \gamma$ respectively (see Figure 5.10). The sub-time step for the advection in the subdomain and in the fracture is defined by

$$\Delta t_i = L_i \Delta t_{i,a},\ i = 1, 2, \gamma,$$

and we denote by $\mathscr{T}_i^a$, $i = 1, 2, \gamma$ the corresponding partition in time for the advection. We denote by $P_0(\mathscr{T}_i, \Lambda_h)$ the space of piecewise constant functions in time on grid $\mathscr{T}_i$ with values in Λ_h. Then define $\Pi_{i\gamma}$ the average-valued projection from $P_0(\mathscr{T}_\gamma, \Lambda_h)$ to $P_0(\mathscr{T}_i, \Lambda_h)$, and $\Pi_{i\gamma}^a$ the projection from $P_0(\mathscr{T}_\gamma^a, \Lambda_h)$ to $P_0(\mathscr{T}_i^a, \Lambda_h)$.

For Method 1

As the interface unknown is the concentration in the fracture, we choose it to be piecewise constant on the fracture time grid $\mathscr{T}_\gamma^a$:

$$\lambda_f \in (\Lambda_h)^{N_\gamma\times(L_\gamma+1)}.$$

Because Dirichlet data at each diffusion time step λ_h^n is identified with $\lambda_h^{n,0}$, Dirichlet data of the associated advection step, we only need to project λ_f onto the advection

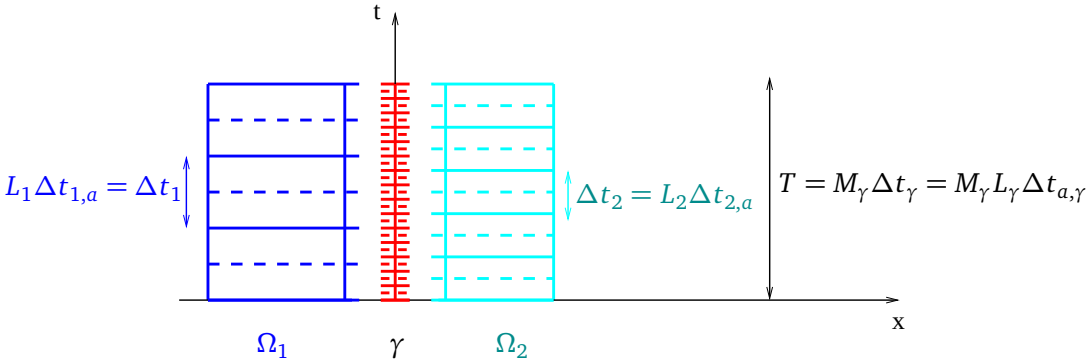

Figure 5.10: Nonconforming advection and diffusion time grids in the rock matrix and in the fracture.

time grid $\mathscr{T}_i^a$ of each subdomain. After the subdomain problem is solved, information corresponding to the transmission condition of the advection equation is projected back to $\mathscr{T}_\gamma^a$ and information corresponding to the transmission condition of the diffusion equation is projected to $\mathscr{T}_\gamma$.

The interface problem (5.45) becomes:

$$\underline{\mathscr{L}}\lambda_f = \underline{\chi},$$

where

$$\underline{\mathscr{L}}\lambda_f = \left(\begin{array}{l} \displaystyle\int_E \phi_\gamma \frac{\lambda_h^{n,l+1} - \lambda_h^{n,l}}{\Delta t_{\gamma,a}} + \int_{\partial E} \hat{\lambda}_h^{n,l} (\boldsymbol{u}_\gamma \cdot \boldsymbol{n}_E) \\ \displaystyle\int_E \phi_\gamma \frac{\lambda_h^{n+1} - \lambda^{n,L}}{\Delta t_\gamma} + \int_E \operatorname{div} \boldsymbol{r}_{h,\gamma}^{n+1} \end{array} \right)_{\substack{E\in\mathscr{G}_h \\ n=0,\dots,N_\gamma-1 \\ l=0,\dots,L_\gamma-1}} +$$

$$\left(\begin{array}{l} \displaystyle -\frac{1}{\Delta t_{\gamma,a}} \int_{t_\gamma^{n,l}}^{t_\gamma^{n,l+1}} \int_E \sum_{i=1}^2 \boldsymbol{u}_i \cdot \boldsymbol{n}_i \, \Pi_{\gamma i}^a \left(\mathscr{H}_i \mathscr{D}_i (\Pi_{i\gamma}^a(\lambda_f), 0, 0) \right) \\ \displaystyle -\frac{1}{\Delta t_\gamma} \int_{t_\gamma^n}^{t_\gamma^{n+1}} \int_E \sum_{i=1}^2 \Pi_{\gamma i} \left(\mathscr{F}_i \mathscr{D}_i (\Pi_{i\gamma}^a(\lambda_f), 0, 0) \right) \end{array} \right)_{\substack{E\in\mathscr{G}_h \\ n=0,\dots,N_\gamma-1 \\ l=0,\dots,L_\gamma-1}}$$

and

$$\underline{\chi} = \left(\begin{array}{l} \displaystyle \frac{1}{\Delta t_{\gamma,a}} \int_{t_\gamma^{n,l}}^{t_\gamma^{n,l+1}} \int_E \sum_{i=1}^2 \boldsymbol{u}_i \cdot \boldsymbol{n}_i \, \Pi_{\gamma i}^a \left(\mathscr{H}_i \mathscr{D}_i (0, q_{c,i}, c_{0,i}) \right) \\ \displaystyle \int_E q_{c,\gamma}(t_\gamma^{n+1}) + \frac{1}{\Delta t_\gamma} \int_{t_\gamma^n}^{t_\gamma^{n+1}} \int_E \sum_{i=1}^2 \Pi_{\gamma i} \left(\mathscr{F}_i \mathscr{D}_i (0, q_{c,i}, c_{0,i}) \right) \end{array} \right)_{\substack{E\in\mathscr{G}_h \\ n=0,\dots,N_\gamma-1 \\ l=0,\dots,L_\gamma-1}}$$

For Method 2

We recall that one advantage of operator splitting in this case is that one may efficiently make use of small time step for the advection in the fracture. Thus $\check{\lambda}$ is piecewise

constant on grid $\mathscr{T}_\gamma^a$ and is used for solving the advection equation in the fracture (without projecting on the advection time grid of the subdomain, $\mathscr{T}_i^a$). As in the pure diffusion case, θ_i is piecewise on grid $\mathscr{T}_\gamma$. The interface problem (5.48) of Method 2 is

$$\begin{aligned}
\int_{t_\gamma^{n,l}}^{t_\gamma^{n,l+1}} \int_E \check{\lambda} &= \int_{t_\gamma^{n,l}}^{t_\gamma^{n,l+1}} \int_E \sum_{i=1}^{2} \boldsymbol{u}_i \cdot \boldsymbol{n}_i \, \Pi_{\gamma i}^a \left(\widetilde{\mathscr{H}_i} \mathscr{R}_i(\check{\lambda}, \Pi_{i\gamma}(\theta_i), q_{c,i}, c_{0,i}, q_{c,\gamma}, c_{0,\gamma}) \right), \\
\int_{t_\gamma^n}^{t_\gamma^{n+1}} \int_E \theta_1 &= \int_{t_\gamma^n}^{t_\gamma^{n+1}} \int_E \left(\Pi_{\gamma 2} \left(\mathscr{B}_2 \mathscr{R}_2(\check{\lambda}, \Pi_{2\gamma}(\theta_2), q_{c,2}, c_{0,2}, q_{c,\gamma}, c_{0,\gamma}) \right) + q_\gamma(t_\gamma^{n+1}) \right), \\
\int_{t_\gamma^n}^{t_\gamma^{n+1}} \int_E \theta_2 &= \int_{t_\gamma^n}^{t_\gamma^{n+1}} \int_E \left(\Pi_{\gamma 1} \left(\mathscr{B}_1 \mathscr{R}_1(\check{\lambda}, \Pi_{1\gamma}(\theta_1), q_{c,1}, c_{0,1}, q_{c,\gamma}, c_{0,\gamma}) \right) + q_\gamma(t_\gamma^{n+1}) \right), \\
&\forall E \in \mathscr{G}_h, \ \forall n = 0, \ldots, N_\gamma - 1, \ \forall l = 0, \ldots, L_\gamma - 1.
\end{aligned}$$

5.5.4 Some remarks on numerical implementation

Because of the time availability, we haven't carried out numerical experiments to verify the performance of the two methods derived in this section. Otherwise we have two remarks concerning the use of preconditioners for Method 1 and of the optimized parameters for Method 2:

- For Method 1, the local and Neumann-Neumann preconditioners derived in Subsection 5.3.1 can be extended to this problem of advection-diffusion equation and with operator splitting. The extension of the local preconditioner is straightforward, while for the Neumann-Neumann preconditioner, we use an idea similar to that used in the case of domain decomposition without fracture (Chapter 3): the preconditioning system is obtained by solving in the subdomain the advection equation with inflow Dirichlet data and the diffusion equation with Neumann data on the space-time fracture-interface.
- For Method 2, the Robin optimized parameters are computed by solving the same min-max problem as in the pure diffusion case since the optimized transmission conditions are derived for the diffusion equation only (see Chapter 3 for a related result).

Conclusion

We apply two domain decomposition methods for modeling the compressible flow in fractured porous media in which the fractures are assumed to be much more permeable than the surrounding medium. Two space-time interface problems are formulated using the time-dependent Dirichlet-to-Neumann and the Ventcell-to-Robin operators respectively, so that different time discretizations in the subdomains and in the fracture can be adapted. For Method 1, two different preconditioners - the local and the Neumann-Neumann preconditioners- are considered and are first validated for a simple test case with one fracture. For Method 2, the optimized parameter is used to accelerate the convergence of the associated iterative algorithm. Preliminary numerical experiments show that Method 2 converges much faster than Method 1 (with either the preconditioner) in terms of the number of iterations. The Neumann-Neumann

preconditioner works better than the local preconditioner in the sense that its convergence is faster and is only weakly dependent on the mesh size of the discretizations. Method 2 also has a weak dependence on the mesh size. When nonconforming time steps are used, only the local preconditioner preserves the accuracy in time: the L^2 error in the fracture of the nonconforming time grid is close to that of the conforming fine grid. For the other algorithms, the L^2 error in the fracture of the nonconforming time grid is close to that of the conforming coarse grid instead. There are several possibilities to overcome this problem as mention in Subsection 5.4, and this work is still in progress. The two methods are then extended to the transport problem with advection and diffusion, where operator splitting is used. Two discrete interface problems are formulated in which the advection and the diffusion transmission conditions are taken into account. Numerical results have not yet completed due to lack of time.

Conclusion and future work

In this thesis, we have developed two different types of space-time domain decomposition methods for diffusion and advection-diffusion problems in the mixed formulations: one method (Method 1) is based on the Steklov-Poincaré operator and one method (Method 2) is based on the OSWR method with Robin or Ventcell transmission conditions. For all problems considered, each method is formulated as a problem defined on the space-time interfaces between the subdomains, which facilitates the use of a matrix-free iterative method to solve such an interface problem (in our case, we use GMRES for Method 1 and Jacobi iterations or GMRES for Method 2). This unified presentation also helps to understand the similarities and differences between the formulations of the two methods, and between their formulations for different model problems. As the main interest of this work is to use different time steps in the subdomains, we have formulated the semi-discrete-in-time interface problem with nonconforming time grids in which the transmission conditions are enforced by using L^2 projections in time. In the advection-diffusion problems, with the use of operator splitting, both the advection and the diffusion time steps can be different from one subdomain to another, and they can be different in each subdomain as well. Thus, depending on the physical properties of the problem, we can choose the time steps efficiently in the sense that the multi-domain solution with a nonconforming time grid preserves the accuracy in time of the solution compared with a monodomain solution computed with a conforming fine grid. This has been observed for different test cases in 2D, both academic and realistic , with two subdomains or many subdomains, with constant and discontinuous coefficients or variable coefficients.

Another objective of this work was to compare the convergence performance of the two methods. From our numerical experiments, we observe that for pure diffusion problems with piecewise constant and continuous coefficients, Method 1 outperforms Method 2, while with piecewise constant and discontinuous coefficients, the convergence speed (in terms of subdomain solves) of Method 1 and Method 2 are comparable. These results are obtained for Method 1 enhanced with a time dependent Neumann-Neumann preconditioner and weight matrices to deal with heterogeneous problems, and for Method 2 with optimized Robin or Ventcell parameters. Asymptotically, both methods have been observed depend weakly on the discretization parameters.

For advection-diffusion problems in the operator splitting context: Method 2 is more robust than Method 1 since Method 2 can efficiently handle both advection-dominated (high Péclet number) and diffusion-dominated (low Péclet number) problems and the convergence of Method 2 is almost independent of the Péclet number. Method 1 with a generalized Neumann-Neumann preconditioner works well when the diffusion is dominant, but it becomes slow when the advection is dominant - even

slower than Method 1 without preconditioner. In terms of accuracy in time, both methods are good since the multidomain solution with the nonconforming time grid has the same accuracy as that with a conforming fine grid. Of course, one need to choose the time steps adapted to the physics of the problem - smaller time steps are chosen where the coefficient is large (i.e. where the solution varies most).

Since a fracture in a porous medium seems to provide an ideal setting in which the use of different time steps could be useful, we have extended the two methods to the modeling of flow and transport in fractured porous medium. In particular, we consider a reduced fracture model in which the fracture is treated as an interface and there is a dynamic system in the fracture that is coupled with the dynamic system in the surrounding medium. Preliminary results show that in terms of convergence Method 2 is very efficient and converges very fast compared with Method 1 using different types of preconditioner.

Because the purpose of using domain decomposition is to take advantage of using different numerical schemes, in both spatial and time discretizations, we would like to extend the work for the advection-diffusion equation to nonmatching grids in space as well, using a mortar mixed finite element method. Dispersion might also be taken into account for better modeling the physical processes in the porous medium.

For the fracture applications, we will first complete the numerical results for the transport problem and then improve Method 2 so that it can actually take advantage of the smaller diffusion time step in the fracture.

Since another reason for using domain decomposition methods is to solve the subdomain problems in parallel and to obtain a significant gain in terms of computational time, we would like to perform parallel computing on a supercomputer.

From a more long-term perspective, a possible direction for extension is to do numerical experiments in $3D$ for modeling more realistic environmental phenomena.

Appendix A

Convergence factor and optimized parameters

We present the formulas for the convergence factor of the Optimized Schwarz and Optimized Schwarz Waveform Relaxation (OSWR) algorithms for problems with discontinuous coefficients. These formulas are used to calculate the optimized parameters associated with the zero-order (Robin) or second-order (Ventcell) transmission conditions. We derive such formulas for three different problems involved in the thesis: the stationary problem (in Chapter 4), the time-dependent diffusion problem (in Chapter 2) and the reduced fracture model for compressible flow (in Chapter 5).

The derivation of the convergence factor is carried out using Fourier transform, where the solution is assumed to be indefinitely differentiable (actually it is in the Schwarz space). In such a context, the mixed formulation is equivalent to the primal formulation and since finding the convergence factor (not the solution) is what we are interested here, in the sequel we will write the problems in primal form.

For simplicity, we consider 2D problems and note that the results presented below can be extended to higher dimensions.

In the following, we recall the formula for convergence factor for stationary problems (Section A.1) and for time-dependent problems (Section A.2). Then in Section A.3, we extend the analysis to the OSWR algorithm associated with the formulation derived in Chapter 5 for a reduced fracture model.

A.1 Stationary problems

We consider the following elliptic problem

$$Lp := -\mathrm{div}\,(\mathfrak{K}\nabla p) = f, \quad \text{on } \Omega = \mathbb{R}^2, \tag{A.1}$$

where $\mathfrak{K} > 0$ is assumed to be constant on each half space $\mathbb{R}^+ \times \mathbb{R}$ and $\mathbb{R}^- \times \mathbb{R}$, but may be discontinuous at $x = 0$,

$$\mathfrak{K} = \begin{cases} \mathfrak{K}_+ & (x,y) \in \mathbb{R}^+ \times \mathbb{R}, \\ \mathfrak{K}_- & (x,y) \in \mathbb{R}^- \times \mathbb{R}. \end{cases}$$

In addition, the solution of (A.1) is assumed to decay at infinity. We decompose Ω into two nonoverlapping subdomains, $\Omega_- = \mathbb{R}^- \times \mathbb{R}$ and $\Omega_+ = \mathbb{R}^+ \times \mathbb{R}$ with an interface

$\Gamma = \partial\Omega_+ \cap \partial\Omega_- = \{x = 0\}$. In order to write the multi-domain problem of (A.1), we denote by

$$L_\pm p := -\mathrm{div}\,(\mathfrak{K}_\pm \nabla p), \quad (x,y) \in \Omega_\pm,$$

and introduce the normal trace operators on the interface as follows

$$\mathscr{B}_\pm p := \mathfrak{K}_\pm \frac{\partial p_\pm}{\partial \boldsymbol{n}_\pm} = \mp \mathfrak{K}_\pm \frac{\partial p}{\partial x}, \quad (x,y) \in \Gamma,$$

where $\boldsymbol{n}_-$ and $\boldsymbol{n}_+$ are the unit outward normal vectors on $\partial\Omega_-$ and $\partial\Omega_+$ respectively.

The multi-domain problem equivalent to (A.1) consists of the subdomain problems:

$$L_- p = f, \ \text{ on } \Omega_-, \ \text{ and } \ L_+ p = f, \ \text{ on } \Omega_+,$$

together with the transmission conditions

$$\begin{array}{c} p_- = p_+, \\ \mathscr{B}_- p_- + \mathscr{B}_+ p_+ = 0 \end{array} \quad \text{on } \Gamma. \tag{A.2}$$

These conditions can be replaced equivalently by

$$\begin{array}{l} \left(\mathscr{B}_- + S_-\right) p_- = \left(-\mathscr{B}_+ + S_-\right) p_+ \\ \left(\mathscr{B}_+ + S_+\right) p_- = \left(-\mathscr{B}_- + S_+\right) p_- \end{array} \quad \text{on } \Gamma, \tag{A.3}$$

where $S_\pm$ is some positive linear operators defined along the y direction. We will see in the following that the choice of $S_\pm$ has an important effect on the convergence of the Jacobi algorithm applied to solve the multi-domain problem with transmission conditions (A.3). Such an algorithm is called the Optimal Schwarz algorithm (see [44] and references therein) and is defined by: starting with an initial guess

$$\left(\mathscr{B}_\pm + S_\pm\right) p_\pm^0 = g_\pm^0,$$

at the k^{th} iteration, $k = 1, \ldots$, solving

$$\begin{array}{rll} L_- p_-^k &= f & \text{in } \Omega_-, \\ \left(\mathscr{B}_- + S_-\right) p_-^k &= \left(-\mathscr{B}_+ + S_-\right) p_+^{k-1} & \text{on } \Gamma, \\ L_+ p_+^k &= f & \text{in } \Omega_+, \\ \left(\mathscr{B}_+ + S_+\right) p_+^k &= \left(-\mathscr{B}_- + S_+\right) p_-^{k-1} & \text{on } \Gamma. \end{array} \tag{A.4}$$

Because the problem is linear, we only consider $f = 0$ and analyse the convergence of the algorithm to the zero solution. Using a Fourier transform in the y direction with parameter η, we obtain the Fourier functions $\hat{p}_\pm^k$ in y of $p_\pm^k$, are solutions to an ODE in the x variable

$$\begin{array}{rll} -\mathfrak{K}_- \dfrac{\partial^2 \hat{p}_-^k}{\partial x^2} + \mathfrak{K}_- \eta^2 \hat{p}_-^k &= 0, & x < 0, \ \eta \in \mathbb{R}, \\ \left(\mathfrak{K}_- \dfrac{\partial}{\partial x} + \sigma_-\right) \hat{p}_-^k &= \left(\mathfrak{K}_+ \dfrac{\partial}{\partial x} + \sigma_-\right) \hat{p}_+^{k-1}, & x = 0, \ \eta \in \mathbb{R}, \end{array}$$

and

$$\begin{array}{rll} -\mathfrak{K}_+ \dfrac{\partial^2 \hat{p}_+^k}{\partial x^2} + \mathfrak{K}_+ \eta^2 \hat{p}_+^k &= 0, & x > 0, \ \eta \in \mathbb{R}, \\ \left(-\mathfrak{K}_+ \dfrac{\partial}{\partial x} + \sigma_+\right) \hat{p}_+^k &= \left(-\mathfrak{K}_- \dfrac{\partial}{\partial x} + \sigma_+\right) \hat{p}_-^{k-1}, & x = 0, \ \eta \in \mathbb{R}, \end{array}$$

where $\sigma_\pm$ are the symbols of the operators $S_\pm$ respectively:

$$\widehat{S_\pm c}(\eta) = \sigma_\pm(\eta)\hat{p}(\eta).$$

The subdomain solutions in the Fourier transformed domain are of the form

$$\hat{p}(x,\eta) = A(\eta)e^{|\eta|x} + B(\eta)e^{-|\eta|x}.$$

As the solution decays at infinity, we obtain

$$\begin{aligned} \hat{p}_-^k &= A^k(\eta)e^{|\eta|x}, \\ \hat{p}_+^k &= B^k(\eta)e^{-|\eta|x}. \end{aligned} \tag{A.5}$$

Substitute these into the transmission conditions on the interface we find

$$\begin{aligned} \left(\mathfrak{K}_-|\eta| + \sigma_-\right)\hat{p}_-^k(0,\eta) &= \left(-\mathfrak{K}_+|\eta| + \sigma_-\right)\hat{p}_+^{k-1}(0,\eta), \\ \left(\mathfrak{K}_+|\eta| + \sigma_+\right)\hat{p}_+^k(0,\eta) &= \left(-\mathfrak{K}_-|\eta| + \sigma_+\right)\hat{p}_-^{k-1}(0,\eta). \end{aligned}$$

Then by induction we obtain

$$\begin{aligned} \hat{p}_-^{2k}(0,\eta) &= \frac{-\mathfrak{K}_+|\eta| + \sigma_-}{\mathfrak{K}_-|\eta| + \sigma_-} \cdot \frac{-\mathfrak{K}_-|\eta| + \sigma_+}{\mathfrak{K}_+|\eta| + \sigma_+} \quad \hat{p}_-^{2k-2}(0,\eta) \\ &= \ldots \rho^k \hat{p}_-^0(0,\eta), \end{aligned}$$

where

$$\rho(\mathfrak{K}_-, \mathfrak{K}_+, \eta) = \frac{-\mathfrak{K}_+|\eta| + \sigma_-}{\mathfrak{K}_-|\eta| + \sigma_-} \cdot \frac{-\mathfrak{K}_-|\eta| + \sigma_+}{\mathfrak{K}_+|\eta| + \sigma_+} < 1. \tag{A.6}$$

Similarly, we deduce

$$\hat{p}_+^{2k}(0,\eta) = \rho^k \hat{p}_+^0(0,\eta).$$

On the other hand, from (A.5) we have

$$\begin{aligned} \hat{p}_-^k(0,\eta) &= A^k(\eta), \\ \hat{p}_+^k(0,\eta) &= B^k(\eta). \end{aligned}$$

Thus

$$\begin{aligned} \hat{p}_-^{2k}(x,\eta) &= \rho^k \hat{p}_-^0(x,\eta), \\ \hat{p}_+^{2k}(x,\eta) &= \rho^k \hat{p}_+^0(x,\eta), \end{aligned}$$

which implies that $\rho(\mathfrak{K}_-, \mathfrak{K}_+, \eta)$ is the convergence factor of algorithm (A.4). An obvious choice made by

$$\sigma_-^{\text{opt}} = \mathfrak{K}_+|\eta|, \text{ and } \sigma_+^{\text{opt}} = \mathfrak{K}_-|\eta|,$$

leads to $\rho(\mathfrak{K}_-, \mathfrak{K}_+, \eta) = 0$, which makes the algorithm converges in 2 iterations independently of the coefficient $\mathfrak{K}$ and the intial guess. However, this choice results in nonlocal operator $S_\pm$ as $\sigma_\pm^{\text{opt}}$ contains the absolute value of the frequency. One possibility is to approximate $\sigma_\pm^{\text{opt}}$ by polynomials. In the following, we consider the zero order and the second order polynomials since the operator of the underlying problem is second order.

A.1.1 Zero order (Robin) transmission conditions

We approximate the optimal symbol σ_-^{opt} by

$$\sigma_-^{\text{Robin}} = \mathfrak{K}_+ a_-, \text{ and } \sigma_+^{\text{Robin}} = \mathfrak{K}_- a_+,$$

where $a_\pm$ are positive constants.

The convergence factor (A.6) becomes

$$\rho^{\text{Robin}}(\mathfrak{K}_-, \mathfrak{K}_+, a_-, a_+, \eta) = \frac{\mathfrak{K}_+|\eta| + \mathfrak{K}_+ a_-}{\mathfrak{K}_-|\eta| + \mathfrak{K}_+ a_-} \cdot \frac{-\mathfrak{K}_-|\eta| + \mathfrak{K}_- a_+}{\mathfrak{K}_+|\eta| + \mathfrak{K}_- a_+}.$$

The parameters $a_\pm$ are calculated in a way such that they minimize the convergence factor over some range of frequencies relevant to the problem:

$$\min_{a_+, a_-} \left(\max_{|\eta| \le \eta_{\max}, |\omega| \le \omega_{\max}} |\rho^{\text{Robin}}(\mathfrak{K}_-, \mathfrak{K}_+, a_-, a_+, \eta)| \right).$$

For numerical computations in a finite domain, denoting by h the mesh size over the interface with length L, it is sufficient to search for the minimum value of $|\rho|$ over a bounded range of frequencies:

$$\min_{a_+, a_-} \left(\max_{|\eta| \in \left[\frac{\pi}{L}, \frac{\pi}{h}\right]} |\rho^{\text{Robin}}(\mathfrak{K}_-, \mathfrak{K}_+, a_-, a_+, \eta)| \right). \tag{A.7}$$

One can choose a_+ and a_- to be equal or different. The former is called weighted Robin parameters, and the latter is referred as two-sided Robin parameters:

- Weighted Robin parameters:

  $$\alpha_- := \mathfrak{K}_+ a, \text{ and } \alpha_+ := \mathfrak{K}_- a,$$

  hence the optimization problem (A.7) is defined for only one free parameter a.

- Two-sided Robin parameters:

  $$\alpha_- := \mathfrak{K}_+ a_- \text{ and } \alpha_+ := \mathfrak{K}_- a_+, \text{ where } a_- \neq a_+.$$

  The optimized parameters are obtained by solving the min-max problem for two free parameters.

Obviously, the convergence given by the optimized two-sided Robin parameters can not be worse than the weighted Robin ones. Thus for numerical results of the Optimized Schwarz methods with Robin transmission conditions, we show the performance of two-sided Robin parameters only (unless otherwise specified).

A.1.2 Second order (Ventcell) transmission conditions

In this case, we approximate the optimal symbol σ_-^{opt} by second order polynomials:

$$\sigma_-^{\text{Ventcell}} = \mathfrak{K}_+ \left(a_- + b_- \mathfrak{K}_+ \eta^2\right), \text{ and } \sigma_+^{\text{Ventcell}} = \mathfrak{K}_- \left(a_+ + b_+ \mathfrak{K}_- \eta^2\right),$$

where $a_\pm$ and $b_\pm$ are positive constants. The first order term is not considered because the operator of the model problem is self-adjoint.

The convergence factor (A.6) is now

$$\rho^{\text{Ventcell}}(\mathfrak{K}_-,\mathfrak{K}_+,a_-,b_-,a_+,b_+,\eta) = \left(\frac{\mathfrak{K}_+|\eta|+\mathfrak{K}_+\left(a_-+b_-\mathfrak{K}_+\eta^2\right)}{\mathfrak{K}_-|\eta|+\mathfrak{K}_+\left(a_-+b_-\mathfrak{K}_+\eta^2\right)}\right)\left(\frac{-\mathfrak{K}_-|\eta|+\mathfrak{K}_-\left(a_++b_+\mathfrak{K}_-\eta^2\right)}{\mathfrak{K}_+|\eta|+\mathfrak{K}_-\left(a_++b_+\eta^2\right)}\right).$$

The parameters $a_\pm$ and $b_\pm$ are computed by solving the following min-max problem:

$$\min_{a_\pm,b_{pm}}\left(\max_{|\eta|\in\left[\frac{\pi}{L},\frac{\pi}{h}\right]}|\rho^{\text{Ventcell}}(\mathfrak{K}_-,\mathfrak{K}_+,a_-,b_-,a_+,b_+,\eta)|\right). \tag{A.8}$$

As in the Robin case, one can choose a_+ and a_-, and b_- and b_+ to be equal or different. However, in practice it's difficult to solve numerically an optimization with four parameters. Thus we consider only the case where $a_- = a_+ = a$ and $b_+ = b_+ = b$, namely weighted Ventcell parameters:

$$\begin{aligned}\alpha_- &= \mathfrak{K}_+ a, \quad \beta_- = \mathfrak{K}_+ b,\\ \alpha_+ &= \mathfrak{K}_- a, \quad \beta_+ = \mathfrak{K}_- b.\end{aligned}$$

Note that with such a choice of $\sigma_\pm^{\text{Ventcell}}$, we have accordingly

$$S_-^{\text{Ventcell}}p = \alpha_- p + \beta_-\,\text{div}_\tau\left(\mathfrak{K}_+\nabla_\tau p\right),\ \text{ and }\ S_+^{\text{Ventcell}}p = \alpha_+ p + \beta_+\,\text{div}_\tau\left(\mathfrak{K}_-\nabla_\tau p\right),$$

where div_τ and ∇_τ are the tangential divergence and gradient with respect to the interface Γ.

A.2 Time-dependent diffusion problems

In this section, we consider the OSWR method for the time-dependent diffusion problems. This method is an extension of the Optimized Schwarz method to evolution problems using waveform relaxation algorithms, in which time-dependent subdomain problems are solved and information is exchanged on the space-time interface. Optimized transmission conditions are derived in an analogous was as in the stationary case using Fourier transform, but now in time direction also. In the following, we briefly recall the convergence factor of the OSWR method and the calculation of the optimized Robin and Ventcell parameters for a two-half space decomposition [12, 44] (as considered in Section A.1). However, it was shown in [60, 75] that for some applications where the subdomains has different lengths, one might need to take into account the size of the subdomain of small scale to efficiently improve the convergence of the algorithm. Thus we consider additionally the three domain decomposition and show in detail the derivation of the convergence factor obtained in this case.

A.2.1 Two half-space analysis

The model problem is the two dimensional time-dependent diffusion equation:

$$\begin{aligned}\mathscr{L}c := \phi\,\partial_t c - \text{div}\left(d\nabla c\right) &= f \quad \text{in } \Omega\times\mathbb{R},\\ c(\cdot,0) &= c_0 \quad \text{in } \Omega,\end{aligned} \tag{A.9}$$

where $\Omega = \mathbb{R}^2$, the porosity ϕ and the diffusion coefficient $d > 0$ are assumed constant on each half space $\mathbb{R}^+ \times \mathbb{R}$ and $\mathbb{R}^- \times \mathbb{R}$, but may be discontinuous at $x = 0$,

$$\phi = \begin{cases} \phi_+ & (x,y) \in \mathbb{R}^+ \times \mathbb{R}, \\ \phi_- & (x,y) \in \mathbb{R}^- \times \mathbb{R}, \end{cases} \qquad d = \begin{cases} d_+ & (x,y) \in \mathbb{R}^+ \times \mathbb{R}, \\ d_- & (x,y) \in \mathbb{R}^- \times \mathbb{R}. \end{cases}$$

In addition, the solution to (A.9) is required to decay at infinity. We decompose Ω into two half-spaces

$$\Omega_- = \mathbb{R}^- \times \mathbb{R}, \quad \Omega_+ = \mathbb{R}^+ \times \mathbb{R},$$

with an interface $\Gamma = \{x = 0\}$. In order to define the multi-domain problem of (A.9), we introduce the notation

$$\begin{aligned} \mathscr{L}_\pm c &:= \phi_\pm \partial_t c - d_\pm \Delta c, && (x,y,t) \in \Omega^\pm \times \mathbb{R}, \\ \mathscr{B}_\pm c &:= d_\pm \frac{\partial c}{\partial \boldsymbol{n}^\pm} = \mp d_\pm \frac{\partial c}{\partial x}, && (x,y,t) \in \Gamma \times \mathbb{R}, \end{aligned}$$

where $\boldsymbol{n}_-$ and $\boldsymbol{n}_+$ are the unit outward normal vectors on $\partial\Omega_-$ and $\partial\Omega_+$ respectively.

It is well-known that (A.9) is equivalent to the decomposed problem

$$\begin{aligned} \mathscr{L}_- c_- &= f \quad \text{in } \Omega_- \times \mathbb{R}, & \mathscr{L}^+ c_+ &= f \quad \text{in } \Omega_+ \times \mathbb{R}, \\ c_-(\cdot,0) &= c_0 \quad \text{in } \Omega_-, & c_+(\cdot,0) &= c_0 \quad \text{in } \Omega_+, \end{aligned}$$

together with the transmission conditions which are defined on the space-time interface (not only in space as in the stationary problem)

$$\begin{aligned} c_- &= c_+ \\ \mathscr{B}_- c_- + \mathscr{B}_+ c_+ &= 0 \end{aligned} \qquad \text{on } \Gamma \times \mathbb{R}.$$

As for the Optimized Schwarz method, we again replace these physical conditions by new transmission conditions, which results in the optimal Schwarz waveform relaxation algorithm defined by: starting with an initial guess on the space-time interface

$$(\mathscr{B}_\pm + \mathscr{S}_\pm) c_\pm^0 = g_\pm^0,$$

at the k^{th} Jacobi iteration, $k = 1, hdots$, solve

$$\begin{aligned} \mathscr{L}_- c_-^k &= f && \text{in } \Omega_- \times \mathbb{R}, \\ c_-^k(\cdot,0) &= c_0 && \text{in } \Omega_-, \\ (\mathscr{B}_- + \mathscr{S}_-) c_-^k &= (-\mathscr{B}_+ + \mathscr{S}_-) c_+^{k-1} && \text{on } \Gamma \times \mathbb{R}, \\ \mathscr{L}_+ c_+^k &= f && \text{in } \Omega_+ \times \mathbb{R}, \\ c_+^k(\cdot,0) &= c_0 && \text{in } \Omega_+, \\ (\mathscr{B}_+ + \mathscr{S}_+) c_+^k &= (-\mathscr{B}_- + \mathscr{S}_+) c_-^{k-1} && \text{on } \Gamma \times \mathbb{R}, \end{aligned} \tag{A.10}$$

where $\mathscr{S}_-$ and $\mathscr{S}_+$ are linear pseudo-differential operators.

Because the problem is linear, we only consider $f = 0$ and $c_0 = 0$, and analyze the convergence of (A.10) to the zero solution. Using a Fourier transform in time with parameter ω and in the y direction with parameter η, we obtain the Fourier transforms $\hat{c}_\pm^k$ in time t and in y of $c_\pm^k$ are solutions to the following ODE in the x variable:

$$-d \frac{\partial^2 \hat{c}}{\partial x^2} + (\phi i\omega + d\eta^2)\hat{c} = 0.$$

Hence, the Fourier transforms of the subdomain solutions are of the form

$$\hat{c}(x,\eta,\omega) = A(\eta,\omega)\, e^{r^+(\phi,d,\eta,\omega)x} + B(\eta,\omega)\, e^{r^-(\phi,d,\eta,\omega)x},$$

where $r^{\pm}(\phi,d,\eta,\omega)$ are the roots (with positive and negative real parts) of the characteristic equation

$$-dr^2 + \phi i\omega + d\eta^2 = 0.$$

Thus we have

$$r^{\pm} = \pm\frac{\sqrt{\Delta}}{d}, \quad \text{where } \Delta = d(\phi i\omega + d\eta^2). \tag{A.11}$$

As the solution decays at infinity, we deduce that

$$\begin{aligned} \hat{c}_-^k(x,\eta,\omega) &= A_k(\eta,\omega)\, e^{r^+(\phi_-,d_-,\eta,\omega)x}, \\ \hat{c}_+^k(x,\eta,\omega) &= B_k(\eta,\omega)\, e^{r^-(\phi_+,d_+,\eta,\omega)x}. \end{aligned} \tag{A.12}$$

We also note that

$$\begin{aligned} \mathscr{B}_-\hat{c}_-^k &= d_- r^+(\phi_-,d_-,\eta,\omega)\hat{c}_-^k, \\ \mathscr{B}_+\hat{c}_+^k &= -d_+ r^-(\phi_+,d_+,\eta,\omega)\hat{c}_+^k. \end{aligned} \tag{A.13}$$

Substituting (A.12) and (A.13) into the transmission conditions (the 3rd and 6th equations of (A.10)) and denoting by $\sigma^{\pm}$ the symbols of the operators $\mathscr{S}^{\pm}$, i.e.

$$\widehat{\mathscr{S}^{\pm}c}(\eta,\omega) = \sigma^{\pm}(\eta,\omega)\hat{c}(\eta,\omega),$$

we obtain the transmission conditions in the Fourier domain

$$\begin{aligned} \left(d_- r^+(\phi_-,d_-,\eta,\omega) + \sigma_-\right)\hat{c}_-^k(0,\eta,\omega) &= \left(d_+ r^-(\phi_+,d_+,\eta,\omega) + \sigma_-\right)\hat{c}_+^{k-1}(0,\eta,\omega), \\ \left(-d_+ r^-(\phi_+,d_+,\eta,\omega) + \sigma_+\right)\hat{c}_+^k(0,\eta,\omega) &= \left(-d_- r^+(\phi_-,d_-,\eta,\omega) + \sigma_+\right)\hat{c}_-^{k-1}(0,\eta,\omega). \end{aligned}$$

By induction, we have on the space-time interface $\Gamma\times\mathbb{R}$

$$\begin{aligned} \hat{c}_{2k}^-(0,\eta,\omega) &= \frac{d_+ r^-(\phi_+,d_+,\eta,\omega)+\sigma_-}{d_- r^+(\phi_-,d_-,\eta,\omega)+\sigma_-}\,\hat{c}_+^{2k-1}(0,\eta,\omega) \\ &= \left(\frac{d_+ r^-(\phi_+,d_+,\eta,\omega)+\sigma_-}{d_- r^+(\phi_-,d_-,\eta,\omega)+\sigma_-}\right)\left(\frac{-d_- r^+(\phi_-,d_-,\eta,\omega)+\sigma_+}{-d_+ r^-(\phi_+,d_+,\eta,\omega)+\sigma_+}\right)\,\hat{c}_-^{2k-2}(0,\eta,\omega) \\ &= \ldots \rho^k \hat{c}_-^0(0,\eta,\omega). \end{aligned}$$

Similarly,

$$\hat{c}_+^{2k}(0,\eta,\omega) = \rho^k \hat{c}_+^0(0,\eta,\omega),$$

where $\rho = \rho(\phi_+,d_+,\phi_-,d_-,\sigma_+,\sigma_-,\eta,\omega)$ is the convergence factor, defined by:

$$\rho = \left(\frac{d_+ r^-(\phi_+,d_+,\eta,\omega)+\sigma_-}{d^- r^+(\phi_-,d_-,\eta,\omega)+\sigma_-}\right)\left(\frac{-d^- r^+(\phi_-,d_-,\eta,\omega)+\sigma_+}{-d^+ r^-(\phi_+,d_+,\eta,\omega)+\sigma_+}\right). \tag{A.14}$$

Hence, the optimal convergence (i.e. in two iterations and independently of the coefficients and the initial guess) is obtained by choosing for the symbols

$$\begin{aligned} \sigma_-^{\text{opt}} &= -d_+ r^-(\phi_+,d_+,\eta,\omega) &&= \sqrt{\Delta(\phi_+,d_+,\eta,\omega)}, \\ \sigma_+^{\text{opt}} &= d^- r^+(\phi_-,d_-,\eta,\omega) &&= \sqrt{\Delta(\phi_-,d_-,\eta,\omega)}. \end{aligned}$$

This choice leads to non-local operators $\mathscr{S}^{\pm}$ as the symbol $\sigma_{\pm}^{\text{opt}}$ contains a square root of the frequencies. As in the Optimized Schwarz method, we will approximate the optimal choice of $\sigma^{\pm}$ by polynomials. We consider again the zero order and the second order approximations though one may use higher order approximations (see, e.g., [96, 72, 71, 12, 62]. In fact, this approach is originally introduced for absorbing boundary conditions where higher order approximations are very useful (see, e.g.,[58, 9]).

A.2.1.1 Robin transmission conditions

We approximate the optimal transmission conditions by Robin type conditions:

$$\begin{array}{ll} \sigma_{-}^{\text{Robin}} & = d_+ a_-, \\ \sigma_{+}^{\text{Robin}} & = d_- a_+, \end{array} \quad \text{for } a_+ \text{ and } a_- > 0.$$

Note that the weights d_+ and d_- comes from the fact that there is a factor d in the definition of Δ. In fact, this choice is well-adapted to problems with highly discontinuous coefficients.

Consequently, the convergence factor (A.14) becomes

$$\rho^{\text{Robin}}(\phi_+, d_+, \phi_-, d_-, a_-, a_+, \eta, \omega) = \left(-\frac{\sqrt{\Delta(\phi_+, d_+, \eta, \omega)} + d_- a_+}{\sqrt{\Delta(\phi_-, d_-, \eta, \omega)} + d_- a_+} \right) \left(-\frac{\sqrt{\Delta(\phi_-, d_-, \eta, \omega)} + d_+ a_-}{\sqrt{\Delta(\phi_+, d_+, \eta, \omega)} + d_+ a_-} \right). \quad \text{(A.15)}$$

To accelerate the convergence, the parameters a_+ and a_- in (A.2.1.1) are chosen to minimize the convergence factor (A.15) over low and high frequencies. Thus, we end up with a min-max problem as follows:

$$\min_{a_+, a_-} \left(\max_{|\eta| \le \eta_{\max}, |\omega| \le \omega_{\max}} |\rho^{\text{Robin}}(\phi_+, d_+, \phi_-, d_-, a_-, a_+, \eta, \omega)| \right).$$

In practice, for Δt the time step of a uniform partition of $[0, T]$ and h the mesh size over the interface with length L, it is sufficient to search for the minimum value of $|\rho^{\text{Robin}}|$ over a bounded range of frequencies

$$\min_{a_+, a_-} \left(\max_{|\eta| \in \left[\frac{\pi}{L}, \frac{\pi}{h}\right], |\omega| \in \left[\frac{\pi}{T}, \frac{\pi}{\Delta t}\right]} |\rho^{\text{Robin}}(\phi_+, d_+, \phi_-, d_-, a_-, a_+, \eta, \omega)| \right). \quad \text{(A.16)}$$

As in the stationary case, we distinguish two types of Robin parameters:

- Weighted Robin parameters: with one free parameter a and

$$\alpha_- := d_+ a, \text{ and } \alpha_+ := d_- a.$$

- Two-sided Robin parameters: with two parameters $a_{\pm}$ and

$$\alpha_- := d_+ a_- \text{ and } \alpha_+ := d_- a_+, \text{ where } a_- \neq a_+.$$

Again for numerical experiments presented in the thesis, we consider only the optimized two-sided Robin parameters when the OSWR method with Robin transmission conditions is considered.

A.2.1.2 Ventcell transmission conditions

We use second-order polynomials to approximate $\sigma_{\pm}^{\text{opt}}$:

$$\begin{aligned} \sigma_{-}^{\text{Ventcell}} &= d_+\left(a_- + b_-(i\,\phi_+\omega + d_+\eta^2)\right), \\ \sigma_{+}^{\text{Ventcell}} &= d_-\left(a_+ + b_+(i\,\phi_-\omega + d_-\eta^2)\right), \end{aligned} \quad \text{for } a_\pm \text{ and } b_\pm > 0.$$

Consequently, we obtain

$$\rho^{\text{Ventcell}} = \left(\frac{d_+ r^-(s_+,d_+,\eta,\omega) + d_+\left(a_- + b_-(i\,\phi_+\omega + d_+\eta^2)\right)}{d_- r^+(s_-,d_-,\eta,\omega) + d_+\left(a_- + b_-(i\,\phi_+\omega + d_+\eta^2)\right)}\right) \cdot \left(\frac{-d_- r^+(s_-,d_-,\eta,\omega) + d_-\left(a_+ + b_+(i\,\phi_-\omega + d_-\eta^n)\right)}{-d_+ r^-(s_+,d_+,\eta,\omega) + d_-\left(a_+ + b_+(i\,\phi_-\omega + d_-\eta^n)\right)}\right).$$

The optimized parameters $a_\pm$ and $b_\pm$ are then computed by solving the min-max problem

$$\min_{a_\pm, b_\pm}\left(\max_{|\eta|\in\left[\frac{\pi}{L},\frac{\pi}{h}\right],|\omega|\in\left[\frac{\pi}{T},\frac{\pi}{\Delta t}\right]} |\rho^{\text{Ventcell}}(\phi_+,d_+,\phi_-,d_-,a_-,b_-,a_+,b_+,\eta,\omega)|\right). \quad \text{(A.17)}$$

For the same reasons as in the stationary case (see Section A.1), we consider the weighted Ventcell parameters and optimize the convergence factor for two free parameters a and b:

$$\begin{aligned} \alpha_- &= d_+ a, \quad \beta_- = d_+ b, \\ \alpha_+ &= d_- a, \quad \beta_+ = d_- b. \end{aligned}$$

Note that with this choice, we have accordingly

$$\begin{aligned} \mathscr{S}_{-}^{\text{Ventcell}} c &= \alpha_-\, c + \beta_-\left(\phi_+\partial_t c + \text{div}_\tau\left(d_+\nabla_\tau c\right)\right), \text{ and} \\ \mathscr{S}_{+}^{\text{Ventcell}} c &= \alpha_+\, c + \beta_+\left(\phi_-\partial_t c + \text{div}_\tau\left(d_-\nabla_\tau c\right)\right), \end{aligned}$$

where div_τ and ∇_τ are the tangential divergence and gradient with respect to the interface Γ.

Remark A.1. *Since the optimization depends on the mesh size $h = \max h_i$ and the time step $\Delta t = \max \Delta t_i$, the optimized parameters serve in some sense as a preconditioner. See [12] and the numerical results in Chapters 2, 3 and Chapter 4 where the asymptotic behaviours of the Optimized Schwarz or OSWR methods with either Robin or Ventcell transmission conditions are studied.*

A.2.2 Three domain analysis

It has been shown in [60, 75] that for a domain consisting of layers with highly different sizes and physical properties, the classical optimization, based on two half-space analysis presented above, is not well-adapted to the problem. Thus another optimization that takes into account the size of the domain of small scale has been derived in these papers and it has good numerical performance compared to the classical optimization (see Subsection 2.5.3 where we consider a realistic test case inspired from the nuclear waste repository simulations). In this subsection, we will recall the formulation for this adapted optimization.

Consider a decomposition into three domains

$$\Omega_1 = (-\infty, 0) \times \mathbb{R},\ \Omega_2 = (0, L) \times \mathbb{R} \text{ and } \Omega_3 = (L, \infty) \times \mathbb{R} \text{ with } L \ll 1.$$

As in the previous subsection, we assume that the porosity and the diffusion are piecewise constant in each subdomain (but may be discontinuous across the interface)

$$\phi = \phi_i,\ d = d_i \quad \forall (x, y) \in \Omega_i,\ i = 1, 2, 3.$$

The new transmission conditions, equivalent to the physical ones, are

$$\begin{aligned}
d_1 \frac{\partial c_1^k}{\partial x} + \mathscr{S}_{1,2} c_1^k &= d_2 \frac{\partial c_2^{k-1}}{\partial x} + \mathscr{S}_{1,2} c_2^{k-1}, && \text{on } \{x = 0\} \times \mathbb{R}, \\
-d_2 \frac{\partial c_2^k}{\partial x} + \mathscr{S}_{2,1} c_2^k &= -d_1 \frac{\partial c_1^{k-1}}{\partial x} + \mathscr{S}_{2,1} c_1^{k-1}, && \text{on } \{x = 0\} \times \mathbb{R}, \\
d_2 \frac{\partial c_2^k}{\partial x} + \mathscr{S}_{2,3} c_2^k &= d_3 \frac{\partial c_3^{k-1}}{\partial x} + \mathscr{S}_{2,3} c_3^{k-1}, && \text{on } \{x = L\} \times \mathbb{R}, \\
-d_3 \frac{\partial c_3^k}{\partial x} + \mathscr{S}_{3,2} c_3^k &= -d_2 \frac{\partial c_2^{k-1}}{\partial x} + \mathscr{S}_{3,2} c_2^{k-1}, && \text{on } \{x = L\} \times \mathbb{R}.
\end{aligned}$$

Proceeding as in Subsection A.2.1, the solutions of (A.9) are

$$\begin{aligned}
\hat{c}_1^k(x, \eta, \omega) &= A_1^k(\eta, \omega) e^{r^+(d_1, \phi_1, \eta, \omega) x}, && x < 0, \\
\hat{c}_2^k(x, \eta, \omega) &= A_2^k(\eta, \omega) e^{r^+(d_2, \phi_2, \eta, \omega) x} + B_2^k(\eta, \omega) e^{r^-(d_2, \phi_2, \eta, \omega) x}, && 0 < x < L, \\
\hat{c}_3^k(x, \eta, \omega) &= B_3^k(\eta, \omega) e^{r^-(d_3, \phi_3, \eta, \omega) x}, && x > L,
\end{aligned}$$

where $r^\pm$ are defined in (A.11). We further denote by

$$r_i^\pm = r^\pm(d_i, \phi_i, \eta, \omega).$$

The transmission conditions in the Fourier domain can be written, for a.e. $t \in \mathbb{R}$, as follows

$$\left(d_1 r_1^+ + \sigma_{1,2}\right) A_1^k = \left(d_2 r_2^+ A_2^{k-1} + d_2 r_2^- B_2^{k-1}\right) + \sigma_{1,2} \left(A_2^{k-1} + B_2^{k-1}\right), \quad \text{on } \{x = 0\}, \tag{A.18}$$

$$\left(-d_2 r_2^+ A_2^k - d_2 r_2^- B_2^k\right) + \sigma_{2,1} \left(A_2^k + B_2^k\right) = \left(-d_1 r_1^+ + \sigma_{2,1}\right) A_1^{k-1}, \quad \text{on } \{x = 0\}, \tag{A.19}$$

$$\left(d_2 r_2^+ e^{r_2^+ L} A_2^k + d_2 r_2^- e^{r_2^- L} B_2^k\right) + \sigma_{2,3} \left(e^{r_2^+ L} A_2^k + e^{r_2^- L} B_2^k\right) = \left(d_3 r_3^- + \sigma_{2,3}\right) e^{r_3^- L} B_3^{k-1}, \quad \text{on } \{x = L\}, \tag{A.20}$$

$$\left(-d_3 r_3^- + \sigma_{3,2}\right) e^{r_3^- L} B_3^k = \left(-d_2 r_2^+ e^{r_2^+ L} A_2^{k-1} - d_2 r_2^- e^{r_2^- L} B_2^{k-1}\right) + \sigma_{3,2} \left(e^{r_2^+ L} A_2^{k-1} + e^{r_2^- L} B_2^{k-1}\right), \quad \text{on } \{x = L\}. \tag{A.21}$$

- From (A.18), we have

$$\left(d_1 r_1^+ + \sigma_{1,2}\right) A_1^k = \left(d_2 r_2^+ + \sigma_{1,2}\right) A_2^{k-1} + \left(d_2 r_2^- + \sigma_{1,2}\right) B_2^{k-1}.$$

  Thus

$$A_1^k = s_1 A_2^{k-1} + s_2 B_2^{k-1}, \quad \text{on } \{x = 0\} \times \mathbb{R}, \tag{A.22}$$

  where

$$s_1 = \frac{d_2 r_2^+ + \sigma_{1,2}}{d_1 r_1^+ + \sigma_{1,2}}; \quad s_2 = \frac{d_2 r_2^- + \sigma_{1,2}}{d_1 r_1^+ + \sigma_{1,2}}.$$

- From (A.21), we have

$$\left(-d_3 r_3^- + \sigma_{3,2}\right) B_3^k = \left(-d_2 r_2^+ + \sigma_{3,2}\right) e^{r_2^+ L} A_2^{k-1} + \left(-d_2 r_2^- + \sigma_{3,2}\right) e^{r_2^- L} B_2^{k-1}.$$

Thus

$$B_3^k = s_7 A_2^{k-1} + s_8 B_2^{k-1}, \quad \text{on } \{x = L\} \times \mathbb{R}, \tag{A.23}$$

where

$$s_7 = \frac{-d_2 r_2^+ + \sigma_{3,2}}{-d_3 r_3^- + \sigma_{3,2}} e^{(r_2^+ - r_3^-)L}; \quad s_8 = \frac{-d_2 r_2^- + \sigma_{3,2}}{-d_3 r_3^- + \sigma_{3,2}} e^{(r_2^- - r_3^-)L}.$$

- Rewrite (A.19) as

$$\left(-d_2 r_2^+ + \sigma_{2,1}\right) A_2^k + \left(-d_2 r_2^- + \sigma_{2,1}\right) B_2^k = \left(-d_1 r_1^+ + \sigma_{2,1}\right) A_1^{k-1}, \quad \text{on } \{x = 0\},$$

Thus, we can deduce

$$A_2^k = s_4 A_1^{k-1} - s_5 B_2^k, \quad \text{on } \{x = 0\} \times \mathbb{R}, \tag{A.24}$$

where

$$s_4 = \frac{-d_1 r_1^+ + \sigma_{2,1}}{-d_2 r_2^+ + \sigma_{2,1}}, \quad s_5 = \frac{-d_2 r_2^- + \sigma_{2,1}}{-d_2 r_2^+ + \sigma_{2,1}}.$$

Similarly, rewrite (A.20) as

$$\left(d_2 r_2^+ + \sigma_{2,3}\right) e^{r_2^+ L} A_2^k + \left(d_2 r_2^- + \sigma_{2,3}\right) e^{r_2^- L} B_2^k = \left(d_3 r_3^- + \sigma_{2,3}\right) e^{r_3^- L} B_3^{k-1}, \text{ on } \{x = L\},$$

and obtain

$$B_2^k = -s_3 A_2^k + s_6 B_3^{k-1}, \quad \text{on } \{x = L\} \times \mathbb{R}, \tag{A.25}$$

where

$$s_3 = \frac{d_2 r_2^+ + \sigma_{2,3}}{d_2 r_2^- + \sigma_{2,3}} e^{(r_2^+ - r_2^-)L}, \quad s_6 = \frac{d_3 r_3^- + \sigma_{2,3}}{d_2 r_2^- + \sigma_{2,3}} e^{(r_3^- - r_2^-)L}.$$

To obtain a representation of A_2^k depending only on the terms at the $(k-1)^{\text{th}}$ iteration, we substitute (A.25) into (A.24) and have

$$A_2^k = \frac{s_4}{D} A_1^{k-1} - \frac{s_5 s_6}{D} B_3^{k-1}, \tag{A.26}$$

where $D = 1 - s_5 s_3$. Then substituting this into (A.25), we obtain

$$B_2^k = -\frac{s_3 s_4}{D} A_1^{k-1} + \frac{s_6}{D} B_3^{k-1}. \tag{A.27}$$

Finally denoting by $\xi^k = [A_1^k; A_2^k; B_2^k; B_3^k]$, from (A.22), (A.23), (A.26) and (A.27), we have

$$\xi^k = \boldsymbol{M} \xi^{k-1},$$

where

$$\boldsymbol{M} = \begin{bmatrix} 0 & s_1 & s_2 & 0 \\ s_4/D & 0 & 0 & -s_5 s_6/D \\ -s_3 s_4/D & 0 & 0 & s_6/D \\ 0 & s_7 & s_8 & 0 \end{bmatrix}.$$

Thus, the convergence factor ρ is the spectral radius of the matrix $\boldsymbol{M}$.

If we choose the symbols

$$\sigma_{1,2}^{\text{opt}} = -d_2 r_2^-,\ \sigma_{2,1}^{\text{opt}} = d_1 r_1^+,\ \sigma_{2,3}^{\text{opt}} = -d_3 r_3^- \text{ and } \sigma_{3,2}^{\text{opt}} = d_2 r_2^+,$$

then $A_2^k = 0$ for $k \geq 1$, $A_1^k = B_3^k = 0$ for $k \geq 2$ and $B_2^k = 0$ for $k \geq 3$. This gives the optimal convergence of the algorithm, i.e. in three iterations and independently of the initial guess. As in Subsection A.2.1, we approximate this optimal choice $\sigma_{i,j}$ by zero-order polynomials (the second order case can be considered, but we do not treat such a case here):

$$\begin{array}{llll} \sigma_{1,2}^{\text{app}} & = -d_2 a_{1,2}, & \sigma_{2,1}^{\text{app}} & = d_1 a_{2,1}, \\ \sigma_{2,3}^{\text{app}} & = -d_3 a_{2,3}, & \sigma_{3,2}^{\text{app}} & = d_2 a_{3,2}. \end{array} \tag{A.28}$$

Then parameters $a_{i,j}$ can be computed by solving the min-max problem

$$\min_{a_{i,j}} \left(\max_{|\eta| \leq \eta_{\max}, |\omega| \leq \omega_{\max}} |\rho^{\text{Robin}}(\phi_1, d_1, \phi_2, d_2, \phi_3, d_3, a_{1,2}, a_{2,1}, a_{2,3}, a_{3,2}, \eta, \omega)| \right).$$

Remark A.2. *In practice, the optimization for four parameters is complicated (for instance, using "fminsearch" of Matlab may give you local minimum value which can be much larger than the global minimum value). We propose two possible choices to handle this problem:*

- *If subdomains Ω_1 and Ω_3 have the same physical properties, i.e.*

  $$\phi_1 = \phi_3 = \phi_{13}, \quad d_1 = d_3 = d_{13},$$

  then (A.28) *reduces to*

  $$\begin{array}{llll} \sigma_{1,2}^{app} & = -d_2 a_{13}, & \sigma_{2,1}^{app} & = d_{13} a_2, \\ \sigma_{2,3}^{app} & = -d_{13} a_2, & \sigma_{3,2}^{app} & = d_2 a_{13}. \end{array}$$

  The associated min-max problem is then for only two parameters

  $$\min_{a_{13}, a_2} \left(\max_{|\eta| \leq \eta_{\max}, |\omega| \leq \omega_{\max}} |\rho(\phi_{13}, d_{13}, \phi_2, d_2, a_{13}, a_2 \eta, \omega)| \right).$$

- *Otherwise, i.e. if each subdomain has different physical properties, one could optimize on two parameters by letting*

  $$\begin{array}{llll} \sigma_{1,2}^{app} & = -d_2 a_1, & \sigma_{2,1}^{app} & = d_1 a_1, \\ \sigma_{2,3}^{app} & = -d_3 a_2, & \sigma_{3,2}^{app} & = d_2 a_2. \end{array}$$

A.3 Reduced fracture model of the incompressible flow

In this section, we extend the two domain analysis above (Subsection A.2) to derive the convergence factor associated with the OSWR type method which we have introduced in Chapter 5 for a reduced fracture model of the incompressible flow. With this

aim, we consider the two half-space decomposition and write the fractured OSWR algorithm (obtained by performing Jacobi iterations on the interface problem (5.28), see Chapter 5) in the primal formulation: at the k^{th} Jacobi iteration, solve

$$\begin{aligned} s_-\partial_t p_-^k + \operatorname{div}\left(-\boldsymbol{K}_-\nabla p_-^k\right) &= q && \text{in } \Omega_- \times (0,T), \\ \boldsymbol{K}_-\frac{\partial p_-^k}{\partial \boldsymbol{n}_-} + \alpha_- p_-^k + s_\gamma \partial_t p_-^k + \operatorname{div}_\tau\left(-\boldsymbol{K}_{f,\tau}\delta\nabla_\tau p_-^k\right) &= \boldsymbol{K}_+\frac{\partial p_+^{k-1}}{\partial \boldsymbol{n}_-} + \alpha_- p_+^{k-1} + q_f && \\ & && \text{on } \gamma \times (0,T), \\ p_-^k(\cdot,0) &= p_0 && \text{in } \Omega_-, \end{aligned} \tag{A.29}$$

and

$$\begin{aligned} s_+\partial_t p_+^k + \operatorname{div}\left(-\boldsymbol{K}_-\nabla p_+^k\right) &= q && \text{in } \Omega_+ \times (0,T), \\ \boldsymbol{K}_+\frac{\partial p_+^k}{\partial \boldsymbol{n}_+} + \alpha_+ p_+^k + s_\gamma \partial_t p_+^k + \operatorname{div}_\tau\left(-\boldsymbol{K}_{f,\tau}\delta\nabla_\tau p_+^k\right) &= \boldsymbol{K}_-\frac{\partial p_-^{k-1}}{\partial \boldsymbol{n}_+} + \alpha_+ p_-^{k-1} + q_f && \\ & && \text{on } \gamma \times (0,T), \\ p_+^k(\cdot,0) &= p_0 && \text{in } \Omega_+, \end{aligned} \tag{A.30}$$

where

$$\Omega_- = \mathbb{R}^- \times \mathbb{R}, \quad \Omega_+ = \mathbb{R}^+ \times \mathbb{R},$$

and $\gamma = \{x = 0\}$ is the fracture. We assume that the permeability is isotropic:

$$\boldsymbol{K}_{pm} = \mathfrak{K}_\pm \boldsymbol{I}, \text{ and } \boldsymbol{K}_{f,\tau} = \mathfrak{K}_f,$$

where $\boldsymbol{I}$ is the 2D identity matrix. In addition, the solution of the problem is assumed to decay at infinity. As the problem is linear, we only consider $q = 0$, $q_f = 0$ and $p_0 = 0$, and analyse the convergence of (A.29)-(A.30) to the zero solution. As in previous sections, we use Fourier transform in time with parameter ω and in y direction with parameter η to obtain the Fourier functions $\hat{p}_\pm^k$ in time t and y of $p_\pm^k$, are solutions to the Ordinary Differential Equation (ODE) in the x variable

$$-\mathfrak{K}\frac{\partial^2 \hat{p}}{\partial x^2} + \left(si\omega + \mathfrak{K}\eta^2\right)\hat{p} = 0.$$

Thus

$$\hat{p} = A(\eta,\omega)e^{r^+ x} + B(\eta,\omega)e^{r^- x},$$

where $r^\pm$ are the roots of the characteristic equation

$$-\mathfrak{K}r^2 + \left(si\omega + \mathfrak{K}\eta^2\right) = 0,$$

so

$$r^\pm = \pm\frac{\sqrt{\Delta}}{2\mathfrak{K}}, \quad \Delta = 4\mathfrak{K}\left(si\omega + \mathfrak{K}\eta^2\right).$$

As the solution decays at infinity, we obtain

$$\begin{aligned} \hat{p}_-^k &= A^k(\eta,\omega)e^{r^+(s_-,\mathfrak{K}_-,\eta,\omega)x}, \\ \hat{p}_+^k &= B^k(\eta,\omega)e^{r^-(s_+,\mathfrak{K}_+,\eta,\omega)x}. \end{aligned}$$

Substitute these into the transmission conditions on the interface $\Gamma \times (0,T)$ (i.e. the second equations of (A.29) and (A.30)), we find

$$\begin{aligned}
\left[\mathfrak{K}_- r^+(s_-,\mathfrak{K}_-,\eta,\omega)+\alpha_- + s_\gamma i\omega + \mathfrak{K}_f \delta\eta^2\right] \quad & \hat{p}_-^k(0,\eta,\omega) \\
&= \left[\mathfrak{K}_+ r^-(s_+,\mathfrak{K}_+,\eta,\omega)+\alpha_-\right] \hat{p}_+^{k-1}(0,\eta,\omega), \\
\left[-\mathfrak{K}_+ r^-(s_+,\mathfrak{K}_+,\eta,\omega)+\alpha_+ + s_\gamma i\omega + \mathfrak{K}_f \delta\eta^2\right] \quad & \hat{p}_+^k(0,\eta,\omega) \\
&= \left[-\mathfrak{K}_- r^+(s_-,\mathfrak{K}_-,\eta,\omega)+\alpha_+\right] \hat{p}_-^{k-1}(0,\eta,\omega).
\end{aligned} \tag{A.31}$$

Denote by

$$\theta = s_\gamma i\omega + \mathfrak{K}_f \delta\eta^2,$$

then from (A.31) and by induction we obtain

$$\begin{aligned}
\hat{p}_-^{2k}(0,\eta,\omega) &= \frac{\mathfrak{K}_+ r^-(s_+,\mathfrak{K}_+,\eta,\omega)+\alpha_-}{\mathfrak{K}_- r^+(s_-,\mathfrak{K}_-,\eta,\omega)+\alpha_-+\theta} \quad \hat{p}_+^{2k-1}(0,\eta,\omega) \\
&= \left(\frac{\mathfrak{K}_+ r^-(s_+,\mathfrak{K}_+,\eta,\omega)+\alpha_-}{\mathfrak{K}_- r^+(s_-,\mathfrak{K}_-,\eta,\omega)+\alpha_-+\theta}\right)\left(\frac{-\mathfrak{K}_- r^+(s_-,\mathfrak{K}_-,\eta,\omega)+\alpha_+}{-\mathfrak{K}_+ r^-(s_+,\mathfrak{K}_+,\eta,\omega)+\alpha_++\theta}\right) \quad \hat{p}_-^{2k-2}(0,\eta,\omega) \\
&= \ldots \rho_{\mathrm{f}}^k \hat{p}_-^0(0,\eta,\omega).
\end{aligned}$$

Similarly,

$$\hat{p}_+^{2k}(0,\eta,\omega) = \rho_f^k \hat{p}_+^0(0,\eta,\omega),$$

where

$$\rho_{\mathrm{f}} = \left(\frac{\mathfrak{K}_+ r^-(s_+,\mathfrak{K}_+,\eta,\omega)+\alpha_-}{\mathfrak{K}_- r^+(s_-,\mathfrak{K}_-,\eta,\omega)+\alpha_-+\theta}\right)\left(\frac{-\mathfrak{K}_- r^+(s_-,\mathfrak{K}_-,\eta,\omega)+\alpha_+}{-\mathfrak{K}_+ r^-(s_+,\mathfrak{K}_+,\eta,\omega)+\alpha_++\theta)}\right),$$

is the convergence factor of the algorithm (A.29)-(A.30). Thus, we can calculate the parameters $\alpha_\pm$ such that it minimizes this continuous convergence factor:

$$\min_{\alpha_+,\alpha_-}\left(\max_{|\eta|\in\left[\frac{\pi}{L},\frac{\pi}{h}\right],|\omega|\in\left[\frac{\pi}{T},\frac{\pi}{\Delta t}\right]} |\rho_{\mathrm{f}}(s_+,\mathfrak{K}_+,s_-,\mathfrak{K}_-,\alpha_-,\alpha_+,\eta,\omega)|\right), \tag{A.32}$$

where L is the length of the fracture, h is the spatial mesh size, T is the final time and Δt is the maximum time step of the discretization in time.

Note that α_- and α_+ can be equal or different. In the numerical results of Chapter 5, as the first step we have used the optimized one-sided Robin parameters:

$$\alpha_- = \alpha_+ = \alpha.$$

Of course one may make use of the two-sided Robin as in the previous section. In Chapter 5, the optimized one-sided Robin parameter works well since in the test case we considered, the two subdomains Ω_1 and Ω_2 (representing the rock matrix) have similar physical properties (though a comparison of the performance of the one-sided and two-sided parameters might be considered).

Appendix B

Discretizations in space using mixed finite element methods

We present the mixed finite element method for a 2D parabolic equation - which can be a model for compressible flow in porous media or for contaminant transport with an effect of diffusion only (see Chapter 1). Different boundary conditions (Dirichlet, Neumann and Robin types) are treated.

We first give the variational formulation of the model problem, then discretize the problem in space using the lowest order Raviart-Thomas spaces on rectangles. In time, the discontinuous Galerkin method of zero order (or the modified backward Euler method) is considered. Details of the calculation of the basis functions and the matrices of the resulting algebraic system is shown.

In addition, a type of mixed-hybrid mixed finite element method, where Lagrange multipliers for the scalar unknown are introduced on some part of the boundary, is considered. This is the case when one uses the OSWR method with Ventcell transmission conditions in the context of mixed formulations (see Chapter 4) or when the OSWR method is used for modeling flow and transport in fractured porous media (see Chapter 5).

Note that the discretization in space for an elliptic problem can be easily obtained from the results presented in this appendix.

Remark B.1. *Our purpose here is to formulate the discrete problem and show how to calculate the terms of the matrices of the algebraic system for implementation purposes.*

B.1 A model problem and its mixed variational formulation

For a polygonal domain $\Omega \subset \mathbb{R}^2$ and some fixed $T > 0$, consider a model problem written in mixed form as follows:

$$\begin{aligned}
\boldsymbol{K}^{-1}\boldsymbol{u} + \nabla p &= 0 && \text{in } \Omega \times (0,T),\\
s\frac{\partial p}{\partial t} + \operatorname{div} \boldsymbol{u} &= f && \text{in } \Omega \times (0,T),\\
p &= g_D && \text{on } \Gamma_D \times (0,T),\\
-\boldsymbol{K}\frac{\partial p}{\partial \boldsymbol{n}} &= g_N && \text{on } \Gamma_N \times (0,T),\\
\varphi p + \boldsymbol{K}\frac{\partial p}{\partial \boldsymbol{n}} &= g_R && \text{on } \Gamma_R \times (0,T),\\
p(x,0) &= p_0(x) && \text{in } \Omega,
\end{aligned} \tag{B.1}$$

where Γ_i, $i = D,N,R$, is a subset of $\partial\Omega$ such that $\Gamma_i \cap \Gamma_j = \emptyset$, $i \neq j$ and $\overline{\Gamma_D} \cup \overline{\Gamma_N} \cup \overline{\Gamma_R} = \partial\Omega$, $\boldsymbol{n}$ is the outward unit normal vector on $\partial\Omega$, s is a strictly positive function on Ω, $\boldsymbol{K}$ is a symmetric, positive definite tensor, φ is a strictly positive function on Γ_R, f, g_D, g_N and g_R are given.

In order to write the variational formulation of (B.1), we need to introduce the following spaces (for the Robin boundary conditions)

$$\begin{aligned}
&M = L^2(\Omega),\\
&\Sigma = \mathscr{H}(\operatorname{div},\Omega) := \left\{\boldsymbol{v} \in H(\operatorname{div},\Omega) : \boldsymbol{v}\cdot\boldsymbol{n} \in L^2(\partial\Omega)\right\}.
\end{aligned}$$

To handle Neumann boundary conditions, we need also the space

$$\Sigma^{g_N} := \left\{\boldsymbol{v} \in \Sigma : \boldsymbol{v}\cdot\boldsymbol{n} = g_N \text{ on } \Gamma_N\right\} \subset \Sigma.$$

Consequently,

$$\Sigma^0 = \left\{\boldsymbol{v} \in \Sigma : \boldsymbol{v}\cdot\boldsymbol{n} = 0 \text{ on } \Gamma_N\right\} \subset \Sigma.$$

Note that Σ^0 is a vector space whereas Σ^{g_N} is not.

Remark B.2. *If there is no Robin boundary condition, we take $\Sigma = H(div\ ,\Omega)$. However, the mixed finite element subspace of Σ does not change whether the Robin boundary condition is present or not.*

We now derive the variational formulation of (B.1): we multiply the first equation of (B.1) by a test function $\boldsymbol{v} \in \Sigma^0$ and integrate over Ω. Then using Green's formula as well as boundary conditions we obtain

$$\int_\Omega \left(\boldsymbol{K}^{-1}\boldsymbol{u}\right)\cdot\boldsymbol{v} - \int_\Omega p\nabla\cdot\boldsymbol{v} + \int_{\Gamma_R} \varphi^{-1}(\boldsymbol{u}\cdot\boldsymbol{n})(\boldsymbol{v}\cdot\boldsymbol{n}) = -\int_{\Gamma_D} g_D\,\boldsymbol{v}\cdot\boldsymbol{n} - \int_{\Gamma_R} \varphi^{-1} g_R\,\boldsymbol{v}\cdot\boldsymbol{n}, \quad \forall \boldsymbol{v} \in \Sigma^0.$$

Next multiplying the second equation of (B.1) by a test function $\mu \in M$ and integrating over Ω, we have

$$\int_\Omega s\frac{\partial p}{\partial t}\mu + \int_\Omega \operatorname{div}\boldsymbol{u}\,\mu = \int_\Omega f\,\mu, \quad \forall \mu \in M.$$

Before writing the variational problem, we introduce the following bilinear forms a, b and r and the linear forms L_D and L_R:

$$\begin{aligned}
a: \quad & \boldsymbol{L^2(\Omega)} \times \boldsymbol{L^2(\Omega)} \longrightarrow \mathbb{R}, \quad a(\boldsymbol{u},\boldsymbol{v}) = \int_\Omega \left(\boldsymbol{K}^{-1}\boldsymbol{u}\right)\cdot\boldsymbol{v},\\
b: \quad & \Sigma \times M \longrightarrow \mathbb{R}, \quad b(\boldsymbol{v},\mu) = \int_\Omega \mu \nabla\cdot\boldsymbol{v},\\
r: \quad & \Sigma \times \Sigma \longrightarrow \mathbb{R}, \quad r(\boldsymbol{u},\boldsymbol{v}) = \int_{\Gamma_R} \varphi^{-1}(\boldsymbol{u}\cdot\boldsymbol{n})(\boldsymbol{v}\cdot\boldsymbol{n}),\\
L_D: \quad & \Sigma \longrightarrow \mathbb{R}, \quad L_D(\boldsymbol{v}) = -\int_{\Gamma_D} g_D\,\boldsymbol{v}\cdot\boldsymbol{n},\\
L_R: \quad & \Sigma \longrightarrow \mathbb{R}, \quad L_R(\boldsymbol{v}) = -\int_{\Gamma_R} \varphi^{-1} g_R\,\boldsymbol{v}\cdot\boldsymbol{n}.
\end{aligned}$$

We denote by $(\cdot,\cdot)_\Omega$ the scalar product in $M = L^2(\Omega)$:

$$(f,\mu)_\Omega = \int_\Omega f\mu, \qquad \text{for } f,\mu \in M. \tag{B.2}$$

The variational formulation of problem (B.1) is written as follows:
Find $\boldsymbol{u} : (0,T) \to \Sigma^g$ *and* $p : (0,T) \to M$ *such that*

$$\begin{aligned}
a(\boldsymbol{u},\boldsymbol{v}) - b(\boldsymbol{v},p) + r(\boldsymbol{u},\boldsymbol{v}) &= L_D(\boldsymbol{v}) + L_R(\boldsymbol{v}), && \forall \boldsymbol{v} \in \Sigma^0,\ t \in (0,T),\\
\left(s\frac{\partial p}{\partial t},\mu\right)_\Omega + b(\boldsymbol{u},\mu) &= (f,\mu)_\Omega, && \forall \mu \in M,\ t \in (0,T),\\
(p(\cdot,0),\mu)_\Omega &= (p_0,\mu)_\Omega, && \forall \mu \in M.
\end{aligned} \tag{B.3}$$

In the next section, we formulate the semi-discrete-in-space problem of (B.3) using mixed finite element spaces. In particular, we use the lowest order Raviart-Thomas spaces on rectangles.

B.2 Semi-discrete approximations in space

We denote by

- h a positive number,
- $\mathscr{K}_h$ a conforming triangulation of Ω into rectangles of diameters no greater than h, with card $(\mathscr{K}_h) = nc =$ number of the cells in the mesh,
- $\mathscr{E}_h$ the set of all edges of rectangles in $\mathscr{K}_h$, with card $(\mathscr{E}_h) = ne =$ number of the edges,
- $\hat{\mathscr{E}}_h$ the subset of $\mathscr{E}_h$ containing the edge in $\mathscr{E}_h$ that are not contained in Γ_N, with card $(\hat{\mathscr{E}}_h) = ne - nne$, where nne is the number of edges not in Γ_N.

Now we come to the definition of the finite dimensional subspaces $M_h \subset M$ and $\Sigma_h \subset \Sigma$ and the approximations $p_h(t) \in M$ and $\boldsymbol{u}_h(t) \in \Sigma_h$ of $p(t)$ and $\boldsymbol{u}(t)$ respectively.

- M_h is the space of functions $\mu_h \in M$ which are constant over each cell:

- $\dim M_h = \text{card}\left(\mathscr{K}_h\right) = nc =$ number of the cells in the mesh $\mathscr{K}_h$.
- A basis of M_h is $\left\{\chi_K\right\}_{K\in\mathscr{K}_h}$ where:

$$\chi_K(x) = \begin{cases} 1 & \text{if } x \in K, \\ 0 & \text{otherwise.} \end{cases}$$

- The degrees of freedom are $\left\{p_K(t)\right\}_{K\in\mathscr{K}_h}$, $p_K(t)$ is the average value of $p(t)$ over the cell K for $K \in \mathscr{K}_h$.

The approximate scalar solution $p_h : (0,T) \mapsto M_h$ has a unique representation as follows

$$p_h(x,t) = \sum_{K\in\mathscr{K}_h} p_K(t)\ \chi_K(x), \qquad (x,t) \in \Omega \times (0,T).$$

- Σ_h is the lowest order Raviart-Thomas on $\mathscr{K}_h$ (see [22, 104]), i.e. the space of vector functions $\boldsymbol{v}_h \in \Sigma$ such that the restriction of $\boldsymbol{v}_h$ to each element $K \in \mathscr{K}_h$, $\boldsymbol{v}_{h|K}$ is in Σ_K

$$\Sigma_K = \left\{ \boldsymbol{v}_h \in \Sigma : \boldsymbol{v}_{h|K} = \begin{pmatrix} \bar{a}x_1 + \bar{b} \\ \bar{c}x_2 + \bar{d} \end{pmatrix}, (\bar{a},\bar{b},\bar{c},\bar{d}) \in \mathbb{R}^4 \right\}, \ K \in \mathscr{K}_h.$$

The properties of Σ_h are as follows

- $\dim \Sigma_h = \text{card}\left(\mathscr{E}_h\right) = ne =$ the number of edges in the mesh.
- A basis of Σ_h is $\left\{\boldsymbol{w}_E\right\}_{E\in\mathscr{E}_h}$ defined by:

$$\int_F \boldsymbol{w}_E \cdot \boldsymbol{n}_F = \delta_{E,F}, \ \ \forall F \in \mathscr{E}_h.$$

  where $\boldsymbol{n}_E$ is a chosen unit normal to the edge $E \in \mathscr{E}_h$:
  - for $E \subset \partial\Omega$, $\boldsymbol{n}_E$ is the outward unit normal to $\partial\Omega$;
  - for $E = \partial K_i \cap \partial K_j$ for K_i, $K_j \in \mathscr{K}_h$, $\boldsymbol{n}_E$ is either unit vector orthogonal to the edge E. However, after choosing $\boldsymbol{n}_E$ (which may be an outward normal to ∂K_i or ∂K_j) we will fix and record its direction for further computations.
- The degrees of freedom are $\left\{u_E(t)\right\}_{E\in\mathscr{E}_h}$, where $u_E(t)$ is the flow rate of $\boldsymbol{u}(t)$ across E $\in \mathscr{E}_h$:

$$u_E = \int_E \boldsymbol{u} \cdot \boldsymbol{n}_E.$$

Hence the approximate vector solution $\boldsymbol{u}_h : (0,T) \to \Sigma_h$ has a unique representation as follows

$$\boldsymbol{u}_h(x,t) = \sum_{E\in\mathscr{E}_h} u_E(t)\boldsymbol{w}_E(x), \qquad (x,t) \in \Omega \times (0,T).$$

We define the corresponding finite dimensional spaces of Σ^{g_N} and Σ^0 by

$$\Sigma_h^{g_N} = \left\{\boldsymbol{v}_h \in \Sigma_h : \boldsymbol{v}_h \cdot \boldsymbol{n} = g_N \text{ on } \Gamma_N\right\}, \text{ and } \Sigma_h^0 = \left\{\boldsymbol{v}_h \in \Sigma_h : \boldsymbol{v}_h \cdot \boldsymbol{n} = 0 \text{ on } \Gamma_N\right\}.$$

Using the notation introduced above, one can write the semi-discrete problem of (B.3) as follows

Find $\boldsymbol{u}_h : (0,T) \to \Sigma_h^g$ *and* $p_h : (0,T) \to M_h$ *such that*

$$\begin{aligned} a\left(\boldsymbol{u}_h, \boldsymbol{v}_h\right) - b\left(\boldsymbol{v}_h, p_h\right) + r\left(\boldsymbol{u}_h, \boldsymbol{v}_h\right) &= L_D\left(\boldsymbol{v}_h\right) + L_R\left(\boldsymbol{v}_h\right), && \forall \boldsymbol{v}_h \in \Sigma_h^0,\ t \in (0,T), \\ \left(s\frac{\partial p_h}{\partial t}, \mu_h\right)_\Omega + b\left(\boldsymbol{u}_h, \mu_h\right) &= \left(f, \mu_h\right)_\Omega, && \forall \mu_h \in M_h,\ t \in (0,T), \\ \left(p_h(\cdot,0), \mu_h\right)_\Omega &= \left(p_0, \mu_h\right)_\Omega, && \forall \mu_h \in M_h. \end{aligned} \tag{B.4}$$

Since $\boldsymbol{v}_h = \sum_{E \in \mathscr{E}_h} \vartheta_E \boldsymbol{w}_E(x)$ and $\mu_h = \sum_{K \in \mathscr{K}_h} \eta_K \chi_K(x)$, the system (B.4) is equivalent to

$$\sum_{F \in \mathscr{E}_h} a\left(\boldsymbol{w}_F, \boldsymbol{w}_E\right) u_F(t) - \sum_{K \in \mathscr{K}_h} b\left(\boldsymbol{w}_E, \chi_K\right) p_K(t) + \sum_{F \in \mathscr{E}_h} r\left(\boldsymbol{w}_F, \boldsymbol{w}_E\right) u_F(t) = L_D\left(\boldsymbol{w}_E\right) + L_R\left(\boldsymbol{w}_E\right),$$
$$\forall E \in \mathscr{E}_h,\ E \notin \Gamma_N,\ t \in (0,T),$$

$$\begin{aligned} \sum_{S \in \mathscr{K}_h} \left(s\chi_S, \chi_K\right)_\Omega \frac{dp_S(t)}{dt} + \sum_{E \in \mathscr{E}_h} b\left(\boldsymbol{w}_E, \chi_K\right) u_E(t) &= \left(f, \chi_K\right)_\Omega, && \forall K \in \mathscr{K}_h,\ t \in (0,T), \\ \sum_{S \in \mathscr{K}_h} \left(\chi_S, \chi_K\right)_\Omega p_S(0) &= \left(p_0, \chi_K\right)_\Omega, && \forall K \in \mathscr{K}_h, \\ u_E(t) &= \int_E g_N, && \forall E \in \mathscr{E}_h, E \subset \Gamma_N,\ t \in J. \end{aligned}$$

This is a linear system of $(ne + nc)$ equations in $(ne + nc)$ unknowns $\left\{u_E(t)\right\}_{E \in \mathscr{E}_h}$ and $\left\{p_K(t)\right\}_{K \in \mathscr{K}_h}$. It can be rewritten in matrix form

$$\begin{aligned} \mathbf{A}\mathbf{u}(t) + \mathbf{B}\mathbf{p}(t) &= \mathbf{G}_{\mathbf{DNR}}(t), && t \in (0,T), \\ \mathbf{B}^{\mathrm{T}}\mathbf{u}(t) - \mathbf{M}\frac{d\mathbf{p}(t)}{dt} &= -\mathbf{F}(t), && t \in (0,T), \\ \mathbf{M}\mathbf{p}(0) &= \mathbf{p_0}, \end{aligned} \tag{B.5}$$

where $\mathbf{u} = \left(u_E\right)_{E \in \mathscr{E}_h}$ is a vector of size ne, $\mathbf{p} = \left(p_K\right)_{K \in \mathscr{K}_h}$ is a vector of size nc, and

- $\mathbf{A}$ is an $ne \times ne$ matrix:

$$\mathbf{A}(E,F) = \begin{cases} a\left(\boldsymbol{w}_E, \boldsymbol{w}_F\right) + r\left(\boldsymbol{w}_F, \boldsymbol{w}_E\right), & \text{if } E \notin \Gamma_N, \\ 1, & \text{if } E \subset \Gamma_N \text{ and } F = E, \\ 0, & \text{if } E \subset \Gamma_N \text{ and } F \neq E, \end{cases}$$

- $\mathbf{B}$ is an $ne \times nc$ matrix:

$$\mathbf{B} = \left(-b\left(\boldsymbol{w}_E, \chi_K\right)\right)_{E \in \mathscr{E}_h, K \in \mathscr{T}_h},$$

- $\mathbf{M}$ is an $nc \times nc$ diagonal matrix:

$$\mathbf{M} = \left(\left(s\chi_S, \chi_K\right)_\Omega\right)_{K,S \in \mathscr{K}_h},$$

- $\mathbf{G}_{\mathbf{DNR}}$ is a vector of size ne:

$$\mathbf{G}_{\mathbf{DNR}}(E) = \begin{cases} L_D\left(\boldsymbol{w}_E\right) + L_R\left(\boldsymbol{w}_E\right), & \text{if } E \notin \Gamma_N, \\ \displaystyle\int_E g_N, & \text{if } E \subset \Gamma_N. \end{cases}$$

- $\mathbf{F}$ is a vector of size nc:
$$\mathbf{F} = \left((f, \chi_K)_\Omega \right)_{K \in \mathscr{K}_h}.$$
- $\mathbf{p_0}$ is a vector of size nc:
$$\mathbf{p_0} = \left((p_0, \chi_K)_\Omega \right)_{K \in \mathscr{K}_h}.$$

B.3 Fully discrete problem with an implicit scheme in time

Now we solve the system of ordinary differential equations (B.5) by discretizing the time derivative using the discontinuous Galerkin method of order zero (which is equivalent to a modified Euler method). Let $0 = t^0 < t^1 < \cdots < t^N = T$ be a partition of J into N subintervals $\left(t^n, t^{n+1}\right)$ of length $\Delta t^n = t^{n+1} - t^n$. For a generic function v of time, we denote by $v^n = v(t^n)$.

The fully discrete variational formulation of (B.3) is

Find $\boldsymbol{u}_h^n \in \Sigma_h^g$ *and* $p_h^n \in M_h$ *for* $n = 1, 2, \cdots, N$ *such that*

$$\begin{aligned}
a\left(\boldsymbol{u}_h^{n+1}, \boldsymbol{v}_h\right) - b\left(\boldsymbol{v}_h, p_h^{n+1}\right) - r\left(\boldsymbol{u}_h^{n+1}, \boldsymbol{v}_h\right) &= \int_{t^n}^{t^{n+1}} \left(L_D\left(\boldsymbol{v}_h\right) + L_R\left(\boldsymbol{v}_h\right)\right), \quad \forall \boldsymbol{v}_h \in \Sigma_h^0, \\
\left(p_h^{n+1} - p_h^n, \mu_h\right) + \Delta t^n b\left(\boldsymbol{u}_h^n, \mu_h\right) &= \int_{t^n}^{t^{n+1}} (f, \mu_h)_\Omega, \qquad \forall \mu_h \in M_h, \\
\left(p_h^0, \mu_h\right) &= (p_0, \mu_h), \qquad \forall \mu_h \in M_h,
\end{aligned}$$

or equivalently in matrix form

$$\begin{aligned}
\mathbf{A}\mathbf{u}^{n+1} + \mathbf{B}\mathbf{p}^{n+1} &= \int_{t^n}^{t^{n+1}} \mathbf{G_{DNR}}, \\
\Delta t^n \mathbf{B^T}\mathbf{u}^{n+1} - \mathbf{M}\mathbf{p}^{n+1} &= -\mathbf{M}\mathbf{p}^n - \int_{t^n}^{t^{n+1}} \mathbf{F}^{n+1}, \\
\mathbf{M}\mathbf{p}(0) &= \mathbf{p_0},
\end{aligned} \tag{B.6}$$

where $\mathbf{u}^n = \left(u_E^n\right)_{E \in \mathscr{E}_h}$ and $\mathbf{p}^n = \left(p_K^n\right)_{K \in \mathscr{K}_h}$ with

$$\begin{aligned}
p_h^n &= \sum_{K \in \mathscr{K}_h} p_K^n \chi_K, \\
\boldsymbol{u}_h^n &= \sum_{E \in \mathscr{E}_h} u_E^n \boldsymbol{w}_E,
\end{aligned} \qquad \text{for } n = 1, 2, \cdots, N.$$

B.4 Detailed calculation of the matrices in the linear system

We present detailed calculation of the matrices in (B.6) for a rectangular mesh $\mathscr{K}_h$ whose horizontal and vertical edges are parallel to the x_1- and x_2-coordinate axes, respectively (see Figure B.1). We assume that s and $\boldsymbol{K}$ are piecewise constant on each element $K_{ij} \in \mathscr{K}_h$ and write

$$s_{ij} = s_{|K_{ij}}, \ \boldsymbol{K} = \boldsymbol{K}_{|K_{ij}}, \quad \forall K_{ij} \in \mathscr{K}_h.$$

In order to compute the basis functions $\boldsymbol{w}_E$ of Σ_h, we fix the normal vector $\boldsymbol{n}_E$ in a way that $\boldsymbol{n}_E = \boldsymbol{n}_1 = (1, 0)$ if E is vertical, and $\boldsymbol{n}_E = \boldsymbol{n}_2 = (0, 1)$ if E is horizontal. We give the explicit formula for $\boldsymbol{w}_E$ for a vertical edge E and for a horizontal edge E.

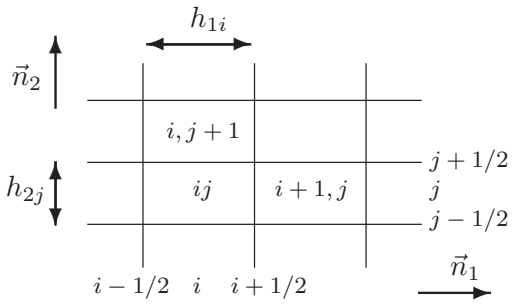

Figure B.1: A conforming triangulation into rectangles.

Remark B.3. *By the definition of the basis function $\boldsymbol{w}_E$ of Σ_h, the restriction of $\boldsymbol{w}_E$ to the cells which are not adjacent to E is equal to zero.*

- If E is a vertical edge (not on the boundary $\partial\Omega$): $E = E_{i+1/2,j}$. Due to Remark B.3, we only consider the restriction of $\boldsymbol{w}_E$ to two adjacent cells T_{ij} and $T_{i+1,j}$ of the edge $E_{i+1/2,j}$. By definition, we have

$$\boldsymbol{w}_{i+1/2,j}\,|_{T_{ij}} = \begin{pmatrix} ax_1 + b \\ cx_2 + d \end{pmatrix},$$

for some $a, b, c, d \in \mathbb{R}$ and

$$\int_{E_{i+1/2,j}} \boldsymbol{w}_{i+1/2,j} \cdot \boldsymbol{n}_{i+1/2,j} = 1, \qquad \int_{E_{i-1/2,j}} \boldsymbol{w}_{i+1/2,j} \cdot \boldsymbol{n}_{i-1/2,j} = 0,$$
$$\int_{E_{i,j+1/2}} \boldsymbol{w}_{i+1/2,j} \cdot \boldsymbol{n}_{i,j+1/2} = 0, \qquad \int_{E_{i,j-1/2}} \boldsymbol{w}_{i+1/2,j} \cdot \boldsymbol{n}_{i,j-1/2} = 0,$$

or equivalently,

$$\begin{cases} ax_{i+1/2} + b &= 1/h_{2j} \\ ax_{i-1/2} + b &= 0 \\ c = d &= 0 \end{cases} \Leftrightarrow \begin{cases} a &= \dfrac{1}{\left(x_{i+1/2} - x_{i-1/2}\right) h_{2j}} = \dfrac{1}{h_{1i}h_{2j}} = \dfrac{1}{|\,T_{ij}\,|}, \\ b &= -\dfrac{x_{i-1/2}}{|\,T_{ij}\,|}, \\ c &= d = 0. \end{cases}$$

Thus

$$\boldsymbol{w}_{i+1/2,j}\,|_{T_{ij}} = \begin{pmatrix} \dfrac{x_1 - x_{i-1/2}}{|\,T_{ij}\,|} \\ 0 \end{pmatrix}.$$

Similarly, we have

$$\boldsymbol{w}_{i+1/2,j}\,|_{T_{i+1,j}} = \begin{pmatrix} \dfrac{-x_1 + x_{i+3/2}}{|\,T_{i+1,j}\,|} \\ 0 \end{pmatrix}.$$

From these two equations, we obtain an explicit formula for the basis function $\boldsymbol{w}_{i+1/2,j}$:

$$\boldsymbol{w}_{i+1/2,j}\,(x_1, x_2) = \begin{pmatrix} v_{i+1/2,j}\,(x_1) \\ 0 \end{pmatrix},$$

where $v_{i+1/2,j}(x_1)$ is the hat function (see Figure B.2):

$$v_{i+1/2,j}(x_1) = \begin{cases} \dfrac{x_1 - x_{i-1/2}}{|\,T_{ij}\,|} & \text{if } x_1 \in \left[x_{i-1/2}, x_{i+1/2}\right], \\ \dfrac{-x_1 + x_{i+3/2}}{|\,T_{i+1,j}\,|} & \text{if } x_1 \in \left[x_{i+1/2}, x_{i+3/2}\right], \\ 0 & \text{otherwise.} \end{cases}$$

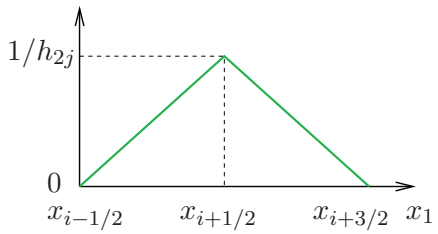

Figure B.2: The hat function $v_{i+1/2,j}(x_1)$.

- E is a horizontal edge (not on the boundary $\partial\Omega$): $E = E_{i,j+1/2}$. Proceeding as above, we obtain the corresponding basis

$$\boldsymbol{w}_{i,j+1/2}(x_1, x_2) = \begin{pmatrix} 0 \\ v_{i,j+1/2}(x_2) \end{pmatrix},$$

where

$$v_{i,j+1/2}(x_2) = \begin{cases} \dfrac{x_2 - x_{j-1/2}}{|\,T_{ij}\,|} & \text{if } x_2 \in \left[x_{j-1/2}, x_{j+1/2}\right], \\ \dfrac{-x_2 + x_{j+3/2}}{|\,T_{i,j+1}\,|} & \text{if } x_2 \in \left[x_{j+1/2}, x_{j+3/2}\right], \\ 0 & \text{otherwise .} \end{cases}$$

Remark B.4. *If the edge E is on the boundary, then E has only one adjacent cell. The corresponding basis function $\boldsymbol{w}_E$ is defined using its the restriction to that cell only. For example, If E is on the left boundary ($i = 0$), then*

$$\boldsymbol{w}_{1/2,j}(x_1, x_2) = \begin{pmatrix} w_{1/2,j}(x_1) \\ 0 \end{pmatrix},$$

where

$$w_{1/2,j}(x_1) = \begin{cases} \dfrac{-x_1 + x_{3/2}}{|\,T_{1j}\,|} & \textit{if } x_1 \in \left[x_{1/2}, x_{3/2}\right], \\ 0 & \textit{otherwise.} \end{cases}$$

We now compute explicitly the coefficients in the system (B.6). We begin with the 2nd equation: since the basis functions χ_K of M_h are characteristic functions , we have

$$\sum_{E \in \mathcal{E}_h} u_E^n \int_\Omega \chi_K \nabla \cdot \boldsymbol{w}_E = \sum_{E \in \partial K} u_E^n \int_K \nabla \cdot \boldsymbol{w}_E.$$

Using the explicit formulas derived above for the basis function $\boldsymbol{w}_E$, we deduce

$$\int_{T_{ij}} \nabla \cdot \boldsymbol{w}_{i+1/2,j} = \int_{T_{ij}} \frac{1}{|\,T_{ij}\,|} = 1,$$
$$\int_{T_{ij}} \nabla \cdot \boldsymbol{w}_{i-1/2,j} = \int_{T_{ij}} -\frac{1}{|\,T_{ij}\,|} = -1.$$

Then the i,j row (corresponding to K_{ij}) of the second matrix equation of (B.6) can be rewritten as

$$-\Delta t^n \left(u^{n+1}_{i+1/2,j} - u^{n+1}_{i-1/2,j} + u^{n+1}_{i,j+1/2} - u^{n+1}_{i,j-1/2}\right) - |T_{ij}| s_{ij} p^{n+1}_{ij} = -|T_{ij}| p^n_{ij} - \int_{t^n}^{t^{n+1}} \int_{T_{ij}} f.$$

From this we see that $\boldsymbol{M}$ is a diagonal matrix with entries s_{ij} and $\boldsymbol{B}^T$ is a matrix having 4 nonzero entries per row.

Now to calculate the coefficients of $\boldsymbol{A}$, we use the first equation of (B.6) and first consider a row corresponding to an interior edge E or to $\boldsymbol{w}_E$. Since E is an interior edge, the boundary terms on the right hand side vanish, and thus is $\boldsymbol{K}$ constant on each element, we may write $\boldsymbol{K}^{-1}_{|K_{ij}}$ in the form

$$\boldsymbol{K}^{-1}_{|K_{ij}} = \begin{bmatrix} \alpha^1_{ij} & \alpha^{12}_{ij} \\ \alpha^{12}_{ij} & \alpha^2_{ij} \end{bmatrix}.$$

Using the definition of the basis function $\boldsymbol{w}_E$, we rewrite the rows of the first equation of (B.6) as

- For an interior vertical edge $E = E_{i+1/2,j}$:

$$\frac{\alpha^1_{ij}}{3}\frac{h_{1i}}{h_{2j}} u^{n+1}_{i+1/2,j} + \frac{\alpha^1_{ij}}{6}\frac{h_{1i}}{h_{2j}} u^{n+1}_{i-1/2,j} + \frac{\alpha^{12}_{ij}}{4}\left(u^{n+1}_{i,j+1/2} + u^{n+1}_{i,j-1/2}\right) + \frac{\alpha^1_{i+1,j}}{3}\frac{h_{1,i+1}}{h_{2j}} u^{n+1}_{i+1/2,j} +$$
$$\frac{\alpha^1_{i+1,j}}{6}\frac{h_{1,i+1}}{h_{2j}} u^{n+1}_{i+3/2,j} + \frac{\alpha^{12}_{i+1,j}}{4}\left(u^{n+1}_{i+1,j+1/2} + u^{n+1}_{i+1,j-1/2}\right) + p^{n+1}_{i+1,j} - p^{n+1}_{ij} = 0.$$

- For an interior horizontal edge $E = E_{i,j+1/2}$:

$$\frac{\alpha^2_{ij}}{3}\frac{h_{2j}}{h_{1i}} u^{n+1}_{i,j+1/2} + \frac{\alpha^2_{ij}}{6}\frac{h_{2j}}{h_{1i}} u^{n+1}_{i,j-1/2} + \frac{\alpha^{12}_{ij}}{4}\left(u^{n+1}_{i+1/2,j} + u^{n+1}_{i-1/2,j}\right) + \frac{\alpha^2_{i,j+1}}{3}\frac{h_{2,j+1}}{h_{1,i}} u^{n+1}_{i,j+1/2}$$
$$+ \frac{\alpha^2_{i,j+1}}{6}\frac{h_{2,j+1}}{h_{1,i}} u^{n+1}_{i,j+3/2} + \frac{\alpha^{12}_{i,j+1}}{4}\left(u^{n+1}_{i+1/2,j+1} + u^{n+1}_{i-1/2,j+1}\right) + p^{n+1}_{i,j+1} - p^{n+1}_{ij} = 0.$$

Now if E lies on Γ_D, for instance, on the left boundary $E = E_{1/2,j}$, as there is only one adjacent cell, the first equation of (B.6) corresponding to E or $\boldsymbol{w}_E = \boldsymbol{w}_{1/2,j}$ becomes

$$\frac{\alpha^1_{1j}}{3}\frac{h_{11}}{h_{2j}} u^{n+1}_{1/2,j} + \frac{\alpha^1_{1j}}{6}\frac{h_{11}}{h_{2j}} u^{n+1}_{3/2,j} + \frac{\alpha^{12}_{1j}}{4}\left(u^{n+1}_{1,j+1/2} + u^{n+1}_{1,j-1/2}\right) + p^{n+1}_{1,j} = \frac{1}{h_{2j}} \int_{t^n}^{t^{n+1}} \int_{E_{1/2,j}} g_D.$$

If E lies on Γ_R, the first equation of (B.6) corresponding to E or $\boldsymbol{w}_E = \boldsymbol{w}_{1/2,j}$ is written as

$$\frac{\alpha^1_{1j}}{3}\frac{h_{11}}{h_{2j}}u^{n+1}_{1/2,j} + \frac{\alpha^1_{1j}}{6}\frac{h_{11}}{h_{2j}}u^{n+1}_{3/2,j} + \frac{\alpha^{12}_{1j}}{4}\left(u^{n+1}_{1,j+1/2} + u^{n+1}_{1,j-1/2}\right) + p^{n+1}_{1,j} + \frac{1}{h^2_{2j}}\int_{E_{1/2,j}} \varphi^{-1}u^{n+1}_{1/2,j} = \frac{1}{h_{2j}}\int_{t^n}^{t^{n+1}}\int_{E_{1/2,j}} \varphi^{-1}g_R.$$

If E lies on Γ_N, the first equation of (B.6) corresponding to E or $\boldsymbol{w}_E = \boldsymbol{w}_{1/2,j}$ is

$$u^{n+1}_{1/2,j} = \int_{t^n}^{t^{n+1}}\int_{E_{1/2,j}} g_N.$$

Thus on a row that corresponds to an interior edge E: the matrix $\boldsymbol{A}$ has 7 nonzero entries associated with the degrees of freedom of $\boldsymbol{u}_h$ on the edges of the two cells adjacent to E while the matrix $\boldsymbol{B}$ has 2 nonzero entries associated with the degrees of freedom of p_h on the two adjacent cells; on a row corresponding to a boundary edge of Dirichlet or Robin conditions: the matrix $\boldsymbol{A}$ has 4 nonzero entries while the matrix $\boldsymbol{B}$ has only 1 nonzero entry. Recall that in the mixed setting, the Neumann boundary condition is explicitly imposed in the finite dimensional space, $\Sigma_h^{g_N}$.

B.5 Mixed finite elements for Ventcell type boundary conditions

In Chapter 4, we have formulated the OSWR method with Ventcell transmission conditions for a problem in mixed formulation. This requires the solution of the subdomain problems with Ventcell boundary conditions. These subdomain problems take the form:

$$\begin{aligned}
\boldsymbol{K}^{-1}\boldsymbol{u} + \nabla p &= 0 && \text{in } \Omega\times(0,T),\\
s\frac{\partial p}{\partial t} + \operatorname{div}\boldsymbol{u} &= f && \text{in } \Omega\times(0,T),\\
\tilde{\boldsymbol{K}}_\Gamma^{-1}\tilde{\boldsymbol{u}}_\Gamma + \nabla_\tau p_\Gamma &= 0, && \text{on } \Gamma\times(0,T),\\
-\boldsymbol{u}\cdot\boldsymbol{n} + \alpha p_\Gamma + \tilde{s}_\Gamma\frac{\partial p_\Gamma}{\partial t} + \operatorname{div}_\tau(\tilde{\boldsymbol{u}}_\Gamma) &= g && \text{on } \Gamma\times(0,T),\\
p(\cdot,0) &= p_0 && \text{in } \Omega,\\
p_\Gamma(\cdot,0) &= p_{0|_\Gamma} && \text{in } \Gamma,
\end{aligned} \tag{B.7}$$

where we have imposed pure Ventcell boundary conditions on $\Gamma = \partial\Omega$ for simplicity. Recall that p_Γ represent the trace of p on Γ while $\tilde{\boldsymbol{u}}_\Gamma$ is not the tangential trace of $\boldsymbol{u}$ on Γ. Similarly, $\tilde{s}_\Gamma$ and $\tilde{\boldsymbol{K}}_\Gamma$ do not necessarily have any connection with s and $\boldsymbol{K}$ respectively.

Remark B.5. *Problem* (B.7) *can be seen as a coupling between a 2D (in Ω) and a 1D (in Γ) problems, both are written in mixed form. This remark will be useful later for the mixed approximations of the 2D and 1D unknowns.*

In this section, we explain how to discretize problem (B.7) using the lowest order Raviart-Thomas spaces on rectangles. We first write the variational formulation of

(B.7). Toward this end, we introduce the spaces

$$M = L^2(\Omega), \quad \Lambda = L^2(\Gamma),$$
$$\Sigma = \mathscr{H}(\mathrm{div}\,, \Omega), \quad \Sigma_\Gamma = H(\mathrm{div}_\tau, \Gamma).$$

We define the bilinear forms a and b as in Section B.1 and their 1D counterparts defined on Γ as follows

$$a_\Gamma : \quad \Lambda \times \Lambda \longrightarrow \mathbb{R}, \quad a_\Gamma\left(\boldsymbol{u}_\Gamma, \boldsymbol{\nu}_\Gamma\right) = \int_\Gamma \left(\tilde{\boldsymbol{K}}^{-1}\boldsymbol{u}_\Gamma\right)\cdot\boldsymbol{\nu}_\Gamma,$$
$$b_\Gamma : \quad \Sigma_\Gamma \times \Lambda \longrightarrow \mathbb{R}, \quad b_\Gamma\left(\boldsymbol{\nu}_\Gamma, \mu_\Gamma\right) = \int_\Gamma \mu_\Gamma \nabla_\tau \cdot \boldsymbol{\nu}_\Gamma, .$$

We also make use of the following bilinear form:

$$d : \quad \Lambda \times \Sigma \longrightarrow \mathbb{R}, \quad d\left(\mu_\Gamma, \boldsymbol{\nu}\right) = \int_\Gamma \mu_\Gamma\left(\boldsymbol{\nu}\cdot\boldsymbol{n}\right).$$

Finally we denote by $(\cdot,\cdot)_\Gamma$ the scalar product in $L^2(\Gamma)$.

The variational formulation of (B.7) is written as:

For a.e. $t \in (0,T)$, find $(p, \boldsymbol{u}, p_\Gamma, \tilde{\boldsymbol{u}}_\Gamma)$ such that

$$\begin{aligned}
a\left(\boldsymbol{u},\boldsymbol{\nu}\right) - b\left(\boldsymbol{\nu},p\right) + d(p_\Gamma,\boldsymbol{\nu}) &= 0, && \forall \boldsymbol{\nu}\in\Sigma,\\
\left(s\frac{\partial p}{\partial t},\mu\right)_\Omega + b\left(\boldsymbol{u},\mu\right) &= \left(f,\mu\right)_\Omega, && \forall \mu\in M,\\
a_\Gamma\left(\tilde{\boldsymbol{u}}_\Gamma,\boldsymbol{\nu}_\Gamma\right) - b_\Gamma\left(\boldsymbol{\nu}_\Gamma,p_\Gamma\right) &= 0, && \forall \boldsymbol{\nu}_\Gamma\in\Sigma_\Gamma,\\
-d(\mu_\Gamma,\boldsymbol{u}) + \left(\alpha p_\Gamma,\mu_\Gamma\right)_\Gamma + \left(\tilde{s}_\Gamma\frac{\partial p_\Gamma}{\partial t},\mu_\Gamma\right)_\Gamma + b_\Gamma\left(\tilde{\boldsymbol{u}}_\Gamma,\mu_\Gamma\right) &= \left(g,\mu_\Gamma\right)_\Gamma, && \forall \mu_\Gamma\in\Lambda,\\
\left(p\left(\cdot,0\right),\mu\right)_\Omega &= \left(p_0,\mu\right)_\Omega, && \forall \mu\in M,\\
\left(p_\Gamma\left(\cdot,0\right),\mu_\Gamma\right)_\Gamma &= \left(p_{0|\Gamma},\mu_\Gamma\right)_\Gamma, && \forall \mu_\Gamma\in\Lambda.
\end{aligned} \tag{B.8}$$

Using the conforming triangulation $\mathscr{K}_h$ of Ω into rectangles and the nonuniform partition in time defined in previous sections, we obtain the fully discrete problem of (B.9) (with zero order discontinuous Galerkin method in time and mixed finite elements in space):

For $n = 1,\ldots,N$, find $(p_h^n, \boldsymbol{u}_h^n, p_{h,\Gamma}^n, \tilde{\boldsymbol{u}}_{h,\Gamma}^n)$ such that

$$\begin{aligned}
a\left(\boldsymbol{u}_h^{n+1},\boldsymbol{\nu}_h\right) - b\left(\boldsymbol{\nu}_h,p_h^{n+1}\right) + d(p_{h,\Gamma}^{n+1},\boldsymbol{\nu}_h) &= 0, && \forall \boldsymbol{\nu}_h\in\Sigma_h,\\
\left(s\,p_h^{n+1},\mu_h\right)_\Omega + \Delta t^n b\left(\boldsymbol{u}_h^{n+1},\mu_h\right) &= \left(s\,p_h^{n},\mu_h\right)_\Omega + \int_{t^n}^{t^{n+1}} (f,\mu_h)_\Omega, && \forall \mu_h\in M_h,\\
a_\Gamma\left(\tilde{\boldsymbol{u}}_{h,\Gamma}^{n+1},\boldsymbol{\nu}_{h,\Gamma}\right) - b_\Gamma\left(\boldsymbol{\nu}_{h,\Gamma},p_{h,\Gamma}^{n+1}\right) &= 0, && \forall \boldsymbol{\nu}_{h,\Gamma}\in\Sigma_{\Gamma,h},\\
-\Delta t^n\, d(\mu_{h,\Gamma},\boldsymbol{u}_h^{n+1}) + \Delta t^n\left(\alpha p_{h,\Gamma}^{n+1},\mu_{h,\Gamma}\right)_\Gamma + \left(\tilde{s}_\Gamma p_{h,\Gamma}^{n+1},\mu_{h,\Gamma}\right)_\Gamma + \Delta t^n b_\Gamma\left(\tilde{\boldsymbol{u}}_{h,\Gamma}^{n+1},\mu_{h,\Gamma}\right)&\\
= \left(\tilde{s}_\Gamma p_{h,\Gamma}^{n},\mu_{h,\Gamma}\right)_\Gamma + \int_{t^n}^{t^{n+1}} (g,\mu_{h,\Gamma})_\Gamma, && \forall \mu_{h,\Gamma}\in\Lambda_h,\\
\left(p_h^0,\mu_h\right)_\Omega &= \left(p_0,\mu_h\right)_\Omega, && \forall \mu_h\in M_h,\\
\left(p_{h,\Gamma}^0,\mu_{h,\Gamma}\right)_\Gamma &= \left(p_{0|\Gamma},\mu_{h,\Gamma}\right)_\Gamma, && \forall \mu_{h,\Gamma}\in\Lambda_h,
\end{aligned} \tag{B.9}$$

where $\Sigma_h \times M_h$ and $\Sigma_{\Gamma,h} \times \Lambda_h$ are 2D and 1D respectively mixed finite elements of Raviart-Thomas type of lowest order. Proceeding as in the previous sections, we obtain a matrix form of (B.9) as follows:

$$\begin{bmatrix} \boldsymbol{A} & \boldsymbol{B} & 0 & \boldsymbol{D} \\ \boldsymbol{B}^T & -\boldsymbol{M} & 0 & 0 \\ 0 & 0 & \boldsymbol{A}_\Gamma & \boldsymbol{B}_\Gamma \\ \boldsymbol{D}^T & 0 & \boldsymbol{B}_\Gamma^T & -\boldsymbol{M}_\alpha - \boldsymbol{M}_\Gamma \end{bmatrix} \begin{bmatrix} \boldsymbol{u}^{n+1} \\ \boldsymbol{p}^{n+1} \\ \tilde{\boldsymbol{u}}_\Gamma^{n+1} \\ \boldsymbol{p}_\Gamma^{n+1} \end{bmatrix} = \begin{bmatrix} 0 \\ -\boldsymbol{M}\boldsymbol{p}^n - \boldsymbol{F}^{n+1} \\ 0 \\ -\boldsymbol{M}\boldsymbol{p}_\Gamma^n - \boldsymbol{G}^{n+1} \end{bmatrix}, \tag{B.10}$$

where

- $\boldsymbol{u}^n, \boldsymbol{p}^n, \tilde{\boldsymbol{u}}_\Gamma^n$ and $\boldsymbol{p}_\Gamma^n$ are vectors of the degrees of freedom of $\boldsymbol{u}_h, p_h, \tilde{\boldsymbol{u}}_{h,\Gamma}$ and $p_{h,\Gamma}$ in their associated finite dimensional spaces.
- $\boldsymbol{A}, \boldsymbol{B}$ and $\boldsymbol{M}$ are defined as in Section B.2, but now for the interior edges $E \subset \Omega$ only (as there is the 1D problem defined on the boundary).
- $\boldsymbol{A}_\Gamma, \boldsymbol{B}_\Gamma$ and $\boldsymbol{M}_\Gamma$ can be seen as the 1D counterparts of $\boldsymbol{A}, \boldsymbol{B}$ and $\boldsymbol{M}$ respectively and one can easily calculate the coefficients of these matrices following steps similar to those of Section B.4.
- $\boldsymbol{D}$ represents the coupling term between the normal flux and the pressure trace on the boundary,
$$\boldsymbol{D} = d(\chi_E, \boldsymbol{w}_E)_{E \in \mathscr{E}_h \cap \Gamma},$$
where χ_E is a basis function of Λ_h and $\boldsymbol{w}_E$ is a basis function of Σ_h.
- $\boldsymbol{M}_\alpha$ is a diagonal matrix defined by
$$\boldsymbol{M}_\alpha = (\alpha \chi_E, \chi_F)_{E,F \in \mathscr{E}_h \cap \Gamma}.$$
- $\boldsymbol{F}$ and $\boldsymbol{G}$ are vectors representing the source term and the Ventcell data,
$$\boldsymbol{F}^{n+1} = \left(\int_{t^n}^{t^{n+1}} \int_K f \right)_{K \in \mathscr{K}_h},$$
$$\boldsymbol{G}^{n+1} = \left(\int_{t^n}^{t^{n+1}} \int_E g \right)_{E \in \mathscr{E}_h \cap \Gamma}.$$

Appendix C

Space-time domain decomposition with time windows

In many applications, such as the simulation of contaminant transport around a nuclear waste repository site, the simulation of radioactive transport for a CO2 geological storage, etc. one has to deal with a dynamic system for a very long time interval $(0,T)$. In this case, the discretization on the whole time interval may be very expensive for implementation. In addition, if a waveform relaxation algorithm or a space-time domain decomposition method is used for a large T, it will lead to a slow convergence rate (see, e.g. [116] and Chapter 2). A technique called windowing waveform relaxation was introduced to handle this problem, in which one decomposes $(0,T)$ into subintervals, namely time windows and perform the iteration on each time window successively. Such a technique was incorporated in the context of Optimized Schwarz Waveform Relaxation (OSWR) methods, such as for the 1D wave equation [48], the viscous shallow water equation [91], the 1D or 2D convection-diffusion equation involved in ocean-atmostphere coupling [17, 62], the advection-diffusion-reaction equation in porous media [60], etc. The question of how to choose an efficient window length in practical computation was addressed in [116, 77] for waveform relaxation methods and in [48] for OSWR methods.

In this appendix, we explain in detail how time windows are used in the context of the two space-time domain decomposition methods presented in Chapters 2 and 4. The formulations are derived through a space-time interface problem, which facilitates the use of different iterative solvers, such as Jacobi iterations, GMRES, etc. An important point is that an adapted initial guess for the $(m+1)^{\text{th}}$ time window calculated from the m^{th} time window can be used to improve the convergence in the time windows, which enhances the global performance on the whole time interval (see [62]).

We first recall the model problem and briefly describe the two methods involved. Consider the time-dependent diffusion equation in mixed form:

$$\begin{aligned} \phi\,\partial_t c + \operatorname{div} \boldsymbol{r} &= f, \quad && \text{in } \Omega \times (0,T), \\ \nabla c + \boldsymbol{D}^{-1}\boldsymbol{r} &= 0, && \text{in } \Omega \times (0,T), \\ c(\cdot,0) &= c_-, && \text{in } \Omega. \end{aligned} \tag{C.1}$$

(we have omitted the boundary conditions as it is not the main interest here). For simplicity, we decompose Ω into two nonoverlapping subdomains Ω_1 and Ω_2 with an interface $\Gamma = \partial\Omega_1 \cap \partial\Omega_2 \cap \Omega$. Problem (C.1) can be formulated as an equivalent

multidomain problem:

$$\begin{aligned} \phi_i \partial_t c_i + \operatorname{div} \boldsymbol{r}_i &= f \quad \text{in } \Omega_i \times (0,T), \\ \nabla c_i + \boldsymbol{D}_i^{-1} \boldsymbol{r}_i &= 0 \quad \text{in } \Omega_i \times (0,T), \quad \text{for } i = 1,2, \\ c_i(0) &= c_0 \quad \text{in } \Omega_i, \end{aligned}$$

coupled with the transmission conditions on the interface

$$\begin{aligned} c_1 = c_2, &\quad \text{on } \Gamma \times (0,T), \\ \boldsymbol{r}_1 \cdot \boldsymbol{n}_1 + \boldsymbol{r}_2 \cdot \boldsymbol{n}_2 = 0, &\quad \text{on } \Gamma \times (0,T), \end{aligned} \tag{C.2}$$

where $\boldsymbol{n}_i$, $i = 1,2$, is the unit outward normal on $\partial\Omega_i$.

In the OSWR methods, one replaces (C.2) by equivalent transmission conditions:

$$\begin{aligned} \mathfrak{B}_1^{OSWR} p_1 &= \mathfrak{B}_1^{OSWR} p_2 \\ \mathfrak{B}_2^{OSWR} p_2 &= \mathfrak{B}_2^{OSWR} p_1 \end{aligned} \quad \text{on } \Gamma \times (0,T), \tag{C.3}$$

where $\mathfrak{B}_i^{OSWR}$, $i = 1,2$, are optimized operators representing Robin or Ventcell transmission conditions (cf. Appendix A).

We now give a short description of the two space-time domain decomposition methods that are studied in Chapters 2 and 4.

Method 1: using the time-dependent Steklov-Poincaré operator

In the first method, we impose Dirichlet boundary conditions, representing the equality of the concentration trace, on the interface to solve the time-dependent subdomain problem. Then we calculate the resulting flux and enforce it to be continue across the space-time interface. This leads to an interface problem in a form:

$$\mathscr{S}(\lambda) = \chi(f, c_0), \quad \text{on } \Gamma \times (0,T), \tag{C.4}$$

where λ representing the concentration trace on the interface, $\mathscr{S} = \mathscr{S}_1 + \mathscr{S}_2$ is the time-dependent Steklov-Poincaré operator and is linear in λ, and χ is an operator affine in each component c_0 and f (for precise definitions of $\mathscr{S}$ and χ, see Chapter 2). Importantly, $\mathscr{S}(\lambda)$ is the jump of the flux across the interface, obtained by solving the subdomain problems with interface Dirichlet data λ and with a zero source term and a zero initial condition; while $\chi(f, c_0)$ is also the jump of the flux but obtained by solving the subdomain problems with zero Dirichlet data on the interface and with a source term f and an initial data c_0.

The discrete counterpart of the interface problem is solved by using an iterative method: one start with an initial guess λ_h, which is a vector representing the approximation in space and in time of the concentration trace, and solve the time-dependent subdomain problems to calculate $\mathscr{S}_h(\lambda_h)$, then iterate until convergence. Note that the right-hand side is computed once as it does not depend on λ_h.

Method 2: using the OSWR method with Robin or Ventcell transmission conditions

In the second method, we impose Robin or Ventcell boundary conditions on the interface

$$\mathfrak{B}_i^{OSWR} p_i = \xi_i, \quad \text{on } \left(\partial\Omega_i \cap \Gamma\right) \times (0,T),\ i = 1,2,$$

and solve the corresponding time-dependent subdomain problem. The resulting solutions are enforced to verify the transmission conditions (C.3), which leads to a space-time interface problem with two Lagrange multipliers (see Chapters 2 and 4):

$$\mathscr{S}_{OSWR}\begin{pmatrix} \xi_1 \\ \xi_2 \end{pmatrix} = \chi_{OSWR}(f, c_0), \quad \text{on } \Gamma \times (0,T). \tag{C.5}$$

Here $\mathscr{S}_{OSWR}$ is the Robin-to-Robin or Ventcell-to-Ventcell operators, calculating by first solving the subdomain problem with Robin/Ventcell boundary data ξ_i (for Ω_i), $i = 1, 2$, and with a zero source term and a zero intial condition, then computing the jumps of the Robin/Ventcell terms for each subdomain. A similar calculation is applied for $\chi_{OSWR}(f, c_0)$ but now with zero Robin/Ventcell boundary data, a source term f and an initial data c_0.

As in Method 1, we solve iteratively by starting with a space-time initial guess as a pair of vectors $(\xi_{h,1}, \xi_{h,2})$, then iterating until the algorithm converges.

Time windows for the space-time interface problem

Both methods presented above can be formulated as a space-time interface problem in a form:

$$\underline{\mathscr{S}}\vartheta = \underline{\chi}(f, c_0), \quad \text{on } \Gamma \times (0,T), \tag{C.6}$$

where the left and right hand sides are computed by solving the associated subdomain problems with Dirichlet/Robin/Ventcell boundary conditions on the interface.

We now use time windows for solving the interface problem (C.6). Toward this end, we divide $(0,T)$ into M sub-intervals

$$(0,T) = \bigcup_{m=1}^{M} \left(T^{m-1}, T^m\right), \text{ with } T^0 = 0 \text{ and } T^M = T.$$

Instead of solving (C.6) on the whole time interval $(0,T)$, now we solve it successively in each time window with an updated initial condition given by the solution of the previous time window. In particular, the interface problem solved on the $(m+1)^{\text{th}}$ time window is defined by

$$\underline{\mathscr{S}}\vartheta_{m+1} = \underline{\chi}\left(f, c(\cdot, T^m)\right), \quad \text{on } \Gamma \times (T^m, T^{m+1}),\ m = 0, \ldots, M-1, \tag{C.7}$$

where $c(\cdot, T^m)$ is the converged solution (i.e. corresponding to a relative residual of a iterative solver (GMRES) less than a fixed tolerance) at the final time of the m^{th} time window (T^{m-1}, T^m):

$$c(\cdot, T^0) = c_0,$$

and

$$c(\cdot, T^m) = \begin{cases} c_1(\cdot, T^m) & \text{in } \Omega_1, \\ c_2(\cdot, T^m) & \text{in } \Omega_2, \end{cases} \qquad \forall m = 1, \ldots, M-1.$$

Importantly, instead of using a random initial guess for ϑ_{m+1}, we compute an adapted value obtained from the solution at the previous time window. Such an adapted initial guess is closer to the converged ϑ_{m+1} than a random. In order to

explain how to construct this adapted initial guess, we consider the fully discrete interface problem and denote by $\vartheta_{h,m}$ the discrete counterpart of $\vartheta_{h,m}$. In particular, $\vartheta_{h,m}$ is a vector corresponding to discretizations in space and in time on the interface:

$$\vartheta_{h,m} = \left(\vartheta_h^{m,1}, \ldots, \vartheta_h^{m,N_m}\right),$$

where N_m is the number of time subintervals corresponding to the partition in time of the m^{th} time window $\left(T^{m-1}, T^m\right)$:

$$\left(T^{m-1}, T^m\right) = \bigcup_{n=1}^{N_m} \left(t^{m,n-1}, t^{m,n}\right), \text{ for } m = 1, \ldots, M.$$

Assume now we have solved the interface problem (C.7) on the m^{th} time window and obtained the converged interface solution $\vartheta_{h,m}$. An adapted initial guess θ_{m+1} for the $(m+1)^{\text{th}}$ time window, (T^m, T^{m+1}), is defined by using values of $\vartheta_{h,m}$ at its final time T^m and duplicating them N_{m+1} times:

$$\theta_{m+1} = (\underbrace{\vartheta_h^{m,N_m}, \ldots, \vartheta_h^{m,N_m}}_{N_{m+1} \text{ times}}).$$

Thus θ_{m+1} incorporates the information of the solution at the initial time T^m of the $(m+1)^{\text{th}}$ time window and obviously, such a choice is better than a zero initial guess for the convergence of the associated iterative algorithm.

Bibliography

[1] Y. Achdou, C. Japhet, Y. Maday, and F. Nataf, *A New Interface Cement Equilibrated Mortar (NICEM) method with Robin interface conditions : the P1 finite element case*, M3AS, 23 (1991), pp. 2253–2292.

[2] ——, *A new cement to glue non-conforming grids with Robin interface conditions: the finite volume case*, Numer. Math., 92 (2002), pp. 593–620.

[3] V. I. Agoshkov, *Poincaré-Steklov's operators and domain decomposition methods in finite-dimensional spaces*, in First International Symposium on Domain Decomposition Methods for Partial Differential Equations (Paris, 1987), SIAM, Philadelphia, PA, 1988, pp. 73–112.

[4] V. I. Agoshkov and V. I. Lebedev, *Poincaré-Steklov operators and methods of partition of the domain in variational problems*, in Computational processes and systems, No. 2, "Nauka", Moscow, 1985, pp. 173–227.

[5] C. Alboin, J. Jaffré, J. E. Roberts, and C. Serres, *Modeling fractures as interfaces for flow and transport in porous media*, in Fluid flow and transport in porous media: mathematical and numerical treatment (South Hadley, MA, 2001), vol. 295 of Contemp. Math., Amer. Math. Soc., Providence, RI, 2002, pp. 13–24.

[6] L. Amir, *Modèles couplés en milieu poreux: transport réactif et fractures*, PhD thesis, University of Paris Dauphine, 2008.

[7] L. Amir, M. Kern, V. Martin, and J. E. Roberts, *Décomposition de domaine pour un milieu poreux fracturé: un modéle en 3D avec fractures qui s'intersectent*, Arima, 5 (2006), pp. 11–25.

[8] P. Angot, F. Boyer, and F. Hubert, *Asymptotic and numerical modelling of flows in fractured porous media*, M2AN Math. Model. Numer. Anal., 43 (2009), pp. 239–275.

[9] X. Antoine, C. Besse, and P. Klein, *Absorbing boundary conditions for the two-dimensional Schrödinger equation with an exterior potential. Part I: Construction and a priori estimates*, Math. Models Methods Appl. Sci., 22 (2012), pp. 1250026, 38.

[10] P. Bastian, Z. Chen, R. E. Ewing, R. Helmig, H. Jakobs, and V. Reichenberger, *Numerical simulation of multiphase flow in fractured porous media*, in Numerical treatment of multiphase flows in porous media (Beijing, 1999), vol. 552 of Lecture Notes in Phys., Springer, Berlin, 2000, pp. 50–68.

[11] J. BEAR, *Dynamics of fluids in porous media*, Dover, New York, 1988.

[12] D. BENNEQUIN, M. J. GANDER, AND L. HALPERN, *A homographic best approximation problem with application to optimized Schwarz waveform relaxation*, Math. Comp., 78 (2009), pp. 185–223.

[13] C. BERNARDI, Y. MADAY, AND A. T. PATERA, *A new nonconforming approach to domain decomposition: the mortar element method*, in Nonlinear partial differential equations and their applications. Collège de France Seminar, Vol. XI (Paris, 1989–1991), vol. 299 of Pitman Res. Notes Math. Ser., Longman Sci. Tech., Harlow, 1994, pp. 13–51.

[14] P. E. BJØRSTAD, J. BRÆKHUS, AND A. HVIDSTEN, *Parallel substructuring algorithms in structural analysis, direct and iterative methods*, in Fourth International Symposium on Domain Decomposition Methods for Partial Differential Equations (Moscow, 1990), SIAM, Philadelphia, PA, 1991, pp. 321–340.

[15] P. E. BJØRSTAD AND O. B. WIDLUND, *Solving elliptic problems on regions partitioned into substructures*, in Elliptic problem solvers, II (Monterey, Calif., 1983), Academic Press, Orlando, FL, 1984, pp. 245–255.

[16] E. BLAYO, L. DEBREU, AND F. LEMARIÉ, *Toward an optimized global-in-time Schwarz algorithm for diffusion equations with discontinuous and spatially variable coefficients. Part 1: the constant coefficients case*, Accepted in ETNA.

[17] E. BLAYO, L. HALPERN, AND C. JAPHET, *Optimized Schwarz waveform relaxation algorithms with nonconforming time discretization for coupling convection-diffusion problems with discontinuous coefficients*, in Domain decomposition methods in science and engineering XVI, vol. 55 of Lect. Notes Comput. Sci. Eng., Springer, Berlin, 2007, pp. 267–274.

[18] D. BOFFI AND L. GASTALDI, *Analysis of finite element approximation of evolution problems in mixed form*, SIAM J. Numer. Anal., 42 (2004), pp. 1502–1526.

[19] J.-F. BOURGAT, R. GLOWINSKI, P. LE TALLEC, AND M. VIDRASCU, *Variational formulation and algorithm for trace operator in domain decomposition calculations*, in Domain decomposition methods (Los Angeles, CA, 1988), SIAM, Philadelphia, PA, 1989, pp. 3–16.

[20] J. H. BRAMBLE, J. E. PASCIAK, AND A. H. SCHATZ, *The construction of preconditioners for elliptic problems by substructuring. I*, Math. Comp., 47 (1986), pp. 103–134.

[21] F. BREZZI, *On the existence, uniqueness and approximation of saddle-point problems arising from lagrangian multipliers*, RAIRO Anal. Numér., 8 (1974), pp. 129–151.

[22] F. BREZZI AND M. FORTIN, *Mixed and hybrid finite elements methods*, Springer-Verlag, New York, 1991.

[23] X.-C. CAI, *Additive Schwarz algorithms for parabolic convection-diffusion equations*, Numer. Math., 60 (1991), pp. 41–61.

[24] GUY CHAVENT, *Mathematical models and finite elements for reservoir simulation : single phase, multiphase, and multicomponent flows through porous media*, North-Holland Sole distributors for the U.S.A. and Canada, Elsevier Science Pub. Co, Amsterdam New York New York, N.Y., U.S.A, 1986.

[25] G. CHAVENT AND J. E. ROBERTS, *A unified physical presentation of mixed, mixed-hybrid finite elements and usual finite differences for the determination of velocities in waterflow problems*, Advances in Water Resources, 14 (1991), pp. 329–348.

[26] Z. CHEN, G. HUAN, AND Y. MA, *Computational methods for multiphase flows in porous media*, Society for Industrial and Applied Mathematics, Philadelphia, 2006.

[27] A. CHERTOCK AND A. KURGANOV, *On splitting-based numerical methods for convection-diffusion equations*, in Numerical methods for balance laws, vol. 24 of Quad. Mat., Dept. Math., Seconda Univ. Napoli, Caserta, 2009, pp. 303–343.

[28] L. C. COWSAR, J. MANDEL, AND M. F. WHEELER, *Balancing domain decomposition for mixed finite elements*, Math. Comp., 64 (1995), pp. 989–1015.

[29] C. DAWSON, *Godunov-mixed methods for advection-diffusion equations in multidimensions*, SIAM J. Numer. Anal., 30 (1993), pp. 1315–1332.

[30] ——, *High resolution upwind-mixed finite element methods for advection-diffusion equations with variable time-stepping*, Numer. Methods Partial Differential Equations, 11 (1995), pp. 525–538.

[31] Y.-H. DE ROECK AND P. LE TALLEC, *Analysis and test of a local domain-decomposition preconditioner*, in Fourth International Symposium on Domain Decomposition Methods for Partial Differential Equations (Moscow, 1990), SIAM, Philadelphia, PA, 1991, pp. 112–128.

[32] J. DOUGLAS, JR., R. E. EWING, AND M. F. WHEELER, *The approximation of the pressure by a mixed method in the simulation of miscible displacement*, RAIRO Anal. Numér., 17 (1983), pp. 17–33.

[33] J. DOUGLAS, JR., P. J. PAES-LEME, J. E. ROBERTS, AND J. P. WANG, *A parallel iterative procedure applicable to the approximate solution of second order partial differential equations by mixed finite element methods*, Numer. Math., 65 (1993), pp. 95–108.

[34] J. DOUGLAS, JR. AND J. E. ROBERTS, *Numerical methods for a model for compressible miscible displacement in porous media.*, Math. Comp., 41 (1983), pp. 441–459.

[35] M. DRYJA, *Substructuring methods for parabolic problems*, in Fourth International Symposium on Domain Decomposition Methods for Partial Differential Equations (Moscow, 1990), SIAM, Philadelphia, PA, 1991, pp. 264–271.

[36] O. DUBOIS, *Optimized Schwarz methods for the advection-diffusion equation and for problems with discontinuous coefficients*, PhD thesis, McGill University, 2007.

[37] L. C. EVANS, *Partial differential equations*, American Mathematical Society, Providence, 1998.

[38] R. E. EWING, R. D. LAZAROV, T. F. RUSSELL, AND P. S. VASSILEVSKI, *Local refinement via domain decomposition techniques for mixed finite element methods with rectangular Raviart-Thomas elements*, in Third International Symposium on Domain Decomposition Methods for Partial Differential Equations (Houston, TX, 1989), SIAM, Philadelphia, PA, 1990, pp. 98–114.

[39] R. E. EWING, T. F. RUSSELL, AND M. F. WHEELER, *Convergence analysis of an approximation of miscible displacement in porous media by mixed finite elements and a modified method of characteristics*, Comput. Methods Appl. Mech. Engrg., 47 (1984).

[40] I. FAILLE, E. FLAURAUD, S. NATAF, F.AND PÉGAZ-FIORNET, F. SCHNEIDER, AND F. WILLIEN, *A new fault model in geological basin modelling. Application of finite volume scheme and domain decomposition methods*, in Finite volumes for complex applications, III (Porquerolles, 2002), Hermes Sci. Publ., Paris, 2002, pp. 529–536.

[41] N. FRIH, V. MARTIN, J. E. ROBERTS, AND A. SAÂDA, *Modeling fractures as interfaces with nonmatching grids*, Computational Geosciences, 16 (2012), pp. 1043–1060.

[42] A. FUMAGALLI AND A. SCOTTI, *Numerical modelling of multiphase subsurface flow in the presence of fractures*, Commun. Appl. Ind. Math., 3 (2012), pp. e–380, 23.

[43] M. J GANDER, *Personal communication*.

[44] M. J. GANDER, *Optimized Schwarz methods*, SIAM J. Numer. Anal., 44 (2006), pp. 699–731.

[45] M. J. GANDER AND L. HALPERN, *Optimized Schwarz waveform relaxation methods for advection reaction diffusion problems*, SIAM J. Numer. Anal., 45 (2007), pp. 666–697.

[46] M. J. GANDER, L. HALPERN, AND M. KERN, *A Schwarz waveform relaxation method for advection-diffusion-reaction problems with discontinuous coefficients and nonmatching grids*, in Domain decomposition methods in science and engineering XVI, vol. 55 of Lect. Notes Comput. Sci. Eng., Springer, Berlin, 2007, pp. 283–290.

[47] M. J. GANDER, L. HALPERN, AND F. NATAF, *Optimal convergence for overlapping and non-overlapping Schwarz waveform relaxation*, in Proceedings of the 11th International Conference on Domain Decomposition Methods, C-H. Lai, P. Bjørstad, M. Cross, and O. Widlund, eds., 1999, pp. 27–36.

[48] ——, *Optimal Schwarz waveform relaxation for the one dimensional wave equation*, SIAM J. Numer. Anal., 41 (2003), pp. 1643–1681.

[49] M. J. GANDER AND C. JAPHET, *Algorithm PANG: Software for non-matching grid projections in 2d and 3d with linear complexity*, TOMS, (2013).

[50] M. J. GANDER, C. JAPHET, Y. MADAY, AND F. NATAF, *A new cement to glue nonconforming grids with Robin interface conditions: the finite element case*, in Domain decomposition methods in science and engineering, vol. 40 of Lect. Notes Comput. Sci. Eng., Springer, Berlin, 2005, pp. 259–266.

[51] M. J. GANDER AND A. M. STUART, *Space-time continuous analysis of waveform relaxation for the heat equation*, SIAM J. Sci. Comput., 19 (1998), pp. 2014–2031.

[52] L. GASTALDI, *A domain decomposition for the transport equation*, in Domain decomposition methods in science and engineering (Como, 1992), vol. 157 of Contemp. Math., Amer. Math. Soc., Providence, RI, 1994, pp. 97–102.

[53] A. GENTY, G. MATHIEU, AND E. WEETJENS, *PAMINA: Performance assessment methodologies in application to guide the development of the safety case. Final report on benchmark calculation in clay*, Deliverable D-N^o: 4.2.4 of the European Contract Number FP6-036404, (2009). Available at http://www.ip-pamina.eu/downloads/pamina4.2.4.pdf.

[54] E. GILADI AND H. B. KELLER, *Space-time domain decomposition for parabolic problems*, Numer. Math., 93 (2002), pp. 279–313.

[55] R. GLOWINSKI, Q. V. DINH, AND J. PERIAUX, *Domain decomposition methods for nonlinear problems in fluid dynamics*, Comput. Methods Appl. Mech. Engrg., 40 (1983), pp. 27–109.

[56] R. GLOWINSKI AND M. F. WHEELER, *Domain decomposition and mixed finite element methods for elliptic problems*, in First International Symposium on Domain Decomposition Methods for Partial Differential Equations (Paris, 1987), SIAM, Philadelphia, PA, 1988, pp. 144–172.

[57] F. HAEBERLEIN, *Time space domain decomposition methods for reactive transport - Application to CO_2 geological storage*, PhD thesis, Institut Galilée, Université Paris 13, 2011.

[58] L. HALPERN, *Artificial boundary conditions for the linear advection diffusion equation*, Math. Comp., 46 (1986), pp. 425–438.

[59] L. HALPERN AND C. JAPHET, *Discontinuous Galerkin and Nonconforming in Time Optimized Schwarz Waveform Relaxation for Heterogeneous Problems*, in Decomposition Methods in Science and Engineering XVII, U. Langer, M. Discacciati, D.E. Keyes, O.B. Widlund, and W. Zulehner, eds., vol. 60 of Lecture Notes in Computational Science and Engineering, Springer, 2008, pp. 211–219.

[60] L. HALPERN, C. JAPHET, AND P. OMNES, *Nonconforming in time domain decomposition method for porous media applications.*, in Proceedings of the 5th European Conference on Computational Fluid Dynamics ECCOMAS CFD 2010., J. C. F. Pereira and A. Sequeira, eds., Lisbon, Portugal, 2010.

[61] L. HALPERN, C. JAPHET, AND J. SZEFTEL, *Discontinuous Galerkin and nonconforming in time optimized Schwarz waveform relaxation*, in Domain decomposition methods in science and engineering XIX, vol. 78 of Lect. Notes Comput. Sci. Eng., Springer, Heidelberg, 2011, pp. 133–140.

[62] ——, *Optimized Schwarz waveform relaxation and discontinuous Galerkin time stepping for heterogeneous problems*, SIAM J. Numer. Anal., 50 (2012), pp. 2588–2611.

[63] K. HELLAN, *Analysis of elastic plates in flexure by a simplified finite element method*, Acta Polytechnica Scandinavia, Civil Engineering Series, 46 (1967), pp. 1–19.

[64] L. R. HERRMANN, *Finite element bending analysis for plates*, J. Eng. Mech. Div. ASCE, 93 (1967), pp. 13–26.

[65] T. T. P. HOANG, J. JAFFRÉ, C. JAPHET, M. KERN, AND J. E ROBERTS, *Space-time domain decomposition methods for diffusion problems in mixed formulations*.

[66] T. T. P. HOANG, J. JAFFRÉ, C. JAPHET, M. KERN, AND J. E. ROBERTS, *Space-time domain decomposition methods for diffusion problems in mixed formulations*, SIAM J. Numer. Anal., (Accepted).

[67] U. HORNUNG, ed., *Homogenization and porous media*, vol. 6 of Interdisciplinary Applied Mathematics, Springer-Verlag, New York, 1997.

[68] W. HUNDSDORFER AND J.G. VERWER, *Numerical solution of time-dependent advection-diffusion-reaction equations*, Springer, Berlin Heidelberg New York etc, 2010.

[69] J. JANSSEN AND S. VANDEWALLE, *Multigrid waveform relaxation of spatial finite element meshes: the continuous-time case*, SIAM J. Numer. Anal., 33 (1996), pp. 456–474.

[70] ——, *On SOR waveform relaxation methods*, SIAM J. Numer. Anal., 34 (1997), pp. 2456–2481.

[71] C. JAPHET, *Méthode de décomposition de domaine et conditions aux limites artificielles en mécanique des fluides: méthode optimisée d'Ordre 2*, PhD thesis, University of Paris XIII, 1998.

[72] ——, *Optimized Krylov-Ventcell method. Application to convection-diffusion problems*, in Domain decomposition methods in science and engineering IX, U. Bjørstad, M. Espedal, and D.E. Keyes, eds., John Wiley & Sons Ltd, 1998, pp. 382–389.

[73] C. JAPHET, Y. MADAY, AND F. NATAF, *A new interface cement equilibrated mortar method with Ventcel conditions*, in Proceedings of the 21st International Conference on Domain Decomposition Methods., 2013, to appear.

[74] C. JAPHET, F. NATAF, AND F. ROGIER, *The Optimized Order 2 method. application to convection-diffusion problems*, Future Gener. Comp. Sy., 18 (2001), pp. 17–30.

[75] C. JAPHET AND P. OMNES, *Optimized Schwarz waveform relaxation for porous media applications.*, in Proceedings of the 20th International Conference on Domain Decomposition Methods., 2013.

[76] R. JELTSCH AND B. POHL, *Waveform relaxation with overlapping splittings*, SIAM J. Sci. Comput., 16 (1995), pp. 40–49.

[77] Y.-L. JIANG, *Windowing waveform relaxation of initial value problems*, Acta Math. Appl. Sin. Engl. Ser., 22 (2006), pp. 575–588.

[78] Y. A. KUZNETSOV, *Domain decomposition methods for unsteady convection-diffusion problems*, in Computing methods in applied sciences and engineering (Paris, 1990), SIAM, Philadelphia, PA, 1990, pp. 211–227.

[79] F. KWOK, *Neumann-Neumann waveform relaxation for the time-dependent heat equation.*, in Proceedings of the 21st International Conference on Domain Decomposition Methods, 2013, to appear.

[80] P. LE TALLEC, Y. H. DE ROECK, AND M. VIDRASCU, *Domain decomposition methods for large linearly elliptic three-dimensional problems*, J. Comput. Appl. Math., 34 (1991), pp. 93–117.

[81] J. LI, T. ARBOGAST, AND Y. HUANG, *Mixed methods using standard conforming finite elements*, Comput. Methods Appl. Mech. Engrg., 198 (2009), pp. 680–692.

[82] J.-L. LIONS AND E. MAGENES, *Problèmes aux limites non homogènes et applications. Vol. 1*, Travaux et Recherches Mathématiques, No. 17, Dunod, Paris, 1968.

[83] P.-L. LIONS, *On the Schwarz alternating method. I*, in First International Symposium on Domain Decomposition Methods for Partial Differential Equations, G. A. Meurant R. Glowinski, G. H. Golub and J. Périaux, eds., Philadelphia, PA, SIAM, 1988, pp. 1–42.

[84] ——, *On the Schwarz alternating method. II*, in Second International Symposium on Domain Decomposition Methods for Partial Differential Equations, J. Périaux T. Chan, R. Glowinski and O. Widlund, eds., Philadelphia, PA, SIAM, 1989, pp. 47–70.

[85] ——, *On the Schwarz alternating method. III: a variant for nonoverlapping subdomains*, in Third International Symposium on Domain Decomposition Methods for Partial Differential Equations, held in Houston, Texas, March 20-22, 1989„ J. Périaux T. F. Chan, R. Glowinski and O. Widlund, eds., Philadelphia, PA, SIAM, 1990, pp. 202–223.

[86] A. LUMSDAINE AND D. WU, *Krylov subspace acceleration of waveform relaxation*, SIAM J. Numer. Anal., 41 (2003), pp. 90–111.

[87] C. MAKRIDAKIS AND R. H. NOCHETTO, *A posteriori error analysis for higher order dissipative methods for evolution problems*, Numer. Math., 104 (2006), pp. 489–514.

[88] J. MANDEL, *Balancing domain decomposition*, Comm. Numer. Methods Engrg., 9 (1993), pp. 233–241.

[89] J. MANDEL AND M. BREZINA, *Balancing domain decomposition for problems with large jumps in coefficients*, Math. Comp., 65 (1996), pp. 1387–1401.

[90] V. MARTIN, *An optimized Schwarz waveform relaxation method for the unsteady convection diffusion equation in two dimensions*, Appl. Numer. Math., 52 (2005), pp. 401–428.

[91] ——, *Schwarz waveform relaxation method for the viscous shallow water equations*, in Domain decomposition methods in science and engineering, vol. 40 of Lect. Notes Comput. Sci. Eng., Springer, Berlin, 2005, pp. 653–660.

[92] V. MARTIN, J. JAFFRÉ, AND J. E. ROBERTS, *Modeling fractures and barriers as interfaces for flow in porous media*, SIAM J. Sci. Comput., 26 (2005), pp. 1667–1691 (electronic).

[93] W. MARTINSON AND P. BARTON, *A differentiation index for partial differential-algebraic equations*, SIAM Journal on Scientific Computing, 21 (2000), pp. 2295–2315.

[94] T. MATHEW, *Domain Decomposition Methods for the Numerical Solution of Partial Differential Equations*, vol. 61 of Lecture Notes in Computational Science and Engineering, Springer, 2008.

[95] A. MAZZIA, L. BERGAMASCHI, C. N. DAWSON, AND M. PUTTI, *Godunov mixed methods on triangular grids for advection-dispersion equations*, Comput. Geosci., 6 (2002), pp. 123–139.

[96] F. NATAF AND F. ROGIER, *Factorization of the convection-diffusion operator and the Schwarz algorithm*, Math. Models Methods Appl. Sci., 5 (1995), pp. 67–93.

[97] F. NATAF, F. ROGIER, AND E. DE STURLER, *Optimal interface conditions for domain decomposition methods*, I.R. n^{o}301, CMAP (Ecole Polytechnique).

[98] O. NEVANLINNA, *Power bounded prolongations and Picard-Lindelöf iteration*, Numer. Math., 58 (1990), pp. 479–501.

[99] J. E. PASCIAK, *Domain decomposition preconditioners for elliptic problems in two and three dimensions: first approach*, in First International Symposium on Domain Decomposition Methods for Partial Differential Equations (Paris, 1987), SIAM, Philadelphia, PA, 1988, pp. 62–72.

[100] A. QUARTERONI AND A. VALLI, *Theory and application of Steklov-Poincaré operators for boundary-value problems: the heterogeneous operator case*, in Fourth International Symposium on Domain Decomposition Methods for Partial Differential Equations (Moscow, 1990), SIAM, Philadelphia, PA, 1991, pp. 58–81.

[101] ——, *Domain decomposition methods for partial differential equations*, Clarendon Press, Oxford New York, 1999.

[102] P-A. RAVIART AND J.-M. THOMAS, *A mixed finite element method for second order elliptic prolems*, in Mathematical Aspects of Finite Element Methods, I. Galligani and E. Magenes, eds., vol. 606 of Lecture Notes in Mathematics, Springer, Berlin, 1977, pp. 292–315.

[103] M. RENARDY AND R. C. ROGERS, *An introduction to partial differential equations*, Springer-Verlag, New York, 1993.

[104] J. E. ROBERTS AND J.-M. THOMAS, *Mixed and hybrid methods*, in Handbook of numerical analysis, Vol. II, Handb. Numer. Anal., II, North-Holland, Amsterdam, 1991, pp. 523–639.

[105] H. A. SCHWARZ, *Gesammelte mathematische Abhandlungen. Band I, II*, Chelsea Publishing Co., Bronx, N.Y., 1972. Nachdruck in einem Band der Auflage von 1890.

[106] R. E. SHOWALTER, *Nonlinear degenerate evolution equations in mixed formulation*, SIAM J. Math. Anal., 42 (2010), pp. 2114–2131.

[107] U. STEFANELLI AND A. VISINTIN, *Some nonlinear evolution problems in mixed form*, Boll. Unione Mat. Ital. (9), 2 (2009), pp. 303–320.

[108] V. THOMÉE, *Galerkin finite element methods for parabolic problems*, Springer, Berlin New York, 1997.

[109] A. TOSELLI AND O. WIDLUND, *Domain decomposition methods—algorithms and theory*, vol. 34 of Springer Series in Computational Mathematics, Springer-Verlag, 2005.

[110] X. TUNC, I. FAILLE, T. GALLOUËT, M. C. CACAS, AND P. HAVÉ, *A model for conductive faults with non-matching grids*, Computational Geosciences, 16 (2012), pp. 277–296.

[111] B. FRAEIJS DE VEUBEKE, *Displacement and equilibrium models in the finite element method*, in Stress Analysis, O. C. Zienkiewica and G. S. Holister, eds., Wiley, New York, 1965, ch. 9, pp. 145–197.

[112] O. B. WIDLUND, *Iterative substructuring methods: algorithms and theory for elliptic problems in the plane*, in First International Symposium on Domain Decomposition Methods for Partial Differential Equations (Paris, 1987), SIAM, Philadelphia, PA, 1988, pp. 113–128.

[113] B. I. WOHLMUTH, *Hierarchical a posteriori error estimators for mortar finite element methods with Lagrange multipliers*, SIAM J. Numer. Anal., 36 (1999), pp. 1636–1658 (electronic).

[114] ——, *Discretization methods and iterative solvers based on domain decomposition*, Springer, Berlin New York, 2001.

[115] I. YOTOV, *Mixed finite element methods for flow in porous media*, Ph.D. thesis, Rice University, Houston, Texas, 1996.

[116] H. ZHANG, *A note on windowing for the waveform relaxation method*, Appl. Math. Comput., 76 (1996), pp. 49–63.